ABSTRACT

Title of dissertation: CONTROL AND VERIFICATION OF QUANTUM MECHANICAL SYSTEMS

Dvir Kafri, Doctor of Philosophy, 2015

Dissertation directed by: Professor Jacob Taylor
Department of Physics

Quantum information science uses the distinguishing features of quantum mechanics for novel information processing tasks, ranging from metrology to computation. This manuscript explores multiple topics in this field. We discuss implementations of hybrid quantum systems composed of trapped ions and superconducting circuits, protocols for detecting signatures of entanglement in small and many-body systems, and a proposal for ground state preparation in quantum Hamiltonian simulators.

Control and Verification of Quantum Mechanical Systems

by

Dvir Kafri

Dissertation submitted to the Faculty of the Graduate School of the
University of Maryland, College Park in partial fulfillment
of the requirements for the degree of
Doctor of Philosophy
2015

Advisory Committee:
Christopher Monroe (Chair)
Jacob M. Taylor
Christopher Jarzynski
Mohammad Hafezi
Alexey Gorshkov

Preface

In 1935, Einstein, Podolsky, and Rosen (EPR) published a paper claiming that quantum mechanics was incomplete, that there exist 'elements of reality' which cannot be described by the quantum wave-function of a system [1]. The key to their argument was their definition of an element of reality: whenever a physical quantity of a system can be predicted with certainty without disturbing that system, there must necessarily be a corresponding element of reality. In quantum mechanics, an observable of a system can only be predicted with certainty if that system's wave-function is an eigenvector of that observable. Thus two non-commuting observables (with non-complementary eigenvectors) cannot be simultaneous elements of reality. Considering wave-functions describing composites of two systems, EPR showed that by measuring one system it appeared possible to 'steer' the second to a wave-function corresponding to two different non-commuting observables. Therefore, by making an appropriate measurement on the first system, it seemed possible to predict the values of *both* non-commuting observables of the second, and therefore both observables would be elements of reality. Since this is forbidden in quantum mechanics, EPR concluded that the theory was incapable of completely describing nature [1].

Building on the comments of Einstein, Podolsky, and Rosen, Erwin Schrödinger [2] considered a class of composite quantum states for which the value of every observ-

[1] Many physicists today would argue that the issue with this conclusion is not in quantum mechanics, but rather in EPR's defintion of an 'element of reality'. We can instead interpret EPR's paper as showing that quantum mechanics is in direct conflict with local realism, i.e. that elements of reality must be associated with objects localized in space.

able of one system can be inferred by measuring a corresponding observable in the other [2]. An extraordinary feature of these states is that, prior to any measurement, one cannot make predictions with certainty about *any* observable of a single subsystem, and yet all of them are elements of reality. Schrödinger called systems displaying this bizzare property "entangled", and stressed the importance of this phenomenon to quantum theory:

"I would not call that **one** *but rather* **the** *characteristic trait of quantum mechanics, the one that enforces its entire departure from classical lines of thought."*

This unique form of correlation, and more generally the ability to form superpositions of composite systems, is arguably the key ingredient of quantum information science. From it stem novel applications in computation [3], communication [4], and metrology [5].

[2] Today these are called maximally entangled states. In the case of two qubits (an 'EPR pair'), they are called Bell states.

This thesis focuses on different aspects of quantum information science, and entanglement will be relevant throughout the work. The following chapters are based on the following publications and pre-prints (in press or pending submission):

- Dvir Kafri, Prabin Adhikari, and Jacob M. Taylor. Dynamics of an ion coupled to a parametric superconducting circuit. 04 2015. arXiv:1504.03993
- D. Kielpinski, D. Kafri, M. J. Woolley, G. J. Milburn, and J. M. Taylor. Quantum interface between an electrical circuit and a single atom. *Phys. Rev. Lett.*, 108:130504, Mar 2012.
- Dvir Kafri and Jacob M. Taylor. A noise inequality for entanglement generation, 2013. arXiv:1311.4558
- D Kafri, J M Taylor, and G J Milburn. A classical channel model for gravitational decoherence. *New Journal of Physics*, 16(6):065020, 2014.
- Dvir Kafri and Jacob M. Taylor. Distinguishing quantum and classical many-body systems. 04 2015. arXiv:1504.01187
- Dvir Kafri and Jacob M. Taylor. Algorithmic cooling of a quantum simulator, 07 2012. arXiv:1207.7111

Table of Contents

List of Figures

List of Abbreviations

EPR	Einstein, Podolsky and Rosen
RWA	Rotating Wave Approximation
BAW	Bulk-Acousting-Wave (microelectromechanical modulator)
LOCC	Local Operations with Classical Communication
MBS	Many-body System
QSC	Quantum Simulated Cooling
TCP	Trace-preserving, Completely Positive

Chapter 1: Introduction

While quantum information science has seen impressive advances in the last two decades, it has also generated unique challenges. Experiments in atom and ion traps have been approaching the coherence and size limits required to simulate exotic states of matter [6–8]. Success in these efforts will provide insight into strongly correlated many-body systems in condensed matter [8–10], as well as quantum field theories that cannot be studied with classical numerical methods [11, 12]. Yet it is exactly the fact that they simulate such quantum systems that makes confirming the output of these simulators so difficult [13–15]. Along similar lines, progress in quantum optics has led to some of the first industrial applications of quantum information, including provably secure long-range distribution of cryptographic keys [16–19] and generation of truly random numbers [20–22]. All of these advances inherit the same problem: given a device purported to achieve a uniquely quantum task, how does one verify it is working with only limited quantum resources? There have also been several impressive achievements in quantum metrology [5]. Since the 1950's [23] there have been orders of magnitude improvements in timekeeping of atomic clocks [24].The extreme precision of these devices

(currently one part in 10^{18} [25, 26]) make them ideal for defining time standards[1], as well as testing for space-time variations of fundamental constants [28, 29]. Developments in precision measurement from quantum optics have also recently been applied in gravitational wave detection [30]. These experiments use systems displaying uniquely quantum features, such as squeezed states, to achieve precisions surpassing the Standard Quantum Limit [31, 32]. The generation of such states is non-trivial, and understanding the practical physical limits of measurement remains an active area of research.

Future successes in quantum information science will rely on advances in the following categories:

1. *The ability to correlate distant quantum systems through controlled interactions while avoiding decoherence.* For example, interactions between at least two qubits are required for universal quantum computation [33] as well as the entanglement required for generating provably secure cryptographic keys [4, 34]. Decoherence from interactions with the environment causes these superpositions of correlated states to break down, forming useless statistical mixtures.

2. *Procedures for verifying the correct operation of quantum devices.* Indeed, techniques for measuring error rates [35–38] are invaluable in quantum computing, since there exists error correction thresholds which a computation is guaranteed to succeed [39, 40].In many settings (such as in quantum simula-

[1]According to the International Bureau of Weights and Measures (BIPM) [27]:"The second is the duration of 9,192,631,770 periods of the radiation corresponding to the transition between the two hyperfine levels of the ground state of the caesium 133 atom."

tion [13, 41] and boson sampling [42]) it is impossible to completely verify the system of interest using known classical methods. Indeed, for such systems the many-body quantum processes involved are not believed to be reproduceable by classical computation.

3. *Quantum state preparation.* Specifically prepared quantum states serve as practical resources, such as in measurement based quantum computing [43] and quantum state teleportation [44, 45]. Alternatively, the preparation of certain states can be viewed as computational goals, such as for ground states corresponding to physically interesting Hamiltonians [46] or as outputs of quantum computation [47].

This thesis will describe efforts to address each of these challenges.

1.1 Decoherence and controlled interactions

Minimizing decoherence and maintaining strong desired couplings between constituents of a quantum system can be conflicting goals. Decoherence is caused by unwanted interactions with an inaccessible environment. This can be viewed as a measurement of the system by the environment, whose back-action degrades the stored information in a quantum memory or disentangles multi-partite systems. (Although not a main focus in this thesis, the strength of decoherence will be of relevant interest in several of the following chapters.) Conversely, certain quantum systems (e.g., photons) have intrinsically weak interactions with their environment and therefore low decoherence rates, but for this same reason they require sophisti-

cated measures to correlate them with other systems. Both of these issues are crucial in nearly every aspect of quantum information science, from proposed large scale quantum computing networks [48–50], to cryptographically secure communication schemes [51, 52], to preservation of sensitive states used in metrology [53, 54].

Many applications stem from the ability to controllably and strongly couple distinct quantum systems. This is the basis of sympathetic cooling, in which artificial baths thermalize target systems far below their ambient temperatures (e.g., in ultracold atoms [55–57] or micromechanical oscillators [58–60]). Likewise, atom-light couplings can be used to generate effective interactions between photons, allowing for novel many-body photonic systems [61, 62], single photon detectors [63–65], and scalable light-based quantum computation [66–68]. Future devices will likely be hybrid quantum systems, combining components with distinct properties needed in a quantum computing architecture. For example, with their long lifetimes and ease of measurement [69], trapped ions make good canditates for quantum memories. There has been recent interest in interfacing these systems with superconducting circuits, which have fast gate times, can be fabricated to user specifications, and sized to macroscopic scales [70]. In Chapters 2 and 3 we will discuss two related implementations of these hybrid systems.

1.2 Verification of quantum systems

The ability to verify entanglement between distant objects is fundamental to our understanding of quantum physics. Indeed, some of the earliest protocols

for quantum key distribution [18] were based on detecting violations of Bell's inequalities [71, 72]. The amount of entanglement between two subsystems after one subsystem is sent through a quantum communication channel defines the channel's quantum capacity, which characterize its ability to coherently transmit quantum states [45, 73, 74]. The quantum capacity is at least as large as the classical capacity since classical information can be encoded in quantum states [75]. Long-range interactions can also be viewed as communication channels, since they induce statistical correlations between distant objects. In Chapters 4 and 5 we study interactions in the presence of decoherence that can correlate quantum systems but never produce distillable entanglement between them. In other words, they have a finite classical channel capacity but zero quantum channel capacity. From this analysis we derive a generic test verifying that an observed interaction can entangle.

As quantum systems grow beyond a few tens of constituents, the exponential growth of their Hilbert space makes it impossible to directly simulate their evolution or even completely characterize them through measurement (a procedure known as state or process tomography). In fact, this was one of the first motivations for making such quantum simulators [13, 14]. Instead, current experimental efforts must use incomplete tests to verify the correct operation of quantum devices. For example, state tomography based on compressed sensing assumes that the studied state is described by a low rank density matrix, allowing for substantially fewer measurements than full tomography [76, 77]. Similarly, randomized benchmarking [36, 78] and fidelity estimation [37, 38] techniques can be used to quantify error rates in quantum gates. In Chapter 6 we will describe another partial test, intended to ver-

ify that the simulated evolution of quantum system can be used to generate long range entanglement.

1.3 State preparation

Exotic quantum states are key to applications within quantum information science. Indeed, highly entangled 'Schrodinger cat states' have the potential to enhance signal to noise ratios in interferometry [53], but for this same sensitivity to noise they are very hard to prepare in practice (the largest photonic cat state to date was composed of 8 distinct modes [79]). On the information theoretic side, instances of classically intractable problems can be encoded in the ground states of quantum Hamiltonians with three-body interactions [47, 80]. In fact, the ability to generically measure the ground state energy of 3-local Hamiltonians is believed to be even outside the capability of quantum algorithms (the 3-local Hamiltonian problem is QMA-complete) [81][2].

There are a variety of state preparation algorithms for achieving specific tasks. For example, quantum Metropolis sampling [82, 83] can be used to prepare Gibbs states of simulated Hamiltonians on a quantum computer (this is a challenge in classical simulations due to the 'sign problem'), while more generally there is also a quantum version of rejection sampling (a primary subroutine in the classical Metropolis algorithm) [84]. Likewise adiabatic quantum computation [47] is premised on using an adiabatically changing a system's Hamiltonian to prepare ground states relevant

[2]In this context, a k-local Hamiltonian is a sum of terms, each acting on at most k subsystems.

to computational problems. It has been shown to be computationally equivalent to the circuit-based model [85]. Recently these problems have been approached from the perspective of quantum query complexity, producing lower bounds on the required number of operations to prepare a given state [86–88]. In Chapter 7 we will study the computational power of cooling quantum systems with limited resources. Relevant to this discussion, we present a novel scheme for ground state preparation in quantum simulators, based on cooling the simulated system through resonant, local interactions with a single qubit 'bath'.

1.4 Thesis outline

The upcoming chapters are grouped according to three sets of related categories:

- *2,3 – Control of hybrid quantum systems.* Chapter 2 describes a hybrid quantum system composed of a superconducting circuit capacitively coupled to a nearby trapped ion. The circuit's photonic excitations and the ion's motional mode are modeled as coupled harmonic oscillators with highly off-resonant frequencies. To overcome the frequency mismatch and achieve a fast exchange of excitations between these modes, we modulate the characteristic inductance of the circuit. Our method is based on the reaction of a non-linear circuit element (a Josephson junction) to a time-dependent, external magnetic flux. The inductance modulation adds a sideband to circuit dynamics that is resonant with the ion motion, so that the ion-circuit coupling is time-independent in

the interaction picture. Similarly, Chapter 3 describes how to couple these systems by instead modulating the circuit's capacitancee. The capacitive driving allows for much larger resonant sideband in the circuit's charge, and is therefore much more effective than the previous scheme. Based on this enhanced coupling we describe several applications, each premised on using the ion motional mode as a 'quantum bus' between the circuit and ion's spin degree of freedom.

- *4,5,6 – Verification of entanglement in quantum systems.* Moving from control to verification of quantum systems, in Chapter 4 we study the effects of dissipation on linearly coupled oscillators. We derive a necessary and sufficient condition for a given class of master equations to generate distillable entanglement. This leads to a generic experimental test, premised on observing the canonical variables as a witness to the interaction's ability to correlate the systems. We compare the witness to the observed noise in these variables, which must increase at a finite rate in order to prevent entanglement from emerging. Chapter 5 ties these results to the question of gravitational decoherence. It proposes a simple gravitational model between two pendulums based on continuous measurement and feedback, studies this model in the context of the previous chapter's results, and discusses the challenges in experimentally testing whether gravity can entangle distant objects. Finally, Chapter 6 focuses on verification of entanglement in many-body quantum simulators. It describes a generic test for distinguishing classical and quantum systems, by checking

whether the time evolution of a system can be used to produce long-range entanglement.

- *7 – State preparation in quantum simulators.* Chapter 7 investigates the cost of state preparation in quantum simulators. It describes a technique for cooling these systems to their ground states using only local interactions a small ancillary 'bath'. By comparing total cooling time to query cost in terms of computational complexity, it shows that this technique is as powerful as standard quantum computation[3].

[3]More specifically, we show that any algorithm that can be carried out efficiently using circuit-based quantum computation can also be achieved efficiently by ground state preparation.

Chapter 2: Dynamics of an Ion Coupled to a Parametric Superconducting Circuit

Superconducting circuits and trapped ions are promising architectures for quantum information processing. However, the natural frequencies for controlling these systems – radio frequency ion control and microwave domain superconducting qubit control – make direct Hamiltonian interactions between them weak. In this paper we describe a technique for coupling a trapped ion's motion to the fundamental mode of a superconducting circuit, by applying to the circuit a carefully modulated external magnetic flux. In conjunction with a non-linear element (Josephson junction), this gives the circuit an effective time-dependent inductance. We then show how to tune the external flux to generate a resonant coupling between the circuit and ion's motional mode, and discuss the limitations of this approach compared to using a time-dependent capacitance.

2.1 Introduction

Superconducting circuits and trapped ions have distinct advantages in quantum information processing. Circuits are known for fast gate times, flexible fabrication methods, and macroscopic sizes, allowing multiple applications in quantum

information science [89–92]. Unfortunately, they have short coherence times and their decoherence mechanisms are hard to address [50]. Trapped ions, on the other hand, serve as ideal quantum memories. Indeed, the hyperfine transition displays coherence times on the order of seconds to minutes [93–96], while high fidelity state readout is available through fluorescence spectroscopy [69, 97]. Unfortunately, ions depend mainly on motional gates for interactions [98–101]; these are typically slow, susceptible to motional heating associated with traps [102–104], and usually occur only at relatively short – dipolar – ranges (as compared with the size scales of interconnected superconducting circuits). The distinct advantages of ion and superconducting systems therefore motivates a hybrid system comprising both architectures, producing a long-range coupling between high-quality quantum memories.

Early proposals for hybrid atomic and solid state systems [105, 106] have yet to be implemented experimentally. Other approaches involve coupling solid state systems to atomic systems with large dipole moments, such as ensembles of polar molecules [107] or Rydberg atoms [108]. Although the motional dipole couplings with the electric field of superconducting circuits can be several hundred kHz, these systems suffer from a large mismatch between motional ($\sim$ MHz) and circuit ($\sim$ GHz) frequencies. This causes the normal modes of the coupled systems to be either predominantly motional or photonic in nature, thereby limiting the rate at which information is carried between them. Implementation of a practical hybrid device therefore requires something additional.

Parametric processes allow for efficient conversion of excitations between off-resonant systems. In the field of quantum optics, they are widely used in the fre-

quency conversion of photons using nonlinear media [109, 110]. In the realm of superconducting quantum devices, parametric amplifiers provide highly sensitive, continuous readout measurements while adding little noise [111–114]. Parametric processes can also be used to generate controllable interactions between superconducting qubits and microwave resonators [115–117]. In the context of hybrid systems, Ref. [118] presents a parametric coupling scheme between the resonant modes of an LC circuit and trapped ion. The ion, confined in a trap with frequency ω_i, is coupled to the driven sidebands of a high quality factor parametric LC circuit whose capacitance is modulated at frequency $\omega_{LC} - \omega_i$. This gives rise to a coupling strength on the order of tens of kHz for typical ion chip-trap parameters.

In this chapter we describe an alternative parametric driving scheme to produce coherent interactions between atoms and circuits. By using a time-dependent external flux, we drive a superconducting loop containing a Josephson junction, which causes the superconductor to act as a parametric oscillator with a tunable inductance. By studying the characteristic, time-dependent excitations of this system, we show how to produce a resonant interaction between it and the motional mode of a capacitively coupled trapped ion. Although in principle our approach could be used to produce a strong coupling, we find that, in contrast with capacitive driving schemes, the mismatch between inductive driving and capacitive (charge-mediated) interaction causes a significant loss in coupling strength.

The chapter proceeds as follows: In the first section, we describe the experimental setup of the circuit and ion systems and motivate the method used to couple them. To understand how the Josephson non-linearity and external flux affect the

circuit, we transform to a reference frame corresponding to the classical solution of its non-linear Hamiltonian. We then linearize about this solution, resulting in a Hamiltonian that describes fluctuations about the classical equations of motion and corresponds to an LC circuit with a sinusoidally varying inductance. This periodic, linear Hamiltonian is characterized by the quasi-periodic solutions to Mathieu's equation. From these functions we define the 'quasi-energy' annihilation operator for the system and transform to a second reference frame where it is time-independent. Finally, we derive the circuit-ion interaction in the interaction picture, which allows us to directly compute the effective coherent coupling strength between the systems. We conclude by comparing our results to previous work [118] (a capacitive driving scheme) and analyzing why inductive modulation is generically ineffective for capacitive couplings.

2.2 Physical System and Hamiltonian

We begin with a basic physical description of the ion-circuit system, and as in Ref. [119], construct the classical Lagrangian before deriving the quantized Hamiltonian. We consider a single ion placed close to two capacitive plates of a superconducting circuit. We assume that the ion is trapped in an effective harmonic potential with a characteristic frequency ω_z in the direction parallel to the electric field between the two plates [69]. The associated ion Lagrangian is

$$\mathcal{L}_{ion}(z, \dot{z}, t) = \frac{1}{2} m \dot{z}^2 - \frac{1}{2} m \omega_z^2 z^2 \,, \tag{2.1}$$

where m is the ion mass and z its displacement from equilibrium. Since the LC circuit will only couple to the ion motion in the z direction, we ignore the Lagrangian terms associated with motion in the other axial directions.

The circuit interacting with the ion contains a Josephson junction [120] (Fig. 2.1) shunted by an inductive outer loop with inductance L. This configuration is known as a radio frequency superconducting quantum interference device (rf-SQUID) [90]. The SQUID is connected in parallel to a capacitor C, whose plates are coupled to the nearby trapped ion. An external, time-dependent magnetic flux $\phi_x(t)$ through the circuit is used to tune the characteristic frequencies of this system. In our proposed configuration, the SQUID Lagrangian can be written in terms of the node flux ϕ as [119]

$$\mathcal{L}_q(\phi, \dot{\phi}, t) = \frac{1}{2} C_\Sigma \dot{\phi}^2 + E_J \cos(\phi/\tilde{\phi}_0) - \frac{1}{2L}(\phi + \phi_x(t))^2 \,, \tag{2.2}$$

where $\tilde{\phi}_0 = \hbar/(2e)$ is the reduced flux quantum and $C_\Sigma = C + C_J$ is the effective capacitance of the circuit including the capacitance C_J of the Josephson junction. The Josephson energy is defined in terms of the critical current of the junction, $E_J = I_c \tilde{\phi}_0$. The Josephson term adds a non-linearity to the system $\propto E_J$ which will, in conjunction with the external driving, allow us to map the circuit to a linear LC system with time dependent inductance. The modulation of the inductance, in turn, will allow for coherent transfer of excitations between the otherwise off-resonant LC circuit (typical frequency $\sim 1 - 10$ GHz) and ion motional mode ($\sim 1 - 10$ MHz). Finally, we include the interaction between the two systems, associated with the ion

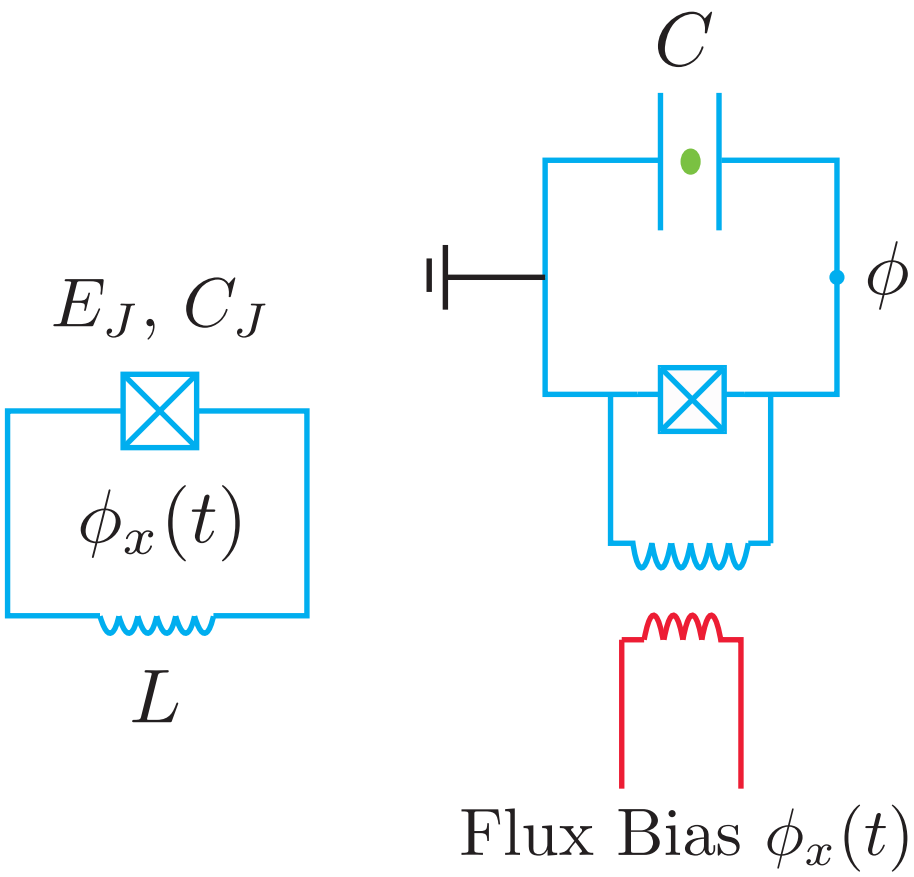

Figure 2.1: Simplified diagram of experimental setup. Left: An rf-Squid with Josephson energy E_J and junction capacitance C_J driven by a time-dependent external flux $\phi_x(t)$. The outer loop with inductance L contributes an energy E_L. Right: Schematic of an ion confined by a capacitor with capacitance C. The capacitor is connected in parallel to the rf-SQUID system.

motion through the electric field between the two plates in the dipole approximation:

$$\mathcal{L}_I = -e\left(\frac{\xi}{d}\dot{\phi}\right) z\,, \tag{2.3}$$

where d is the distance between the two plates and $\xi \sim 0.25$ a dimensionless factor associated with the capacitor geometry [118].

With the full Lagrangian $\mathcal{L} = \mathcal{L}_q + \mathcal{L}_{ion} + \mathcal{L}_I$ we follow the standard prescription to define the canonical variables conjugate to z and ϕ:

$$p_z = \frac{\partial \mathcal{L}}{\partial \dot{z}} = m\dot{z} \tag{2.4}$$

$$q = \frac{\partial \mathcal{L}}{\partial \dot{\phi}} = C_\Sigma \dot{\phi} - \xi\frac{e}{d}z\,. \tag{2.5}$$

These are identified as the momentum of the ion in the z direction and the effective Cooper-pair charge in the Josephson junction, respectively. We use the canonical Legendre transformation $H = q\dot{\phi} + p_z\dot{z} - \mathcal{L}$ to define the Hamiltonian and quantize the system, giving

$$\hat{H}(t) = \hat{H}_{ion} + \hat{H}_q(t) + \hat{H}_I\,, \tag{2.6}$$

where

$$\hat{H}_{ion} = \frac{\hat{p}_z^2}{2m} + \frac{1}{2}m\omega_i^2\hat{z}^2, \tag{2.7}$$

$$\hat{H}_q(t) = \frac{\hat{q}^2}{2C_\Sigma} - E_J\cos(\hat{\phi}/\tilde{\phi}_0) + \frac{1}{2L}(\hat{\phi} - \phi_x(t))^2, \tag{2.8}$$

$$\hat{H}_I = -e\frac{\xi}{dC_\Sigma}\hat{q}\hat{z}\,, \tag{2.9}$$

As the canonical charge q of equation (2.5) has a term proportional to z, the ion Hamiltonian $\hat{H}_{ion}$ gains an extra potential term proportional to $\hat{z}^2$. Accounting for this term, we define the dressed trap frequency,

$$\omega_i^2 = \omega_z^2 + \frac{e^2\xi^2}{d^2C_\Sigma m}\,. \tag{2.10}$$

The latter correction is small compared to ω_z; it is on the order of 50kHz for the parameters suggested in Ref. [118] ($d \approx 25\mu$m, $C_\Sigma \approx 50$fF and $m \approx 1.5\times10^{-26}$kg the atomic mass of Beryllium). Finally, we note the resulting commutation relations, $[\hat{\phi}, \hat{q}] = [\hat{z}, \hat{p}_z] = i\hbar$.

To motivate the method for coherently coupling the ion and circuit, we consider the Hamiltonian in the interaction picture, i.e., in the frame rotating with respect to $\hat{H}_q(t) + \hat{H}_{ion}$. In this frame the Hamiltonian takes the form,

$$\hat{H}_{int}(t) = -\frac{\xi e}{dC_\Sigma}\hat{q}(t)\left(\hat{b}e^{-i\omega_i t} + \hat{b}^\dagger e^{i\omega_i t}\right)\sqrt{\frac{\hbar}{2m\omega_i}}\,, \tag{2.11}$$

where $\hat{b} = \sqrt{\frac{m\omega_i}{2\hbar}}\hat{z} + i\sqrt{\frac{1}{2\hbar m\omega_i}}\hat{p}_z$ is the annihilation operator associated with excitations of the ion motional mode, and $\hat{q}(t)$ is propagated according to the time-dependent Hamiltonian $\hat{H}_q(t)$. Observe that if we set both $\phi_x(t)$ and E_J to 0 in the definition of $\hat{H}_q(t)$, the charge $\hat{q}(t)$ will oscillate as a harmonic oscillator,

$$\hat{q}(t) \to i\sqrt{\frac{\hbar C_\Sigma \omega_0}{2}}(\hat{a}e^{-i\omega_0 t} - \hat{a}^\dagger e^{i\omega_0 t})\,, \tag{2.12}$$

with $\hat{a}$ the circuit annihilation operator analogous to $\hat{b}$, and ω_0 the undriven frequency LC,

$$\omega_0 = 1/\sqrt{LC_\Sigma}\,. \tag{2.13}$$

In order to coherently exchange excitations between the systems, $\hat{H}_{int}(t)$ should only contain beam splitter like terms, $\hat{a}\hat{b}^\dagger$ and $\hat{a}^\dagger\hat{b}$, while suppressing the excitation non-conserving terms, $\hat{a}^\dagger\hat{b}^\dagger$ and $\hat{a}\hat{b}$. Yet since $\omega_0 \gg \omega_i$, the $ab^\dagger$ terms oscillate at a frequency comparable to the $a^\dagger b^\dagger$ terms, both of which have negligible effect in the rotating wave approximation (RWA). Our goal is therefore the following: design E_J

and $\phi_x(t)$ such that $\hat{a}\hat{b}^\dagger$ contains a time-independent component in the interaction picture, while $\hat{a}\hat{b}$ contains only oscillating terms that drop out in the RWA.

2.3 Linearization of the Parametric Oscillator

Before we can determine the parameters $\phi_x(t)$ and E_J allowing for coherent exchange of excitations, we must first bring $\hat{H}_q(t)$ into a more agreeable form. To begin, we linearize the circuit Hamiltonian about the classical solution to its equations of motion. This makes it possible (in the next section) to identify effective annihilation and creation operators for the LC system, and to analyze their spectrum.

We linearize by displacing the charge and flux variables by time-dependent scalars, $q_c(t)$ and $\phi_c(t)$, through the unitary transformations

$$\begin{aligned} \hat{U}_1(t) &= e^{i\hat{\phi}q_c(t)/\hbar}, \\ \hat{U}_2(t) &= e^{-i\hat{q}\phi_c(t)/\hbar}. \end{aligned} \tag{2.14}$$

Specifically, we consider the LC circuit in terms of the displaced states,

$$\left|\tilde{\Psi}(t)\right\rangle = \hat{U}_2^\dagger(t)\hat{U}_1^\dagger(t)\left|\Psi(t)\right\rangle , \tag{2.15}$$

whose equation of motion satisfies

$$\begin{aligned} \partial_t \left|\tilde{\Psi}(t)\right\rangle &= -i\hbar^{-1}\tilde{H}_q(t)\left|\tilde{\Psi}(t)\right\rangle , \\ \tilde{H}_q &= \hat{U}_2^\dagger\hat{U}_1^\dagger\hat{H}_q\hat{U}_1\hat{U}_2 - i\hbar\hat{U}_2^\dagger\hat{U}_1^\dagger\frac{\partial\hat{U}_1}{\partial t}\hat{U}_2 \\ &\quad - i\hbar\hat{U}_2^\dagger\frac{\partial\hat{U}_2}{\partial t}. \end{aligned} \tag{2.16}$$

Given $[\hat{\phi}, \hat{q}] = i\hbar$, we have that $\hat{U}_1^\dagger \hat{q} \hat{U}_1 = \hat{q} + q_c(t)$ and $\hat{U}_2^\dagger \hat{\phi} \hat{U}_2 = \hat{\phi} + \phi_c(t)$, while clearly $\hat{U}_1^\dagger \hat{\phi} \hat{U}_1 = \hat{\phi}$ and $\hat{U}_2^\dagger \hat{q} \hat{U}_2 = \hat{q}$. The displaced state Hamiltonian is therefore

$$\begin{aligned} \tilde{H}_q(t) &= \frac{(\hat{q} + q_c(t))^2}{2C_\Sigma} + V_q(\hat{\phi} + \phi_c(t)) \\ &\quad + (\hat{\phi} + \phi_c(t))\partial_t q_c(t) - \hat{q}\partial_t \phi_c(t), \end{aligned} \tag{2.17}$$

where we have defined the nonlinear potential,

$$V_q(\hat{\phi}) = -E_J \cos(\hat{\phi}/\tilde{\phi}_0) + \frac{1}{2L}(\hat{\phi} - \phi_x(t))^2 \,, \tag{2.18}$$

with $\tilde{\phi}_0 = \hbar/(2e)$. We now Taylor expand V_q about $\phi_c(t)$, and collect all first and second order terms in $\hat{q}$ and $\hat{\phi}$, giving

$$\begin{aligned} \tilde{H}_q(t) &= \hat{q}\,(q_c(t)/C_\Sigma - \partial_t \phi_c) + \hat{\phi}\left(V_q'(\phi_c) + \partial_t q_c\right) \\ &\quad + \frac{\hat{q}^2}{2C_\Sigma} + \frac{V_q''(\phi_c)}{2!}\hat{\phi}^2 + R(\hat{\phi}) \,, \end{aligned} \tag{2.19}$$

where we have dropped all scalar terms, and

$$R(\hat{\phi}) = \sum_{k \geq 3} \tilde{\phi}_0^k V_q^{(k)}(\phi_c) \left(\hat{\phi}/\tilde{\phi}_0\right)^k \frac{1}{k!} \tag{2.20}$$

represents all higher order terms in the Taylor expansion.

To complete the linearization, the displacements q_c and ϕ_c are chosen so that the first order terms in $\hat{q}$ and $\hat{\phi}$ vanish, and therefore $\tilde{H}_q$ is quadratic to leading order:

$$\begin{aligned} \partial_t \phi_c &= q_c/C_\Sigma \\ \partial_t q_c &= -V_q'(\phi_c) \,. \end{aligned} \tag{2.21}$$

These relations are the solutions to the classical, driven Hamiltonian, $H_q = \frac{q_c^2}{2C_\Sigma} + V_q(\phi_c, t)$, and can be substituted into each other to give

$$\partial_t^2 \phi_c + \omega_0^2(\phi_c + \beta\tilde{\phi}_0 \sin(\phi_c/\tilde{\phi}_0)) = \omega_0^2 \phi_x(t)\,, \tag{2.22}$$

where

$$\beta = LE_J/\tilde{\phi}_0^2 = \frac{LI_c}{\tilde{\phi}_0} \tag{2.23}$$

represents the strength of the non-linearity and $\omega_0 = 1/\sqrt{LC_\Sigma}$ is the bare LC resonance frequency. Substituting from (2.21) and computing $V_q''(\phi_c) = \frac{1}{L}(1 + \beta\cos(\phi_c/\tilde{\phi}_0))$, we can now express the circuit Hamiltonian as

$$\tilde{H}_q(t) = \frac{\hat{q}^2}{2C_\Sigma} + \frac{1}{2L}(1 + \beta\cos(\phi_c(t)/\tilde{\phi}_0))\hat{\phi}^2\,. \tag{2.24}$$

Note that we have dropped the higher order terms $R(\hat{\phi})$ of equation (2.20). Understanding when this is valid will require us to express the flux operator $\hat{\phi}$ in the interaction picture, which we carry out below. A complete analysis is deferred to the appendix.

With equation (2.24) we have converted to the Hamiltonian of a harmonic oscillator with time-dependent inductance. Although it is explicitly dependent on the classical solution $\phi_c(t)$, we note that engineering this function is rather straightforward. Given a desired $\phi_c(t)$, the external driving $\phi_x(t)$ needed to produce it is given explicitly by equation (2.22) (see Fig. 2.2). For simplicity we assume that $\phi_c(t)$ satisfies the relation

$$\beta\cos(\phi_c(t)/\tilde{\phi}_0) = \eta\cos(\omega_d t)\,, \tag{2.25}$$

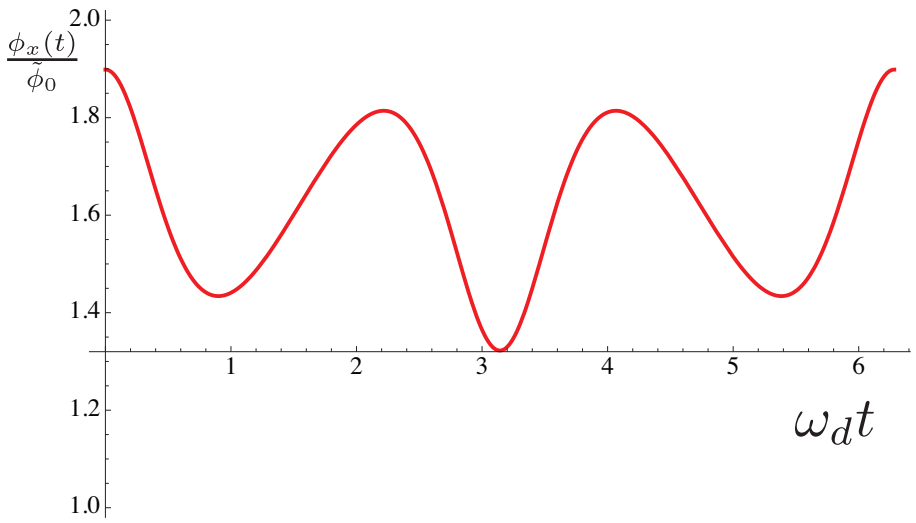

Figure 2.2: External flux drive $\phi_x(t)/\tilde{\phi}_0$ required for a sinusoidal modulation of circuit inductance. The flux $\phi_x(t)$ is defined explicitly by equation (2.22), where the classical solution $\phi_c(t)$ satisfies $\beta\cos(\phi_c(t)/\tilde{\phi}_0) = \eta\cos(\omega_d t)$. The plotted function corresponds to drive parameters $\omega_d = 0.999\omega_0$, $\eta = 0.06 = (3/4)\times\beta$, where $\beta = E_J(\tilde{\phi}_0^2/L)^{-1}$ represents the strength of the non-linearity compared to the bare linear inductance. The relative scaling $\eta/\beta < 1$ is chosen so that ϕ_c is a smooth function of time; the $\eta \to \beta^-$ limit corresponds to a saw-tooth wave with undefined second derivative.

where we assume $\eta < \beta$ so that ϕ_c is well defined at all t. This corresponds to an LC circuit with inverse inductance L^{-1} modulated at amplitude η and frequency ω_d,

$$\tilde{H}_q(t) = \frac{\hat{q}^2}{2C_\Sigma} + \frac{1}{2L}(1+\eta\cos(\omega_d t))\hat{\phi}^2\,. \tag{2.26}$$

In the following section we will see how the design parameters η and ω_d determine the evolution of this system.

2.4 Time-Dependent Quantum Harmonic Oscillator

Although we now have a quadratic Hamiltonian for the SQUID, since $\tilde{H}_q(t) = \frac{\hat{q}^2}{2C_\Sigma} + \frac{1}{2L}(1 + \eta\cos(\omega_d t))\hat{\phi}^2$ is time-dependent, it is not immediately clear how to define its associated annihilation operator. To do so, we follow the approach of Ref. [121] to obtain an effective operator $\hat{a}$ retaining useful properties of the time-independent case. Specifically, it satisfies $[\hat{a}, \hat{a}^\dagger] = 1$ and, in the appropriate reference frame, is explicitly time-independent. Further, in this frame the Hamiltonian can be written as $\hbar(\partial_t\theta(t))(\hat{a}^\dagger\hat{a} + 1/2)$, where $\theta(t)$ is the effective phase accumulated by $\hat{a}$ in the Heisenberg picture. This new Hamiltonian commutes with itself at all times, allowing us to directly transform to the interaction picture in the next section. We will then describe how to control the spectral properties of $\hat{q}(t)$ in the interaction Hamiltonian (2.11), producing the desired time-independent beam splitter-like interaction between circuit and ion motion.

Following Ref. [121], we use unitary transformations to change $\tilde{H}_q(t)$ so that it is of the form $\sim g(t)(\alpha\hat{q}^2 + \beta\hat{\phi}^2)$, where α and β are explicitly time-independent. To do this, we first analyze the classical equation of motion for the flux ϕ associated with $\tilde{H}_q(t)$, as derived from equation (2.26),

$$\partial_t^2 f(t) + \omega_0^2(1 + \eta\cos(\omega_d t))f(t) = 0\,. \tag{2.27}$$

Since the drive has period $\tau = 2\pi/\omega_d$, from Floquet's theorem [122,123] we can find

a quasi-periodic solution f satisfying

$$\begin{aligned} f(0) &= 1\,, \\ f(t+\tau) &= e^{i\mu\pi} f(t)\,. \end{aligned} \tag{2.28}$$

In order for the solution to be stable, the characteristic exponent μ must be real valued. This imposes constraints on the parameters ω_d and η, which we discuss later. As we shall see, the properties of the function f will be closely related to the spectrum of $\hat{q}(t)$ in the interaction picture.

It is useful to express f in polar form,

$$f(t) = r(t)e^{i\theta(t)}\,, \tag{2.29}$$

where $r > 0$ and θ is real valued. Substituting this relation into the characteristic equation (2.27) determines equations of motion for r and θ,

$$\begin{aligned} \partial_t^2 r &= \left((\partial_t\theta)^2 - \omega_0^2(1+\eta\cos(\omega_d t))\right) r\,, \\ 0 &= r\partial_t^2\theta_t + 2(\partial_t r)(\partial_t\theta)\,. \end{aligned} \tag{2.30}$$

We define the associated Wronskian, which sets a characteristic frequency scale for the evolution,

$$\begin{aligned} W &= \frac{1}{2i}\left(f^*(t)\partial_t f(t) - f(t)\partial_t f^*(t)\right) \\ &= \mathrm{Im}\left(re^{-i\theta}\partial_t\left(re^{i\theta}\right)\right) \\ &= r^2\partial_t\theta\,. \end{aligned} \tag{2.31}$$

We note that $\frac{1}{r}\partial_t W$ is equal to the second line of (2.30), so $\partial_t W = 0$ and W is time-independent.

The above definitions are key to the transformations bringing $\tilde{H}_q(t)$ into the desired form. Our first transformation is

$$\hat{U}_3 = \exp(i\chi(t)\hat{\phi}^2/\hbar)\,, \tag{2.32}$$

where

$$\chi(t) \equiv \frac{C_\Sigma}{2}\frac{\partial_t r}{r} \tag{2.33}$$

is the real part of the effective admittance, $\frac{C_\Sigma}{2}\frac{\partial_t f}{f}$. Using $[\hat{\phi},\hat{q}] = i\hbar$, we note

$$\begin{aligned}
\hat{U}_3^\dagger \hat{q} U_3 &= \hat{q} + 2\chi\hat{\phi} \\
\hat{U}_3^\dagger \hat{\phi} U_3 &= \hat{\phi} \\
-i\hbar\hat{U}_3^\dagger \partial_t \hat{U}_3 &= (\partial_t\chi)\hat{\phi}^2
\end{aligned} \tag{2.34}$$

After some algebra, the Hamiltonian of Eq. (2.26) is transformed to $\hat{U}_3^\dagger \tilde{H}_q(t)\hat{U}_3 - i\hbar\hat{U}_3^\dagger\partial_t\hat{U}_3$ and becomes

$$\begin{aligned}
&\frac{\hat{q}^2}{2C_\Sigma} + \frac{\chi}{C_\Sigma}(\hat{\phi}\hat{q} + \hat{q}\hat{\phi}) \\
&+\frac{C_\Sigma\hat{\phi}^2}{2}\left(\omega_0^2\left(1+\eta\cos(\omega_d t)\right) + (2\chi/C_\Sigma)^2 + 2\partial_t\chi/C_\Sigma\right) \\
= \;& \frac{\hat{q}^2}{2C_\Sigma} + \frac{\chi}{C_\Sigma}(\hat{\phi}\hat{q} + \hat{q}\hat{\phi}) + \frac{C_\Sigma}{2}(\partial_t\theta)^2\hat{\phi}^2\,.
\end{aligned} \tag{2.35}$$

In the last line we used $2\chi/C_\Sigma = (\partial_t r)/r$ and the first line of (2.30) to compute $2\partial_t\chi/C_\Sigma = (\partial_t\theta)^2 - \omega_0^2\left(1+\eta\cos(\omega_d t)\right) - (2\chi/C_\Sigma)^2$.

The next transformation removes the cross term and rescales $\hat{q}$ and $\hat{\phi}$:

$$\hat{U}_4 = e^{-iF(t)(\hat{\phi}\hat{q}+\hat{q}\hat{\phi})/\hbar}\,, \tag{2.36}$$

where $F(t) = \frac{1}{2}\log(r)$ satisfies $\partial_t F = \chi/C_\Sigma$. Given $[(\hat{\phi}\hat{q} + \hat{q}\hat{\phi}),\hat{\phi}] = -2i\hbar\hat{\phi}$ and

$[(\hat{\phi}\hat{q} + \hat{q}\hat{\phi}), \hat{q}] = 2i\hbar\hat{q}$, we compute

$$\begin{aligned} \hat{U}_4^\dagger \hat{q} U_4 &= e^{-2F}\hat{q} = \frac{\hat{q}}{r} \\ \hat{U}_4^\dagger \hat{\phi} U_4 &= e^{2F}\hat{\phi} = r\hat{\phi} \\ -i\hbar\hat{U}_4^\dagger \partial_t \hat{U}_4 &= -\frac{\chi}{C_\Sigma}(\hat{\phi}\hat{q} + \hat{q}\hat{\phi})\,. \end{aligned} \tag{2.37}$$

The final transformed Hamiltonian is therefore

$$\begin{aligned} \hat{H}_{LC} &= \frac{\hat{q}^2}{2C_\Sigma r^2} + \frac{C_\Sigma}{2}(\partial_t\theta)^2 r^2 \hat{\phi}^2 \\ &= \frac{\partial_t\theta}{W}\left(\frac{\hat{q}^2}{2C_\Sigma} + \frac{1}{2}C_\Sigma W^2 \hat{\phi}^2\right), \end{aligned} \tag{2.38}$$

where the last line follows from equation (2.31).

Equation (2.38) allows us to define the effective annihilation operator in the standard way,

$$\hat{a} = \sqrt{\frac{C_\Sigma W}{2\hbar}}\hat{\phi} + i\sqrt{\frac{1}{2\hbar C_\Sigma W}}\hat{q}\,, \tag{2.39}$$

so that the Hamiltonian is also equal to

$$\hat{H}_{LC}(t) = \hbar(\partial_t\theta)(\hat{a}^\dagger\hat{a} + 1/2)\,. \tag{2.40}$$

In this reference frame, we can interpret $\hat{a}^\dagger$ as the creation operator for the instantaneous eigenstates of $\hat{H}_{LC}(t)$, whose energies are integer multiples of $\hbar(\partial_t\theta)(t)$.

2.5 Interaction Picture

Using the series of unitary transformations derived above, we now compute the operators $\hat{\phi}$ and $\hat{q}$ in the interaction picture with respect to Eq. (2.40). This serves two purposes. First, it will allow us calculate in the interaction picture the higher

order terms $R(\hat{\phi})$ of equation (2.20), which we we dropped in order to the reach driven, quadratic Hamiltonian of equation (2.26). In the appendix we evaluate the size of these corrections in the rotated frame, and suggest a technique for minimizing their effect. Second, going to the interaction picture will allow us to write the original interaction $\hat{H}_I = -e\frac{\xi}{dC_\Sigma}\hat{q}\hat{z}$ in terms of the effective annihilation operators of equation (2.39), allowing for a straightforward calculation of the coherent coupling strength in the next section.

It is easier to first compute $\hat{\phi}$ in the interaction picture; the first two transformations are the displacements involved in linearization,

$$\hat{\phi} \to \hat{\phi} + \phi_c \,, \tag{2.41}$$

while the third unitary $\hat{U}_3 = \exp(i\chi\hat{\phi}^2/\hbar)$ has no effect on $\hat{\phi}$. The final unitary $\hat{U}_4$ rescales $\hat{\phi}$ by the factor r, giving

$$\sqrt{\frac{\hbar}{2C_\Sigma W}} r(\hat{a} + \hat{a}^\dagger) + \phi_c(t) \,, \tag{2.42}$$

where we have used (2.39) to express $\hat{\phi}$ in terms of the annihilation operator $\hat{a}$. Finally, since in this rotated frame the circuit Hamiltonian is of the form $\hat{H}_{LC} = \hbar(\partial_t\theta)\left(\hat{a}^\dagger\hat{a} + 1/2\right)$, in the corresponding interaction picture $\hat{a} \to \hat{a}e^{-i\theta}$. The final form of $\hat{\phi}$ in the interaction picture is thus

$$\begin{aligned} \hat{\phi}_{int}(t) &= \phi_c(t) + \sqrt{\tfrac{\hbar}{2C_\Sigma W}} r(\hat{a}e^{-i\theta} + \hat{a}^\dagger e^{i\theta}) \\ &= \phi_c(t) + \sqrt{\tfrac{\hbar}{2C_\Sigma W}}(f^*\hat{a} + f\hat{a}^\dagger) \,, \end{aligned} \tag{2.43}$$

where we have used $f = re^{i\theta}$. Using this expression for the interaction picture flux operator, we bound the effect of the higher order corrections $R(\hat{\phi})$ to the linearized

Hamiltonian of equation (2.24). A parameter of interest arising in this discussion is the relative size of the characteristic flux, which is set by

$$\gamma \equiv \frac{1}{\tilde{\phi}_0}\sqrt{\frac{\hbar}{2C_\Sigma W}}\,. \tag{2.44}$$

Importantly, the final coupling strength is linearly proportional to this parameter, which we shall see limits the efficacy of our approach.

The derivation of $\hat{q}_{int}$ is analogous to that of $\hat{\phi}_{int}$. From the action of the four transformations $\hat{U}_1$ through $\hat{U}_4$, $\hat{q}$ takes the form

$$q_c(t) + \frac{1}{r}\hat{q} + 2\chi r\hat{\phi}\,. \tag{2.45}$$

Expressing these operators in terms of $\hat{a}$ of equation (2.39) then going to the rotating frame $\hat{a} \to \hat{a}e^{-i\theta}$ gives

$$\hat{q} \to q_c(t) + \sqrt{\frac{\hbar C_\Sigma}{2W}}\left(g(t)\hat{a} + g(t)^*\hat{a}^\dagger\right)\,, \tag{2.46}$$

where $g(t) = (\partial_t r - i\frac{W}{r})e^{-i\theta}$. Using the Wronskian identity $W = r^2\partial_t\theta$ of equation (2.31), we see that $g(t) = \partial_t(re^{-i\theta}) = \partial_t f^*$, so the final form of $\hat{q}$ in the interaction picture is

$$\hat{q}_{int}(t) = q_c(t) + \sqrt{\frac{\hbar C_\Sigma}{2W}}\left(\partial_t f^*\hat{a} + \partial_t f\hat{a}^\dagger\right)\,. \tag{2.47}$$

With this result, we may immediately compute the final ion-circuit interaction,

$$\begin{aligned}
\hat{H}_{int}(t) &= -e\frac{\xi}{dC_\Sigma}\hat{q}_{int}(t)\hat{z}_{int}(t) \\
&= -\xi\frac{ez_0}{C_\Sigma d}\sqrt{\frac{\hbar C_\Sigma}{2W}}\left(\partial_t f^*\hat{a} + \partial_t f\hat{a}^\dagger\right) &(2.48)\\
&\quad\times(\hat{b}e^{-i\omega_i t} + \hat{b}^\dagger e^{i\omega_i t})\,, &(2.49)
\end{aligned}$$

where $\hat{z}_{int}(t) = z_0(\hat{b}e^{-i\omega_i t} + \hat{b}^\dagger e^{i\omega_i t})$, with $z_0 = \sqrt{\frac{\hbar}{2m\omega_i}}$ the characteristic displacement of the ion. Note that we have dropped the term $q_c(t)\hat{z}_{int}(t)$ by using the rotating wave approximation, since q_c oscillates at characteristic frequency $\omega_d \gg \omega_i$.

2.6 Coupling strength

In order to compute the effective coupling strength between the circuit and ion motion, we must first analyze the Fourier spectrum of the characteristic function f. We begin by expressing the interaction Hamiltonian of (2.49) in terms of dimensionless factors,

$$\begin{aligned} \tilde{H}_{int}(u) &= -\frac{\hbar\omega_d}{4}\frac{z_0}{d}\xi\gamma\left(\partial_u f^*\hat{a} + \partial_u f\hat{a}^\dagger\right) \\ &\quad \times(\hat{b}e^{-i2\omega_i u/\omega_d} + \hat{b}^\dagger e^{i2\omega_i u/\omega_d})\,, \end{aligned} \tag{2.50}$$

where we have used $\tilde{\phi}_0 = \hbar/(2e)$ to get an expression in terms of the flux parameter γ of equation (2.44). Here we have rewritten f in terms of the dimensionless parameter $u = \omega_d t/2$, to better match the canonical form of Mathieu's equation,

$$\left[\partial_u^2 + (A - 2Q\cos 2u)\right] f = 0,\ . \tag{2.51}$$

Using the substitution $A = 4(\omega_0/\omega_d)^2$, and $Q = -\eta a/2$, this equation is equivalent to (2.27). By Floquet's Theorem, f can be expressed as a quasi-periodic function

$$f(u) = e^{i\mu u}\sum_k c_k e^{2iku}\,, \tag{2.52}$$

where the sum has period $u_0 = \pi$ corresponding to $t = 2\pi/\omega_d$. Multiplying the cross terms of equation (2.50), we see that the coupling strength is proportional to the

time-independent part of $e^{i2\omega_i u/\omega_d}\partial_u f^* \hat{a}\hat{b}^\dagger$ (the only term to survive under the RWA). This constant is exactly proportional to the Fourier component of f corresponding to the ion motional frequency, which is specified by the resonance condition

$$(\mu + 2k) = 2\omega_i/\omega_d \,. \tag{2.53}$$

Accounting for the derivative $\partial_u f^*$ in this expression, the coupling strength is

$$\hbar|\Omega| = \frac{\hbar\omega_d}{4}\frac{z_0}{d}\xi\gamma(\mu + 2k)|c_k| = \frac{\hbar\omega_i}{2}\frac{z_0}{d}\xi\gamma|c_k| \,, \tag{2.54}$$

where in the second equality we used condition (2.53). Note that although Ω is not explicitly dependent on the driving amplitude η and frequency ω_d, both γ and c_k are functions of these parameters since both are dependent on the characteristic function f.

With equation (7.37) we can now evaluate the strength of the coupling for a driving strategy similar to that of Ref. [118]. Specifically, we set the drive frequency to be approximately the difference between the circuit's bare frequency and the ion's motional frequency: $\omega_d \approx \omega_0 - \omega_i$. Since the ion frequency $\omega_i \ll \omega_0$ is much smaller than the LC frequency, the drive frequency ω_d is nearly resonant with the LC circuit. This means that even a relatively small drive amplitude leads to a mathematical instability in the system. Indeed, for η sufficiently large, the characteristic exponent μ describing the quasi-periodic function f gains an imaginary component, causing the interaction picture charge operator $\hat{q}_{int}(t)$ to diverge over time. This instability is alleviated in the presence environmental dissipation, as the system dynamics are then damped, though for simplicity we neglect these effects in our analysis. As seen in Fig. 2.3, for $\omega_0 \approx \omega_d \gg \omega_i$ the boundary between mathematically stable

and unstable regions is set by $\eta \lesssim 2\sqrt{\omega_i/\omega_0}$. For near-resonant driving to be mathematically stable, the parameter η must therefore be perturbatively small. In this $\eta \ll 1$ limit, the characteristic exponent is equal to $\mu = 2\omega_0/\omega_d + O(\eta^2)$ [124], so the solution of the frequency matching condition $\mu + 2k = 2\omega_i/\omega_d$ corresponds to $k = -1$. Using the relations $A = 4(\omega_0/\omega_d)^2 \approx 4$ and $Q = -\eta A/2 \approx -2\eta$, these parameters can be mapped to the canonical form of equation (2.51). The coefficient $c_{-1} = Q/4 + O(Q^2) = -\eta/2 + O(\eta^2)$ is known from standard perturbative expansions [124]. Substituting this value into equation (7.37), we conclude that in the perturbative regime $\eta \lesssim 2\sqrt{\omega_i/\omega_0}$, the coupling strength between LC and ion modes scales as

$$\begin{aligned} \hbar|\Omega| &= \frac{\hbar\omega_i}{4}\left(\frac{z_0}{d}\xi\gamma\eta\right)(1+O(\eta)) \\ &\lesssim \frac{\hbar\omega_i}{2}\left(\frac{z_0}{d}\xi\gamma\right)\sqrt{\frac{\omega_i}{\omega_0}}\left(1+O(\sqrt{\omega_i/\omega_0})\right) . \end{aligned} \tag{2.55}$$

We note that this driving scheme may not be optimal. When ω_d is set far from resonance and $\eta \sim 1$, the characteristic exponent μ can be stable and vary over a large range of values, allowing for the resonance condition (2.53) to be satisfied at stronger driving. Note that this also changes the Wronskian W (which changes $\gamma \propto 1/\sqrt{W}$) in a non-linear way, so a general analysis for the best driving parameters is difficult. Strong driving may be infeasible for experimental reasons, since it may require too large a Josephson energy (which is proportional to $\beta > \eta$).

Unfortunately, we find that the final effective coupling Ω is substantially weaker than in the proposal of Ref. [118]. In that work, the ion's motional degree of freedom was also capacitively coupled to the circuit, but the characteristic

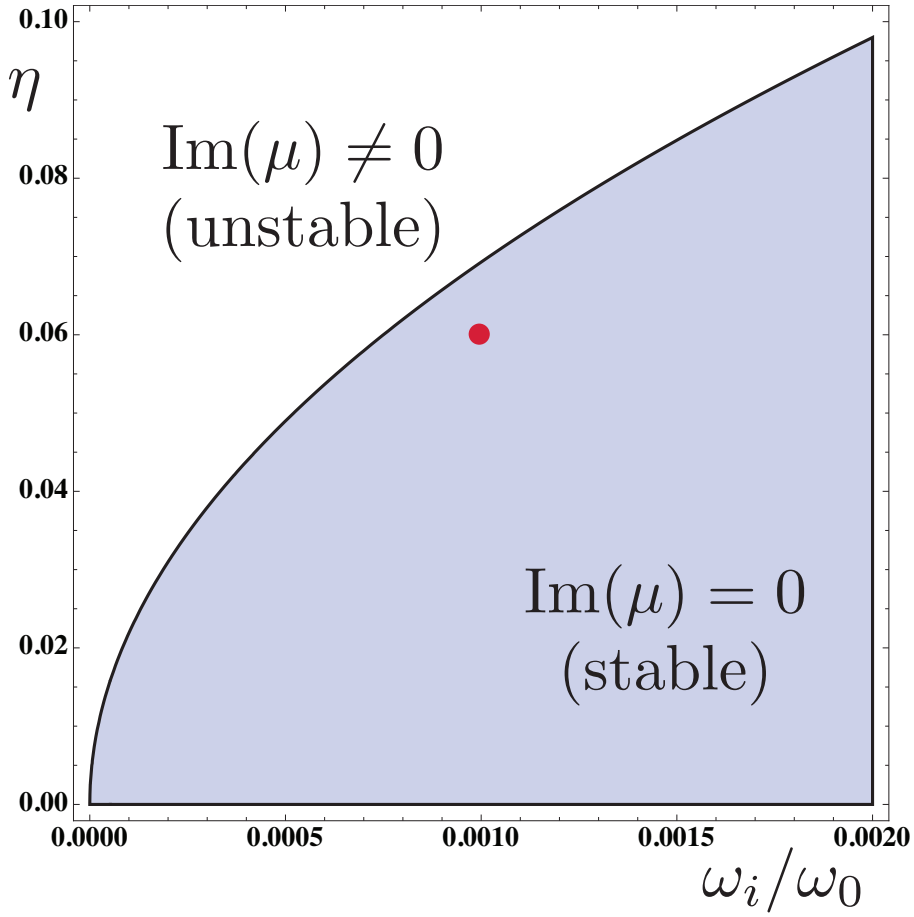

Figure 2.3: Stability diagram of Mathieu's equation. The parameters ω_i/ω_0 and η map to the canonical variables of equation (2.51) as $A = 4(1 - \omega_i/\omega_0)^2$ and $Q = -2\eta(1 - \omega_i/\omega_0)^2$. The shaded region corresponds to stable quasi-periodic solutions, i.e. those with characteristic exponent μ having no imaginary part. The red dot at $\omega_i = 0.001\omega_0, \eta = 0.06$ corresponds to the driving parameters used in Fig. 2.4.

equation of the circuit was instead modulated by a time varying capacitive element. The same driving scheme as above was used, leading to an effective coupling strength of the form,

$$\hbar\Omega_{cap} \sim \frac{eQ_0}{C_\Sigma}\left(\xi\frac{z_0}{d}\eta\right) \approx \hbar(2\pi \times 60 \text{ kHz})\,. \tag{2.56}$$

Here $Q_0 = \sqrt{\frac{\hbar C_\Sigma W}{2}}$ is the characteristic charge fluctuation in the driven circuit, and η the relative amplitude of the time-varying capacitance, $C(t) = C_\Sigma(1+\eta\sin(\omega_d t))$. For comparison, from equation (2.55) we obtain a coupling rate $\Omega \simeq 1$ Hz. Decoherence rates for these systems are expected to be on the order of kHz, while leading order corrections from linearization scale as $\hbar\omega_i(\beta\gamma\omega_0/\omega_i)^2$, both of which make this approach infeasible as currently described. Note that we are making the same assumptions as Ref. [118] about trap geometry ($\xi = 0.25, d = 25\mu$m) and ion mass ($m \simeq 1.5\times10^{-26}$kg for $^9\text{Be}_+$), as well as ion motional frequency ($\omega_i \approx 2\pi\times$1MHz, so $z_0 = \sqrt{\frac{\hbar}{2m\omega_i}} \approx 25$ nm). Finally, the parameter $\gamma \sim 1.3$ is set by the circuit capacitance $C_\Sigma = 46$ fF and the Wronskian $W \approx \omega_0 = 2\pi\times 1$ GHz.

As seen from the above comparison, when the ion-circuit interaction is capacitive (proportional to charge), modulating the circuit inductance at frequency $\omega_d \gg \omega_i$ is significantly less effective than modulating the capacitance. This results from the asymmetric dependence between charge and flux operators on the characteristic function f, as demonstrated by the interaction picture expressions for these operators (equations (2.43) and (2.47)). While the flux scales with $f(t)$, charge is explicitly dependent on $\partial_t f(t)$. This means that the Fourier component of $\hat{q}_{int}(t)$ oscillating at frequency ω_i (and thus the time-independent component of $\hat{H}_{int}(t)$)

picks up a factor of $\omega_i/\omega_d \ll 1$ compared to $\hat{\phi}_{int}(t)$. The opposite is true for capacitance modulation (for which the roles of q and ϕ are reversed in transformations $\hat{U}_3$ and $\hat{U}_4$), which explains why it achieves a much larger effective coupling for a charge based interaction.

2.7 Conclusions

We have studied a technique to coherently couple a superconducting circuit to the motional mode of a trapped ion by careful variation of the circuit's inductance. We describe a means of tuning the inductance (an external magnetic flux with a Josephson Junction) through an approximation mapping the circuit's non-linear Hamiltonian to that of a driven harmonic oscillator. Notwithstanding corrections to this approximation (as well as the technical challenges of trapping and optically addressing an ion near a Josephson junction) the mismatch between the inductive driving and capacitive interaction is the major reason why the resulting coupling strength is impractically small. We confirm this in a direct comparison with a capacitive modulation scheme for a specific driving strategy, though the general form of the coupling suggests our conclusions hold for a broader class of strategies as well. Indeed, equation (7.37) holds for any choice of drive parameters ω_d, η, and in fact can be applied more generally to any periodic modulation of inductance[1]. Conversely, our work suggests that for an inductive interaction (e.g. one based on

[1]Specifically, we may replace Mathieu's equation (2.27) with the more general Hill equation, $\partial_t^2 f + Q(t)f = 0$, where $Q(t)$ is any periodic function. The bare LC resonance frequency would then correspond to $\omega_0^2 = \frac{1}{\tau}\int_0^\tau Q(t)\mathrm{d}t$, where $Q(t+\tau) = Q(t)$.

mutual inductance between off-resonant circuits) an inductive modulation is the preferred approach.

2.8 Appendix – Linearization Procedure

The expression for $\hat{\phi}_{int}(t)$ allows us to evaluate the higher order corrections to the linearized Hamiltonian of equation (2.26). Since these corrections arise after the first two transformations ($(\hat{\phi},\hat{q}) \rightarrow (\hat{\phi}+\phi_c, \hat{q}+q_c)$), they can be expressed as $\hat{R}_{int}(t) = R(\hat{\phi}_{int}(t) - \phi_c)$. Using relations (2.20) and $E_J = \beta\tilde{\phi}_0^2/L$ we obtain

$$\begin{aligned}
\hat{R}_{int}(t) &= \sum_{k\geq 3} \tilde{\phi}_0^k V_q^{(k)}|_{\phi_c(t)} \tilde{\phi}_0^{-k} \left(\hat{\phi}_{int}(t) - \phi_c(t)\right)^k /k! \\
&= \frac{\tilde{\phi}_0^2}{L} \sum_{k\geq 3} \beta c_k(t) \left(\sqrt{\frac{\hbar}{2C_\Sigma W}} \frac{1}{\tilde{\phi}_0}\right)^k \left(\hat{a}f^* + \hat{a}^\dagger f\right)^k \frac{1}{k!} \\
&= \frac{\hbar}{LC_\Sigma W} \sum_{k\geq 3} \beta c_k(t) \gamma^{k-2} \left(\hat{a}f^* + \hat{a}^\dagger f\right)^k \frac{1}{k!},
\end{aligned}$$

where we have defined the characteristic flux parameter

$$\gamma \equiv \frac{1}{\tilde{\phi}_0}\sqrt{\frac{\hbar}{2C_\Sigma W}}. \tag{2.57}$$

Here $c_k(t) = E_J^{-1}\tilde{\phi}_0^k \frac{\partial^k V_q}{\partial \phi^k}|_{\phi=\phi_c}$ is defined according to equation (2.18), giving

$$\begin{aligned}
\beta c_3(t) &= \beta \sin(\phi_c(t)/\tilde{\phi}_0) &&= \sqrt{\beta^2 - \eta^2\cos^2(\omega_d t)} \\
\beta c_4(t) &= \beta \cos(\phi_c(t)/\tilde{\phi}_0) &&= \eta\cos(\omega_d t) \\
\beta c_k(t) &= -\beta\partial_x^k \cos(x)|_{x=\phi_c(t)/\tilde{\phi}_0} &&,
\end{aligned}$$

where we have used $\beta\cos(\phi_c(t)/\tilde{\phi}_0) = \eta\cos(\omega_d t)$.

To bound the error introduced by $\hat{R}_{int}(t)$ we begin by considering only the

$k = 3$ contribution. Using $\omega_0^2 = 1/LC_\Sigma$ this term can be written as

$$\hbar\omega_0 \frac{\omega_0}{W} \frac{\gamma\beta}{3!} \sqrt{1 - (\eta/\beta)^2 \cos^2(\omega_d t)} \left(\hat{a} f^* + \hat{a}^\dagger f\right)^3 . \tag{2.58}$$

To analyze this term under the rotating wave approximation, we note that our coupling scheme is premised on giving f a Fourier component matching the ion motional frequency, ω_i. Specifically, in the driving scheme described in the text, the parameters $\omega_d \approx \omega_0 - \omega_i$ and $\eta < \beta \ll 1$ are chosen such that f has the form

$$f(t) = e^{i(\omega_d + \omega_i)t} \left(1 + \frac{\eta}{2}\left(e^{i\omega_d t}/3 - e^{-i\omega_d t}\right) + ...\right) , \tag{2.59}$$

where all other terms are of order $O(\eta^2)$ and correspond to frequencies $n\omega_d$ ($|n| \geq 2$). Thus the only slowly rotating term in equation (2.58) is of order $\hbar\omega_0\gamma\eta$ (since $W \approx \omega_0$ for these parameters) and rotates at frequency ω_i. This slowly rotating part is the main contribution of (2.58) for evolutions over a time scale $\sim 1/\omega_i$, and we may compute its effective size over this timescale by using a second-order Magnus expansion [125, 126],

$$\hat{R}_{int}(t) \sim \hbar\omega_i \left(\gamma\beta\frac{\omega_0}{\omega_i}\right)^2 . \tag{2.60}$$

Using a similar procedure, we can derive analogous estimates for the higher ($k > 3$) order terms as well. But because these terms pick up extra factors of γ, equation (2.60) represents the overall scaling of all higher order terms. This is true when the scale of $|f|$ is on the order of ~ 1 (as in Fig. 2.4), the characteristic flux is small ($\gamma \lesssim 1$), and there are only small fluctuations above the classical solution, $\langle \hat{a}^\dagger \hat{a} \rangle \sim 1$.

One technique to reduce the effective size of corrections $\hat{R}_{int}(t)$ is to replace

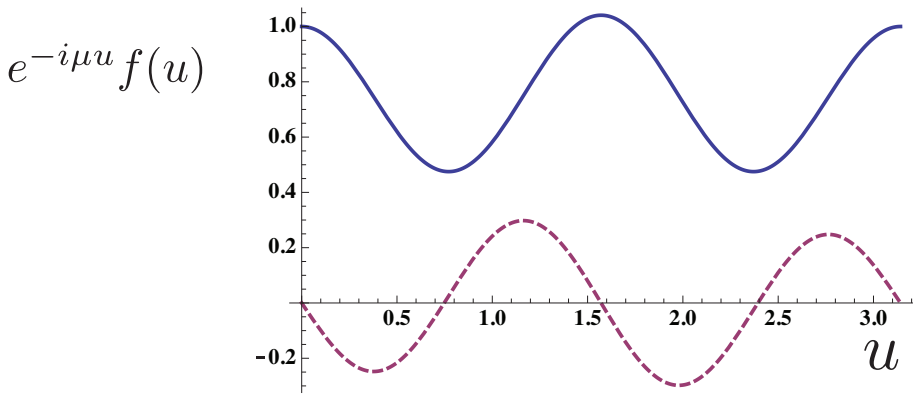

Figure 2.4: A plot of the periodic component of the characteristic function, $p(u) = e^{-i\mu u} f(u)$. The blue, solid line and red, dashed lines represent the real and imaginary parts of $p(u)$, respectively. Because the driving frequency $\omega_d = 0.999\,\omega_0$ is nearly resonant with the bare LC frequency, even a small driving amplitude $\eta = 0.06$ causes significant deviations from the undriven case (for which $\mu u = 2\pi\omega_0 t$ and $p(u) = 1$).

the single Josephson junction with a linear array of these elements. In the simplest approximation [127], using a stack of N junctions we get that the Josephson Hamiltonian contribution is transformed as

$$-E_J \cos\left(\frac{\hat{\phi}}{\tilde{\phi}_0}\right) \rightarrow -NE_J \cos\left(\frac{\hat{\phi}}{N\tilde{\phi}_0}\right) \tag{2.61}$$

In terms of the parameters in the definition of $\hat{R}_{int}(t)$, this corresponds to the map $\beta \rightarrow \beta/N$, $\tilde{\phi}_0 \rightarrow N\tilde{\phi}_0$ (or equivalently $\gamma \rightarrow \gamma/N$). From equation (2.60), this rescales the leading order contribution of $\hat{R}_{int}(t)$ by a factor of $1/N^4$. For the resonance ratio $\omega_0/\omega_i = 1000$, an array of $N \sim 100$ junctions should suffice to limit the effect of all higher order corrections.

Chapter 3: Quantum interface between an electrical circuit and a single atom

As alluded to in the previous chapter, we develop a more successful scheme to bridge the divide between atomic systems and electronic devices, based on engineering a coupling between the motion of a single ion and the quantized electric field of a capacitively modulated circuit. Our method can be used to couple the internal state of an ion to the quantized circuit with the same speed as the internal-state coupling between two ions. All the well-known quantum information protocols linking ion internal and motional states can be converted to protocols between circuit photons and ion internal states. Our results enable quantum interfaces between solid state qubits, atomic qubits, and light, and lay the groundwork for a direct quantum connection between electrical and atomic metrology standards.

3.1 Introduction

Atomic systems are remarkably well suited to storage and processing of quantum information [128, 129]. However, their properties are tightly constrained by nature, causing difficulties in interfacing to other optical or electronic devices. On the other hand, quantum electronic circuits, such as superconducting interference

devices, may be easily engineered to the designer's specifications and are readily integrated with existing microelectronics [130]. The naturally existing couplings between a single atom and a single microwave photon in a superconducting circuit are too weak for practical coherent interfaces. The coupling has been estimated at tens of Hz [131], much smaller than the decoherence rate of $10^3\,\mathrm{s}^{-1}$. For trapped ions, the coupling between the electric dipole induced by ion motion and the electric field of the superconducting circuit can be much larger, on the order of several hundred kHz. Unfortunately, this coupling is far off resonance. Motional frequencies of trapped ions are limited to tens of MHz, while any superconducting circuit must maintain GHz operating frequencies to avoid thermal noise, even in the extreme cryogenic environment of a dilution refrigerator.

In this chapter, we propose a method to couple single trapped ions with microwave circuits, bridging the gap between the very different frequencies of ion motion and microwave photon by parametric modulation of the microwave frequency. The resulting coupling strength of $\sim 2\pi \times 60$ kHz is sufficient for high-fidelity coherent operations and similar to the strength of currently obtained ion-ion couplings [132, 133]. A simple model system illustrating the key concepts is shown in Fig. 3.1. Microwave photons reside in a superconducting LC circuit with natural frequency $\omega_{\mathrm{LC}} = 1/\sqrt{LC} \approx 1$ GHz. A single ion is confined within the capacitor C_s and can oscillate at the motional frequency $\omega_i \approx 10$ MHz. The circuit voltage across C_s generates an electric field that couples to the ion's motional electric dipole. Modulating the circuit capacitance by C_{mod} at a frequency ν causes the superconducting voltage to acquire sidebands at frequencies $\omega_{\mathrm{LC}} \pm \nu$. The coupling

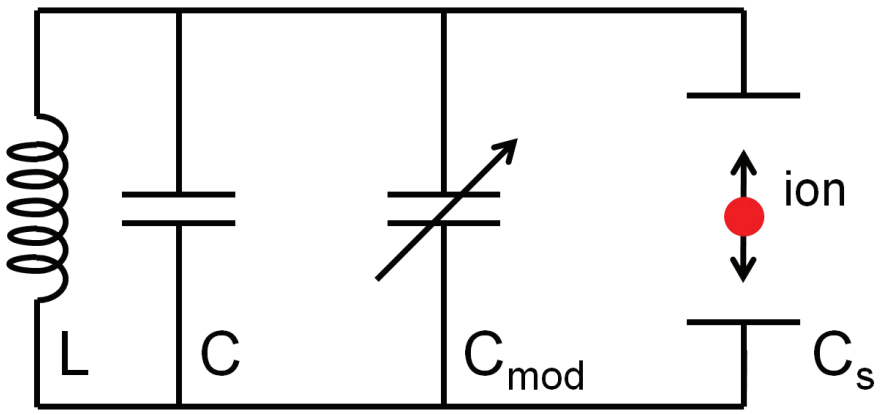

Figure 3.1: Equivalent-circuit model of scheme for ion-circuit coupling.

between the superconducting circuit and the ion motion becomes resonant when $\omega_i \approx \omega_{\mathrm{LC}} - \nu$. The interaction Hamiltonian is then

$$H_{\mathrm{int}} = \hbar g\, a b^{\dagger} + \mathrm{h.c.} \tag{3.1}$$

where a and b are the annihilation operators of the microwave photon mode and the ion motional mode, respectively. As shown below, $g \sim 2\pi \times 60$ kHz.

The coupling between the LC circuit and the ion motion allows us to generalize all the well-known protocols operating on ion spin and motion to protocols operating on ion spin and LC state. Ion spin-motion protocols based on laser [134] or microwave fields [135, 136] now allow for generation of nearly arbitrary spin/motion entangled states. If the capacitance modulation is switched on for a time $T = \pi/(2g)$, Eq. (3.1) shows that the mode operators evolve as $a(T) = -ib(0), b(T) = -ia(0)$, i.e., a perfect swap between LC and motional modes. For a unitary operator $U(b, \vec{\sigma})$ describing a protocol between the ion motion and the ion spin operator $\vec{\sigma}$, the sequence 1) swap LC/motion, 2) apply $U(b, \vec{\sigma})$, 3) swap LC/motion implements the same unitary $U(a, \vec{\sigma})$ between the LC and spin modes. By this means, one can es-

tablish a quantum communications channel between LC circuits in separate dewars, couple ion spins through a common LC circuit for large-scale quantum computing on a single chip, and perform Heisenberg-limited voltage metrology in the microwave domain by generating large Schrödinger cat states of the LC mode.

3.2 Realisation of ion-CQED coupling

Figure 3.2 shows a schematic of a device implementing the simple model described above. The device combines an ion trap, a microwave LC circuit, and a bulk-acoustic-wave (BAW) microelectromechanical modulator to coherently couple the quantized motion of trapped ions at MHz frequencies with microwave photons at 1 GHz. We now describe a specific design to give real-world parameters relevant to our system.

Ions are confined above a planar electrode structure of a type now widely used for microfabricated trap arrays [137]. Applying appropriate voltages to the electrodes generates RF electric fields, which provide a ponderomotive confining potential transverse to the trap axis, and DC fields that give rise to a harmonic potential along the axis. The ion trap parameters are taken to be typical for planar traps [138], with ions confined at height $h = 25\ \mu$m above the plane with an axial frequency ω_i of $2\pi\times1$ MHz. For the commonly used $^9Be^+$ ion, the harmonic oscillator length is then $z_0 = \sqrt{\hbar/(2m\omega_i)} = 24$ nm.

A superconducting inductor is attached to the island electrodes and a silicon bulk-acoustic-wave resonator (BAW) is mounted near the inductor (see the Supple-

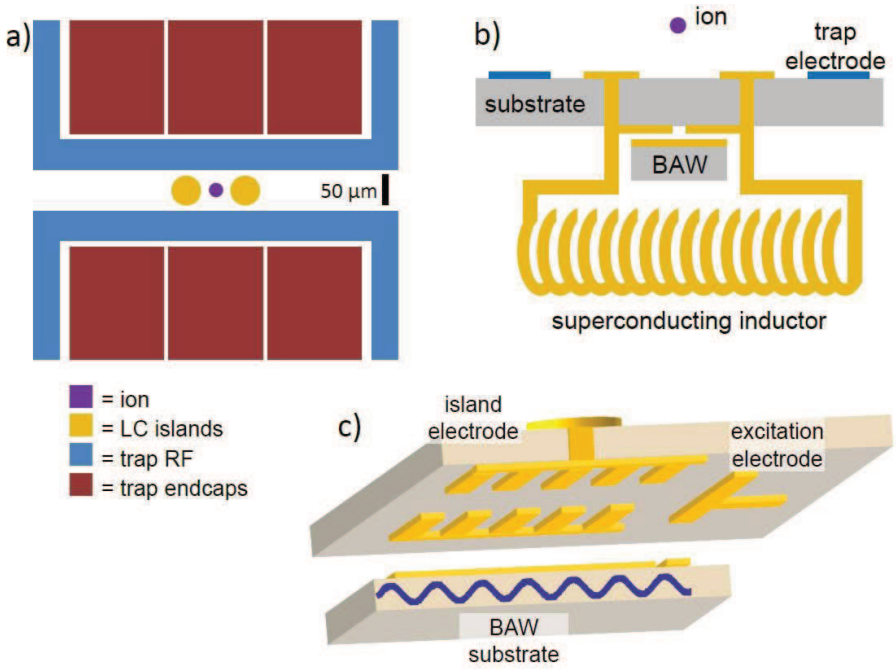

Figure 3.2: Schematic of a device for coupling trapped ions to a microwave resonant circuit. a) Top view of surface ion trap showing RF and DC trapping electrodes. The "LC island" electrodes couple the ion motion to the LC circuit excitation. b) Side view of device, showing ion trap, superconducting inductor, and BAW device. c) Exploded side view of BAW device. Purple line: transverse displacement of BAW substrate due to classical driving.

mental Material for technical details). The inductance of 440 nH, combined with the total static circuit capacitance of $C_0 = 46$ fF, then yields $\omega_{\mathrm{LC}} = 1$ GHz, with characteristic impedance of $Z = 2.7\,\mathrm{k}\Omega$. The zero-point charge fluctuation on the resonator is $q_0 = \sqrt{\hbar/(2Z)} = 0.9$ electrons.

The ion-circuit coupling is provided through two coplanar islands near the ion position that are each connected to a terminal of the superconducting inductor. The microwave electric field between these islands couples to the ion motion along the trap axis through the electric dipole of the moving ion charge. To activate the ion-circuit coupling, one excites acoustic waves in the BAW at frequency $\nu_B \approx \omega_{\mathrm{LC}} - \omega_i$ by voltage driving of metallic electrodes on the BAW surface. The modulation of the BAW-substrate gap distance provides the desired capacitance modulation.

The classical dipole interaction energy of the ion due to the axial electric field E_z from the island electrodes is

$$U_{\mathrm{cl}} = ezE_z = \frac{e\zeta}{h} z\, V = \frac{e\zeta}{hC} zQ \tag{3.2}$$

where h is the ion height, V is the voltage between the islands, ζ is a dimensionless constant of order unity set by the electrode geometry, C is the total circuit capacitance, and Q is the total charge on the circuit. Simulation of the electric field near the island electrodes gives $\zeta = 0.25$. The BAW drive modulates the capacitance as $C = C_0(1 + \eta \sin \nu t)$ with modulation depth $\eta = 0.3$, so that

$$U_{\mathrm{cl}}(Q, z, t) = \frac{e\zeta}{hC}(1 - \eta \sin \nu t) zQ \tag{3.3}$$

We now quantize the LC and ion motion, but keep the BAW motion classical. In the rotating frame with respect to LC and motion, the total Hamiltonian of

the ion-LC system becomes (for details of the calculation, see the Supplemental Material)

$$H_{\rm int}/\hbar = \frac{2ig_0\eta}{3} e^{-i\Delta t} ab^\dagger + \text{h.c.} \tag{3.4}$$

where $g_0 = e\zeta z_0 q_0/(hC_0)$ and $\Delta \equiv \nu - (\omega_{\rm LC} - \omega_i)$. For the numerical parameters given above, $g_0 = 2\pi \times 200$ kHz and $\eta = 0.3$, giving $g = 2\pi \times 60$ kHz.

Because the BAW is only used as a parametric drive in our scheme, it contributes negligible noise to the LC and motional modes. To first order, the only semiclassical effect of the BAW is variation in the coupling parameter η between the ion motion and the LC–there is no direct (linear) coupling between the motion of the BAW and these other two variables. Hence parametric heating is the main source of noise added by the BAW. While thermal motion of the BAW can in principle produce parametric heating, in most practical settings errors in η will be determined by classical control errors in setting the BAW amplitude.

The chief quantum noise contribution of the BAW arises from the entanglement induced by the LC and ion systems with the BAW and, indirectly, its environment. This entanglement occurs via the parametric coupling, and manifests as a static displacement of the BAW that depends on LC photon number n_{LC}. The displacement can be estimated as

$$\zeta_{\rm LC} \sim \frac{x_B}{\zeta_0} \frac{n_{\rm LC}\omega_{\rm LC}}{\omega_{\rm LC} - \nu + i\kappa_B/2} \tag{3.5}$$

where x_B is the harmonic oscillator length of the BAW and κ_B is the BAW damping rate. For typical BAW parameters at $\nu \sim 1$ GHz, one finds $x_B \sim 10^{-16}$ m and $\kappa_B \sim 100$ kHz, so that $\zeta_{\rm LC}/\zeta_0 \lesssim 10^{-3}$ even for $n_{\rm LC} \sim 100$. Hence the BAW

contributes negligible quantum noise for our purposes.

3.3 LC/spin protocols

LC/spin protocols can be executed by the swapping method with fidelity well over 95%. Q as high as 5×10^5 have been reported for an LC circuit [139], giving a decoherence rate of 2 ms^{-1}. Motional decoherence rates of 0.5 s^{-1} have been demonstrated in a cryogenically cooled ion trap with an ion height of 150 μm and 1 MHZ motional frequency [140]. This rate scales as $\sim 1/d^4$ [141], so at our 25 μm height, we estimate a rate of 0.5 ms^{-1}. Spin decoherence is negligible on these timescales [134]. Hence the overall decoherence rate is 2.5 ms^{-1}, limited by LC damping. The total spin/LC operation requires two LC/motion swaps, each taking 3 μs, and the spin/motion protocol, with typical Rabi frequency $\Omega_0 \sim 2\pi \times 100$ kHz [134]. A typical spin/motion protocol requires approximately a $\pi/2$-pulse time, so the total time required for the LC/spin protocol is 10 μs. The infidelity is given by the ratio of decoherence rate to operation rate, i.e., 0.03.

Quantum interfaces between LC and spin can be achieved through a Jaynes-Cummings spin/motion interaction [134]. If the LC mode is regarded as the microwave analog of a linear-optical qubit, this interaction serves as a quantum logic interface between ion spin and single-rail microwave photon qubits. A $\pi/2$ pulse of the interaction performs an LC/spin CNOT gate.

An alternative LC-spin quantum interface swaps spin-dependent displacement of the ion motion into the LC mode. The unitary evolution for such a protocol is

given by

$$U_{\text{eff}}(\alpha) = \exp\left[(\alpha a + \alpha^* a^\dagger)\sigma_x\right] \tag{3.6}$$

Such an operation could be used to teleport a superposition of spin states into a superposition of coherent LC states.

These interactions allow us to use the LC and ion modes as quantum buses for more complex tasks. The Jaynes-Cummings LC/spin interaction enables quantum communication between LC circuits in independent cryogenic environments, as shown in Figure 3.3(a). Each ion interface is controllably coupled to a high-finesse optical resonator. After LC/spin coupling, the spin is mapped to the polarisation state of an outgoing optical photon, as in recent experiments [142]. Overall, this set of operations coherently couples the microwave photon state to the optical domain. In particular, one could entangle independent superconducting qubits via conditional photon measurements [143]. This task is impossible using direct microwave signaling, owing to the thermal noise of microwave links at room temperature.

The spin-dependent LC displacement also lets one perform nonlocal ion spin-spin gates on a single chip through a shared LC mode (Fig 3.3(b)). The spin-spin bus is based on the spin-dependent displacement operation $D(\alpha q \sigma_y)$. Two ions (with identical phonon frequencies) in multiple traps are capacitively coupled to the LC circuit. Performing four spin-dependent displacements that enclose a square in phase space with side length $L = \alpha J_z$, one picks up a phase of $2|L|^2 = 4|\alpha|^2(1 + \sigma_z^{(1)}\sigma_z^{(2)})$, which is the desired spin-spin interaction [144]. Along with single qubit gates, this

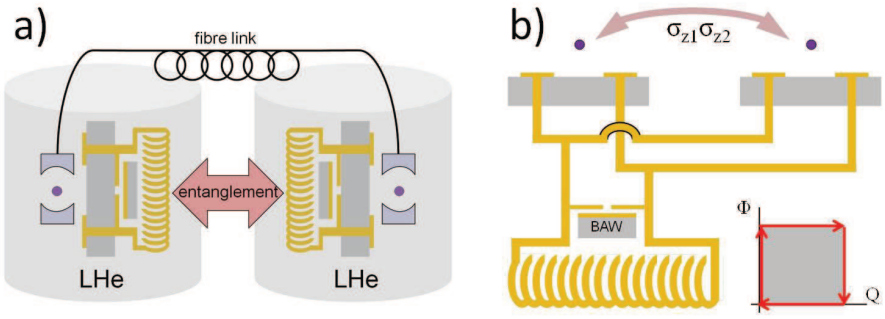

Figure 3.3: Quantum buses enabled by LC/motion coupling. a) Quantum communication between LC circuits in independent cryogenic environments. b) Nonlocal ion spin-spin gates on a single chip.

interaction provides a sufficient gate set for universal quantum computation [145].

Spin-dependent displacement of the LC causes a superposition of spin states to evolve into a superposition of LC coherent states. Such superposed coherent states can detect field displacements with Heisenberg-limited sensitivity [146]. In the present context, these states enable Heisenberg-limited metrology of small voltages at microwave frequencies. The mean photon number in the generated state can exceed 100 for our parameters. The RMS voltage is then $\sim$ 0.1 mV and can be estimated at sub-μV precision in a single shot.

3.4 Resistance to motional heating

Rapid technical advances in superconducting circuits mean that the LC coherence time may substantially increase in the near future, leaving ion motional heating as the primary source of decoherence. We have developed a modified LC/spin cou-

pling scheme similar to [144, 147] that resists ion heating. We simultaneously apply bichromatic LC/motion and motion/spin couplings at detunings $\pm\delta$ from the blue-sideband and red-sideband resonances. In the frame rotating with ion motion, the Hamiltonian becomes

$$H_{\rm int}/\hbar = \sqrt{2}M\left(x\cos\delta t + p\sin\delta t\right)) \tag{3.7}$$

$$M \equiv \frac{2i\eta g_0}{3}q + \frac{\Omega_0}{4}\sigma_x \tag{3.8}$$

where $x = (b + b^\dagger)/\sqrt{2}$, $p = -i(b - b^\dagger)/\sqrt{2}$ are dimensionless motional operators, $q = (a + a^\dagger)/\sqrt{2}$ is the dimensionless charge operator, and we approximate $\Omega_0 \ll \delta \ll \omega_i$. The Hamiltonian (3.7) is identical to that of [148], except that the collective spin operator J_y is replaced by the collective spin-LC operator M. The ion motional state undergoes M-dependent phase-space displacement along a closed trajectory, giving rise to an M^2 dependent geometric phase. At times $t_n = 2\pi n/|\delta|$ with n an integer, the evolution operator becomes simply

$$U_n = \exp\left[-i\,\mathrm{sign}(\delta)\frac{2\pi n}{\delta^2}M^2\right] \tag{3.9}$$

The undesired q^2 term in Eq. (3.9) can be removed by a spin echo sequence $ZU_n^\dagger ZU_n$, where $Z = e^{-i\pi\sigma_z}$ is a fast π-pulse of the spin, and $U^\dagger$ is obtained by changing $\delta \to -\delta$. The overall time evolution is then $\exp(\alpha q\sigma_x)$ with $\alpha = -4i\pi n g_0\Omega_0\eta/(3\delta^2)$.

A straightforward modification of the arguments of Sørensen and Mølmer [148] shows that this coupling can be made arbitrarily resistant to ion motional heating. The loss of fidelity due to heating is $\propto 1/\delta^2$ in the limit of low infidelity, while the effective coupling constant is $\propto 1/\delta$. Even if the heating rate is larger than the coupling constant, one can still achieve near-perfect coupling.

3.5 Outlook

Our ion-circuit coupling enables a powerful hybrid quantum system with operation speeds similar to those for ion spins. This system can perform nonlocal quantum gates between ions on a single chip, nonlocal quantum communication between electrical circuits, and Heisenberg-limited voltage metrology. The coupling can be made resistant to ion motional heating. Implementing our proposal will present new challenges arising from the need to isolate these systems from the devices used to manipulate them. For example, errors may arise when stray fields from the BAW drive displacing the ion's motion, or from circuit heating through interactions with trap electrodes and light used to address the ion. Despite these issues, we believe that current experiments in classical ion-circuit coupling [135,136] can be extended in a natural way to realise our scheme.

Chapter 4: A universal test for entangling dynamics

Interactions between particles, typically called forces, lead to the emergence of correlated dynamics. Seen from an information theoretic perspective, we infer that interactions are primarily a means of communication. Here we present a method of confirming that a given, continuous interaction actually provides a means of quantum communication. More specifically, we show that for a system with linear couplings between canonical variables of two separated subsystems, disallowing the quantum communication necessary to produce distillable entanglement leads to excess noise in the subsystems' conjugate variables. Analogously to Bell's inequality for quantum states, this gives a straightforward, local test verifying the capacity for an interaction to entangle systems. We conclude with a simple experimental proposal demonstrating these ideas.

4.1 Introduction

Entanglement is an ubiquitous phenomenon in modern quantum mechanics arising from interactions between quantum systems [2]. While a complete understanding of entanglement and its characterization remains elusive in experimental settings [149–151], the crucial insight of Bell [71] provides the current "gold stan-

dard" for testing the existence of entanglement between separated systems. This has developed into the general class of entanglement witnesses [72, 152, 153], from which physical approaches to quantum information have validated their quantum performance [154–156]. However, in practice the increasing complexity of quantum information experiments – particularly going to large numbers of qubits – makes validation more difficult [77,157,158], and one is forced to ask if the character of the interactions may instead be probed. For example, one might attempt to bound the quantum channel capacity [45, 73, 74] of interactions between two systems directly rather than verify the entanglement produced by the channel. While we do not have a general solution to this problem, a subcase of interest – Gaussian channels – may admit a path forward [159, 160].

In this chapter we propose an inequality for interacting open quantum systems whose violation indicates the interaction between these systems distillably entangles them. This effectively verifies that the interaction has an effective, non-zero quantum channel capacity, i.e., that it can be used in conjunction with distillation protocols to coherently transmit quantum information [41, 44, 74]. Analogously to Bell's inequality, assuming the interaction correlates but does *not* entangle distant subsystems leads to local, observable consequences. Thus, as a substitute for Bell's inequality violation experiments, one can verify entanglement generation with a two step approach: first, measure the linear response as a "witness" of the interaction strength; second, measure the corresponding noise and compare to the rate of information transfer suggested by the witness. This enables a noise-based test of entanglement generation which may be easier to confirm in laboratory settings and

in scenarios where a detailed physical model of the interaction remains unknown.

4.2 Main result

Consider an open quantum system comprised of two (infinite dimensional) subsystems, $\mathcal{A}$ and $\mathcal{B}$. Assume that they evolve under a Hamiltonian $\hat{H}_{loc}$, which contains only local terms that are quadratic in canonical variables. Define $\hat{A}$ and $\hat{B}$ as canonical variables acting on subsystems $\mathcal{A}$ and $\mathcal{B}$, meaning that they have conjugate variables $\hat{A}_c$ and $\hat{B}_c$ satisfying $[\hat{A}, \hat{A}_c] = [\hat{B}, \hat{B}_c] = i$ (for simplicity we set $\hbar = 1$ and assume that $\hat{A}$ and $\hat{B}$ are both dimensionless). Now add an interaction between the two systems, with the following witness:

$$\partial_t \langle \hat{A}_c \rangle_I = \frac{1}{2}(2\eta - \xi)\langle \hat{B} \rangle_I \text{ and } \partial_t \langle \hat{B}_c \rangle_I = \frac{1}{2}(2\eta + \xi)\langle \hat{A} \rangle_I \,, \tag{4.1}$$

where $\langle \hat{O} \rangle_I$ represents an average in the interaction picture with respect to $\hat{H}_{loc}$. For $\xi = 0$, this witness to the coupling strength can be interpreted as a statement of Ehrenfest's theorem [161] and is satisfied by simple addition of $\hat{V} = \eta \hat{A}\hat{B}$ to the Hamiltonian. However, it is generically compatible with any dissipative component that is both Markovian and quadratic in variables $\hat{A}$ and $\hat{B}$. Expressed in the Heisenberg picture, we therefore consider the equation

$$\partial_t \hat{O} = \mathcal{L}(\hat{O}) = i[\hat{H}_{loc} + \eta \hat{A}\hat{B}, \hat{O}] + \mathcal{D}(\hat{O}) \,, \tag{4.2}$$

where

$$\mathcal{D}(\hat{O}) = i\frac{\xi}{2}(\hat{A}\hat{O}\hat{B} - \hat{B}\hat{O}\hat{A}) + \\ -\frac{1}{4}\Big(Y_{xx}[\hat{A},[\hat{A},\hat{O}]] + Y_{pp}[\hat{B},[\hat{B},\hat{O}]] \\ +2Y_{xp}[\hat{A},[\hat{B},\hat{O}]]\Big)\ . \tag{4.3}$$

As discussed in the appendix, this is the most general (quadratic and Markovian) time-homogeneous dynamical equation that satisfies equation (4.1). In contrast to the first term of equation (4.2), corresponding to unitary evolution, $\mathcal{D}$ is an adjoint superoperator representing irreversible information exchange with the environment [162].

Defining Δ_n as the n component symplectic matrix

$$\Delta_n = \bigoplus_{i=1}^{n} \begin{pmatrix} 0 & 1 \\ -1 & 0 \end{pmatrix}_i , \tag{4.4}$$

and Y as the matrix composed of the parameters Y_{uv} defining $\mathcal{D}$ in equation (4.3), we can state the main result of this work:

Theorem: *For Gaussian states evolving under generator $\mathcal{L}$ of equation* (4.2)*, if $Y - 2i\eta\Delta_1$ is positive semi-definite, then non-zero distillable entanglement never develops between $\mathcal{A}$ and $\mathcal{B}$. Conversely, let $|\psi_a\rangle\otimes|\psi_b\rangle$ denote the (separable, Gaussian) ground state of $\hat{H}_{loc}$. If $Y - 2i\eta\Delta_1$ has a negative eigenvalue, then after some $t > 0$ the initial state $|\psi_a\rangle \otimes |\psi_b\rangle$ is mapped to a state with finite distillable entanglement.*

The full proof of the theorem is given in the appendix, though we summarize it here. We first assume that $\mathcal{A}$ and $\mathcal{B}$ are Gaussian states of single harmonic oscillators (described below). Defining the vector $M = [\hat{x}_a, \hat{p}_a, \hat{x}_b, \hat{p}_b]^T$ from the (dimensionless)

canonical variables of $\mathcal{A}$ and $\mathcal{B}$, we consider the covariance matrix of the system,

$$\gamma_{ij} = \langle \hat{M}_i \hat{M}_j + \hat{M}_j \hat{M}_i \rangle - 2\langle \hat{M}_i \rangle \langle \hat{M}_j \rangle \,. \tag{4.5}$$

Up to a displacement of the means $m_i = \langle \hat{M}_i \rangle$, this matrix uniquely defines the 2-mode Gaussian states (i.e. the states whose characteristic function is of the form $\langle \exp(iz^T M) \rangle \propto \exp(iz^T m - \frac{1}{4} z^T \gamma z)$) [159, 163]. We note that since it is quadratic in canonical variables, the generator $\mathcal{L}$ of (4.2) necessarily maps Gaussian states to Gaussian states [164]. It therefore suffices to consider the evolution of m and γ alone. We then use the fact that a bipartite Gaussian state is not distillably entangled if and only if its partial time reverse is also a valid state [165, 166]. That is, if we set $\hat{p}_b \to -\hat{p}_b$ in the definition of γ above, the resulting characteristic function corresponds to a valid Gaussian state. Solving directly for the evolution of γ we show that this is true for all initial γ, as long as $Y - 2i\eta\Delta_1$ is positive semi-definite. Conversely, if this matrix has a negative eigenvalue, then we let γ initially correspond to the separable ground state of $\hat{H}_{loc}$ (which is Gaussian as $\hat{H}_{loc}$ is quadratic). After time $t > 0$ sufficiently small, we show that the partial time reverse of this state violates the uncertainty principle [167–169]. Since the time evolved state is no longer valid under partial time reversal, it is distillably entangled [166].

This result characterizes when distillable entanglement (i.e., entanglement useful in quantum teleportation protocols [45,170]) can emerge between Gaussian states of $\mathcal{A}$ and $\mathcal{B}$. Our theorem will allow us to define a direct test of the effective quantum channel capacity of the interaction arising from $\mathcal{L}$. Specifically, it will allow us

to verify if, for finite times $t > 0$, the map $e^{t\mathcal{L}}$ could be used in conjunction with a distillation protocol [171, 172] to transmit quantum information between separate parties controlling each subsystem.

To motivate our test, we notice that the matrix $Y - 2i\eta\Delta_1$ can be understood heuristically as a comparison between the observed witness parameters and the decoherence caused by the dissipator $\mathcal{D}$. Accordingly, we define the 'witness' dynamics of an operator $\hat{O}$ as

$$\begin{aligned}\mathcal{L}_w(\hat{O}) = i[\hat{H}_{loc} + \eta\hat{A}\hat{B}, \hat{O}] \\ + i\frac{\xi}{2}\left(\hat{A}\hat{O}\hat{B} - \hat{B}\hat{O}\hat{A}\right) .\end{aligned} \tag{4.6}$$

Strictly speaking, the generator $\mathcal{L}_w$ cannot be written in Lindblad form [173] and does not generate a completely positive time evolution [164]. Indeed, the effect of the term proportional to ξ is to cause an apparent violation of Newton's third law. Even so, the dynamics generated by $\mathcal{L}_w$ agree with $\mathcal{L}$ for any canonical variable $\hat{O}$, and it is exactly the component of $\mathcal{L}$ which determines the evolution of $\langle\hat{O}\rangle$.

Our test compares the observed noise in the canonical variables to the noise predicted by $\mathcal{L}_w$. Specifically, we define the excess noise rate of an observable $\hat{O}$ as

$$N(\hat{O}, t) = \partial_t \left(\mathrm{Var}\left(e^{t\mathcal{L}}(\hat{O})\right) - \mathrm{Var}\left(e^{t\mathcal{L}_w}(\hat{O})\right)\right) , \tag{4.7}$$

where $e^{t\mathcal{L}}(\hat{O})$ defines the propagation of $\hat{O}$ for time t under generator $\mathcal{L}$ and $\mathrm{Var}(\hat{O}) = \langle\hat{O}^2\rangle - \langle\hat{O}\rangle^2$ is the variance in $\hat{O}$. Using the theorem we can bound the amount of excess noise added to the systems in order to prevent distillable entanglement from emerging. More specifically,

Corollary: *Let $\mathcal{A}$ and $\mathcal{B}$ evolve under $\mathcal{L}$ of equation* (4.2). *Assume that Gaussian*

states of these systems cannot become distillably entangled. Then for any state of $\mathcal{A}$ *and* $\mathcal{B}$*, the excess noise rate in the conjugate variables* $\hat{A}_c$ *and* $\hat{B}_c$ *should exceed twice their coupling strength* η*. That is, at all times* t*,*

$$N(\hat{A}_c, t) + N(\hat{B}_c, t) \geq 2|\eta|\,. \tag{4.8}$$

Hence if this bound does not hold, then the (separable) ground state of $\hat{H}_{loc}$ *becomes distillably entangled at some later time.*

From the corollary we can derive a local test of the ability of an interaction to entangle distant objects. First, observers of $\mathcal{A}$ and $\mathcal{B}$ monitor the first moments of their canonical variables, establishing a witness to the parameters of the interacting Hamiltonian $\hat{H}_{loc} + \eta\hat{A}\hat{B}$ and the parameter ξ, which completely characterize the witness generator $\mathcal{L}_w$. This can be inferred directly from the full equations of motion, for if $\hat{A}'$ and $\hat{B}'$ represent canonical variables for $\mathcal{A}$ and $\mathcal{B}$, respectively,

$$\begin{aligned} \partial_t \langle e^{t\mathcal{L}} \hat{A}' \rangle &= \langle e^{t\mathcal{L}} \left(i[\hat{H}_{loc} + (\eta - \frac{\xi}{2})\hat{A}\hat{B}, \hat{A}'] \right) \rangle \\ \partial_t \langle e^{t\mathcal{L}} \hat{B}' \rangle &= \langle e^{t\mathcal{L}} \left(i[\hat{H}_{loc} + (\eta + \frac{\xi}{2})\hat{A}\hat{B}, \hat{B}'] \right) \rangle\,. \end{aligned} \tag{4.9}$$

(Since $\hat{H}_{loc}$ is quadratic, the output of the commutators is a sum of canonical variables.) Observers then monitor the variance in $\hat{A}_c$ and $\hat{B}_c$ and compare to the predictions of the witness variables determined above. If the excess noise rate is less than $2|\eta|$, they may immediately conclude that the interaction can distillably entangle $\mathcal{A}$ and $\mathcal{B}$.

The corollary follows directly from the theorem. Let $\hat{O}$ be any canonical variable. First notice that since every term of $\mathcal{L}$ is quadratic in canonical variables,

$\mathcal{L}^k(\hat{O})$ is also a canonical variable for every $k \geq 0$ [1]. Further, $(\mathcal{L} - \mathcal{L}_w)(\hat{O})$ vanishes since it involves only double commutators. We conclude then that $\mathcal{L}^k(\hat{O}) = \mathcal{L}_w^k(\hat{O})$ for every $k \geq 0$ and therefore $e^{t\mathcal{L}}(\hat{O}) = e^{t\mathcal{L}_w}(\hat{O})$. Similarly, for any pair of canonical variables $\hat{O}$ and $\hat{O}'$, $\mathcal{L}(\hat{O}\hat{O}')$ is quadratic in canonical variables, and $(\mathcal{L}-\mathcal{L}_w)(\hat{O}\hat{O}')$ is proportional to the identity operator $\hat{I}$. Since $\mathcal{L}(\hat{I}) = (\mathcal{L}-\mathcal{L}_w)(\hat{I}) = 0$, by expanding the Taylor series for $e^{t\mathcal{L}}$ we conclude that $e^{t\mathcal{L}}(\hat{O}\hat{O}') = \left(e^{t\mathcal{L}_w} + t(\mathcal{L} - \mathcal{L}_w)\right)(\hat{O}\hat{O}')$. Combining these facts with the definition of $N(\hat{O}, t)$ in equation (4.7), the left hand side of (4.8) simplifies to $\langle(\mathcal{L}-\mathcal{L}_w)(\hat{A}_c^2+\hat{B}_c^2)\rangle$. Defining the vectors $z_\pm = \frac{1}{\sqrt{2}}[1, \pm i]^T$, from equation (4.3) we see that this quantity is equal to $\frac{1}{2}(Y_{xx} + Y_{pp}) = z_\pm^\dagger Y z_\pm$. We get the desired lower bound by noting that the no entanglement condition of the theorem implies that $z_\pm^\dagger Y z_\pm \geq 2i\eta(z_\pm^\dagger \Delta_1 z_\pm) = \pm 2\eta$.

4.3 Circuit model for long-range interactions

To describe a physical context for our result and motivate the theorem and its corollary, we present a toy model inspired by phonon-mediated spin-spin interactions in ion traps [99, 174]. This will serve as a conceptual aid and provide a clue as to when entanglement can emerge. To mediate the non-local interaction between $\mathcal{A}$ and $\mathcal{B}$, we introduce an ancillary harmonic oscillator $\mathcal{F}$, analogous to the phonon in ion trap systems. Our goal is to derive a linear generator of time evolution, $\mathcal{L}$, that corresponds to the witness dynamics of equation (4.1).

Within our model, the dynamics of $\mathcal{A}$ and $\mathcal{B}$ arise as the limiting process of

[1] The notation $\mathcal{L}^k = \mathcal{L} \circ \mathcal{L} \ldots \circ \mathcal{L}$ denotes a k-fold composition of the superoperator $\mathcal{L}$

n applications of a quantum circuit, involving only $\mathcal{A}-\mathcal{F}$ and $\mathcal{B}-\mathcal{F}$ interactions. In the limit $n\to\infty$, the systems are propagated a time t by setting the effective individual circuit time as t/n. The ancilla $\mathcal{F}$ interacts individually with each system through the chain of unitary evolutions [174],

$$e^{i\sqrt{t/n}\hat{B}\hat{p}}e^{i\sqrt{t/n}\hat{A}\hat{x}}e^{-i\sqrt{t/n}\hat{B}\hat{p}}e^{-i\sqrt{t/n}\hat{A}\hat{x}}=e^{-it\hat{A}\hat{B}/n}\,, \tag{4.10}$$

where $\hat{x}$ and $\hat{p}$ are canonical variables of $\mathcal{F}$ satisfying $[\hat{x},\hat{p}]=i$. We can heuristically picture the ancilla as traveling between $\mathcal{A}$ and $\mathcal{B}$ to produce the effective interaction of a Hamiltonian $\hat{A}\hat{B}$. Following this by the local unitary $e^{-it(\hat{H}_a+\hat{H}_b)/n}$ completes the evolution for a circuit of time t/n. In the large n limit, by the Trotter formula we obtain

$$\lim_{n\to\infty}\left(e^{-i\hat{A}\hat{B}t/n}e^{-it\hat{H}_a+\hat{H}_b/n}\right)^n=\exp(-it(\hat{H}_a+\hat{H}_b+\hat{A}\hat{B}))\,. \tag{4.11}$$

This corresponds to a witness in equation (4.1) with $\eta=1,\xi=0$. This effective interaction is the underlying mechanism describing geometric phase gates [99, 174, 175].

While the unitary above produces the desired witness dynamics, to account for the more general $\mathcal{L}$ we add a 'screen' operation acting on the ancilla. This screen behaves like a measurement in the middle of the circuit, whose strength determines whether the ancilla is able to entangle $\mathcal{A}$ and $\mathcal{B}$. Letting $\mathcal{S}$ be the unital, completely positive map [176] representing the screen's action, the true circuit evolution (Fig. 4.1) is described by the superoperator,

$$\mathcal{V}_t=\mathcal{C}_{\hat{H}_a+\hat{H}_bt}\,\mathcal{C}_{\hat{A}\hat{x}\sqrt{t}}\,\mathcal{C}_{\hat{B}\hat{p}\sqrt{t}}\,\mathcal{S}\,\mathcal{C}_{-\hat{A}\hat{x}\sqrt{t}}\,\mathcal{C}_{-\hat{B}\hat{p}\sqrt{t}}\,, \tag{4.12}$$

where $\mathcal{C}_{\hat{X}}(\hat{O}) = e^{i\hat{X}}\hat{O}e^{-i\hat{X}}$ are superoperators associated with unitary evolution and the products above denote composition. Note that we are working in the Heisenberg picture, so $\mathcal{V}_t$ acts on operators representing observables of the composite system. As expected, when $\mathcal{S}$ is the identity, the Trotter limit is just $\mathcal{C}_{\hat{(}\hat{H}_a+\hat{H}_b+\hat{A}\hat{B})t}$.

The superoperator of equation (4.12) acts non-trivially on the ancilla, and hence cannot determine the dynamics of $\mathcal{A}$ and $\mathcal{B}$ alone. To do this we take the Markovian limit, i.e. we suppose that the ancilla starts in the same density matrix, $\hat{\rho}_f$, between each time step. This is equivalent to saying that the ancilla has no "memory" of its interactions with $\mathcal{A}$ and $\mathcal{B}$, and that it is drawn out of a large reservoir of identical systems. We can then trace out the ancilla, yielding the reduced circuit propagator,

$$\mathcal{V}_t^{red}(\hat{O}_{ab}) = \mathrm{tr}_f \left\{ \mathbb{I}_{ab} \otimes \hat{\rho}_f \mathcal{V}_t(\hat{O}_{ab} \otimes \mathbb{I}_f) \right\} . \tag{4.13}$$

Finally, we take the take the Trotter limit to produce the true time evolution superoperator,

$$e^{t\mathcal{L}} = \lim_{n\to\infty} \left(\mathcal{V}_{t/n}^{red}\right)^n , \tag{4.14}$$

with corresponding generator [173],

$$\mathcal{L} \equiv \partial_t(\mathcal{V}_t^{red})|_{t=0} . \tag{4.15}$$

As we shall see below, the generator $\mathcal{L}$ produces the expected dynamics of equation (4.2).

Before verifying the form of $\mathcal{L}$, we first derive a necessary property of the screen $\mathcal{S}$ based on the requirement that the limit (4.14) converges. This is equivalent to

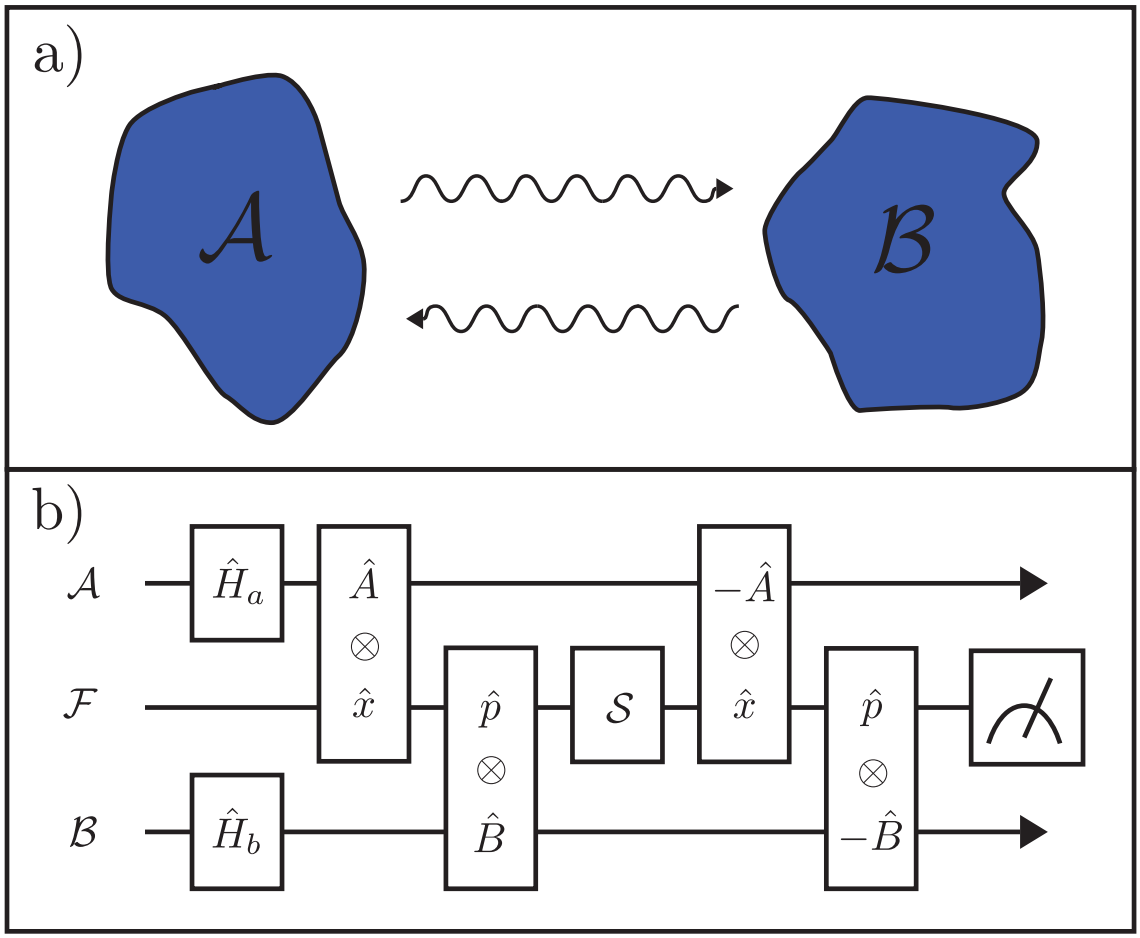

Figure 4.1: **a)** Heuristic diagram representing non-local interaction between distinct quantum subsystems. **b)** Quantum circuit schematic simulating the witness equations (4.1). The local unitaries $\hat{U}_a = \exp(-it\hat{H}_a)$ and $\hat{U}_b = \exp(-it\hat{H}_b)$ account for local Hamiltonian evolution, while the ancilla couplings $\hat{U}_A = \exp(-i\sqrt{t}\hat{A}\hat{x})$, $\hat{U}_B = \exp(-i\sqrt{t}\hat{B}\hat{p})$ produce the effective interaction between $\mathcal{A}$ and $\mathcal{B}$. The decoherence caused by the screen $\mathcal{S}$ can prevent entanglement between $\mathcal{A}$ and $\mathcal{B}$ while still allowing classical correlations to emerge.

assuming that the terms of order $\sqrt{t}$ in the Taylor expansion of $\mathcal{V}_t^{red}$ vanish. To see when this is the case, we use the Baker-Campbell-Hausdorff formula,

$$e^{i\hat{X}}\hat{O}e^{-i\hat{X}} = \hat{O} + \frac{1}{1!}[i\hat{X}, \hat{O}] + \frac{1}{2!}[i\hat{X}, [i\hat{X}, \hat{O}]] + ... \tag{4.16}$$

Substituting into equations (4.12) and (4.13), we see (in the appendix) that the $\sqrt{t}$ terms vanish if and only if $\mathcal{S}$ preserves the mean quadratures of the ancilla,

$$\langle \mathcal{S}(\hat{x}) - \hat{x} \rangle_f = \langle \mathcal{S}(\hat{p}) - \hat{p} \rangle_f = 0\,, \tag{4.17}$$

where $\langle \hat{O} \rangle_f = \mathrm{tr}\{\hat{\rho}_f \hat{O}\}$. Given equation (4.17) holds, we may directly verify that the Trotter limit generator of equation (4.15) matches the dynamics of equation (4.2). We defer this calculation to the appendix, but note that it results from the BCH formula (4.16) and the Jacobi identity $[\hat{X}\hat{Y}, \hat{Z}] = \hat{X}[\hat{Y}, \hat{Z}] + [\hat{X}, \hat{Z}]\hat{Y}$.

The action of the screen modifies the dynamics of $\mathcal{A}$ and $\mathcal{B}$ analogously to the effect of an external environment. First, it adds a Lamb shift-like term to the observed local Hamiltonian,

$$\hat{H}_{loc} = \hat{H}_a + \hat{H}_b + \frac{\nu_a}{2}\hat{A}^2 + \frac{\nu_b}{2}\hat{B}^2\,, \tag{4.18}$$

with associated coupling strengths set by the action of the screen,

$$\begin{aligned} \nu_a &= -i\,\langle [\hat{x}, \mathcal{S}(\hat{x})] \rangle_f \\ \nu_b &= -i\,\langle [\hat{p}, \mathcal{S}(\hat{p})] \rangle_f\,. \end{aligned} \tag{4.19}$$

The observed interaction parameters η and ξ are shifted as well. This is set by the discrepancy in the commutation relations between the input and output canonical

variables of $\mathcal{F}$,

$$\begin{aligned} \eta &= 1 - \frac{i}{2} \left\langle [\mathcal{S}(\hat{x}), \hat{p}] - [\hat{x}, \mathcal{S}(\hat{p})] \right\rangle_f \\ \xi/2 &= 1 - \frac{i}{2} \left\langle [\hat{x}, \mathcal{S}(\hat{p})] + [\mathcal{S}(\hat{x}), \hat{p}] \right\rangle_f . \end{aligned} \tag{4.20}$$

As expected, when $\mathcal{S}$ is the identity, the generator $\mathcal{L}$ corresponds to the original witness, $\eta = 1$, $\xi = \nu_a = \nu_b = 0$. The components of $\mathcal{D}$ proportional to Y_{uv} (in equation (4.3)) are set by,

$$Y_{uv} = \left\langle \mathcal{S}(\{\hat{u}, \hat{v}\}) + \{\hat{u}, \hat{v}\} - \{\hat{u}, \mathcal{S}(\hat{v})\} - \{\mathcal{S}(\hat{u}), \hat{v}\} \right\rangle_f , \tag{4.21}$$

for indices u and v representing either $\hat{x}$ or $\hat{p}$. These terms can be interpreted as a back-action on the system due to the continuous measurement of $\hat{A}$ and $\hat{B}$ by the environment [177–179].

We can use the toy model to motivate the matrix $Y - 2i\eta\Delta_1$ described in the theorem. For simplicity, assume that the screen $\mathcal{S}$ takes the form of an unbiased heterodyne measurement followed by preparation of a coherent state corresponding to the measured quadratures. Since this is the optimal 'quantum-classical' channel [163] that estimates both quadratures of $\mathcal{F}$ [180–182], we expect that this channel causes the *least* amount of decoherence while still disallowing entanglement. Because this channel is unbiased it does not displace first moments of the ancilla quadratures, i.e., $\mathcal{S}(\hat{x}) = \hat{x}$ and $\mathcal{S}(\hat{p}) = \hat{p}$, so we observe no level shifts ($\nu_a = \nu_b = 0$ in equation (4.19)) or shifts in the witness parameters ($\eta = 1$ and $\xi = 0$). The matrix Y_{uv} of equation (4.21) (representing the noise added to the ancilla by the channel) is thus the only parameter to determine whether $\mathcal{L}$ can distillably entangle $\mathcal{A}$ and $\mathcal{B}$. In this case, the output of the screen is simply a coherent state corresponding to

the measured quadratures. This output is inherently noisier than the input, since $\hat{x}$ and $\hat{p}$ can't be concurrently measured with infinite precision, and further since the output coherent states have variance 1/4 in each quadrature. Combining these effects, we have that the output variance in $\hat{x}$ and $\hat{p}$ satisfies [183],

$$\mathrm{Var}(\mathcal{S}(\hat{x})) + \mathrm{Var}(\mathcal{S}(\hat{p})) \geq 1 + \mathrm{Var}(\hat{x}) + \mathrm{Var}(\hat{p})\,. \tag{4.22}$$

Further, since the screen preserves the first moments of $\hat{x}$ and $\hat{p}$, this inequality still holds under all canonical transformations, $\hat{x} \to \alpha x + \beta\hat{p}$, $\hat{p} \to -\beta\hat{x} + \alpha\hat{p}$, $\alpha^2 + \beta^2 = 1$. In terms of the heterodyne noise matrix corresponding to equation (4.21), this can be expressed as

$$Y_h \geq 2i\Delta_1\,, \tag{4.23}$$

where $i(\Delta_1)_{uv} = [\hat{u}, \hat{v}]$ denotes the commutation relations between $\hat{x}$ and $\hat{p}$. We note that this bound is tight in that it is saturated in the ideal case of minimal channel noise. We may therefore hypothesize that any channel $\mathcal{S}$ which disallows distillable entanglement between $\mathcal{A}$ and $\mathcal{B}$ must also satisfy this inequality. Indeed, generalizing to the case $\eta \neq 1$ immediately gives the condition of our theorem.

4.4 Experimental application

We conclude with a suggested experiment to demonstrate these concepts. We consider two optical cavities, each coupled linearly to one end of a waveguide. This produces an effective normal mode coupling between the cavities, and this coupling would normally entangle them, except that in our setup the waveguide light is 'screened' such that only classical correlations can develop. In order to test whether

this is the case, our approach is to verify the coupling between the two cavities via the average equations of motion. This verification is a "witness" to the necessary communication rate of the channel. By our theorem, if the rate of increase in excess noise in the system is below the bound set by the witness, then the channel must distillably entangle the cavities.

We now describe the experiment in detail. We assume the narrow-band limit, as well as linear interactions between the cavities and waveguide field modes, so that the system can be described within the input-output formalism [184, 185]. We assume the cavities each couple to the wave-guide at a rate $2g$, while also decaying into the environment at a rate κ. The equations of motion for the cavity and field modes are then

$$\begin{aligned}
\partial_t \hat{a} &= \frac{2g+\kappa}{2}\hat{a} - \sqrt{2|g|}\hat{B}_{in} - \sqrt{\kappa}\hat{A}_{in} \\
\hat{A}_{out} &= \hat{A}_{in} + \sqrt{\kappa}\hat{a} \\
\hat{B}_{out} &= \hat{B}_{in} + \sqrt{2g}\hat{a} \\
\partial_t \hat{b} &= \frac{2g+\kappa}{2}\hat{b} - \sqrt{2|g|}\hat{C}_{in} - \sqrt{\kappa}\hat{D}_{in} \\
\hat{C}_{out} &= \hat{C}_{in} + \sqrt{2g}\hat{b} \\
\hat{D}_{out} &= \hat{D}_{in} + \sqrt{\kappa}\hat{b}\,.
\end{aligned} \tag{4.24}$$

Here $\hat{a}$ and $\hat{b}$ describe the cavity modes, while all other terms are input-output field operators for either the waveguide or environment (note that we are working in a frame rotating at the resonance frequency of the two cavities). In order to screen the amount of quantum information transferred through the waveguide, at each cavity interface we pick off some of the outgoing light, measure its quadratures,

and reproduce the corresponding coherent fields at the other end (see Fig. 4.2a). Experimentally this is done through a continuous heterodyne measurement. As seen in Fig. 4.2b, we vary the strength of this 'screen' by measuring a variable fraction T of the outgoing beam intensity. In the narrow band limit, the heterodyne measurement can be modeled as a linear interaction with two auxiliary vacuum fields, whose resulting individual quadratures average to the mean quadrature of the input field [180]. The output is

$$\begin{aligned} \hat{B}_{in} &= i\hat{C}_{out} + \sqrt{T}\hat{R}_1 \\ \hat{C}_{in} &= i\hat{B}_{out} + \sqrt{T}\hat{R}_2 \,. \end{aligned} \tag{4.25}$$

The terms $\hat{R}_j = (\hat{F}_j^\dagger + \hat{G}_j)$ represent auxiliary vacuum fields which account for the noise added to the waveguide field during the measurement process. The transmissivity T determines how much of the cavity output is measured, while the factor i corresponds to the phase acquired in propagating through the waveguide and is set so that no standing waves occur. Through substitution in equations (4.24) and (4.25), we compute reduced equations of motion for the cavity modes,

$$\begin{aligned} \partial_t \hat{a} &= -\frac{\kappa}{2}\hat{a} - ig\hat{b} - \sqrt{|g|T}\hat{N}_a - \sqrt{\kappa}\hat{A}_{in} \\ \partial_t \hat{b} &= -\frac{\kappa}{2}\hat{d} - ig\hat{a} - \sqrt{|g|T}\hat{N}_b - \sqrt{\kappa}\hat{D}_{in} \,, \end{aligned} \tag{4.26}$$

where $\hat{N}_a$ and $\hat{N}_b$ are independent fields satisfying $\langle\langle \hat{N}(t)\rangle\rangle = 0$ and $\langle\langle \hat{N}(t)\hat{N}^\dagger(t')\rangle\rangle = \langle\langle \hat{N}^\dagger(t)\hat{N}(t')\rangle\rangle = \delta(t-t')$.

Matching the reduced Heisenberg-Langevin equations (4.26) to a master equation, we see that the dynamics are reproduced by a Hamiltonian interaction $g(\hat{x}_a\hat{x}_b +$

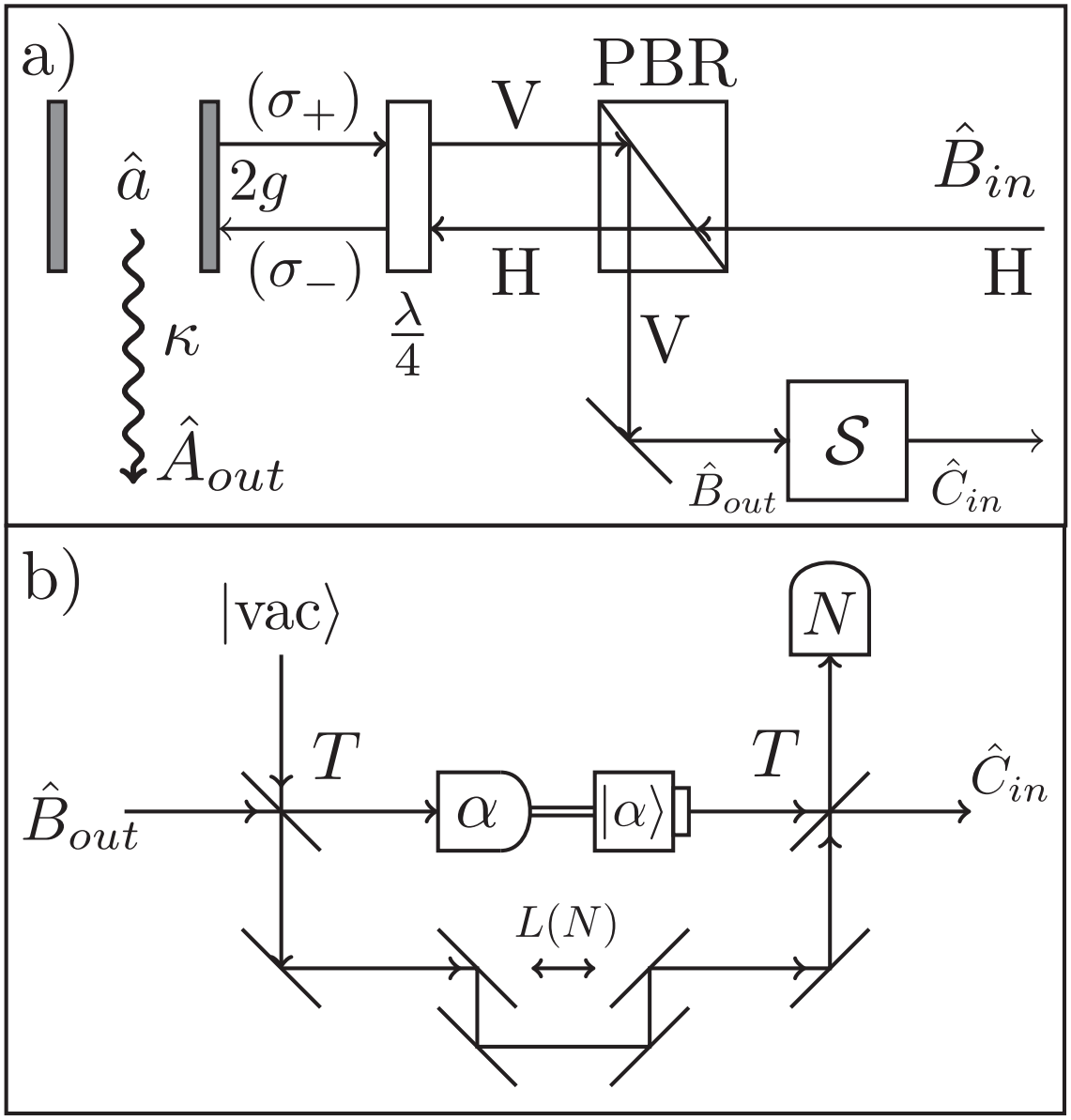

Figure 4.2: **a)** Optical cavity with mode $\hat{a}$ coupled via variable optical isolator (quarter wave plate and variable polarizing beam splitter) to a waveguide with a possible heterodyne measurement system acting as the screen $\mathcal{S}$. An analogous cavity (not shown) receives the vertically polarized output and returns the horizontally polarized input. **b)** Example of the variable-strength screen $\mathcal{S}$ via heterodyne measurement followed by attenuation and phase shift of a coherent source to match the measurement outcome α. The path length of the unmeasured beam is set so that it interferes constructively with the heterodyne output at the second beam splitter.

$\hat{p}_a\hat{p}_b) = g(\hat{a}\hat{b}^\dagger + \hat{b}\hat{a}^\dagger)$, a measurement induced dissipator [177],

$$\mathcal{D}_M^{(a)}(\hat{O}) = -\frac{1}{4}2|g|T\left([\hat{x}_a,[\hat{x}_a,\hat{O}]] + [\hat{p}_a,[\hat{p}_a,\hat{O}]]\right), \tag{4.27}$$

as well as a thermalization dissipator [162],

$$\begin{aligned}\mathcal{D}_T^{(a)}(\hat{O}) =& \kappa(\bar{n}+1)\left(\hat{a}^\dagger\hat{O}\hat{a} - \frac{1}{2}\{\hat{a}^\dagger\hat{a},\hat{O}\}\right) \\ &+ \kappa\bar{n}\left(\hat{a}\hat{O}\hat{a}^\dagger - \frac{1}{2}\{\hat{a}\hat{a}^\dagger,\hat{O}\}\right),\end{aligned} \tag{4.28}$$

and equivalent terms $\mathcal{D}_M^{(b)} + \mathcal{D}_T^{(b)}$. Neglecting the thermal terms, the generator of time evolution is a sum of generators $\mathcal{L}_{xx} + \mathcal{L}_{pp}$, each of the form in equation (4.2). Here $\mathcal{L}_{xx}$ ($\mathcal{L}_{pp}$) produces an $\hat{x}_a\hat{x}_b$ ($\hat{p}_a\hat{p}_b$) coupling of strength $\eta = g$, noise matrix $Y_f = 2|g|TI$, and anomalous term $\xi = 0$. Our theorem predicts that, as expected, when all of the intermediate light is intercepted (i.e. $T = 1$), both $\mathcal{L}_{xx}$ and $\mathcal{L}_{pp}$ have positive semi-definite matrices $Y - 2i\eta\Delta_1$, and therefore the two cavities cannot become entangled. Conversely, when $T < 1$, each generator can entangle the cavities, and the sum $\mathcal{L}_{xx} + \mathcal{L}_{pp}$ does so as well [2].

The actual experimental test is as follows. First, one monitors the evolution of the canonical variables to determine the local Hamiltonian $\hat{H}_{loc} + g(\hat{x}_a\hat{x}_b + \hat{p}_a\hat{p}_b)$ and the thermal decay rate κ. Letting $\hat{m}_a = \frac{1}{\sqrt{2}}(e^{i\theta_a}\hat{a} + \text{h.c.})$, $\hat{m}_b = \frac{1}{\sqrt{2}}(e^{i\theta_b}\hat{d} + \text{h.c.})$ represent arbitrary canonical variables of the systems, one then measures the excess

[2] It may not be true in general that two entangling generators sum to an entangling generator. The statement holds in this case because the two circuit generators involve operators that are canonically conjugate to each other. Considering the proof in the appendix, since they act on different subspaces, the violation of (4.40) is independent for both generators.

noise rates

$$\begin{aligned} N(\hat{m}_a, t) + N(\hat{m}_b, t) &= \langle \mathcal{D}_M^{(a)}(\hat{m}_a) + \mathcal{D}_M^{(b)}(\hat{m}_b) \rangle \\ &= 2|g|T\,. \end{aligned} \tag{4.29}$$

Note that we have incorporated the thermal decay into the definition of $N(\hat{O}, t)$, i.e., we have added the $\mathcal{D}_T$ terms to the definition of the witness generator $\mathcal{L}_w$. This modifies operational definition of the excess noise, since although the parameter κ may be determined by observation of the first moments of the canonical variables, parameter $\bar{n}$ must be determined from the second moments. As expected, when $T < 1$, the noise rate is less than twice the communication rate $2|g|$, hence the systems may become entangled in the $\kappa/|g| \to 0$ limit.

4.5 Conclusion

We have presented a formalism for testing whether a non-local interaction between continuous variables is capable of distillably entangling them. Curiously, our scheme does not require actual verification of entanglement between the interacting objects, allowing one to circumvent these typically challenging measurement procedures. Possible applications of our results range from continuous variable quantum cryptography, to verification of quantum information processing, to the first step towards zero-knowledge reconstruction of models for observed physical interactions.

4.6 Appendix

4.6.1 Calculation of the generator and physical considerations

Generality and complete positivity of the generator: As mentioned previously, $\mathcal{L}$ is the most general time-homogeneous generator for Markovian evolution that can be written as a quadratic expression in operators $\hat{A}$ and $\hat{B}$ and satisfies equation (4.1). To see this, we note that the dissipative component $\mathcal{D}$ (defined in equation (4.3)) can equivalently be written in the canonical Lindblad form [173],

$$\mathcal{D}(\hat{O}) = \sum_k \hat{V}_k^\dagger \hat{O} \hat{V}_k - \frac{1}{2}\{\hat{V}_k^\dagger \hat{V}_k, \hat{O}\}\,, \tag{4.30}$$

where we make the identification,

$$\begin{gathered} \hat{V}_k = \alpha_k \hat{A} + \beta_k \hat{B} \\ \frac{1}{2} Y_{xx} = \sum_k |\alpha_k|^2 \;,\; \frac{1}{2} Y_{pp} = \sum_k |\beta_k|^2 \\ \frac{1}{2}(Y_{xp} + i\xi) = \sum_k \alpha_k^* \beta_k \,. \end{gathered} \tag{4.31}$$

Because it can be expressed in this form, for all $t \geq 0$ the adjoint propagator $e^{t\mathcal{L}}$ is completely positive [164, 173], as expected for a physically realizable map.

Existence of the limit in equation (4.14)*:* To show when the limit exists, we use the Baker-Campbell-Hausdorff relation to expand each term of (4.12) to first order in $\sqrt{t}$. For example, we may expand $\mathcal{C}_{\hat{B}\hat{p}\sqrt{t}}(\hat{O}) = e^{i\hat{B}\hat{p}\sqrt{t}} \hat{O} e^{i\hat{B}\hat{p}\sqrt{t}}$ as

$$\mathcal{C}_{\hat{B}\hat{p}\sqrt{t}} = \mathrm{Id} + i\sqrt{t}[\hat{B}\hat{p}, \cdot\,] - \frac{t}{2}[\hat{B}\hat{p}, [\hat{B}\hat{p}, \cdot\,]] + O(t^{3/2})\,, \tag{4.32}$$

where $\mathrm{Id}(\hat{O}) = \hat{O}$ is the identity super-operator, and $[\hat{B}\hat{p}, \cdot]\hat{O} = [\hat{B}\hat{p}, \hat{O}]$ is the commutation super-operator. Adding all terms of $\mathcal{V}_t$ of order $\sqrt{t}$ gives

$$i\sqrt{t}[\hat{B}, \cdot] \otimes (\mathcal{S}(\hat{p}) - \hat{p}) + i\sqrt{t}[\hat{A}, \cdot] \otimes (\mathcal{S}(\hat{x}) - \hat{x}) \ , \tag{4.33}$$

where we have pulled out $\hat{x}$ and $\hat{p}$ from the commutators since we are only acting on terms of the form $\hat{O}_{ab} \otimes \mathbb{I}_f$. Taking the partial trace over the ancilla Hilbert space in (4.12), we have that the $\sqrt{t}$ terms of $\mathcal{V}_t$ vanish exactly when equation (4.17) holds.

Derivation of $\mathcal{L}$: To calculate the dynamics induced by the reduced circuit (4.13), we continue using Baker-Campbell-Hausdorff (as in equation (4.32)) and expand each superoperator in $\mathcal{V}_t$ to order t. The calculation involves making frequent use of the following identity:

$$\begin{aligned}[\hat{X} \otimes \hat{u}, [\hat{Y} \otimes \hat{v}, \hat{O}_{ab} \otimes \mathbb{I}_f]] =& \frac{1}{2}\{\hat{X}, [\hat{Y}, \hat{O}_{ab}]\} \otimes [\hat{u}, \hat{v}] \\ &+ \frac{1}{2}[\hat{X}, [\hat{Y}, \hat{O}_{ab}]] \otimes \{\hat{u}, \hat{v}\}\end{aligned} \tag{4.34}$$

where we have assumed $\hat{X}$ and $\hat{Y}$ are commuting operators on the composite system $\mathcal{AB}$, and $\hat{u}$ and $\hat{v}$ are operators on $\mathcal{F}$. There are multiple sources of order t terms in $\mathcal{V}_t$. The first is just the commutator

$$i[\hat{H}_a + \hat{H}_b, \cdot] \tag{4.35}$$

obtained from the local unitary $\mathcal{C}_{(\hat{H}_a + \hat{H}_b)t}$. Second, we have products of order $\sqrt{t}$ terms arising from commutators of different ancilla-system interactions (e.g. $\mathcal{C}_{\sqrt{t}\hat{A}\hat{x}}$

and $\mathcal{C}_{\sqrt{t}\hat{B}\hat{p}}$), which – after accounting for the action of the screen – produce

$$\begin{aligned} & i[\hat{A}\hat{B},\,\cdot\,]\otimes\left(\frac{i}{2}([\mathcal{S}(\hat{x}),\hat{p}]-[\hat{x},\mathcal{S}(\hat{p})])+1\right) \\ & -i\left(\hat{A}\,\cdot\,\hat{B}-\hat{B}\,\cdot\,\hat{A}\right)\otimes\left(1-\frac{1}{2i}([\hat{x},\mathcal{S}(\hat{p})]+[\mathcal{S}(\hat{x}),\hat{p}])\right) \\ & -\frac{1}{2}[\hat{A},[\hat{B},\,\cdot\,]]\otimes(\{\hat{x},\hat{p}\}+\mathcal{S}(\{\hat{x},\hat{p}\})-\{\mathcal{S}(\hat{x}),\hat{p}\}-\{\hat{x},\mathcal{S}(\hat{p})\})\ , \end{aligned} \tag{4.36}$$

where we have used $[\hat{x},\hat{p}]=i$.

Finally, we have products of $\sqrt{t}$ terms having only $\hat{A}\otimes\hat{x}$ or $\hat{B}\otimes\hat{p}$ commutators (e.g., from $\mathcal{C}_{\sqrt{t}\hat{A}\hat{x}}$ and $\mathcal{C}_{-\sqrt{t}\hat{A}\hat{x}}$) , as well as individual order t terms involving double commutators from a single interaction (as in the third term of equation (4.32)). This gives

$$\begin{aligned} & i\frac{1}{2}[\hat{A}^2,\,\cdot\,]\otimes(-i[\hat{x},\mathcal{S}[\hat{x}]]) \\ & -\frac{1}{2}[\hat{A},[\hat{A},\,\cdot\,]]\otimes\left(\hat{x}^2+\mathcal{S}(\hat{x}^2)-\{\hat{x},\mathcal{S}(\hat{x})\}\right)\quad . \end{aligned} \tag{4.37}$$

and an analogous contribution from the $\hat{B}$ terms, obtained by substituting $\hat{x}\rightarrow\hat{p}$ and $\hat{A}\rightarrow\hat{B}$ above. Adding all terms together and taking the trace over the ancilla exactly produces the generator in equation (4.2), with parameters set as in equations(4.19)-(4.21).

4.6.2 Proof of the Theorem

Theorem: *For Gaussian states evolving under generator $\mathcal{L}$ of equation* (4.2)*, if $Y-2i\eta\Delta_1$ is positive semi-definite, then non-zero distillable entanglement never develops between $\mathcal{A}$ and $\mathcal{B}$. Conversely, let $|\psi_a\rangle\otimes|\psi_b\rangle$ denote the (separable, Gaussian) ground state of $\hat{H}_{loc}$. If $Y-2i\eta\Delta_1$ has a negative eigenvalue, then after some*

$t > 0$ the initial state $|\psi_a\rangle \otimes |\psi_b\rangle$ is mapped to a state with finite distillable entanglement.

We discuss some preliminary information before giving the proof. As before, we let $M = [\hat{x}_a, \hat{p}_a, \hat{x}_b, \hat{p}_b]^T$ denote the vector of canonical variables of both subsystems. We first note that by its quadratic form, the generator $\mathcal{L}$ does not increase the degree of any polynomial in $\hat{M}_i$, which implies that $e^{t\mathcal{L}}$ preserves Gaussian states [160]. Since Gaussian states are defined uniquely by their first and second moments, we reduce our discussion to the mean vector $m_i = \langle \hat{M}_i \rangle$ and covariance matrix $\gamma_{ij} = \langle \{\hat{M}_i, \hat{M}_j\} \rangle - 2m_i m_j$. For any state of $\mathcal{A}$ and $\mathcal{B}$, a consequence of the positivity of the density matrix is the uncertainty principle [167–169], as implied by the matrix inequality [186–188],

$$\gamma + i\Delta_2 \geq 0\,, \tag{4.38}$$

meaning that the (complex valued) matrix $\gamma + i\Delta_2$ has no negative eigenvalues. Here Δ_n represents the n-mode symplectic matrix,

$$\Delta_n = \bigoplus_{i=1}^{n} \begin{pmatrix} 0 & 1 \\ -1 & 0 \end{pmatrix}_i . \tag{4.39}$$

We note that a 2-mode Gaussian state is *not* distillable if and only if [165,166]

$$\tilde{\gamma} + i\Delta_2 \geq 0\,, \tag{4.40}$$

where $\tilde{\gamma}$ is obtained from γ by setting $\hat{p}_b \to -\hat{p}_b$. In other words, 2-mode Gaussian states are distillably entangled if and only if their partial time reverse does *not* satisfy the uncertainty principle. Given that $\tilde{\gamma}(t) = K\gamma(t)K$, with $K = \mathrm{diag}([1, 1, 1, -1])$,

we have that (4.40) is equivalent to

$$\gamma \geq -i\tilde{\Delta}_2\,, \tag{4.41}$$

where we have defined the operator

$$i\tilde{\Delta}_2 = iK\Delta_2 K = \begin{pmatrix} 0 & 1 \\ -1 & 0 \end{pmatrix} \oplus \begin{pmatrix} 0 & -1 \\ 1 & 0 \end{pmatrix}\,. \tag{4.42}$$

Proving the theorem requires determining when inequality (4.41) can break. To prove the first statement, we analyze the evolution of γ and show that under condition

$$Y - 2i\eta\Delta_1 \geq 0\,, \tag{4.43}$$

if equation (4.41) holds at $t = 0$ then it also holds for $t > 0$ sufficiently small. This implies that equation (4.40) holds for all $t \geq 0$, since the argument may similarly be applied assuming any initial value of t. Conversely, if $Y - 2i\eta\Delta_1$ has a negative eigenvalue, we show that for $\gamma(0)$ corresponding to the (separable, Gaussian) ground state of $\hat{H}_{loc}$, the inequality (4.41) breaks down for some small $t > 0$.

To begin the proof we first determine the evolution of $\gamma(t)$. We consider the operator valued matrix

$$\Gamma_{ij} = \hat{M}_i\hat{M}_j + \hat{M}_j\hat{M}_i\,. \tag{4.44}$$

Written in terms of M and noting that $i(\Delta_2)_{ij} = [\hat{M}_i, \hat{M}_j]$, we can write this matrix as $\Gamma = 2MM^T - i\Delta_2$. From the definition of $\mathcal{L}$ in (4.2), we can then compute the equations of motion,

$$\begin{aligned} \partial_t M &= x^T M \\ \partial_t \Gamma &= x^T\Gamma + \Gamma x + y\,. \end{aligned} \tag{4.45}$$

Here the matrices x and y are

$$x^T = \Delta_2(H + G) \quad y = -\Delta_2 N \Delta_2 \,, \tag{4.46}$$

with matrices H, G and N described below. The real symmetric matrix H parametrizes the Hamiltonian,

$$\frac{1}{2}\sum_{ij} H_{ij}\hat{M}_i\hat{M}_j = \hat{H}_{loc} + \eta\hat{A}\hat{B} \,. \tag{4.47}$$

Since they are canonical variables, we can decompose $\hat{A}$ and $\hat{B}$ as $\hat{A} = \chi_x^T\hat{M}$ and $\hat{B} = \chi_p^T\hat{M}$, where χ_x and χ_p are real vectors. Likewise since $\hat{H}_{loc}$ is a local Hamiltonian, there exist 2×2 real symmetric matrices H_a and H_b such that $\hat{H}_{loc} = \frac{1}{2}\sum_{ij}(H_a \oplus H_b)_{i,j}\hat{M}_i\hat{M}_j$ takes on a block diagonal structure. Combining these statements, we have that

$$H = H_a \oplus H_b + \eta(\chi_x\chi_p^T + \chi_p\chi_x^T) \,. \tag{4.48}$$

The matrix G similarly encodes the effect of the superoperator $i\frac{\xi}{2}(\hat{A}\cdot\hat{B} - \hat{B}\cdot\hat{A})$ appearing in $\mathcal{L}$. It is similar to H in that it appears in the dynamics of both M and Γ, but unlike H it is an antisymmetric matrix,

$$G = \frac{\xi}{2}(\chi_x\chi_p^T - \chi_p\chi_x^T) \,. \tag{4.49}$$

Finally, the operator N represents the noise added to the systems from the dissipative term $\mathcal{D}$,

$$N = \sum_{u,v=x,p} Y_{uv}\chi_u\chi_v^T \,. \tag{4.50}$$

From the definition (4.5), we have $\gamma = \langle\Gamma\rangle - 2\langle M\rangle\langle M\rangle^T$. Hence from (4.45) and noting that $x^T i\Delta_2 = -i\Delta_2 x$, the equation of motion for γ is,

$$\partial_t\gamma = x^T\gamma + \gamma x + y \,. \tag{4.51}$$

The differential equation (4.51) may then be solved directly to give

$$\gamma(t) = Y_t + X_t^T \gamma(0) X_t \,, \tag{4.52}$$

where $X_t = e^{xt}$ and $Y_t = \int_0^t X_{t-s}^T \, y \, X_{t-s} \mathrm{d}s$.

To prove the first statement of the theorem, we assume that $Y - 2i\eta\Delta_1$ is positive semi-definite. We want to show that if any $\gamma(t)$ satisfies matrix inequality (4.41) at $t = 0$, then it also does so for sufficiently small $t > 0$. Hence we must show that if there is some (possibly complex) vector z such that $z^\dagger \left(\gamma(0) + i\tilde{\Delta}_2\right) z = 0$, then $\partial_t z^\dagger(\gamma(t) + i\tilde{\Delta}_2)z|_{t=0}$ is non-negative, and therefore $\gamma(t) - i\tilde{\Delta}_2$ has no negative eigenvalues for small $t > 0$. To do this, we use equations (4.52) and (4.41) to compute

$$\begin{aligned} \gamma(t) + i\tilde{\Delta}_2 &= Y_t + X_t^T \gamma(0) X_t + i\tilde{\Delta}_2 \\ &\geq Y_t - X_t^T i\tilde{\Delta}_2 X_t + i\tilde{\Delta}_2 \\ &\equiv F(t) \,. \end{aligned} \tag{4.53}$$

Since $F(0) = 0$, it suffices to show that $F'(0) \geq 0$: for if $z^\dagger(\gamma(0) + i\tilde{\Delta}_2)z = 0$, then assuming that $\partial_t z^\dagger(\gamma(t) + i\tilde{\Delta}_2)z|_{t=0}$ is negative would produce a contradiction with inequality (4.53). A straightforward calculation shows that

$$\begin{aligned} F'(0) &= y - ix^T\tilde{\Delta}_2 - i\tilde{\Delta}_2 x \\ &= -\Delta_2 N \Delta_2 - i\Delta_2(H+G)\tilde{\Delta}_2 - i\tilde{\Delta}_2(-H+G)\Delta_2 \\ &= (i\Delta_2)N(i\Delta_2) \\ &\quad - i(i\Delta_2)\left((H+G)\tilde{\Delta}_2\Delta_2 + \Delta_2\tilde{\Delta}_2(-H+G)\right)(i\Delta_2) \,. \end{aligned} \tag{4.54}$$

In the first line we used the definition of X_t and Y_t and in the second we used equation (4.46) and the fact that H (G) is symmetric (antisymmetric). Finally, in

the third line we used $\Delta_2\Delta_2 = -I_2$, where I_n is the $2n \times 2n$ identity matrix.

It is easy to see that $\tilde{\Delta}_2\Delta_2 = (-I_1) \oplus I_1 = \Delta_2\tilde{\Delta}_2$, which commutes with any block diagonal matrix. Hence for $H = H_a \oplus H_b + \eta(\chi_x\chi_p^T + \chi_p\chi_x^T)$ (noting that χ_x and χ_p have supports in the first and second blocks, respectively), we may easily compute $H\tilde{\Delta}_2\Delta_2 - \Delta_2\tilde{\Delta}_2 H = 2\eta(\chi_x\chi_p^T - \chi_p\chi_x^T)$. Likewise we see that since $\Delta_2\tilde{\Delta}_2\chi_x\chi_p^T + \chi_x\chi_p^T\Delta_2\tilde{\Delta}_2 = 0$, the contribution of $G = \frac{\xi}{2}(\chi_x\chi_p^T - \chi_p\chi_x^T)$ to $F'(0)$ vanishes. Using the definition of N in (4.50), the expression for $F'(0)$ then becomes,

$$\begin{aligned} F'(0) &= \sum_{u,v}(Y_{uv} - 2i\eta(\Delta_1)_{uv})(i\Delta_2)(\chi_u\chi_v^T)(i\Delta_2) \\ &= (i\Delta_2)\chi(Y - 2i\eta\Delta_1)\chi^T(i\Delta_2)\,, \end{aligned} \tag{4.55}$$

where $\chi = [\chi_x\,\chi_p]$ is the 4×2 matrix with columns χ_x and χ_p. Since $i\Delta_2$ is a Hermitian matrix, we see that $F'(0) \geq 0$ if and only if $Y - 2i\eta\Delta_1 \geq 0$. Thus if $Y - 2i\eta\Delta_1$ is positive semi-definite, $z^\dagger(\gamma(t) + i\tilde{\Delta}_2)z$ can never become negative, so inequality (4.41) holds and Gaussian states do not become distillably entangled.

To prove the converse statement, we assume that $(Y - 2i\eta\Delta_1)$ has a negative eigenvalue. Let us prepare the system in the ground state of $\hat{H}_{loc} = \frac{1}{2}M(H_a \oplus H_b)M^T$. As we argue at the end of the proof, without loss of generality we may assume that $H_a \oplus H_b = (\omega_a I_1 \oplus \omega_b I_1)$, and hence the ground state is described by covariance matrix $\gamma(0) = I_2$. For small times $t > 0$, by equation (4.51) we have

$$\gamma(t) + i\tilde{\Delta}_2 = \gamma(0) + i\tilde{\Delta}_2 + t(y + x^T\gamma(0) + \gamma(0)x) + O(t^2)\,. \tag{4.56}$$

Since $(Y - 2i\eta\Delta_1)$ has a negative eigenvalue, there exists a complex valued vector $z_f = [z_1, z_2]^T$ such that $z_f^\dagger(Y - 2i\eta\Delta_1)z_f < 0$. We use this fact to define a vector $z_{ab} \in \mathbb{C}^4$ such that $z_{ab}^\dagger(\gamma(t) + i\tilde{\Delta}_2)z_{ab}$ (from the equation above) is negative to

leading order in t, and therefore the ground state becomes distillably entangled. Set $\tilde{\chi}_s = \chi_s//||\chi_s||$ for $s = x, p$, and $\tilde{\chi}'_s = i\Delta_2\tilde{\chi}_s$ (which is orthogonal to $\tilde{\chi}_s$, since Δ_2 is antisymmetric). Define the vector

$$z_{ab} = i\Delta_2 \left(\frac{z_1}{||\chi_x||}(\tilde{\chi}_x - \tilde{\chi}'_x) + \frac{z_2}{||\chi_p||}(\tilde{\chi}_p + \tilde{\chi}'_p) \right) . \tag{4.57}$$

Noting that $(i\Delta_2)(i\tilde{\Delta}_2) = (i\tilde{\Delta}_2)(i\Delta_2)$, $i\tilde{\Delta}_2\tilde{\chi}_x = \tilde{\chi}'_x$, and $i\tilde{\Delta}_2\tilde{\chi}_p = -\tilde{\chi}'_p$, it is easy to verify that $(I_2 + i\tilde{\Delta}_2)z_{ab} = 0$. Since $\gamma(0) = I_2$, we see that the zero order term of $z_{ab}^\dagger(\gamma(t) + i\tilde{\Delta}_2)z_{ab}$ in equation (4.56) vanishes. Likewise, since $(i\Delta_2)^2 = I_2$ and $\{\tilde{\chi}_x, \tilde{\chi}'_x, \tilde{\chi}_p, \tilde{\chi}'_p\}$ form an orthonormal basis, one may directly verify that $\chi_x^T(i\Delta_2)z_{ab} = z_1$ and $\chi_p^T(i\Delta_2)z_{ab} = z_2$. Using $i\tilde{\Delta}_2 z_{ab} = -z_{ab}$ with equations (4.54) and (4.55), this implies that the order t term of $z_{ab}^\dagger(\gamma(t) + i\tilde{\Delta}_2)z_{ab}$ is

$$z_{ab}^\dagger(y + x^T + x)z_{ab} = z_{ab}^\dagger F'(0)z_{ab} = z_f^\dagger(Y - 2i\eta\Delta_1)z_f \, , \tag{4.58}$$

which is strictly negative by our original assumption. Thus $z_{ab}^\dagger(\gamma(t) + i\tilde{\Delta}_2)z_{ab}$ is negative for $t > 0$ sufficiently small, so that the ground state corresponding to $\gamma(0)$ at $t = 0$ violates equation (4.41) and becomes distillably entangled.

We now justify the assumption that $H_a \oplus H_b = (\omega_a I_1 \oplus \omega_b I_1)$ by showing that $H_a \oplus H_b$ can be transformed into this form under a local change of basis. Before we do so, we note that we can decompose each original Hamiltonian matrix as $H_s = \omega_s O_s R_s R_s^T O_s^T \equiv \omega_s S_s S_s^T$, for $s = a, b$. Here O_s is an orthogonal matrix that diagonalizes H_s, and $R_s = \begin{pmatrix} r_s & 0 \\ 0 & r_s^{-1} \end{pmatrix}$ for some $r_s > 0$. In the case of 2×2 matrices, the symplectic matrices (i.e. those satisfying $S\Delta_1 S^T = \Delta_1$) are exactly those with determinant 1, so we conclude that each S_s is symplectic. Since the

Gaussian unitary channels (i.e., maps corresponding to $Y_t = 0$ in (4.52)) correspond exactly to the symplectic transformations [163], we conclude that there exists a local Gaussian unitary, $\hat{U}_a \otimes \hat{U}_b$, that implements the symplectic transformation $S = S_a^{-1} \oplus S_b^{-1}$. In this new basis, the local Hamiltonian matrix is mapped to $H_a \oplus H_b \to (\omega_a I_1 \oplus \omega_b I_1)$, and the coupling terms are mapped according to $\chi_s \to S^{-1}\chi_s$. Further, since S^{-1} is block diagonal, the transformed vectors $S^{-1}\chi_s$ still have support in either the $\mathcal{A}$ or $\mathcal{B}$ subspace. Our assumption is therefore valid because the Gaussian separability condition (4.40) is invariant under Gaussian local unitaries.

Chapter 5: A classical channel model for gravitational decoherence

We show that, by treating the gravitational interaction between two mechanical resonators as a classical measurement channel, a gravitational decoherence model results that is equivalent to a model first proposed by Diosi. The resulting decoherence model implies that the classically mediated gravitational interaction between two gravitationally coupled resonators cannot create entanglement. The gravitational decoherence rate (and the complementary heating rate) is of the order of the gravitationally induced normal mode splitting of the two resonators. Failure to see this in an experiment would rule out treating gravitational interactions as purely classical.

5.1 Introduction

The ability to optically cool macroscopic mechanical oscillators close to their ground state, from which highly non-classical superposition states may be prepared, provides a platform in which to study the interplay between gravitational and quantum physics [189–192]. The objective is to engineer quantum states of mechanical systems in which gravitational effects must be taken into account if we are to account for the dynamics. Karolyhazy [193], Penrose [194] and also Diosi [195] have

proposed that in such a setting gravity would lead to a new kind of decoherence and, correspondingly, a new source of noise acting on the quantum degrees of freedom.

There are a number of ways to see why decoherence plays a special role in gravitational interactions. The central point can best be seen by contrasting the case of gravitationally mediated interactions to that of electromagnetically mediated interactions for which a full quantum description is available in QED [196]. Indeed, ion trap quanta computing shows that one can entangle the motional states of many particles using the coulomb interaction. The current limits on this are due to fluctuating charges on nearby electrodes but in principle one can shield from all unwanted Coulomb interactions. This is not the case for the gravitational field of a massive object. There are many ways to measure the gravitational field of a large mass: scattering of test particles, deflection of light, red shifts of clocks, contraction of rulers. Admittedly these effects are weak but in principle there is always an open measurement channel: one cannot shield against gravity. A gravitational source exhibits open measurement channels through its effect on space-time geometry. If one cannot close off a measurement channel then there necessarily remains a source of noise and decoherence even if the measurement results are never known. The key question is, how large is this effect?

If we had a quantum theory of gravity, the appearance of an additional source of noise would not be remarkable: it would ultimately arise from quantum fluctuations in the underlying field that mediates the gravitational interaction between quantum mechanical degrees of freedom [196]. Such effects, it is claimed, are likely to become important at the Planck scale and thus seem unlikely to arise in table-top

opto-mechanical experiments for which the Newtonian description of gravitational interactions would seem to suffice. Surprisingly, the proposals of Penrose and Diosi would indicate that this is not the case and that, given sufficient quantum control over macroscopic mechanical degrees of freedom, opto-mechanical systems might reveal gravitational decoherence.

In this chapter we use the recent proposal [197] for classically mediated long range interactions applied to gravitational interactions. They introduce a picture in which gravitational interactions are regarded as a two-way communication channel. Within this picture we contrast a conventional unitary treatment of the mutual gravitational interaction of two masses with a classical channel modelled as a weak continuous measurement of the position of each mass. Such a channel is classical in so far as the stochastic measurement record may be duplicated through fan-out without introducing noise. A classical measurement channel of this kind is an example of LOCC (local operation with classical communication) and cannot entangle the two masses. If gravitational interactions are of this form it implies one cannot entangle particles through purely gravitational interactions. Henceforth when we refer to a classical channel we mean one that cannot be used to entangle systems.

The continuous measurement record is used to control a reciprocal classical force on each mass via a feedforward control. In essence, the classical measurement record informs each mass of the other's position and applies the corresponding gravitational force. By requiring the effect to be reciprocal, we show that the gravitational decoherence rate is completely determined by the gradient of the gravitational force

between the two masses. This is equivalent to the gravitational decoherence models proposed by Penrose and Diosi. We calculate the size of this effect for an experiment based on two gravitationally coupled oscillators. We show that the decoherence rate saturates the bound required for a classical channel to not entangle the oscillators. The key point is this: a decoherence rate below this level would enable one to entangle particles through gravitational interactions and imply that a quantum theory of gravity must realise a quantum channel.

In [198] Diosi introduces a very similar model to the one we are proposing here for the case of relativistic quantum fields. In that paper a fundamental and universal measurement process measures the field configuration and the measurement results are fed back to modify the future dynamics of the field. In the Markov and non-relativistic limit a special case is made for the mass distribution being subject to the universal measurement. In many ways the model of this chapter is a particular demonstration of the physical consequences of this assumption.

5.2 Combining quantum and gravitational physics

Consider two masses, m_1, m_2 freely suspended so as to move (approximately) harmonically along the x-axis, Fig. 5.1. The gravitational interaction between the two masses couples these harmonic motions. The displacement of mass m_k from equilibrium is denoted x_k. The equilibrium positions are determined by the gravitational attractions between the two suspended masses. The interaction potential energy between the masses, expanded to second order in the relative displacement,

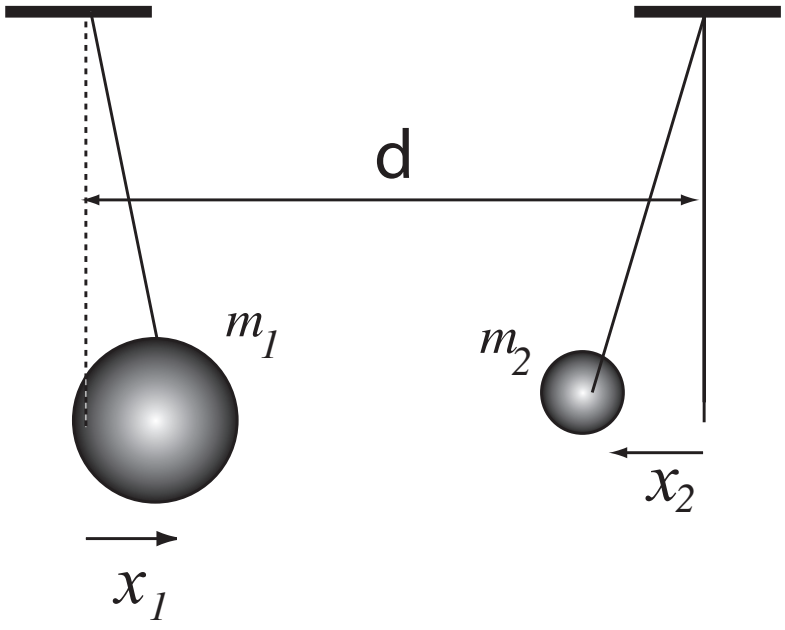

Figure 5.1: A gravitationally coupled system of two harmonic oscillators comprising two suspended masses m_1, m_2.

may be written

$$V(x_1, x_2) = V_0 - \frac{Gm_1m_2}{d^2}(x_1 - x_2) - \frac{Gm_1m_2}{d^3}(x_1 - x_2)^2 \tag{5.1}$$

The term linear in the displacement represents a constant force between the masses and simply modifies the equilibrium position of the masses to $\bar{x}_1 = Gm_2/(d^2\omega_1^2)$, $\bar{x}_2 = -Gm_2/(d^2\omega_2^2)$. We will absorb this into the definition of the displacement coordinates. The quadratic terms proportional to x_k^2 can be incorporated into the definition of the harmonic frequency of each mass. The total mechanical Hamiltonian is then given by

$$H_{qm} = H_0 + K\hat{x}_1\hat{x}_2 \tag{5.2}$$

where

$$H_0 = \sum_{k=1}^{2} \frac{\hat{p}_k^2}{2m_k} + \frac{m_k \Omega_k^2}{2} \hat{x}_k^2 \tag{5.3}$$

with

$$\Omega_k^2 = \omega_k^2 - K/m_k \tag{5.4}$$

and

$$K = \frac{2Gm_1m_2}{d^3} \tag{5.5}$$

and the usual canonical commutation relations hold $[\hat{x}_k, \hat{p}_j] = i\hbar\delta_{kj}$.

The model thus reduces to the very well understood case of two quadratically coupled simple harmonic oscillators. The resulting classical and quantum dynamics is then described as two independent simple harmonic oscillators, the normal modes, which are linear combinations of the local co-ordinates $q_+ = (x_1 + x_2)/\sqrt{2}$ is the *centre-of-mass* mode and $q_- = (x_1 - x_2)/\sqrt{2}$ is the *breathing* mode with frequencies $\omega_\pm$ given by

$$\omega_\pm^2 = (\Omega_1^2 + \Omega_2^2)/2 \pm \frac{1}{2}\left[(\Omega_1^2 - \Omega_2^2)^2 + 4K^2/(m_1m_2)\right]^{1/2} \tag{5.6}$$

In what follows we will consider the symmetric case for which $m_1 = m_2 = m$ and $\Omega_1 = \Omega_2 = \Omega$. In that case the normal mode frequencies become

$$\omega_+ = \omega \quad ; \omega_- = \omega \left[1 - \frac{2K}{m\omega^2}\right]^{1/2} \tag{5.7}$$

In most situations of laboratory relevance, the gravitational coupling is weak and the difference in frequency between the two normal modes, the normal mode splitting, can be written

$$\Delta \equiv \omega_+ - \omega_- \approx \frac{K}{m\omega} \tag{5.8}$$

What is the relevance of the normal modes of two coupled oscillators and gravitational decoherence? Many discussions of gravitational decoherence are concerned with the ability to prepare a single massive object in a pure quantum state of its centre of mass degree of freedom, for example, with a delocalised wave function of the form $\psi(x) = \psi(x+d) + \psi(x-d)$ where d is a macroscopically distinguishable displacement [199]. The ground state of two normal modes is a superposition state of the configuration space variables of two centre-of-mass degrees of freedom (the local modes) and as such the ability to prepare such a state through purely gravitational interactions would be a test of gravitational decoherence. The wave function of the normal mode ground states, $|0\rangle_+ \otimes |0\rangle_-$, in the coordinate basis of the local centre-of-mass coordinates, is a Gaussian two-mode squeezed state [200],

$$|0\rangle_+ \otimes |0\rangle_- = \int\int dx_1 dx_2 \; \psi(x_1, x_2) |x_1\rangle \otimes |x_2\rangle \tag{5.9}$$

where the wave function is

$$\psi(x_1, x_2) = \mathcal{N} \exp\left[-\vec{x}^T L \vec{x}\right] \tag{5.10}$$

where $\vec{x}^T = (x_1, x_2)$ and

$$L = \frac{m\omega}{4} \begin{pmatrix} 1+\sqrt{1-\beta} & 1-\sqrt{1-\beta} \\ 1-\sqrt{1-\beta} & 1+\sqrt{1-\beta} \end{pmatrix} \tag{5.11}$$

and $\beta = 2K/m\omega^2$. Decoherence will suppress the off-diagonal components of this state in the local co-ordinate basis. This state also carries a superposition of correlations through the off diagonal elements of L, that is to say it is also entangled. Thus decoherence will tend to reduce entanglement.

5.3 Gravity as a classical measurement channel

Kafri and Taylor [197] (Chapter 4) have recently proposed a simple way to test if a long range interaction between two particles is mediated by a quantum or a classical channel. They define a quantum channel by introducing an ancillary degree of freedom, a harmonic oscillator. The coherent interactions between two local systems and the channel lead, under appropriate circumstances, to an effective direct non-local interaction between the two local systems. This kind of process is used in geometric phase gates to simulate non-local interactions between internal states of trapped ions, with the ionic vibrational modes serving as the ancilla [201, 202]. The key of course is the ability to implement controlled entangling operations between the electronic and vibrational degrees of freedom of each ion. A classical channel can then be defined by simply allowing the ancillary oscillator to be continually measured.

In this chapter we will take a different, although equivalent, approach to defining a classical mediated interaction by using methods from quantum stochastic control theory [203]. Rather than a direct quantum interaction of the form $\hat{x}_1\hat{x}_2$, we assume the interaction is mediated by a *classical channel*. That is, the gravitational centre of mass co-ordinate, $\hat{x}_i$, of each particle is continuously measured and a classical stochastic measurement record, $J_k(t)$, carrying this information acts reciprocally as a classical control force on the other mass. The effect on the dynamics of the

systems is to produce a Hamiltonian term of the form,

$$H_{grav} = \chi_1 \frac{dJ_1(t)}{dt}\hat{x}_2 + \chi_2 \frac{dJ_2(t)}{dt}\hat{x}_1 \,. \tag{5.12}$$

As we will see, the units can be chosen such that the units of χ_k are Jm^{-2}, the same as the units of K.

In the case of continuous weak measurements of $\hat{x}_k$ the measurement record obeys a stochastic differential equation of the form [203]

$$dJ_k(t) = \langle \hat{x}_k \rangle_c dt + \sqrt{\frac{\hbar}{2\Gamma_k}} dW_k(t) \tag{5.13}$$

where Γ_k is a constant that determines the rate at which information is gained by the measurement, while $dW_{1,2}$ are independent, real valued Wiener increments. The units of $\Gamma_k/\hbar$ are $m^{-2}s^{-1}$. The average $\langle \hat{x}_k \rangle_c$ is a *conditional* quantum mechanical average conditioned on the entire history of measurement records up to time t.

The conditional quantum dynamics of the coupled oscillator system is given by the stochastic master equation

$$d\rho_c = -\frac{i}{\hbar}[H_c, \rho_c]dt - \sum_{k=1}^{2} \frac{\Gamma_k}{2\hbar}[\hat{x}_k, [\hat{x}_k, \rho_c]]dt + \sqrt{\frac{\Gamma_k}{\hbar}} dW_k(t)\mathcal{H}[\hat{x}_k]\rho_c \tag{5.14}$$

where the classical control Hamiltonian is defined by

$$H_c = H_0 + H_{grav} \tag{5.15}$$

and the conditioning super-operator, $\mathcal{H}$ is defined by

$$\mathcal{H}[\hat{X}]\rho = \hat{X}\rho + \rho\hat{X} - \mathrm{Tr}\left(\hat{X}\rho + \rho\hat{X}\right) \tag{5.16}$$

The appearance of the conditional average, $\mathrm{Tr}\left(\hat{x}_k\rho + \rho\hat{x}_k\right)$ in Eq.(5.14) is very similar to the theory of [204] and also [205] although in the latter case the stochastic term is missing and the interpretation is thus very different.

The form of Eq. (5.15) defines a direct feedback model of the kind considered in [203]. Using the results there we find that the corresponding unconditional dynamics (that is to say, the dynamics averaged over all measurement records) is given by

$$\begin{aligned}\frac{d\rho}{dt} &= -\frac{i}{\hbar}[H_0,\rho] - \frac{i}{2\hbar}\left(\chi_2[\hat{x}_1,\hat{x}_2\rho+\rho\hat{x}_2]+\chi_1[\hat{x}_2,\hat{x}_1\rho+\rho\hat{x}_1]\right) \\ &\quad -\sum_{k=1}^{2}\frac{\Gamma_k}{2\hbar}[\hat{x}_k,[\hat{x}_k,\rho]] - \frac{\chi_2^2}{8\hbar\Gamma_1}[\hat{x}_2,[\hat{x}_2,\rho]] - \frac{\chi_1^2}{8\hbar\Gamma_2}[\hat{x}_1,[\hat{x}_1,\rho]]\end{aligned} \tag{5.17}$$

The second term is the systematic effect of the control protocol. It is easy to see that if we fix $\chi_1 = \chi_2 = K$ this reduces to the standard Hamiltonian interaction term given in Eq.(5.2). The final two terms represent the effect of feeding back the white noise on the measurement signals to control the dynamics of the other mass.

In the case of highly asymmetric masses, for example the mass of the earth and the mass of a neutron in the experiments on neutron interferometry [206–208], $m_1 \gg m_2$, so we expect the measurement rates to also be highly asymmetric. In fact for the case of the measurement channel that records the position of the larger mass we expect $\Gamma_1 \gg \Gamma_2$ so that the relative contribution to the noise in the channel from the larger mass to the smaller mass is much smaller than the converse channel. This simply captures the intuition that for large mass the position of the centre of mass should be very classical. Equivalently the rate at which classical information is carried form the larger mass to the smaller mass is much greater than the rate at which information is carried form the smaller mass to the larger mass. This ensures that the decoherence rate of the smaller mass is much less than the decoherence rate of the larger, ‘ classical’ mass.

Let us now consider the symmetric case in which $m_1 = m_2$. In that case we

expect $\Gamma_1 = \Gamma_2 = \Gamma$. The noise added by measurement and feedback is a minimum at $\Gamma = \chi/2$ linking the decoherence rate due to the continuous measurement to the scale of the gravitational interaction as

$$\Gamma = K/2 \tag{5.18}$$

so that the rate at which classical information is transmitted by the classical channel is determined entirely by the gradient of the gravitational field. The resulting unconditional dynamics is

$$\frac{d\rho}{dt} = -\frac{i}{\hbar}[H_0, \rho] - \frac{i}{\hbar}K[\hat{x}_1\hat{x}_2, \rho] - \frac{K}{2\hbar}\sum_{k=1}^{2}[\hat{x}_k, [\hat{x}_k, \rho]] \tag{5.19}$$

This is consistent with Diosi's model [195] which gives the same decoherence rate as obtained here under similar approximations [209]. The form of Eq.(5.19) can be generalized to exactly match the one in reference [197] if we include non-cross terms in the feedback. I.e., in equation (9), we could have terms proportional to $(dJ_1/dt)x_1$ and $(dJ_2/dt)x_2$.

There are similarities between Diosi's approach and the measurement mediated approach described here. Both require that the gravitational interaction between the two degrees of freedom be replaced with a noisy interaction. In the measurement based approach this is incorporated in a way which necessarily preserves positivity as the noise arises from a 'hidden' position measurement of the gravitational centre of has co-ordinate. In Diosi's approach we need to explicitly constrain the noise to preserve positivity. More recently Diosi [210] has pointed out that a system subject to weak continuous measurement is a natural example of a quantum-classical hybrid dynamics.

Using the main result of the previous chapter, we can show that, in the case when the two systems are Gaussian, the master equation Eq. (5.19) can never entangle them. This is also true for Eq. (5.17), assuming $\chi_1 = \chi_2$. Further, the gravitational decoherence in the dynamics is minimal in the sense that, if it were any smaller, evolution under Eq. (5.19) would immediately entangle the ground state of the (uncoupled) Hamiltonian, H_0.

To see this we write the Eq.(5.19) in terms of the dimensionless operators $\tilde{x}_k = x_k \left(m\omega/\hbar\right)^{-1/2}$,

$$\frac{d\rho}{dt} = -\frac{i}{\hbar}[H,\rho] - ig[\tilde{x}_1\tilde{x}_2,\rho] - \frac{1}{4}\sum_{k=1}^{2} Y_{ij}[\tilde{x}_i,[\tilde{x}_j,\rho]] \tag{5.20}$$

where $g = \frac{K}{m\omega}$ measures the strength of the gravitational interaction and the matrix $Y_{ij} = \left(\frac{2K}{m\omega}\right)\delta_{ij}$ is the decoherence matrix. Invoking the theorem of the previous chapter, we note that entanglement is never generated if and only if the matrix $Y - 2ig\sigma$ has no negative eigenvalues, where σ is the 2×2 symplectic matrix

$$\sigma = \begin{pmatrix} 0 & 1 \\ -1 & 0 \end{pmatrix} \tag{5.21}$$

Noting that $Y - 2ig\sigma$ has eigenvalues 0 and $4g$ we see that a slightly less noisy matrix $Y_{ij} - \epsilon\delta_{ij}$ produces entanglement for any positive ϵ.

5.4 An experimental test of gravitational decoherence

We now consider the prospects for an experimental observation of the model proposed here. For simplicity we will assume that the two mechanical resonators have the same mass ($m_1 = m_2 = m$) and frequency ($\omega_1 = \omega_2 = \omega$). The last term

in Eq. (5.19) is responsible for two complementary effects: it drives a diffusion process in momentum of each of the oscillators at the rate $\hbar K$, which we will call the gravitational heating rate

$$D_{grav} = \hbar K \tag{5.22}$$

The momentum diffusion leads to heating of the mechanical resonators. It is convenient to define this in terms of the rate of change of the phonon number; the average mechanical energy divided by $\hbar\omega$. The heating rate is then given by

$$R_{grav} = \frac{K}{2m\omega} \tag{5.23}$$

The double commutator term also leads to the decay of off-diagonal coherence in the position basis of each mechanical resonator,

$$\frac{d\langle x_k'|\rho|x_k\rangle}{dt} = (\ldots) - \frac{K}{2\hbar}(x_k' - x_k)^2 \tag{5.24}$$

This shows that the rate of decay of coherence is more rapid the greater the separation of the superposed states. We can use the natural length scale proceeded by the zero-point position fluctuations in the ground state of each resonator to rewrite the decoherence rate as

$$\Lambda_{grav} = \frac{K}{2\hbar}\Delta x_0^2 = \frac{K}{4m\omega} \tag{5.25}$$

Thus the gravitational decoherence rate for position, in natural units, is one half the gravitational heating rate.

These rates can equivalently be expressed in terms of the normal mode splitting

when the gravitational interaction is weak, Eq. (5.8).

$$R_{grav} = \frac{\Delta}{2} \tag{5.26}$$

$$\Lambda_{grav} = \frac{\Delta}{4} \tag{5.27}$$

We thus see that the key parameter responsible for gravitational decoherence is of the order of the normal mode splitting between the two mechanical resonators due to their gravitational coupling. This has significant consequences for observation.

In order to see gravitational decoherence in this model, we need to arrange for the normal mode splitting to be as large as possible. Writing this in terms of the Newton constant, we see that

$$\Delta = \frac{Gm}{\omega d^3} \tag{5.28}$$

In the case of two spheres of radius r, this may be written in terms of the density of the material as

$$\Delta = \frac{4\pi G\rho}{\omega}\left(\frac{r}{d}\right)^3 \tag{5.29}$$

As $d < 2r$, this quantity is bounded

$$\Delta \leq \frac{\pi G\rho}{6\omega} \tag{5.30}$$

We need to use a material with a large density and a mechanical frequency as small as possible. For example, for depleted uranium spheres and a mechanical frequency of one Hertz, we find that $\Delta \sim 10^{-7}\mathrm{s}^{-1}$, a value so small that a terrestrial experiment would be challenging.

In a realistic experiment with low frequency mechanical resonators of the kind considered here, thermal noise and frictional damping will be unavoidable. We can

estimate the relative size of these effects using the quantum Brownian motion master equation [203],

$$\left.\frac{d\rho}{dt}\right|_{diss} = \sum_{j=1}^{2} -i\gamma_k[\hat{x}_j, \{\hat{p}_j, \rho\}] - 2\gamma_j k_B T m_j[\hat{x}_j, [\hat{x}_j, \rho]] \tag{5.31}$$

where γ_k is the dissipation rate for each of the mechanical resonators assumed to be interacting with a common thermal environment at temperature T. If we compare the form of thermal noise in this equation to the form of gravitational decoherence, for the symmetric case, we see that we can assign an effective temperature to the gravitational decoherence rate given by

$$T_{grav} = \frac{\hbar K}{2m\gamma k_B} \tag{5.32}$$

If we write this in terms of the quality factor, Q, for the mechanical resonators, it gives an effective thermal energy scale of

$$k_B T_{grav} = \hbar Q \Delta \tag{5.33}$$

In the example discussed in the previous paragraph for the relatively high value of $Q = 10^9$ we find that $T_{grav} \sim 10^{-9}$K. One would need an ambient temperature less than this to clearly distinguish gravitational decoherence from environmental effects. Possibly gravitationally coupled Bose-Einstein condensates of atomic gases could reach this regime.

However there is currently much interest in using opto-mechanical systems to look for gravitation decoherence. This is largely due to the ability to use laser cooling techniques to prepare harmonically trapped particles of large mass in the ground state [199, 211]. It is possible that carefully controlled optical levitation [212–215],

or magnetic levitation [199, 216] experiments on two gravitationally coupled masses might reach the regime discussed in this chapter but it will not be easy. It should be noted in connection with Eq. 5.33 that laser cooling also changes both the temperature and the quality factor. There will need to be distinct rounds of cooling and coherent control similar to what is done in ion trap experiments. Perhaps the motivation will come from opto-mechanical attempts to fix a better value for G, the Newton gravitational constant. These efforts will help advance these technologies to the point where the kind of decoherence considered here could be ruled out, thus ruling out the possibility of describing gravity as a classical channel.

5.5 Conclusion

In this chapter we have presented a model in which the force of gravity is mediated by a purely classical channel. The channel is defined by considering a continuous weak measurement of the position of each of two masses and feeding forward the classical stochastic record of measurement results to induce the right gravitational force between the masses. As the weak measurement model is entirely consistent with quantum mechanics, exactly the right amount of noise is introduced to ensure that the resulting master equation, when averaged over all measurement records, is positivity preserving. Using a minimal symmetric argument, we find that the model is equivalent to a gravitational decoherence model first proposed by Diosi. As the systematic effect of the gravitational interaction also fixes the size of the noise, minimising the noise leads to a model with no free parameters.

It is well known that a consistent quantum-classical hybrid dynamics leads to problems with positivity of classical phase space distributions and quantum density operators [217]. In our approach these problems are avoided as the classical dynamical component is in fact a quantum measurement signal, explicitly incorporating quantum back-action noise. Another approach to quantum-classical hybrid dynamics has been considered by Hall and Reginato [218].

Our model is a specific example of a general theory of a classically mediated (i.e. non-entangling) force law considered in the previous chapter. Using a result in that paper we find that a classically mediated gravitational channel based on continuous weak measurement can never entangle Gaussian systems. In an experimental setting of two identical gravitationally coupled resonators, this result is manifest as a direct scaling between the normal mode splitting induced by the gravitational force and the gravitational decoherence rate. An experimental test using two gravitationally coupled opto-mechanical resonators would be difficult, but not impossible, with current technology.

Chapter 6: Distinguishing Quantum and Classical Many-Body Systems

Controllable systems relying on quantum behavior to simulate distinctly quantum models so far rely on increasingly challenging classical computing to verify their results. We develop a general protocol for confirming that an arbitrary many-body system, such as a quantum simulator, can entangle distant objects. The protocol verifies that distant qubits interacting separately with the system can become mutually entangled, and therefore serves as a local test that excitations of the system can create non-local quantum correlations. We derive an inequality analogous to Bell's inequality [71, 72] which can only be violated through entanglement between distant sites of the many-body system. Although our protocol is applicable to general many-body systems, it requires finding system-dependent local operations to violate the inequality. A specific example in quantum magnetism is presented.

6.1 Introduction

Quantum simulators can efficiently model quantum systems [13, 14]. However, characterizing and validating such devices is in general difficult. Indeed, quantum state tomography [176] for even eight qubits has required weeks of classical

computational processing time [219] (in addition to exponentially growing measurement requirements). This issue is also present in process tomography, the analogue for quantum channels [220, 221]. Notwithstanding the number of measurements growing exponentially in system size, for systems with 10+ constituents reliable tomography is expected to break down from systematic errors in preparation and measurement [222]. Although these resource scaling problems are partially alleviated with methods based on compressed sensing [76, 223–226], the cost still scales at least linearly with the Hilbert space dimension, and thus exponentially in the number of constituents. Added difficulties arise when data is limited to experimentally accessible local observables [227].

Despite the costs of completely characterizing large quantum systems, there do exist scalable tests giving incomplete – though useful – descriptions of system behavior. For example, techniques such as randomized benchmarking [35,36,78,228] and fidelity estimation [37,38] require a number of measurements polynomial in system size, while still quantifying useful information such as error rates or average gate fidelities. In the case of locally correlated errors, this is sufficient to guarantee the operation of error-corrected quantum computer [39, 40, 229, 230]. Recent linear optics experiments have likewise partially verified implementations of boson sampling, a task which currently cannot be carried out classically [42]. Although it is impossible to efficiently verify this sampling, by using the results of Ref. [231] the authors of Ref. [232] were able to distinguish the sampled distribution from a uniform one. The experiment of Ref. [233] produced similar results, while also checking whether the photon statistics corresponded to indistinguishable particles.

This chapter presents another incomplete test, in the context of quantum simulators of many-body systems (MBS) [234, 235]. It derives from a constructive procedure to entangle two distant ancilla qubits through local interactions with the many-body system. It starts by preparing the system in an initial, known state, composed of many spatially-fixed sites (see Fig. 6.1). We apply a local perturbation to a single site, conditioned on the state of an ancilla qubit in superposition. The simulator then propagates the system forward in time, correlating the ancilla with other sites of the MBS. At one of these distant sites, we apply a second perturbation controlled by a second ancilla qubit. This interaction is chosen to increase the probability amplitude between the current excited MBS state and its initial state, but only does so if both qubits are in the same control state. Qualitatively, excitations induced by the first qubit are conditionally removed by the second. Although both ancillas are now correlated, their correlation with the MBS prevent them from being entangled. We therefore measure the MBS and post-select for it being in its original state. This both disentangles the MBS from the ancillas and increases the probability that they are in the same eigenstate. Finally, we can directly verify that the qubits are entangled (e.g., through state tomography).

6.2 Toy model

As a toy model, we consider a one dimensional transverse field Ising Hamiltonian,

$$\hat{H} = B \sum_i \sigma_x^{(i)} - J \sum_i \sigma_z^{(i)} \otimes \sigma_z^{(i+1)} \,. \tag{6.1}$$

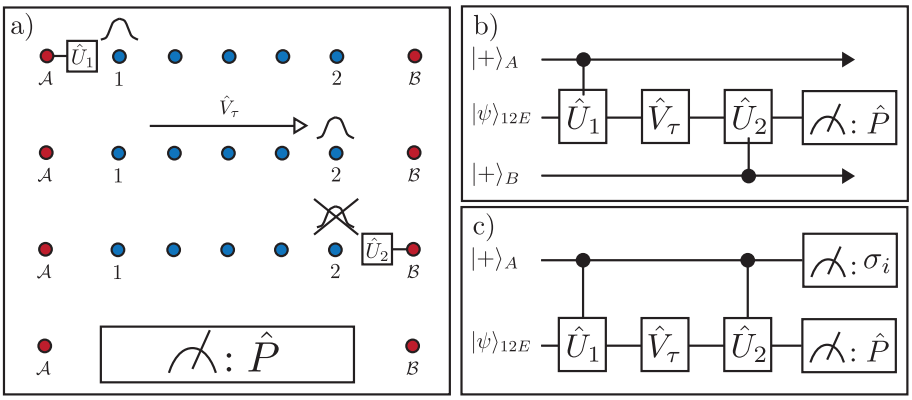

Figure 6.1: **a)** and **b)**: Prototype entangling procedure. Ancilla qubit A prepared as $|+\rangle = (|0\rangle + |1\rangle)/\sqrt{2}$ applies controlled unitary $\hat{U}_1$ to site 1 of the initial MBS state $|\psi\rangle_{12E}$, producing a conditional excited state $(|0\rangle_A \otimes |\psi\rangle_{12E} + |1\rangle \otimes \hat{U}_1 |\psi\rangle_{12E})/\sqrt{2}$. Time evolution $\hat{V}_\tau$ propagates the MBS, spreading the excitation across the system. Ancilla qubit B (also in superposition) then applies controlled unitary $\hat{U}_2$ to site 2, removing the excitation (conditional on its initial state). Finally, a post-selection conditioned on projector $\hat{P}$ is carried out, confirming the MBS has returned to its original state. This projects the ancillas into a (possibly entangled) correlated state. **c)** An analogous protocol using only one ancilla qubit. After post-selection, measurements of the single ancilla are sufficient to determine whether the previous protocol would have entangled the two ancillas.

We write the evolution for a time τ as $\hat{V}_\tau = \exp(-i\tau\hat{H})$. In the $B/J \ll 1$ limit, the eigenstates of $\hat{H}$ are well approximated by eigenstates of the transverse field term, $\hat{H}_J = -J\sum_i \sigma_z^{(i)} \otimes \sigma_z^{(i+1)}$. We therefore assume an initial state of the form

$$|g\rangle = |0\rangle \otimes |0\rangle \otimes \ldots \otimes |0\rangle \ , \tag{6.2}$$

where $\sigma_z |0\rangle = |0\rangle$, which minimizes the energy $\left\langle \hat{H} \right\rangle$ up to corrections of order $B \cdot (B/J)^N$. The lowest lying excitations of $\hat{H}_J$ are described by domain walls. For our protocol to produce entanglement, we use excitations that are indistinguishable from $|g\rangle$ outside a finite region. We therefore consider the evolution of the next lowest excitations of $\hat{H}_J$, involving pairs of domain walls of the form,

$$|e_{i,j}\rangle = \prod_{i \le k \le j} \sigma_x^{(k)} |g\rangle \ , \tag{6.3}$$

where $1 < i \le j < n$. Evolution under $\hat{H} = \hat{H}_J + \hat{H}_B$ disperses these states across the chain [236].

We now consider how to use the MBS to entangle two distant qubits. First, an ancilla qubit (labeled A) in state $|+\rangle = \frac{1}{\sqrt{2}}(|0\rangle + |1\rangle)$ rotates the *second*[1] spin of the chain through controlled-NOT gate, $\hat{U}_{A,2} = |0\rangle\langle 0|_A \otimes \hat{1} + |1\rangle\langle 1|_A \otimes \sigma_x^{(2)}$. This produces the excitation $|e_{2,2}\rangle$ in the chain, conditioned on the state of the ancilla qubit,

$$\hat{U}_{A,2} |+\rangle_A \otimes |g\rangle = \frac{1}{\sqrt{2}} \left(|0\rangle_A \otimes |g\rangle + |1\rangle_A \otimes |e_{2,2}\rangle \right) . \tag{6.4}$$

At this point, the ancilla state is correlated with the MBS, though only at spin 2 of the chain.

[1]Since the first spin only interacts with one neighbor, exciting it would create a single domain wall instead of two.

Continuing with the entangling procedure, we propagate under $\hat{V}_\tau$ for a time $\tau \sim N/B$ in order to spread the correlation with the ancilla across the spin chain as a superposition of excitations. After applying $\hat{V}_\tau$, the $|g\rangle$ component of the MBS acquires only an irrelevant global phase θ, while the excited state $|e_{2,2}\rangle$ disperses over the subspace spanned by $\{|e_{ij}\rangle\}$:

$$\hat{V}_\tau \hat{U}_{A,2} |+\rangle_A \otimes |g\rangle = \frac{1}{\sqrt{2}} \left(e^{i\theta} |0\rangle_A \otimes |g\rangle + |1\rangle_A \otimes \hat{V}_\tau |e_{2,2}\rangle \right) . \tag{6.5}$$

To understand this process, we consider the projection of $\hat{H}_B$ to the linear span of states $|e_{i,j}\rangle$, an approximation valid when $B/J \ll 1$ [237]. We note that $\hat{H}_B$ only couples between adjacent domain walls,

$$\langle e_{i,j}| \hat{H}_B |e_{k,l}\rangle = B(\delta_{i,k+1} + \delta_{i,k-1} + \delta_{j,l+1} + \delta_{j,l-1}) , \tag{6.6}$$

so the evolution of $|e_{2,2}\rangle$ under $\hat{H}$ is equivalent to that of a continuous-time quantum walk in two dimensions [238]. The distinct behaviors of $|g\rangle$ and $|e_{2,2}\rangle$ under $\hat{V}_\tau$ will allow us to distinguish the states of the ancilla through a local operation at spin $N-1$.

After evolving for a time $\tau \sim N/B$, the excitation $\hat{V}_\tau |e_{2,2}\rangle$ has a probability $\sim 1/N^2$ of being localized in state $|e_{N-1,N-1}\rangle$. We verify this numerically by using the quantum walk analogy above. As seen in Fig. 6.2a, the peak transition probability $|\langle e_{N-1,N-1}| \hat{V}_\tau |e_{2,2}\rangle|^2$ scales as $\sim 1/N^2$. Key to the success of our protocol, we note that the unitary σ_x at site $N-1$ maps the excitation $|e_{N-1,N-1}\rangle$ back to the ground state $|g\rangle$. Hence we can applying $\sigma_x^{(N-1)}$ to $\hat{V}_\tau |e_{2,2}\rangle$ to give it a non-zero overlap with the ground state,

$$r = \langle g| \sigma_x^{(N-1)} \hat{V}_\tau |e_{2,2}\rangle = \langle e_{N-1,N-1}| \hat{V}_\tau |e_{2,2}\rangle \neq 0 , \tag{6.7}$$

where $|r|^2 \sim 1/N^2$. The time τ required for the overlap $|r|$ to reach its peak scales linearly with N (Fig. 6.2b), as opposed to a time scale $\sim N^2/B$ observed in diffusive propagation [81].

We can use the fact that $|e_{2,2}\rangle$ can transition to $|e_{N-1,N-1}\rangle$ via $\sigma_x^{(N-1)}$ to entangle ancilla A with a second ancilla, B. After time evolution $\hat{V}_\tau$, we apply a second controlled-NOT gate between B and spin $N-1$,

$$\hat{U}_{N-1,B} = |0\rangle\langle 0|_B \otimes \hat{1} + |1\rangle\langle 1|_B \otimes \sigma_x^{(N-1)}\,. \tag{6.8}$$

The resulting state displays correlations between both ancillas and the MBS,

$$\begin{aligned}
&\hat{U}_{N-1,B}\hat{V}_\tau\hat{U}_{A,2}\,|++\rangle_{AB} \otimes |g\rangle = \\
&\frac{1}{2}\Big(|0\,0\rangle_{AB} \otimes e^{i\theta}\,|g\rangle + |1\,0\rangle_{AB} \otimes \hat{V}_\tau\,|e_{2,2}\rangle + \\
&|0\,1\rangle_{AB} \otimes e^{i\theta}\sigma_x^{(N-1)}\,|g\rangle + |1\,1\rangle_{AB} \otimes \sigma_x^{(N-1)}\hat{V}_\tau\,|e_{2,2}\rangle\Big)\,.
\end{aligned}$$

To motivate the final step, observe that if the ancillas are in either state $|0\,1\rangle_{AB}$ or $|1\,0\rangle_{AB}$, the MBS is necessarily in an excited state. Thus if we measure and post-select the MBS to be in the ground state $|g\rangle$, we project the ancilla qubits into an entangled superposition of states $|0\,0\rangle_{AB}$ and $|1\,1\rangle_{AB}$. This post-selection succeeds with probability $\frac{1+|r|^2}{4}$, and produces the entangled state,

$$\begin{aligned}
&\langle g|\,\hat{U}_{N-1,B}\hat{V}_\tau\hat{U}_{A,2}\,|++\rangle_{AB} \otimes |g\rangle = \\
&\frac{1}{\sqrt{1+|r|^2}}\left(e^{i\theta}\,|0\,0\rangle_{AB} + r\,|1\,1\rangle_{AB}\right)\,.
\end{aligned} \tag{6.9}$$

To conclude the protocol, a measurement of the ancillas would then confirm that the ancillas are entangled.

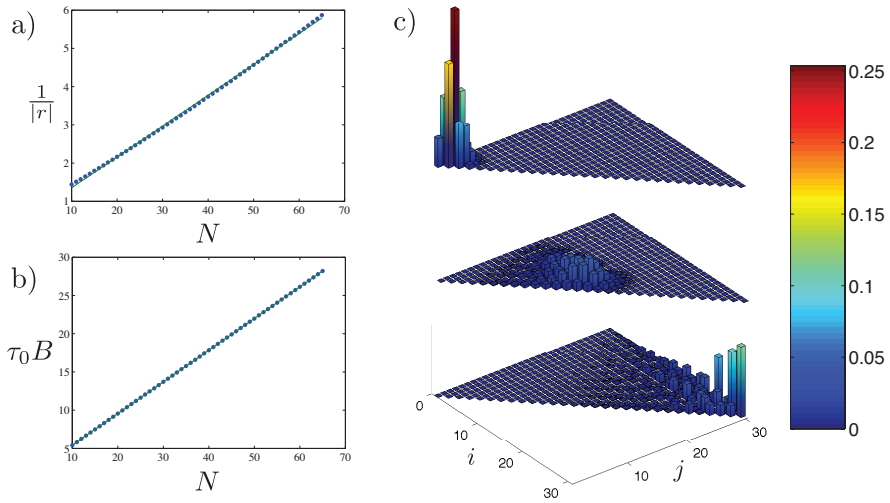

Figure 6.2: Evolution time and ancilla qubit correlation as a function of spin chain length N, in the quantum walk approximation. **a.)** Inverse plot of the peak values of $|r| = |\langle e_{N-1,N-1}| \hat{V}_\tau |e_{2,2}\rangle|$, as a function of chain length N. The numerically calculated values (dots) match closely to the linear fit, with $|r|^{-1} \simeq 0.08N + 0.55$. **b.)** A plot of the time τ_0 taken for the overlap $|r|$ to reach its peak value. The numerically calculated values (dots) match the linear fit as $\tau_0 B \simeq 0.52N + 2.02$. **c.)** A simulation of state occupations $\langle |e_{i,j}\rangle\langle e_{i,j}| \rangle$ in a quantum walk corresponding to $N = 32$ qubits. The system is initialized in state $|e_{2,2}\rangle$ at time $\tau = 0$. The time lapse corresponds to times $\tau = 0.1\tau_0$ (top), $\tau = 0.5\tau_0$ (middle), and $\tau = \tau_0$, where τ_0 corresponds to the peak time determined in the previous fit.

6.3 General protocol

This simple approach can be generalized to a protocol on generic many-body systems. We consider a propagator for an arbitrary many-body Hamiltonian, $\hat{V}_\tau = \exp(-i\hat{H}\tau)$, and an initial prepared ground state $|\psi_{12E}\rangle$ (as we discuss later, this picture can be easily expanded to encompass open quantum systems). The MBS is composed of two local components S_1 and S_2, with E representing the rest of the system. As in the experimental example, we consider two ancilla qubits, interacting locally with S_1 and S_2 at different times. In full, the unitary evolution is

$$C_B(\hat{U}_2)\,\hat{V}_\tau\,C_A(\hat{U}_1)\,|+\rangle_A\,|+\rangle_B\,|\psi_{12E}\rangle\ , \tag{6.10}$$

where $C_A(\hat{U}_1) = |0\rangle\langle 0|_A \otimes \hat{1} + |1\rangle\langle 1|_A \otimes \hat{U}_1$ (with $C_B(\hat{U}_2)$ defined analogously). Importantly, we assume that the local unitaries $\hat{U}_1, \hat{U}_2$ individually bring the MBS to an excited state, though the combined evolution $\hat{U}_2\hat{V}_\tau\hat{U}_1$ produces a non-zero overlap with the ground state. After the second controlled unitary, we make a post-selective measurement on the MBS represented by the projection operator $\hat{P}$. Although this projection can be arbitrary, we assume it confirms that the system has returned to its ground state. As we argued in the example case, this post-selection imparts a known correlation to the ancilla qubits.

The actual test of the MBS derives from verifying that the ancilla qubits are entangled. Writing out the qubit density matrix in the σ_z basis, we have

$$\rho_{ij,i'j'} = \frac{1}{p}\left\langle (\hat{U}_1^\dagger)^{i'}\,\hat{V}_\tau^\dagger\,(\hat{U}_2)^{j'}\,\hat{P}\,(\hat{U}_2^\dagger)^{j}\,\hat{V}_\tau\,(\hat{U}_1)^{i}\right\rangle\ , \tag{6.11}$$

where $\langle\hat{O}\rangle = \langle\psi_{12E}|\,\hat{O}\,|\psi_{12E}\rangle$ refers to an average over the MBS state alone, and p is

the probability of making the projective measurement $\hat{P}$ for the state of Equation (6.10). The product $(\hat{U}_2)^j \hat{V}_\tau (\hat{U}_1)^i$ (with i, j either 0 or 1) represents the unitary evolution of the MBS conditioned on the ancillas being in initial state $|ij\rangle$. Hence to generically determine whether the qubits are entangled, one may carry out full state tomography of the qubits' density matrix which can be done through concurrent local measurements on the individual qubits.

The protocol outlined above is the central result of this chapter. Given the ability to prepare and measure an initial state, it provides a local test verifying that the MBS propagator can generate non-local entanglement. Such a result precludes a description in which subsystems are locally quantum but all correlations between subsystems are essentially classical. In this light, the protocol is akin to a Bell's inequality applied to the system and its dynamics as a whole. Like Bell's inequality, it uses only local operations. It also has a 'loophole': we require that the sites of the MBS are spatially stationary. Otherwise a single site could migrate through the MBS and interact with both ancilla to entangle them, bypassing the need for quantum information to be passed between different sites of the MBS.

The protocol directly extends to the case of open quantum systems. That is, we can apply the same procedure to many-body systems described by a density matrix $\hat{\rho}_{12E}$, whose generic simulator evolution is a trace preserving completely-positive map $\mathcal{S}_\tau$. The extension comes from noting that any such density matrix can be 'purified' by expressing it as a partial trace over an auxiliary system, E':

$$\hat{\rho}_{12E} = \mathrm{tr}_{E'} \left\{ |\psi_{12EE'}\rangle\langle\psi_{12EE'}| \right\} . \tag{6.12}$$

Similarly, the map $\mathcal{S}_\tau$ can be written as a unitary evolution over a larger Hilbert space [239],

$$\mathcal{S}_\tau(\hat{\rho}_{12E}) = \mathrm{tr}_R \left\{ \hat{V}_\tau \left(\hat{\rho}_{12E} \otimes |\psi_R\rangle\langle\psi_R| \right) \hat{V}_\tau^\dagger \right\} . \tag{6.13}$$

Incorporating the extra system R into the auxiliary E', we can generically express the simulator operation as a unitary evolution over an extended pure state, $\hat{V}_\tau|\psi_{12EE'}\rangle\langle\psi_{12EE'}|\hat{V}_\tau^\dagger$, which reduces to $S(\hat{\rho}_{12})$ under the partial trace. Since the system is pure and unitary in this extended picture, the procedure we described previously can be directly applied.

6.4 One qubit protocol

Although the procedure we have presented generically requires two ancilla qubits to be carried out, under certain assumptions this requirement may be loosened. Indeed, although full state tomography on the ancillas is required to generically verify entanglement, we note that by equation (6.11) the qubit density matrix is completely determined by averages over the MBS alone. This means that in certain cases, even in the absence of one of the ancilla qubits, it is possible to test whether entanglement *would* have occurred. Such a test derives from the Peres-Horodecki criterion [149, 240], which states that the ancillas are entangled if and only if the partial transpose matrix ρ^Γ has a negative eigenvalue. This property is characterized by Sylvester's criterion, which states that a square matrix A has no

negative eigenvalues if and only if its principal minors are all non-negative [241],[2]. Hence to confirm that the ancilla qubits are entangled, it is sufficient to check that a single principal minor of ρ^Γ is negative: $\rho^\Gamma_{01,01}\rho^\Gamma_{10,10} - \rho^\Gamma_{01,10}\rho^\Gamma_{10,01} < 0$. We map this statement to an expression on the MBS by using $\rho^\Gamma_{ij,i'j'} = \rho_{ij',i'j}$ and equation (6.11):

$$\left\langle \hat{V}^\dagger \hat{U}_2^\dagger \hat{P} \hat{U}_2 \hat{V} \right\rangle \left\langle \hat{U}_1^\dagger \hat{V}^\dagger \hat{P} \hat{V} \hat{U}_1 \right\rangle < \left| \left\langle \hat{V}^\dagger \hat{P} \hat{U}_2 \hat{V} \hat{U}_1 \right\rangle \right|^2 . \tag{6.14}$$

When this inequality holds, the ancilla qubits become entangled under our protocol. It can only be satisfied when quantum correlations are propagated between spatially distant sites. Importantly, since $\langle \hat{O} \rangle = \langle \psi_{12E} | \hat{O} | \psi_{12E} \rangle$ represents averages over only the state $|\psi_{12E}\rangle$, so it characterizes the many-body system and its evolution alone.

Although inequality (6.14) implies the pair of qubits in the protocol become entangled, it can actually be measured using a single ancilla qubit. First, we note that the product of terms on the left hand side require no ancilla qubits to be measured: for example, the quantity $\langle \hat{V}^\dagger \hat{U}_2^\dagger \hat{P} \hat{U}_2 \hat{V} \rangle$ is simply the probability of measuring the MBS in a state corresponding to projector $\hat{P}$, after having applied the many-body propagator $\hat{V}$ followed by the local unitary $\hat{U}_2$. Contrasting with the left hand terms, the right hand side requires an ancilla qubit to measure. Preparing the ancilla in state $|+\rangle = \frac{1}{\sqrt{2}}(|0\rangle + |1\rangle)$, we follow the same unitary protocol as in equation (6.10), except in this case we use the single ancilla as the control for both unitaries $\hat{U}_1$ and $\hat{U}_2$. Written out, this produces the state

$$|\phi\rangle = \frac{1}{\sqrt{2}} \left(|0\rangle_A \otimes \hat{V} |\psi\rangle + |1\rangle_A \otimes \hat{U}_2 \hat{V} \hat{U}_1 |\psi\rangle \right) . \tag{6.15}$$

[2]The principal minors of a square matrix A_{mn} are the determinants $\det(A^{(s_1, s_2, \cdots s_k)})$, where $A^{(s_1, s_2, \cdots, s_k)}$ is the matrix A truncated to only rows and columns $\{s_1, s_2, \ldots, s_k\}$.

The real and imaginary parts of $\langle \hat{V}^\dagger \hat{P} \hat{U}_2 \hat{V} \hat{U}_1 \rangle$ for the many-body state $|\psi\rangle$ are then the means of $\sigma_x \otimes \hat{P}$ and $\sigma_y \otimes P$ for the compound state $|\phi\rangle$,

$$\left\langle \hat{V}^\dagger \hat{P} \hat{U}_2 \hat{V} \hat{U}_1 \right\rangle = \langle \phi | \, \sigma_x \otimes \hat{P} \, | \phi \rangle + i \, \langle \phi | \, \sigma_y \otimes \hat{P} \, | \phi \rangle \ . \tag{6.16}$$

Preparing the state $|\phi\rangle$ of Equation (6.15) requires the ancilla qubit to interact with both sites of the many-body system, but certain cases require only a single site interaction to measure $\langle \hat{V}^\dagger \hat{P} \hat{U}_2 \hat{V} \hat{U}_1 \rangle$. This occurs when the post-selection projector takes a tensor product form,

$$\hat{P} = \hat{P}_2 \otimes \hat{P}_{1E} \otimes \hat{1}_{E'} \, . \tag{6.17}$$

The product $\hat{P}\hat{U}_2$ can also be written in this way,

$$\hat{P}\hat{U}_2 = \left(\hat{B}_+ + i \hat{B}_- \right) \otimes \hat{P}_{1E} \otimes \hat{1}_{E'} \, . \tag{6.18}$$

where we have written $\hat{P}_2 \hat{U}_2$ in terms of its Hermitian and anti-Hermitian parts, and as before we let E' denote the (inaccessible) environmental degrees of freedom. Using this decomposition, it suffices to prepare the state

$$|\phi'\rangle = \frac{1}{\sqrt{2}} \left(|0\rangle_A \otimes \hat{V} \, |\psi\rangle + |1\rangle_A \otimes \hat{V}\hat{U}_1 \, |\psi\rangle \right) \ , \tag{6.19}$$

which requires only a controlled unitary between the ancilla qubit and site 1 of the MBS. As before, the right hand side of (6.14) can then be written as a sum of observables,

$$\begin{aligned} \left\langle \hat{V}^\dagger \hat{P} \hat{U}_2 \hat{V} \hat{U}_1 \right\rangle \quad &= \langle \phi' | \left(\sigma_x \otimes \hat{B}_+ - \sigma_y \otimes B_- \right) | \phi' \rangle \\ &+ i \, \langle \phi' | \left(\sigma_x \otimes \hat{B}_- + \sigma_y \otimes B_+ \right) | \phi' \rangle \ . \end{aligned} \tag{6.20}$$

We note that with identity (6.11), both of these procedures can be generalized to do complete state tomography.

6.5 Outlook

The ideas we have presented have potential applications in a variety of existing experimental setups. For example, current ion trap experiments have the potential to simulate spin models displaying long-range propagation of correlations [155, 242–246], making them amenable to the single ancilla protocol described above. The models studied have ground states that can be both prepared and measured through direct fluorescence spectroscopy following (if necessary) adiabatic passage. The protocol's ancilla qubit can take the form of either one of the ions present in the system or one of the global motional modes associated with the ion trap. A key requirement in these setups is the ability to individually address single ions in the experiment [247–250]. Alternatively, in optical lattice many-body simulators [7, 251–254] it is possible to use polarization of light as the ancilla qubit. Based on selection rules arising out of angular momentum conservation, the controlled unitary operation of the ancilla would correspond to a polarization-dependent interaction with a localized subsystem. Between interactions the light must be sent through a delay line (e.g., a Fabry-Perot cavity), so that correlations between spatially distant MBS sites are given enough time develop [255, 256].

Chapter 7: Ground State Preparation by Quantum Simulated Cooling

Controlled quantum mechanical devices provide a means of simulating more complex quantum systems exponentially faster than the best known classical simulation methods. Such "quantum simulators" rely heavily upon being able to prepare the ground state of Hamiltonians, whose properties can be used to calculate correlation functions or even the solution to certain classical computations. While adiabatic preparation remains the primary means of producing such ground states, here we provide a different avenue of preparation: cooling to the ground state via simulated dissipation.

7.1 Introduction

Quantum devices provide new opportunities in communication and computation [13,14,16,18,257–261]. One promising application of a well controlled quantum device is simulating a quantum system, which can occur exponentially faster than can be achieved classically [14,15,262,263]. Such simulations could provide insights in many current fields of research, such as BCS-BEC superfluids [6, 7], quantum chemistry [264, 265], and highly correlated condensed matter systems [8–10, 266].

However, a crucial component of such simulation is the specification of the initial state of the system to be simulated. While for some problems such initial states can be prepared [47, 267], in general a means of preparing such states does not exist. Methods for the preparation of specific eigenstates of Hamiltonians, particularly the ground state, therefore remain a pressing challenge for the most interesting quantum simulation applications. A naive approach would be coupling the system to a zero temperature bath to cool it to its ground state. However, fundamental questions about thermalization and convergence to the low T Gibbs ensemble have to date precluded rigorous bounds on cooling efficiency [268–271].

In this chapter we consider the black box query model for cooling a simulated Hamiltonian system. Our approach is inspired by Farhi and Gutmann [272], who introduced the concept of a 'Hamiltonian oracle' as the continuous limit of a discrete oracle. It arises from a common technique for evaluating the complexity of a computational problem, which is to treat a given resource as a black box [273]. That is, one can bound the cost of solving a problem in terms of the number of required queries to an otherwise opaque source of information. In the quantum setting, this approach has provided tight limits on the complexity of many well known problems, including unstructured search [274, 275], abelian hidden subgroup problems such as in period finding [259] and in Simon's algorithm [276], and collision finding [277].

In contrast to the standard query model, we consider a unit query in terms of the simulated evolution time. Within the query model, the black-box 'oracle' can be encoded as a map $|x\rangle \to e^{i\pi s_x} |x\rangle$, where s_x represents the x-th bit of an oracle string s [86, 258]. Connecting this to Hamiltonian evolution, the continuous analogue of a

discrete query is then the maximum total accumulated phase. Indeed, in the binary case, the discrete and continuous models are equivalent in terms of query cost [278]. This also makes sense in terms of computational complexity: the cost of simulating sparse Hamiltonians (including local Hamiltonians) is, up to logarithmic factors, linear in the number of calls to the function describing the non-zero Hamiltonian entries [279–281].

The problem we investigate in this chapter is the quantum query complexity of cooling with limited resources. This is a generalization of the original black box query model, as the goal is no longer to evaluate a function of an oracle string s but rather to generate a specific oracle-dependent state [87, 88]. We assume black box access to time evolution under a Hamiltonian $\hat{H}_S$ and are tasked with preparing its ground state. To do this, we are allowed to include the evolution of a second Hamiltonian, which acts on an ancillary system and allows for interactions with the oracle system. We may also measure and reset the ancilla to allow for energy dissipation; in effect, we cool the system through controlled interactions. We seek to determine the computational power of this model when the allowed interactions with the system are constrained. Specifically, we consider only a finite sized ancilla (a single qubit) that interacts only locally with (i.e., with a small sub-system of) the oracle system. Despite these limitations, we show that, with even one ancilla qubit, the ability to simulate a specific Hamiltonian is sufficient to efficiently reproduce circuit-based quantum computation.

7.2 Grover's Algorithm by Simulated Cooling

As an illustrative example, we apply the method of QSC (Quantum Simulated Cooling) to the Hamiltonian analogue of Grover's algorithm [258]. (Although the arguments given in this section are heuristic, the claims made for the general scheme are rigorously shown in the appendix.) Grover's algorithm is a circuit-based quantum algorithm for finding elements in an unstructured list. In the context of the black box query model, we assume access to the oracle map $|x\rangle \rightarrow e^{i\pi s_x} |x\rangle$, where s_x denotes a single bit in an N bit string. The goal of the search is to find an index x such that $s_x = 0$, while minimizing the required number of calls to the oracle map. Equivalently, we wish to prepare a quantum state that acquires no phase under the oracle operation.

The unstructured search solved by Grover's algorithm may be restated in terms of Hamiltonian evolution. We consider simulated evolution of a Hamiltonian $\hat{H}_S$ on n qubits and which has only two distinct eigenspaces. These are labeled $\mathbf{P}_0$ and $\mathbf{P}_1$, with energies $\omega_0 = 0$ and $\omega_1 > 0$, and correspond to the logical qubit states $|x\rangle$ such that $s_x = 0$ or 1, respectively [1]. For notational simplicity, we let the symbol for a subspace also represent the projector into that subspace. We then have

$$\hat{H}_S \quad = \quad \omega_1 \hat{P}_1. \tag{7.1}$$

Up to a constant factor, the simulation of $\hat{H}_S$ for a fixed time is equivalent in cost to

[1] The logical basis for n qubits is defined by the mutual eigenstates of the individual qubit Pauli Z operators, $\sigma_z |b\rangle = (-1)^b |b\rangle$. For $x = b_0 2^0 + b_1 2^1 + \ldots b_{n-1} 2^{n-1}$, a basis element $|x\rangle$ is denoted by its binary representation $|b_0\rangle |b_1\rangle \ldots. |b_{n-1}\rangle$.

an oracle query of the string s [278]. Hence finding x such that $s_x = 0$ is equivalent to preparing the ground state of $\hat{H}_S$ [176, 272].

The simulated cooling algorithm works by exchanging energy between the simulated Hamiltonian system and a concurrently simulated bath. We consider just a single, two-level bath, with Hamiltonian

$$\hat{H}_B = \omega_B \mathbf{1}_S \otimes \hat{P}_\uparrow \,, \tag{7.2}$$

where $\hat{P}_\uparrow = |\uparrow\rangle\langle\uparrow|$ is the rank one projection operator corresponding to the eigenvector $\sigma_z |\uparrow\rangle = |\uparrow\rangle$. To do cooling we prepare the bath in its ground state $|\downarrow\rangle$ and the system in an initial state $|F\rangle$. (For the moment we assume that $|F\rangle$ is an arbitrarily chosen state.) We then simulate the non-interacting Hamiltonian $\hat{H}_S + \hat{H}_B$ concurrently with an interaction term,

$$\hat{V} = \Omega_0 |F\rangle\langle F| \otimes \sigma_x \,. \tag{7.3}$$

We note that the operator $|F\rangle\langle F|$ is highly non-local: for a system composed of many distinct subsystems, this operator acts non-trivially on all subsystems at once. Such an interaction is difficult to implement in practice, and in the generic case we will assume access to only a local interaction, i.e., between a few subsystems and the bath.

The evolution of the system under the simulated Hamiltonians can be effectively described through perturbation theory [282]. To do so we decompose $|F\rangle$ into its spectral components:

$$|F\rangle = x_0 |0\rangle + x_1 |1\rangle \,, \tag{7.4}$$

where $x_j |j\rangle = \hat{P}_j |F\rangle$ and x_j is real and non-negative. The complete Hamiltonian $\hat{H}_S + \hat{H}_B + \hat{V}$ maps the linear span $\mathbf{S} = \text{Span}\{|0\rangle|\downarrow\rangle, |0\rangle|\uparrow\rangle, |1\rangle|\downarrow\rangle, |1\rangle|\uparrow\rangle\}$ to itself, hence for initial state $|F\rangle|\downarrow\rangle$ we may reduce our analysis to this subspace. Written explicitly, within $\mathbf{S}$ the full Hamiltonian takes the form

$$(\hat{H}+\hat{V})|_{\mathbf{S}} = \left(\begin{array}{c|cccc} & (0\downarrow) & (0\uparrow) & (1\downarrow) & (1\uparrow) \\ \hline (0\downarrow) & 0 & \Omega_0 x_0^2 & 0 & \Omega_0 x_0 x_1 \\ (0\uparrow) & \Omega_0 x_0^2 & \omega_B & \Omega_0 x_0 x_1 & 0 \\ (1\downarrow) & 0 & \Omega_0 x_0 x_1 & \omega_1 & \Omega_0 x_1^2 \\ (1\uparrow) & \Omega_0 x_0 x_1 & 0 & \Omega_0 x_1^2 & \omega_1+\omega_B \end{array}\right).$$

To implement a resonant exchange of energy between system and bath, we set their energies to be approximately equal ($\omega_1 \approx \omega_B$) while keeping the interaction strength Ω_0 perturbatively small. The states $|0\rangle|\uparrow\rangle$ and $|1\rangle|\downarrow\rangle$ are then nearly degenerate, so we expect superpositions of these states to form eigenstates of $\hat{H}_S + \hat{H}_B + \hat{V}$. As $\hat{V}$ has no diagonal terms in the above basis, perturbation theory implies that even orders of Ω_0 cause the energy levels of $\hat{H}_S + \hat{H}_B + \hat{V}$ to shift, while the odd orders cause the eigenstates to mix. Indeed, in the perturbative limit $|\Omega_0/\omega_1| \ll 1$, the dynamics of $|0\rangle|\downarrow\rangle, |1\rangle|\uparrow\rangle$ are effectively governed by the effective Hamiltonian [237]

$$\begin{aligned} \hat{H}_{eff} = &\left(\omega_B + \frac{x_0^4\Omega_0^2}{\omega_B}\right)|0\rangle\langle 0| \otimes |\uparrow\rangle\langle\uparrow| \\ &+ \left(\omega_1 + \frac{x_1^4\Omega_0^2}{\omega_B}\right)|1\rangle\langle 1| \otimes |downn\rangle\langle downn| \\ &+ \Omega_0 x_0 x_1 \left(|0\rangle\langle 0| \otimes |\uparrow\rangle\langle\uparrow| + \text{h.c.}\right), \end{aligned} \tag{7.5}$$

where we have dropped terms of order $O(\Omega_0^3)$.

The form of the effective Hamiltonian gives a prescription for simulated cool-

ing. With knowledge of x_0 and x_1, we could compute the two diagonal entries of $\hat{H}_{eff}$ (in equation (7.5)) to all orders in Ω_0 [283], and adjust ω_B accordingly so that they are equal. Time evolution under $\hat{H}_S + \hat{H}_B + \hat{V}$ then causes coherent oscillations between $|0\rangle|\uparrow\rangle$ and $|1\rangle|\downarrow\rangle$, at a rate $\Omega \approx \Omega_0 x_0 x_1$. Conversely, since the other states $|0\rangle|\downarrow\rangle$ and $|1\rangle|\uparrow\rangle$ are *not* approximately degenerate under the non-interacting Hamiltonian, to leading order they are still eigenstates of $\hat{H}_S + \hat{H}_B + \hat{V}$. An initial state $|F\rangle|\downarrow\rangle$ and evolution time $\tau = \frac{\pi}{2\Omega}$ would therefore satisfy

$$e^{-i\tau(\hat{H}_S+\hat{H}_B+\hat{V})}\left(x_0|0\rangle|\downarrow\rangle + x_1|1\rangle|\downarrow\rangle\right) \approx x_0|0\rangle|\downarrow\rangle + x_1|0\rangle|\uparrow\rangle,$$

so that the system is mapped to a ground state of $\hat{H}_S$.

The simulation time required for cooling scales in the same way as the number of oracle queries in Grover's algorithm. To see this, assume that $\hat{H}_S$ corresponds to an $n-$qubit Hilbert space of dimension $N = 2^n$, and $M = \dim \mathbf{P}_0$ is the rank of the ground space projector $\hat{P}_0$. Assuming the projectors $\hat{P}_0$ and $\hat{P}_1$ are diagonal in the logical basis[2], the initial state we use is $|F\rangle = \frac{1}{\sqrt{N}}\sum_x |x\rangle$, which is equal to the product state $|+\rangle^{\otimes n}$, with $|+\rangle = \frac{1}{\sqrt{2}}(|0\rangle + |1\rangle)$. The amplitude $x_0 = \sqrt{\langle F|\hat{P}_0|F\rangle}$ is then exactly $\sqrt{M/N}$. The evolution time τ needed to map between $|1\rangle|\downarrow\rangle$ and $|0\rangle|\uparrow\rangle$ is set as $\tau = \frac{\pi}{2\Omega}$, where $\Omega = \Omega_0 x_0 x_1$ is the coherent oscillation rate. As expected, τ scales linearly with $|x_0|^{-1} = \sqrt{N/M}$, reflecting the expected quadratic speedup of Grover's algorithm and analogous implementations based on adiabatic state preparation [272,284]. This scaling with $|x_0|^{-1}$ will also apply to generalizations of QSC to more complicated Hamiltonians.

[2]An analogous assumption is made for the oracle in the original Grover's algorithm [274].

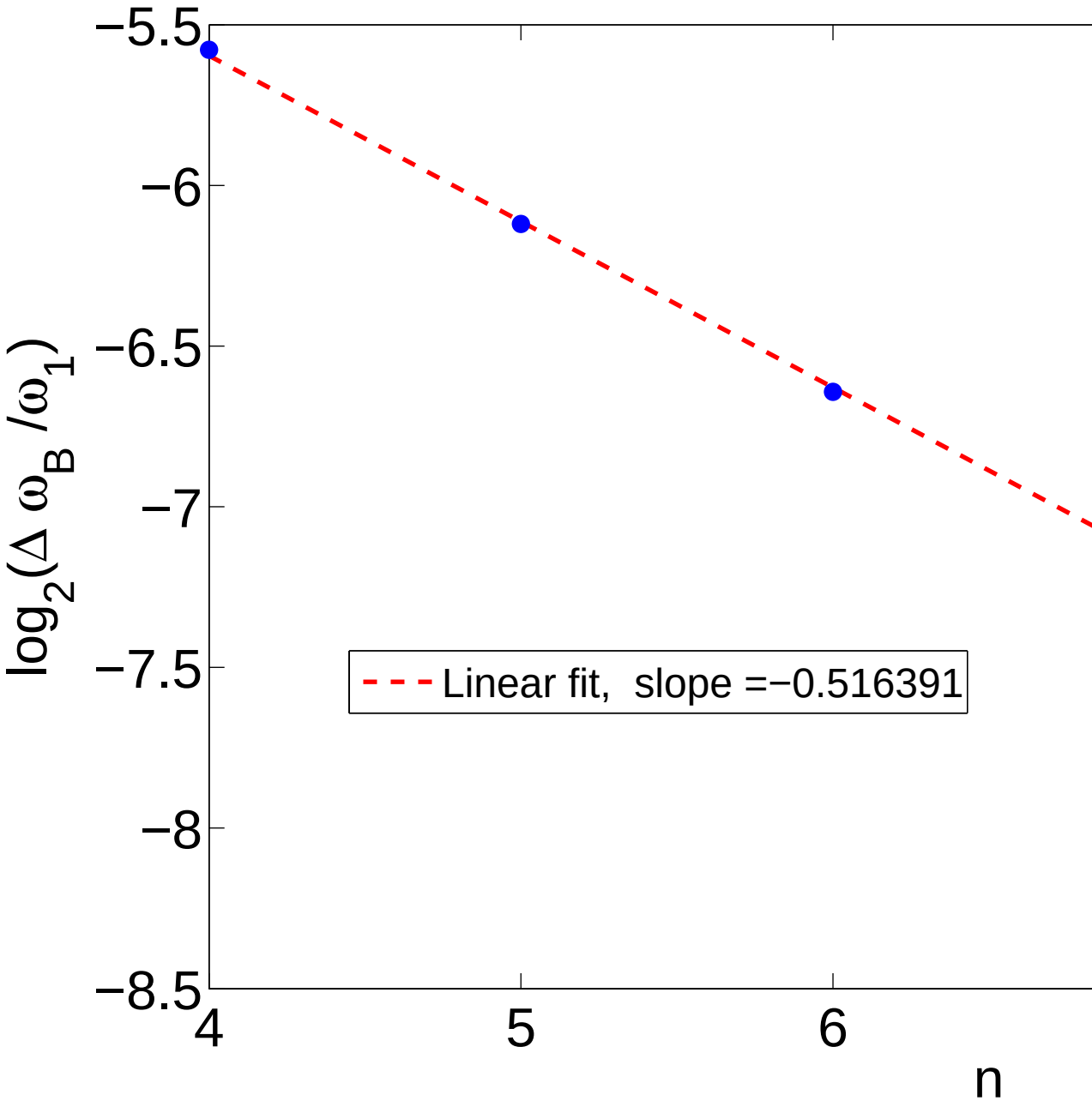

Figure 7.1: The sensitivity of the Grover cooling scheme to errors in bath detuning, as a function of system size. We assume the Hamiltonian $\hat{H}_S$ describes a system of n qubits with corresponding Hilbert space dimension 2^n. In this case the ground overlap of the initial state $|F\rangle$ is exponentially small, $\langle F|\,\hat{P}_0\,|F\rangle = 2^{-n}$. *Inset:* The cooling fidelity $\langle F\uparrow|\,e^{i(\hat{H}_S+\hat{H}_B+\hat{V})\tau}\,\hat{P}_0\,e^{-i(\hat{H}_S+\hat{H}_B+\hat{V})\tau}\,|F\rangle\,|\uparrow\rangle$ as a function of the bath detuning, $(\omega_B-\omega_1)/\omega_1$, for $n=7$ qubits. The vertical dashed line represents the

We note that the values of x_0 and x_1 must be known to set the evolution time τ correctly, as well as account for the energy level shift induced by $\hat{V}$. This is significant, since for $|x_0| \ll |x_1| \approx 1$, the level shift of state $|1\rangle|\downarrow\rangle$ in equation (7.5) is approximately $\frac{\Omega_0^2}{\omega_B}$, which is non-negligible compared to the coupling $\Omega_0 x_0 x_1$. As seen in Figure 7.1, if this shift is not accounted for, the scheme's success rate becomes exponentially small with increasing system size. Thus, as will also be true in the generic case, knowledge of the size of the coefficients x_j is critical to success of our scheme. To circumvent this requirement, in a later section we present a second, modified scheme that succeeds probabilistically in the same time as the original. For the case of the Grover Hamiltonian above, we could then select $|F\rangle$ from a random sample [285], so that on average $|x_0|^2 \approx M/N$. The modified algorithm is analogous to amplitude amplification [286] (a generalization of Grover's algorithm) in the sense that the square root scaling is achieved without knowledge of the initial state.

7.3 Quantum Simulated Cooling

The general QSC algorithm is able to cool a class of Hamiltonians with a specific, known structure. Specifically, we consider a subspace $\mathbf{S}$ that is a direct sum of eigenspaces of $\hat{H}_S$. We assume that $\mathcal{S}$ contains the ground state of $\hat{H}_S$ and that the energies corresponding to $\mathcal{S}$ are non-degenerate with those of its complement, $\mathbf{S}_\perp$. Within $\mathbf{S}$ the simulated Hamiltonian $\hat{H}_S$ has $L+1$ non-degenerate eigenstates,

$$(\hat{H}_S)|_{\mathbf{S}} = \sum_{j=0}^{L} \omega_j |j\rangle\langle j| \,, \tag{7.6}$$

where $\omega_0 = 0$ and $\omega_j > \omega_{j-1}$. A parameter of interest is the general spectral gap between these energies,

$$\Delta = \min_{\omega_j, E} \{ |E - \omega_j| : E \in \mathrm{Spec}(H_S), E \neq \omega_j \} . \tag{7.7}$$

The size of Δ will bound strength of the interaction between the system and bath, since this interaction must be perturbatively small for coherent oscillations to occur. Thus, as in adiabatic quantum computation, the inverse gap Δ^{-1} sets a natural time scale for the algorithm. Importantly, we assume that the energies ω_j are known, and also that we may initialize the system in the subspace $\mathbf{S}$. As in other quantum algorithms [87, 287], these QSC criteria reflect the need for some knowledge about a given problem (e.g., a known symmetry of the system) in order for it to be solved efficiently.

As before, the simulated system is cooled through a simple interaction with a single qubit bath. The bath Hamiltonian is defined in the same way, $\hat{H}_B = \omega_B \mathbf{1}_S \otimes \hat{P}_\uparrow$, where ω_B is the tunable qubit gap. This gap is set resonant with a given system transition, so that a system-bath interaction $\hat{V}$ transfers energy between the system and bath. The interaction is written generically as

$$\hat{V} = \hat{T}_S \otimes \sigma_x , \tag{7.8}$$

where $\hat{T}_S$ is a Hermitian operator acting on the system. Unlike in the Grover example, $\hat{T}_S$ does not need to be highly non-local. Rather, we only require that the projection of $\hat{T}_S$ to $\mathbf{S}$ is of rank one,

$$(\hat{T}_S)|_{\mathbf{S}} = \Omega_0 |G\rangle\langle G| , \tag{7.9}$$

where the state $|G\rangle$ has a spectral decomposition,

$$|G\rangle = \sum_{j=0}^{L} x_j |j\rangle \ . \tag{7.10}$$

As in the Grover case, we assume knowledge of the coefficients x_j so that we may correctly set the bath gap ω_B and evolution time.

Though all of this structure seems cumbersome, in the next section we will show that it applies directly to a variant of Kitaev's clock Hamiltonian [288]. The ground state of this Hamiltonian corresponds to the outcome of a generic circuit-based quantum computation, and the total time for cooling this Hamiltonian scales polynomially with the corresponding circuit's size. Importantly, in that case there exists an operator $\hat{T}_S$ satisfying property (7.9) and acting on only a single degree of freedom of the system. We will therefore show that our model of local simulated cooling is computationally equivalent to standard quantum computation.

The QSC algorithm works by successively implementing transitions from every excited state $|j\rangle$ to the ground state. Letting the system start in any initial state within subspace $\mathbf{S}$, we initialize the bath in state $|\uparrow\rangle$ and its gap ω_B near the maximal system energy ω_L. This makes $|L\rangle|\downarrow\rangle$ and $|0\rangle|\uparrow\rangle$ nearly degenerate eigenstates of $\hat{H}_S + \hat{H}_B$, so that evolution under $\hat{H}_S + \hat{H}_B + \hat{V}$ causes a transition between them. In order for this transition to be favorable, we must calculate the perturbative energy level shifts induced by $\hat{V}$ on these states[3]. We correspondingly adjust ω_B so that $|L\rangle|\downarrow\rangle$ and $|0\rangle|\uparrow\rangle$ are degenerate when accounting for the even order corrections in

[3]Such a calculation – detailed in the appendix – is equivalent to finding a root of a degree L polynomial to accuracy $1/\text{poly}(L)$, and is possible since one may explicitly calculate the coefficients x_j in (7.10).

$\hat{V}$ (see Fig. 7.2). Incorporating the odd order corrections, the approximate eigenstates of $\hat{H}_S + \hat{H}_B + \hat{V}$ become $|0\rangle|\uparrow\rangle \pm |L\rangle|\downarrow\rangle$, with a corresponding energy splitting $\Omega = \Omega_0 |x_0 x_L| (1 + O(\Omega_0/\Delta))$. Evolving under $\hat{H}_S + \hat{H}_B + \hat{V}$ for time $\tau^{(L)} = \frac{\pi}{2\Omega}$ thus coherently maps $|L\rangle|\downarrow\rangle$ to the state $|0\rangle|\uparrow\rangle$. Conversely, since the lower energy states $\{|j\rangle|\downarrow\rangle\}_{j=0}^{L-1}$ of $\hat{H}_S + \hat{H}_B$ are not degenerate with any corresponding $|\uparrow\rangle$ state, by energy conservation their occupation probabilities remain unchanged. A measurement of the bath in state $|\uparrow\rangle$ therefore indicates that the system has transitioned to the ground state, so we may terminate the algorithm. A measurement of $|\downarrow\rangle$, on the other hand, implies that we have projected the system to space spanned by $\{|j\rangle|\downarrow\rangle\}_{j=0}^{L-1}$. We would therefore decrement ω_B to a corresponding value near ω_{L-1}, and implement an analogous procedure for the transition $|L-1\rangle|\downarrow\rangle \to |0\rangle|\uparrow\rangle$. Repeating this process for at most L evolutions, we reach the ground state with high probability.

7.4 Perturbative tools, Simulation errors, and Timing

To rigorously evaluate the fidelity of simulated cooling in the presence simulation errors, we use the method of resolvents [283, 289] to precisely approximate the spectrum and eigenvectors of $\hat{H}_S + \hat{H}_B + \hat{V}$. The resolvent of a generic Hamiltonian $\hat{H}$ (also known as the Green's function) is the meromorphic function

$$\hat{G}(z) = (z\mathbf{1} - \hat{H})^{-1}, \tag{7.11}$$

whose singularities correspond to the eigenvalues of $\hat{H}$ [290]. It can be loosely interpreted as the Fourier transform of $\exp(-i\tau\hat{H})$. Within this formalism we consider

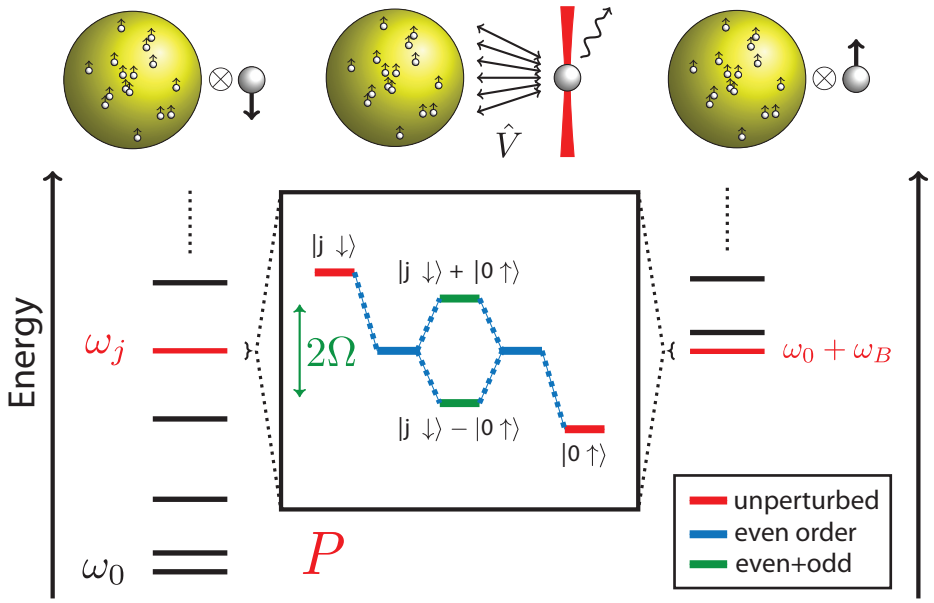

Figure 7.2: The spectrum of $\hat{H}_S + \hat{H}_B$ during the cooling of energy level j. The left and right columns represent the spectrum of the composite system when the bath spin is in its ground and excited state, respectively. The bath gap ω_B is adjusted so that eigenstate $|0\rangle|\uparrow\rangle$ on the right is nearly degenerate with eigenstate $|j\rangle|\downarrow\rangle$ on the left. The inset (center column) shows the effect of the interaction $\hat{V}$ on these unperturbed eigenstates. The blue energy levels are shifted by the even order perturbative corrections in $\hat{V}$ (which are diagonal in the $|j\rangle|\downarrow\rangle, |0\rangle|\uparrow\rangle$ basis). The value of ω_B is accordingly adjusted so that these shifted energies are exactly degenerate. The odd order corrections in $\hat{V}$ couple these states, so including both even and odd orders (green) causes a splitting of 2Ω between the new eigenstates $|j\rangle|\downarrow\rangle \pm |0\rangle|\uparrow\rangle$. Evolving for time $\tau^{(j)} = \pi/(2\Omega)$ maps $|j\rangle|\downarrow\rangle$ to $|0\rangle|\uparrow\rangle$. The bath spin is then measured and, if no transition has occurred, the process is repeated for energy level $j-1$.

a subspace $\mathbf{P}$ spanned by the eigenvectors of $\hat{H}$ corresponding to an isolated energy range (ω_-, ω_+) and study how the dynamics within $\mathbf{P}$ are changed when a perturbation $\hat{V}$ is added to $\hat{H}$. Projecting the perturbed resolvent $\tilde{G}(z) = (z\mathbf{1} - \hat{H} - \hat{V})^{-1}$ into $\mathbf{P}$ defines the corresponding self-energy operator[4] ,

$$(\tilde{G}(z))|_{\mathbf{P}} = \hat{P}\tilde{G}(z)\hat{P} = \frac{1}{z\hat{P} - \hat{\Sigma}(z)} \,. \tag{7.12}$$

Heuristically speaking, if the self-energy $\hat{\Sigma}(z)$ is approximately constant for z near the range (ω_-, ω_+), we can consider it as a Hamiltonian for time evolution within $\mathbf{P}$. Indeed, we can define an effective Hamiltonian $\hat{H}_{eff}$ for $\mathbf{P}$ by approximating $\hat{\Sigma}(z)$. As long as the spectral norm $||\hat{\Sigma}(z) - \hat{H}_{eff}||$ is bounded for an appropriate range of z, the work of Ref. [289] shows that $\hat{H}_{eff}$ closely approximate the eigenvalues of $\hat{H} + \hat{V}$ near the range (ω_-, ω_+). We extend these perturbative results (in the appendix) to show when the eigenvectors of $\hat{H}_{eff}$ also approximate those of $\hat{H} + \hat{V}$. This allows us to give definite bounds on the deviations from the expected transitions in each cooling step of the algorithm.

The calculations describing each step of the algorithm begin by assuming a simplified form for the interaction and neglecting any sources of simulation error. Thus, for the cooling of energy level j we consider the (idealized) unitary

$$\hat{U}_j^{(0)} = \exp\left(-i\tau^{(j)}(\hat{H}_S + \hat{H}_B^{(j)} + \Omega_0 |G\rangle\langle G| \otimes \sigma_x)\right) \,, \tag{7.13}$$

where $\hat{H}_B^{(j)} = \omega_B^{(j)} \mathbf{1}_S \otimes \hat{P}_\uparrow$ is the bath Hamiltonian with gap $\omega_B^{(j)} \approx \omega_j$ and we have projected $\hat{T}_S$ into subspace $\mathbf{S}$ (as in equation (7.9)). We derive the evolution of

[4]This definition is slightly different from the physics literature though we use it here for notational convenience. The typical definition is $\tilde{G}|_{\mathbf{P}} = (z\hat{P} - \hat{P}\hat{H}\hat{P} - \hat{\Sigma}(z))^{-1}$.

states $|j\rangle|\downarrow\rangle$ and $|0\rangle|\downarrow\rangle$ by computing an effective Hamiltonian that approximates their self-energy operator. We set the unperturbed Hamiltonian as $\hat{H} = \hat{H}_S + \hat{H}_B^{(j)}$ and compute $\hat{\Sigma}(z)$ for the subspace spanned by these two states. Letting $\hat{P}$ be the projector into $\mathbf{P}$ and $\hat{Q} = \mathbf{1} - \hat{P}$, the self-energy operator can be written explicitly as [283]:

$$\begin{aligned}\hat{\Sigma}_P(z) &= \hat{P}\hat{H}\hat{P} + \hat{P}\hat{V}\hat{P} + \hat{P}\hat{V}\hat{Q}\frac{1}{z - \hat{Q}(\hat{H}+\hat{V})\hat{Q}}\hat{Q}\hat{V}\hat{P} \\ &= \hat{P}\hat{H}\hat{P} + \hat{P}\hat{V}\hat{P} + \sum_{k\geq 1}\hat{P}\hat{V}(\hat{G}_Q(z)\hat{V})^k\hat{P}\,, \end{aligned} \tag{7.14}$$

where $\hat{G}_Q(z) = (zQ - \hat{Q}\hat{H}\hat{Q})^{-1}$ and $\hat{V} = \Omega_0|G\rangle\langle G| \otimes \sigma_x$. The simplified form of $\hat{V}$ allows us to explicitly compute $\hat{\Sigma}(z)$ to all orders in Ω_0 (see the appendix). We correspondingly define the effective Hamiltonian as $\hat{H}_{eff} = \hat{\Sigma}(\omega_B^{(j)})$, which allows us to bound the difference $||\hat{\Sigma}(z) - \hat{H}_{eff}||$ through Taylor series expansion. With this bound we use the result of ref. [289] and its extension to show that both the two non-trivial eigenvalues and eigenvectors of $\hat{H}_{eff}$ approximately correspond to those of $\hat{H} + \hat{V}$. This allows us to predict the dynamics under the true Hamiltonian, $\hat{H} + \hat{V}$, and to show that the state $|j\rangle|\downarrow\rangle$ is mapped to $|0\rangle|\uparrow\rangle$ with bounded error. Furthermore, the calculation of $\hat{H}_{eff} = \hat{\Sigma}(\omega_B^{(j)})$ allows us to exactly determine bath gap $\omega_B^{(j)}$ and evolution time $\tau^{(j)}$ required for this transition to occur. As in the Grover example, the value of $\omega_B^{(j)}$ is set so that the diagonal entries of the effective Hamiltonian, $\langle j|\langle\downarrow|\hat{H}_{eff}|j\rangle|\downarrow\rangle$ and $\langle 0|\langle\uparrow|\hat{H}_{eff}|0\rangle|\uparrow\rangle$, are identical. Likewise the simulation time is determined by the coupling between these states, $\Omega^{(j)} = |\langle j|\langle\downarrow|\hat{H}_{eff}|0\rangle|\uparrow\rangle| = \Omega_0|x_0x_j|(1 + O(\Omega_0/\Delta))$, so that $\tau^{(j)} = \frac{\pi}{2\Omega^{(j)}}$.

Using the mathematical tools described above, we can bound the error in the

unitary evolution as a function of the perturbative parameter $r = \Omega_0/\Delta$. Furthermore, by using other results from matrix perturbation theory [282], we are able to incorporate the effect of the true interaction $\hat{T}_S \otimes \sigma_x$ and a possible simulation error term $\hat{\delta}_j$. Hence the error in the simulation is set by true measure of infidelity, $1 - |\langle 0| \langle \uparrow| \hat{U}_j |j\rangle |\downarrow\rangle|^2$, where

$$\hat{U}_j = \exp\left(-i\tau^{(j)}(\hat{H}_S + \hat{H}_B^{(j)} + \hat{T}_S \otimes \sigma_x + \hat{\delta}_j)\right) . \tag{7.15}$$

Our error bounds are determined by the Hamiltonian spectral gap Δ and the size of the previously neglected terms. In the appendix we show that the total error in each unitary evolution scales as $O(\Omega_0/\Delta)$ as long as the following inequalities hold:

$$\begin{aligned} r \equiv \Omega_0/\Delta &< 1/8 \\ \frac{||\hat{S}\hat{\delta}_j\hat{S}||}{\Delta} &< r^2 \cdot |x_0 x_j| \\ \frac{||\hat{S}(\hat{T}_S + \hat{\delta}_j)\hat{S}_\perp||^2}{\Delta^2} &< r^2 \cdot |x_0 x_j| \\ \frac{||\hat{S}_\perp(\hat{T}_S + \hat{\delta}_j)\hat{S}_\perp||}{\Delta} &< 1/2\,. \end{aligned} \tag{7.16}$$

Here $\hat{S}$ is the projector into the assumed subspace $\mathbf{S}$ containing the ground state of $\hat{H}_S$, as described in equation (7.6), while $\hat{S}_\perp$ projects into its orthogonal complement. These inequalities ensure that the energy gap between the targeted states and all other states is large enough to prevent unwanted transitions from occurring.

We can express the complete QSC algorithm and compute its fidelity and timing using the language of trace-preserving, completely positive (TCP) maps [291–293]. Accordingly, we consider each step of the algorithm as a measurement of the bath followed by a unitary evolution conditional on the measurement outcome. The

TCP map for the cooling of level j is then

$$\begin{aligned}\mathcal{E}_j(\hat{\rho}) = \hat{U}_j(\mathbf{1}_S \otimes \hat{P}_\downarrow)\,\hat{\rho}\,(\mathbf{1}_S \otimes \hat{P}_\downarrow)\hat{U}_j^\dagger \\ + (\mathbf{1}_S \otimes \hat{P}_\uparrow)\hat{\rho}(\mathbf{1}_S \otimes \hat{P}_\uparrow)\,,\end{aligned} \tag{7.17}$$

where $\hat{\rho}$ is a density matrix for the system and bath, and $\hat{U}_j$ is the defined as in equation (7.13). The TCP map describing the complete algorithm is then $\mathcal{E} = \mathcal{E}_1 \circ \mathcal{E}_2 ... \circ \mathcal{E}_L$. As expected, if the bath transitions into the excited state $|\uparrow\rangle$ during cooling of level j (indicating the algorithm should terminate), the application of steps $\mathcal{E}_{j-1}$ through $\mathcal{E}_1$ acts as an identity operation. Expressing the output of the algorithm, for any density matrix $\hat{\rho}_S$ supported in $\mathbf{S}$ we have

$$\mathcal{E}(\hat{\rho}_S \otimes |\downarrow\rangle\langle\downarrow|) = \lambda_0 \hat{\rho}_0 + \hat{R}, \tag{7.18}$$

where $\lambda_0 \geq 0$ and $\hat{\rho}_0$ is a density matrix made up of states $|0\rangle\,|\downarrow\rangle$ and $|0\rangle\,|\uparrow\rangle$. The operator $\hat{R}$ represents the accumulated error from all L steps of the algorithm and sets the corresponding infidelity,

$$\begin{aligned}\epsilon =& 1 - \mathrm{Tr}[(|0\rangle\langle 0| \otimes \mathbf{1}_B)\mathcal{E}(\rho_S \otimes |\downarrow\rangle\langle\downarrow|)] \\ =& 1 - \lambda_0 - \mathrm{Tr}[(|0\rangle\langle 0| \otimes \mathbf{1}_B)\hat{R}]\,.\end{aligned} \tag{7.19}$$

Building on the analysis described above, we show that both $1 - \lambda_0 = \mathrm{Tr}[\hat{R}]$ and $\mathrm{Tr}[(|0\rangle\langle 0| \otimes \mathbf{1}_B)\hat{R}] \leq 2||\hat{R}||$ scale as $O(L^2\sqrt{L}\Omega_0/\Delta)$. Thus for the algorithm to prepare the ground state with fidelity at least $1-\epsilon$, we must scale the relative interaction strength $r = \Omega_0/\Delta$ as

$$r = O(\frac{\epsilon}{L^2\sqrt{L}})\,. \tag{7.20}$$

Since the time required for cooling step j is $\tau^{(j)} = (r\Delta)^{-1}\frac{\pi}{2|x_0 x_j|}$ (to leading order in

r), the total simulation time of the algorithm may be computed as

$$\begin{aligned}\sum_{j=1}^{L}\tau^{(j)} &= \frac{1}{r\Delta}\frac{\pi}{2}\sum_{j=1}^{L}\frac{1}{|x_0x_j|} \\ &= O\left(\frac{L^2\sqrt{L}}{\epsilon\Delta}\right)\sum_{j=1}^{L}\frac{1}{|x_0x_j|}\,.\end{aligned} \tag{7.21}$$

Generalizing the Grover example case, we see that the cost of the algorithm is related to the inverse amplitudes $|x_j|^{-1}$ describing the interaction state $|G\rangle$ in equation (7.10). In the case where $|x_j|$ is exponentially small in the system size for some $j > 0$, it is possible to skip the cooling of this energy level. As discussed later, doing so increases the error rate ϵ by the probability that the initial state $\hat{\rho}_S$ has energy ω_j.

7.5 Cooling a Quantum Circuit

Here we show how QSC can be used to produce the outcome of a chain of 2-qubit unitary operations, $\hat{U}_c = \hat{U}_L\hat{U}_{L-1}...\hat{U}_1$, with a total simulation time scaling as $O(\text{poly}(L))$. Since 1- and 2-qubit unitaries are sufficient to implement any efficient quantum computation [33, 145], any problem efficiently solved through standard quantum computation can also be solved using QSC with at most a polynomial overhead. The idea behind our result draws from the work of Ref. [85], which shows that adiabatic quantum computation is equivalent to standard quantum computation.

We wish to define a Hamiltonian whose unique ground state (after tracing out any ancilla qubits) can be made arbitrarily close to the outcome of a computation $\hat{U}_c$ on n qubits. One $\hat{H}_S$ satisfying this requirement is a variant of Kitaev's clock

Hamiltonian [288]. To describe it we consider a particle on a one dimensional lattice with $L+1$ sites, whose internal state is described by n qubits [294]. For a given site l, the particle has fixed on-site energy ω, but may also tunnel to neighboring sites $l \pm 1$ through a coupling term $-\frac{\omega}{2} \cdot \hat{U}_l$ acting on the internal states. The Hamiltonian describing such a particle particle is then

$$\hat{H}_{prop}/w = \sum_{l=0}^{L} |s_l\rangle\langle s_l| - \frac{1}{2} \sum_{l=1}^{L} \left(\hat{U}_l \otimes |s_l\rangle\langle s_{l-1}| + \text{h.c.} \right), \tag{7.22}$$

where $|s_l\rangle$ corresponds to the particle being in the lth site. This Hamiltonian is analogous to that of a particle freely propagating through space, and its eigenstates are all of the form [289]:

$$|E(x,j)\rangle = c_0^{(j)} |x\rangle |s_0\rangle + \sum_{l=1}^{L} c_l^{(j)} \left(\hat{U}_l \hat{U}_{l-1} ... \hat{U}_1 \right) |x\rangle |s_l\rangle , \tag{7.23}$$

where $|x\rangle$ is the internal state of the particle at site $l = 0$, denoting a state in the logical basis, and the energy index j runs from 0 to L. The coefficients $c_0^{(j)}$ can be determined by setting each $\hat{U}_l$ in $\hat{H}_{prop}$ to the identity so that it is tri-diagonal. It is then straightforward to diagonalize this matrix [295], giving

$$c_l^{(j)} = \sqrt{\frac{2 - \delta_{0,j}}{L+1}} \cos\left(\frac{(2l+1)j\pi}{2(L+1)} \right) . \tag{7.24}$$

The corresponding energy eigenvalues are

$$\omega_j = \omega \cdot \left(1 - \cos\left(\frac{j\pi}{L+1} \right) \right) , \tag{7.25}$$

each having a 2^n-fold degeneracy indexed by $|x\rangle$.

We now add another term to the Hamiltonian to ensure that the ground state is non-degenerate and corresponds to the properly initialized output of the compu-

tation[5], $|x\rangle = |0^n\rangle$. This is a perturbation of the form

$$\hat{H}_{input} = \Delta_1 \sum_{m=1}^{n} |1\rangle\langle 1|_m \otimes |s_0\rangle\langle s_0|, \tag{7.26}$$

where $\Delta_1 \ll \omega$, and $|1\rangle\langle 1|_m$ acts only on qubit m of the particle's internal state. This lifts the degeneracy between the eigenstates $|E(x,j)\rangle$, and allows us to reduce our analysis to the invariant subspace of eigenstates with $|x\rangle = |0^n\rangle$. Matching the language we used previously, we define the subspace $\mathbf{S}$ as the span of the $L+1$ eigenstates of $\hat{H}_{prop}$ which are also ground states of $\hat{H}_{input}$ (i.e., the states $|E(x,j)\rangle$ with $x = 0^n$). Letting $\hat{H}_S = \hat{H}_{input} + \hat{H}_{prop}$, we thus set the eigenstates in the decomposition (7.6) as

$$|j\rangle = |E(0^n, j)\rangle \ , \tag{7.27}$$

which satisfy $\hat{H}_S |j\rangle = \hat{H}_{prop} |j\rangle = \omega_j |j\rangle$.

It is straightforward to show that the output of the computation can be encoded in the ground state of $\hat{H}_S$. By equation (7.24) the ground states $|E(x,0)\rangle$ of $\hat{H}_{prop}$ correspond to $c_l^{(0)} = \frac{1}{\sqrt{L+1}}$ for all l, and the perturbation $\hat{H}_{input}$ adds positive energy to all these states except the one with $|x\rangle = |0^n\rangle$. Thus, by equation (7.23) the ground state of $\hat{H}_S = \hat{H}_{prop} + \hat{H}_{input}$ has site L component $\frac{1}{\sqrt{L+1}} \hat{U}_c |0^n\rangle |s_L\rangle$. Preparing this state and measuring the position of the particle, with probability $1/(L+1)$ we would observe the particle at site L and project its internal state to the outcome of the computation. Alternatively, we could improve this probability by adding $(L+1)/\epsilon$ sites to the definition of $\hat{H}_{prop}$, with hopping terms correspond-

[5]Here $|x\rangle$ denotes a state in the logical basis, and $|0^n\rangle$ denotes the binary representation of $x = 0$ on n bits

ing to the identity operation on the internal state. The ground state of $\hat{H}_S$ would then have a probability $1-\epsilon$ of being past site L, so after tracing out the particle's position its internal state has an $O(\epsilon)$ trace-norm distance from $\hat{U}_c|0^n\rangle\langle 0^n|\hat{U}_c^\dagger$ [85].

The energy scale determining the timing of the algorithm is the spectral gap Δ of the eigenstates in $\mathbf{S}$ (equation (7.7)). The gap is set by the energy shifts that $\hat{H}_{input}$ adds within the original eigenspaces of $\hat{H}_{prop}$. It is straightforward to compute since $\hat{H}_{input}$ is diagonal in each eigenspace (each is just the span of $\{|E(x,j)\rangle\}$ for fixed j). Considering a single eigenspace with energy ω_j, by equation (7.23) we see that $\hat{H}_{input}$ has diagonal entries

$$\langle E(x,j)|\,\hat{H}_{input}\,|E(x,j)\rangle = \Delta_1 N(x)|c_0^{(j)}|^2 \tag{7.28}$$

where $N(x)$ is the number of 1's in the binary expansion of x and $c_0^{(j)}$ is defined in equation (7.24). Since $\hat{H}_{input}$ vanishes only when $|x\rangle = |0^n\rangle$, the gap is bounded by

$$\Delta \simeq \Delta_1 \cdot 1 \cdot |c_0^{(j)}|^2 \geq \Delta_1/(L+1)\,. \tag{7.29}$$

Note, though, that $\hat{H}_{input}$ and $\hat{H}_{prop}$ do not commute, so this bound only holds when first order degenerate perturbation theory is valid. This is true when $||\hat{H}_{input}|| = n\Delta_1$ is bounded by the minimum level spacing of $\hat{H}_{prop}$, which from equation (7.25) scales as $\omega \cdot L^{-2}$. We therefore scale Δ_1 as $\sim \omega \cdot n^{-1}L^{-2}$, so the gap satisfies

$$\Delta^{-1} \leq (\Delta_1|c_0^{(j)}|^2)^{-1} = \omega^{-1} \cdot O(nL^3)\,. \tag{7.30}$$

The final ingredients for simulated cooling of the circuit are the single qubit bath and the interaction with the system. We define the bath Hamiltonian ($\hat{H}_B = \omega_B \mathbf{1}_S \otimes \hat{P}_\uparrow$) and interaction ($\hat{V} = \hat{T}_S \otimes \sigma_x$) as before, where now the system operator

$\hat{T}_S$ is

$$\hat{T}_S = \Omega_0 \, \mathbf{1}_n \otimes |s_0\rangle\langle s_0| \, . \tag{7.31}$$

Notice that $\hat{T}_S$ does not couple between $\mathbf{S}$ and its complement $\mathbf{S}_\perp$, so it automatically satisfies the bounds implied by equations (7.16). Furthermore, by the decomposition (7.23) and $|j\rangle = |E(0^n, j)\rangle$, the projection of $\hat{T}_S$ into $\mathbf{S}$ has the simple form required by QSC,

$$(\hat{T}_S)|_{\mathbf{S}} = \Omega_0 |G\rangle\langle G| \otimes \sigma_x \, , \tag{7.32}$$

where state $|G\rangle$ satisfies

$$|G\rangle = \sum_j c_0^{(j)} \, |j\rangle \ . \tag{7.33}$$

Importantly, we note that the interaction $\hat{V}$ is local in the sense that the qubit couples only to the particle's position. In fact, by encoding the position as a unary string of logical qubits ($|s_l\rangle \equiv \left|1^l 0^{L-l}\right\rangle$), it is possible to implement the Hamiltonian $\hat{H}_S + \hat{H}_B + \hat{V}$ using at most 5-qubit interactions [85], and we expect that a 2-local QSC scheme is also possible based on Hamiltonian gadget constructions [296, 297].

Using results from the previous section, we can now show that local quantum simulated cooling is polynomially equivalent to standard quantum computation.

Equating the coefficients $x_j = c_0^{(j)}$, from equation (7.21) the total simulation time is

$$\begin{aligned}
\tau_{tot} = \sum_j \tau^{(j)} &= O\left(\frac{L^2\sqrt{L}}{\epsilon\Delta}\right) \sum_{j=1}^{L} \frac{1}{|c_0^{(0)} c_0^{(j)}|} \\
&= O\left(\frac{L^2\sqrt{L}}{\epsilon\Delta}\right) \sum_{j=1}^{L} \left(\frac{L+1}{\sqrt{2}}\right) \left(\cos\left(\frac{j\pi}{2(L+1)}\right)\right)^{-1} \qquad (7.34) \\
&= O\left(\frac{nL^6\sqrt{L}}{\epsilon\omega}\right) \sum_{j=1}^{L} \left(\cos\left(\frac{j\pi}{2(L+1)}\right)\right)^{-1} \\
&= \omega^{-1} O\left(\frac{nL^7\sqrt{L}\log(L)}{\epsilon}\right), \qquad (7.35)
\end{aligned}$$

where the second line follows from equation (7.24) and the third from the bound (7.30). For the final line we noted that the sum grows like $O(L\log(L))$. Assuming that a single 'query' to the Hamiltonian simulator has cost proportional to the maximum accumulated phase, the total cost of simulated cooling scales as $O(||\hat{H}_S||\tau_{tot})$. Given the above bound and the fact that $||\hat{H}_S|| = O(L)\,\omega$ [85], the effective cost of preparing the output of the circuit with error ϵ is bounded by $O(nL^8\sqrt{L}\log(L)/\epsilon)$. Thus Quantum Simulated Cooling with local interactions is, in terms of computational complexity, equivalent to standard quantum computation: any problem on n qubits that may be solved in poly(n) time using a standard quantum computer may also be solved in poly(n) time through QSC.

7.6 Extension

Although the QSC protocol we have presented is in principle as powerful as circuit-based quantum computation, the variety of Hamiltonian systems it can cool is limited by the assumptions placed on $\hat{H}_S$ and $\hat{V}$. To avoid unwanted transitions, it requires access to an approximate eigenspace $\mathbf{S}$ with gap Δ, as well an interaction

$\hat{V}$ described by a known decomposition (equation (7.10)). Here we propose an extension to this scheme that overcomes these constraints. The caveats of this approach are that it is probabilistic and requires $(k+1)$-local interactions for a k-local $\hat{H}_S$. That is, if $\hat{H}_S$ can be written as a sum of terms each acting on at most k subsystems, then the Hamiltonian involved in the extended scheme involves terms acting on $k+1$ subsystems.

We briefly summarize the scheme before describing it in detail. We assume that the spectrum of $\hat{H}_S$ has a non-degenerate ground state $|0\rangle$, as well as an subspace $\mathbf{P}_1$ corresponding to energies near ω_1 that are well separated from the rest of the spectrum. We also assume the ability to simulate evolution under to an operator $\hat{T}_S$ that couples between this space $\mathbf{P}_1$ and $|0\rangle$. We define Hamiltonians $\hat{H}$ and $\hat{V}$ based on $\hat{H}_S$ and $\hat{T}_S$ such that energy is transferred coherently between the system and a qutrit (dimension 3) bath. The system is prepared in $\mathbf{P}_1$ in a state that couples to $|0\rangle$ under $\hat{T}_S$, then propagated with the bath under $\hat{H}+\hat{V}$ for a sufficiently long time. The bath is then measured and, if it has transitioned, we evolve under a second Hamiltonian and measure the bath again in order to verify that the transition mapped the system to its ground state. The scheme is probabilistic since if either measurement fails the process is restarted.

We now specify the scheme's requirements. First, the Hamiltonian $\hat{H}_S$ is of the form

$$\hat{H}_S = \hat{P}_1\hat{H}_S\hat{P}_1 + \hat{P}_2\hat{H}_S\hat{P}_2 + \omega_0|0\rangle\langle 0|\,, \tag{7.36}$$

where $\hat{P}_1$ and $\hat{P}_2$ are projectors into subspaces of the same name and $\omega_0 = 0$ denotes

the ground state energy. The subspace $\hat{P}_1$ represents a narrow band of energies within $(\omega_1 - \delta\omega_1, \omega_1 + \delta\omega_1)$. We assume that $\hat{H}_S$ has a non-degenerate ground state $|0\rangle$ with energy $\omega_0 = 0$, and let $\hat{P}_2$ represent the space orthogonal to both $\hat{P}_1$ and $|0\rangle$. The limiting energy scale for this scheme is $\Delta = \min\left\{\omega_1, E, |E - \omega_1| : E \in \mathrm{Spec}(\hat{H}_S|_{P_2})\right\}$. As before, the size of Δ^{-1} will set an upper bound for the time scale of the simulation.

Along with $\hat{H}_S$, we assume access to a Hermitian operator $\hat{T}_S$ that couples $|0\rangle$ to the space $\hat{P}_1$:

$$\hat{P}_1 \hat{T}_S |0\rangle = \Omega |1\rangle , \tag{7.37}$$

where Ω is real and positive by choice of phase convention. Using this coupling, over a time scale $1/\Omega$ the simulation will cause coherent oscillations of the form $|1\rangle |C\rangle \leftrightarrow |0\rangle |B\rangle$, where $|C\rangle$ and $|B\rangle$ are orthogonal bath states. We must further assume that the energy spread of $\hat{P}_1$ is small compared to the coupling: $\delta\omega_1 \ll \Omega$. This will allow us to treat $|1\rangle$ as an eigenstate of $\hat{H}_S$ in our analysis of the simulated evolution. We must also assume that the energy shift induced by $\hat{T}_S$ on the ground state is small compared to the coupling: $|\langle 0| \hat{T}_S |0\rangle|^2/\omega_1 \ll \Omega$, that $\hat{T}_S$ is perturbative compared to the gap: $\Omega \leq ||\hat{T}_S|| \ll \Delta$, and that $\hat{T}_S$ does not couple strongly between $|0\rangle, \hat{P}_1$ and $\hat{P}_2$: $||(|0\rangle\langle 0| + \hat{P}_1)\hat{T}_S\hat{P}_2|| \ll \sqrt{\Omega\Delta}$. These spectral properties exist, for example, in gapped, translationally invariant many-body systems.

The original scheme succeeds by introducing a 2-level bath and adjusting its energy ω_B so that $|1\rangle |\downarrow\rangle$ and $|0\rangle |\uparrow\rangle$ are nearly degenerate. Within degenerate perturbation theory, the interaction $\hat{V}$ then produces a splitting of 2Ω between approx-

imate eigenstates $\frac{1}{\sqrt{2}}(|1\rangle|\downarrow\rangle \pm |0\rangle|\uparrow\rangle)$, thereby causing coherent oscillations of the form $|1\rangle|\downarrow\rangle \leftrightarrow |0\rangle|\uparrow\rangle$. If not accounted for, the (even-order) level shifts induced by $\hat{V}$ on the state $|1\rangle|\downarrow\rangle$ can be much larger than this splitting, meaning the eigenstates look more like $|1\rangle|\downarrow\rangle$ and $|0\rangle|\uparrow\rangle$, so that the desired oscillation does not occur. Although we may explicitly account for the level shifts by adjusting ω_B, this requires knowledge of the coefficients x_j in (7.10). Instead, one may tailor the unperturbed Hamiltonian $\hat{H}$ so that unwanted level shifts cancel out:

$$\begin{aligned}\hat{H} = \hat{H}_S \otimes (|C\rangle\langle C| + |R\rangle\langle R| - |L\rangle\langle L|) \\ + \omega_1 \mathbf{1}_S \otimes (|R\rangle\langle R| + |L\rangle\langle L|)\ ,\end{aligned} \tag{7.38}$$

where the bath Hilbert space now has dimension 3, with basis vectors $|C\rangle, |R\rangle$ and $|L\rangle$. Since the sign of $\hat{H}_S$ is conditioned on the state of the bath, simulation of $\hat{H}$ is equivalent to applying a conditional evolution of the system Hamiltonian.

We use the operator $\hat{T}_S$ to create the system-bath interaction $\hat{V}$:

$$\begin{aligned}\hat{V} &= \hat{T}_S \otimes (|C\rangle\langle B| + |B\rangle\langle C|) \\ |B\rangle &= \frac{1}{\sqrt{2}}(|L\rangle + |R\rangle)\,.\end{aligned} \tag{7.39}$$

To see how $\hat{H}+\hat{V}$ causes the desired oscillations, we compute the self-energy operator $\hat{\Sigma}(z)$ for the subspace $\mathbf{P}$ of eigenstates of $\hat{H}$ with energy at most $\Delta/4$ away from ω_1 [283]. Written as a projector,

$$\hat{P} = |0\rangle\langle 0| \otimes (|L\rangle\langle L| + |R\rangle\langle R|) + \hat{P}_1 \otimes |C\rangle\langle C|. \tag{7.40}$$

As discussed previously and rigorously shown in the appendix, the eigenstates and eigenvectors of $\hat{\Sigma}(z)$ for z close to ω_1 are good approximations of eigenstates and

eigenvectors of $\hat{H}+\hat{V}$. As before, we have

$$\hat{\Sigma}(z) = \hat{P}\hat{H}\hat{P} + \hat{P}\hat{V}\sum_{k\geq 0}(\hat{G}_Q(z)\hat{V})^k\hat{P}, \tag{7.41}$$

where $\hat{G}_Q(z) = \frac{\hat{Q}}{z\hat{Q}-\hat{Q}\hat{H}\hat{Q}}$ and $\hat{Q}$ projects into the orthogonal complement of $\mathbf{P}$. We observe that for $z=\omega_1$,

$$\begin{aligned}\hat{G}_Q(\omega_1) = &\frac{\hat{P}_1+\hat{P}_2}{\hat{P}_1\hat{H}_S\hat{P}_1+\hat{P}_2\hat{H}_S\hat{P}_2}\otimes(|L\rangle\langle L| - |R\rangle\langle R|)\\ &+\left(\omega_1^{-1}|0\rangle\langle 0| + \frac{\hat{P}_2}{\omega_1\hat{P}_2-\hat{P}_2\hat{H}_S\hat{P}_2}\right)\otimes|C\rangle\langle C|\,,\end{aligned} \tag{7.42}$$

Notice that the bath operator $(|L\rangle\langle L| - |R\rangle\langle R|)$ above has zero expectation value under state under $|B\rangle = \frac{1}{\sqrt{2}}(|L\rangle + |R\rangle)$, so the partial projection of $\hat{G}_Q(\omega_1)$ also vanishes: $\langle B|\,\hat{G}_Q(\omega_1)\,|B\rangle = 0$. Further, since $\hat{V}$ only has matrix elements between bath states $|B\rangle$ and $|C\rangle$, the expansion for $\hat{\Sigma}(z)$ truncates at second order for $z=\omega_1$. Thus the the *only* contributions from $\hat{V}$ in the expansion (7.41) are the first order term $\hat{P}\hat{V}\hat{P} = \Omega\,(|1\rangle\langle 0|\otimes|C\rangle\langle B| + |0\rangle\langle 1|\otimes|B\rangle\langle C|)$ and the ground state energy shift,

$$\omega_0^* = \frac{\left|\langle 0|\,\hat{T}_S\,|0\rangle\right|^2}{\omega_1} + \langle 0|\,\hat{T}_S\frac{\hat{P}_2}{\omega_1\hat{P}_2-\hat{P}_2\hat{H}_S\hat{P}_2}\hat{T}_S\,|0\rangle\,. \tag{7.43}$$

We therefore have

$$\begin{aligned}\hat{\Sigma}(\omega_1) = &\,\omega_1|0\rangle\langle 0|\otimes(|L\rangle\langle L| + |R\rangle\langle R|) + \hat{P}_1\hat{H}_S\hat{P}_1\otimes|C\rangle\langle C|\\ &+\Omega\,(|1\rangle\langle 0|\otimes|C\rangle\langle B| + |0\rangle\langle 1|\otimes|B\rangle\langle C|)\\ &+\omega_0^*|0\rangle\langle 0|\otimes|B\rangle\langle B|\,.\end{aligned} \tag{7.44}$$

This simplified form for the self-energy operator shows that cooling the system is possible without explicit prior knowledge of a spectral decomposition. Indeed, we show in the appendix that as long as the level shift ω_0^* for $|0\rangle\,|B\rangle$ and energy

dispersion $\delta\omega_1$ of the states in $\mathbf{P}_1$ are sufficiently small, the states $|0\rangle|B\rangle$ and $|1\rangle|C\rangle$ are nearly degenerate with respect to the diagonal component of $\hat{\Sigma}(\omega_1)$. And since $\hat{\Sigma}(\omega_1)$ is the effective Hamiltonian for states in $\mathbf{P}$ (as in the previous scheme), its off-diagonal term produces the desired oscillation $|1\rangle|C\rangle \leftrightarrow |0\rangle|B\rangle$ at a rate 2Ω.

Say that the initial prepared state $|F\rangle|C\rangle$ has overlap $|f_1| = |\langle 1|F\rangle|$ with the state described in equation (7.37). Since coherent oscillations between $|1\rangle|C\rangle$ and $|0\rangle|B\rangle$ occur at frequency 2Ω, as long as we evolve for times sampled randomly over a range $\frac{1}{\Omega}$, with probability $O(|f_1|^2)$ we expect to observe a transition of the form $|1\rangle|C\rangle \rightarrow |0\rangle|B\rangle$, heralded by a measurement of the bath. The average simulation time of the algorithm then scales as $O\left(\frac{1}{|f_1|^2\Omega}\right)$. If one is not given an explicit value of Ω, as in Ref. [286] one may implement the scheme with evolution times sampled randomly from $[\tau, 2\tau]$, and iteratively increase $\tau \rightarrow 2\tau$ after $\sim 1/|f_1|^2$ failed attempts. Since the sampling time τ grows exponentially, the total evolution time before success still scales as $O\left(\frac{1}{|f_1|^2\Omega}\right)$.

Unfortunately, a bath measurement of $|B\rangle$ does *not* imply the system is in its ground state, as other resonant transitions could also occur. To account for this, after measuring $|B\rangle$ we map the bath state $|B\rangle \rightarrow |L\rangle$ and evolve under a verification Hamiltonian,

$$\hat{H} + \Omega_0 \mathbf{1}_S \otimes (|L\rangle\langle R| + |R\rangle\langle L|) \ , \tag{7.45}$$

for time $\tau_v = \frac{\pi}{2\Omega_0}$. The form of $\hat{H}$ (equation (7.38))under the symmetric swap $|R\rangle \leftrightarrow |L\rangle$ implies that only the system ground state $|0\rangle$ has degeneracy between its $|L\rangle$ and $|R\rangle$ bath states. All other eigenstates $|\psi\, L\rangle$ have at least Δ less energy

than any $|R\rangle$ eigenstate. Hence by energy conservation only $|0\rangle$ exhibits coherent oscillations from $|L\rangle$ to $|R\rangle$, so measurement of the bath in $|R\rangle$ heralds success of the scheme.

Notice that, as long as $\Omega_0, \delta\omega_1 \ll \Delta$, all of the constraints on $\hat{T}_S$ required for this scheme are satisfied by $\hat{T}_S = \Omega_0 |F\rangle\langle F|$. Since $|F\rangle\langle F|$ is rank 1, the assumption that the ground eigenspace $\mathbf{P}_0$ is non-degenerate is no longer necessary, as $\hat{T}_S$ vanishes on every state in $\mathbf{P}_0$ orthogonal to $f_0 |0\rangle = \hat{P}_0 |F\rangle$ (where $|f_0|^2 = |\langle F| \hat{P}_0 |F\rangle|$). In this case we would have $\Omega |1\rangle = \hat{P}_1 \hat{T}_S |0\rangle = \Omega_0 f_0^* f_1 |1\rangle$, where $|f_1|^2 = \langle F| \hat{P}_1 |F\rangle$. If we use unitary 2-designs (procedures used for efficient random sampling [285]) to randomly generate $|F\rangle$, we then require that there is a fixed probability in n that $\langle F| \hat{P}_i |F\rangle \geq d_i/2^{n+1}$, where d_i is the rank of $\hat{P}_i$. Thus if we are given no information about $\hat{H}_S$ other than $\delta\omega_1$, ω_1, and Δ, by using 2-designs and the probabilistic scheme we may obtain the ground state of $\hat{H}_S$ with an average simulation time scaling as $O\left(\frac{1}{\Delta}\left(\frac{2^n}{d_1}\right)^{3/2}\left(\frac{2^n}{d_0}\right)^{1/2}\right)$, reflecting the quadratic speedup observed in previous sections.

7.7 Concluding Remarks

There are several known alternatives to standard, logic-based quantum computing [47, 298–303]. The advantages of simulated cooling are that it requires the simulation of only time-independent Hamiltonians, as well as measurements of a single qubit (or qutrit) bath. Using the gadget construction [296, 297] we expect that it may be efficiently implemented with only 2-local interactions.

Our work suggests several new avenues for investigation. One question is whether the techniques used in QSC may be applied to prepare other interesting states, such as mixed state ensembles [15, 82–84] or ground states of frustration free Hamiltonians [302]. Using techniques in Ref.'s [125, 126, 304], one may attempt to show whether this scheme is robust against time dependent error terms in the simulation, or non-unitary evolution described by weak interactions with an environment. Finally, we note that the application of QSC to the clock Hamiltonian in Section 3 used only a 2-body system-bath interaction. This prompts the question of when sums of local interactions suffice to produce the ground state of a Hamiltonian, and fundamentally, what the relationship is between a Hamiltonian's computational complexity and the potential to cool it using such interactions.

7.8 Appendix A: Mathematical Tools

The following theorems ensure that the effective Hamiltonian described in Section 7.4 accurately describes the dynamics of the simulator. The goal of these theorems is to bound the error in the unitary evolutions designed to map $|j\rangle|\downarrow\rangle \rightarrow |0\rangle|\uparrow\rangle$ or $|1\rangle|C\rangle \rightarrow |0\rangle|B\rangle$ (in the probabilistic scheme). This will be done by showing that both the eigenstates and eigenvalues corresponding to $\hat{H}_{eff}$ are close to true eigenstates and eigenvalues of $\tilde{H}$.

We consider a finite dimensional Hilbert space on which a Hamiltonian $\hat{H}$ acts, where the subspace $\mathbf{P}$ is spanned by the eigenvectors of $\hat{H}$ whose eigenvalues are in (λ_-, λ_+). We likewise define $\tilde{\boldsymbol{P}}, \tilde{\boldsymbol{Q}}$ with respect to a perturbed Hamiltonian,

$\tilde{H} = \hat{H} + \hat{V}$, using the same bounds. (For simplicity we let the symbol for a subspace also represent its projector.) We will assume that $\hat{H}$ has gap Δ, i.e. that the eigenvalues of $\hat{H}$ in $\mathbf{P}$ are at least Δ away from those in $\mathbf{Q}$. We are interested in the dynamics under $\tilde{H}$ within $\tilde{\boldsymbol{P}}$, which we approximate with an effective Hamiltonian $\hat{H}_{eff}$ acting in $\mathbf{P}$. The approximation is derived from a series expansion of the self-energy operator [283] (equation (7.14)):

$$\begin{aligned}\hat{\Sigma}_P(z) &= \hat{P}\hat{H}\hat{P} + \hat{P}\hat{V}\hat{P} + \hat{P}\hat{V}\hat{Q}\frac{1}{z - \hat{Q}(\hat{H}+\hat{V})\hat{Q}}\hat{Q}\hat{V}\hat{P} \\ &= \hat{P}\hat{H}\hat{P} + \hat{P}\hat{V}\hat{P} + \sum_{k\geq 1}\hat{P}\hat{V}(\hat{G}_Q(z)\hat{V})^k\hat{P}\,, \end{aligned} \tag{7.46}$$

In this notation $\hat{G}(z) = (z\mathbf{1} - \hat{H})^{-1}$ is the Green's function for the unperturbed Hamiltonian.

In all cases below, $||\cdot||$ represents the operator 2-norm,

$$||\hat{X}|| = \sup_{\langle v|v\rangle = 1} ||\hat{X}\,|v\rangle\,||$$

where $\hat{X}$ is a (bounded) linear map between two Hilbert spaces, and $||\,|v\rangle\,||$ is the norm induced by their inner products. This is a consistent norm, satisfying [282]

$$||\hat{A}\hat{B}|| \leq ||\hat{A}|| \cdot ||\hat{B}||\,. \tag{7.47}$$

Finally, we mention a slight abuse of notation: If $|v\rangle$ is a vector in a Hilbert space and $\hat{A}$ an operator acting on that space, then for expressions of the form

$$|v\rangle + O(r)$$

$$\hat{A} + O(r)$$

$O(r)$ represents a vector (operator) with norm scaling as $O(r)$. With this notation in hand, we can state the first theorem. Note that unless otherwise mentioned, the proofs for the following results are at the end of the appendix.

The first result is a slight modification of Theorem 3 in [289]. Within the subspace of interest, the theorem gives a one-to-one correspondence between the spectra of $\hat{H}_{eff}$ and $\tilde{H} = \hat{H} + \hat{V}$, and bounds their difference.

Theorem 7.8.1 ([289]) *Assume that $\hat{H}$ has no eigenvalues in $[\lambda_- - \Delta/2, \lambda_- + \Delta/2]$ and $[\lambda_+ - \Delta/2, \lambda_+ + \Delta/2]$ and that $||\hat{V}|| < \Delta/2$. Let $\mathbf{P}$ correspond to the subspace of $\hat{H}$ spanned by eigenvectors with eigenvalues between (λ_-, λ_+), and likewise define $\tilde{\boldsymbol{P}}$ for the perturbed Hamiltonian $\tilde{H} = \hat{H} + \hat{V}$. Assume there exists an operator $\hat{H}_{eff}$ on $\mathbf{P}$ whose spectrum is contained in some neighborhood $[c, d]$, and denote $\mu_1 \leq \mu_2 \leq ...$ and $\sigma_1 \leq \sigma_2 \leq ...$ as the eigenvalues of $\hat{H}_{eff}$ and $(\tilde{H})|_{\tilde{P}}$, respectively. Also assume that for some $\gamma > 0$, we have that*

$$[c - \gamma, d + \gamma] \subset (\lambda_-, \lambda_+) \, .$$

Finally, for the self-energy operator $\hat{\Sigma}(z)$ defined in equation (7.46), assume that

$$||\hat{\Sigma}(z) - \hat{H}_{eff}|| < \gamma$$

for all $z \in [c-\gamma, d+\gamma]$. Then the eigenvalues of $\hat{H}_{eff}$ are γ-close to those of $(\tilde{H})|_{\tilde{P}}$. That is, for all j,

$$|\mu_j - \sigma_j| < \gamma \, .$$

Reference [289] proves this result for the case $\lambda_- = -\infty$. Since the proof of Theorem 7.8.1 only requires a straightforward modification of the original, we do not show

it here. While Theorem 7.8.1 is used to characterize the spectrum of $\hat{H}_{eff}$, the following corollary characterizes its eigenvectors. It states that if a subspace $\mathbf{P}' \subseteq \mathbf{P}$ of $\hat{H}_{eff}$ is 'well resolved' from its complement, then the corresponding subspace of $\tilde{H}$ is well approximated by $\mathbf{P}'$.

Corollary 7.8.2 *Given the assumptions of Theorem 7.8.1, let $\mathbf{P}' \subseteq \mathbf{P}$ be an subspace of $\hat{H}_{eff}$, and let $\mathbf{P} - \mathbf{P}'$ be its local complement. Define the spectral diameter of $\mathbf{P}'$ as*

$$\nu = \max\left\{|x-y| : x, y \in \mathrm{Spec}(\hat{H}_{eff}|_{P'})\right\},$$

and the spectral distance between $\mathbf{P}'$ and $\mathbf{P} - \mathbf{P}'$ as

$$\eta = \min\left\{|x-y| : x \in \mathrm{Spec}(\hat{H}_{eff}|_{P'}), y \in \mathrm{Spec}(\hat{H}_{eff}|_{P-P'})\right\}.$$

Assume that η is larger than the eigenvalue separation γ. (If $\mathbf{P}' = \mathbf{P}$, set $\eta = \infty$.) Finally, define $\tilde{\boldsymbol{P}}'$ from the eigenvalue correspondence in Theorem 7.8.1: σ_j corresponds to $\tilde{\boldsymbol{P}}'$ if and only if μ_j corresponds to $\mathbf{P}'$.

Then for each eigenstate $|\tilde{v}_i\rangle \in \tilde{\boldsymbol{P}}'$ of $\tilde{H}$,

$$\langle \tilde{v}_i | \hat{P}' | \tilde{v}_i \rangle > \left(1 - \left(\frac{2||\hat{V}||}{\Delta}\right)^2\right)\left(1 - \left(\frac{2\gamma+\nu}{\eta-\gamma}\right)^2\right).$$

The following result is used in the proof of Theorem 7.8.1, as well as in some of the claims below.

Lemma 7.8.3 ([289]) *Let $\hat{H}$, $\tilde{H}$ be two Hamiltonians with ordered eigenvalues $\mu_1 \leq \mu_2 \leq ...$ and $\sigma_1 \leq \sigma_2 \leq ...$. Then for all j,*

$$|\mu_j - \sigma_j| \leq ||\hat{H} - \tilde{H}||.$$

We now give a result derived Theorem 3.6, Chapter V, of Stewart and Sun's *Matrix Perturbation Theory* [282], used to show that transitions in the algorithm which do not conserve energy are suppressed.

Theorem 7.8.4 ([282]) *Let $\hat{H}$ and $\tilde{H}$ be Hermitian operators. Let $\mathbf{P}$ be the subspace of $\hat{H}$ spanning eigenvalues in $[\lambda_- + \Delta/2, \lambda_+ - \Delta/2] \neq \emptyset$, and likewise let $\tilde{\boldsymbol{P}}$ be the subspace of $\tilde{H}$ spanning eigenvalues in (λ_-, λ_+). Suppose that for every eigenvalue E_Q corresponding to the subspace $\mathbf{Q}$ complementary to $\mathbf{P}$, either $E_Q \leq (\lambda_- - \Delta/2)$ or $E_Q \geq (\lambda_+ + \Delta/2)$. Then for any $|v\rangle \in \mathbf{P}$, $|\tilde{v}\rangle \in \tilde{\boldsymbol{P}}$,*

$$\langle \tilde{v}| \hat{P} |\tilde{v}\rangle \geq 1 - \left(\frac{2||\hat{H} - \tilde{H}||}{\Delta} \right)^2$$

$$\langle v| \tilde{P} |v\rangle \geq 1 - \left(\frac{2||\hat{H} - \tilde{H}||}{\Delta} \right)^2$$

The following corollary extends the above theorem to the case of subspaces spanning multiple energy bands.

Corollary 7.8.5 *Let $\hat{H}$ be a Hermitian operator resolved by spaces $\mathbf{P}$ and $\mathbf{Q}$: $\hat{H} = \hat{P}\hat{H}\hat{P} + \hat{Q}\hat{H}\hat{Q}$. Assume that $\mathbf{P} = \mathbf{P}_1 \oplus \mathbf{P}_2 \oplus ... \oplus \mathbf{P}_L$, and that there exist numbers $\lambda_{1-} < \lambda_{1+} < \lambda_{2-} < ... < \lambda_{L+}$ such each $\mathbf{P}_k$ is the subspace of $\hat{H}$ spanning eigenvalues in $[\lambda_{k-} + \Delta/2, \lambda_{k+} - \Delta/2]$. Further assume that the eigenvalues of $\hat{H}$ in the complement $\mathbf{Q}$ are at least $\Delta > 0$ away from those in $\mathbf{P}$. Finally, for $1 \leq k \leq L$ define $\tilde{\boldsymbol{P}}_{\boldsymbol{k}}$ as the subspace of the perturbed operator $\tilde{H}$ corresponding to eigenvalues within $(\lambda_{k-}, \lambda_{k+})$, and set $\tilde{\boldsymbol{P}} = \tilde{\boldsymbol{P}}_{\mathbf{1}} \oplus \mathbf{...} \oplus \tilde{\boldsymbol{P}}_{\boldsymbol{L}}$.*

Then for each $|v\rangle \in \mathbf{P}$, $|\tilde{v}\rangle \in \tilde{\boldsymbol{P}}$,

$$\begin{aligned} \langle v|\,\tilde{P}\,|v\rangle &\geq 1 - L\left(\frac{2||\tilde{H}-\hat{H}||}{\Delta}\right)^2 \\ \langle \tilde{v}|\,\hat{P}\,|\tilde{v}\rangle &\geq 1 - L\left(\frac{2||\tilde{H}-\hat{H}||}{\Delta}\right)^2 . \end{aligned}$$

Finally, the following proofs we will require the following two lemmas about operator norms.

Lemma 7.8.6 *Let* $\hat{A}$, $\hat{B}$ *be Hermitian operators on* $\mathbb{C}^m, \mathbb{C}^n$, *respectively. Suppose that* $||\hat{A}|| \leq \alpha$ *and that* $\hat{B}$ *is invertible, with* $||\hat{B}^{-1}|| \leq \frac{1}{\alpha+\beta}$, *for* $\beta > 0$. *Then for any linear operator* $\hat{X} : \mathbb{C}^n \to \mathbb{C}^m$,

$$||\hat{X}|| \leq \frac{||\hat{A}\hat{X} - \hat{X}\hat{B}||}{\beta} .$$

Lemma 7.8.7 *Let* $\hat{A}$, $\hat{B}$ *be Hermitian operators on some space* $\mathbf{S}_1 \oplus \mathbf{S}_2$. *Suppose that* $\hat{A} = \hat{S}_1\hat{A}\hat{S}_1 + \hat{S}_2\hat{A}\hat{S}_2$, *and that*

$$\begin{aligned} ||\hat{S}_1\hat{A}^{-1}\hat{S}_1|| &< 1/G_1 \\ ||\hat{S}_2\hat{A}^{-1}\hat{S}_2|| &< 1/G_2 \\ b_{11} = ||\hat{S}_1\hat{B}\hat{S}_1|| &< G_1/2 \\ b_{22} = ||\hat{S}_2\hat{B}\hat{S}_2|| &< G_2/2 \\ b_{12} = ||\hat{S}_1\hat{B}\hat{S}_2|| &< \min(G_1, G_2)/2 . \end{aligned}$$

Then $(\hat{A} - \hat{B})$ *is invertible, and*

$$\begin{aligned} ||\hat{S}_1(\hat{A}-\hat{B})^{-1}\hat{S}_2|| &< \frac{b_{12}}{(G_1 - b_{11})(G_2 - b_{22}) - b_{12}^2} \\ ||\hat{S}_1(\hat{A}-\hat{B})^{-1}\hat{S}_1|| &< \frac{1}{G_1 - b_{11}}(1 + b_{12}||\hat{S}_1(\hat{A}-\hat{B})^{-1}\hat{S}_2||) \\ ||\hat{S}_2(\hat{A}-\hat{B})^{-1}\hat{S}_2|| &< \frac{1}{G_2 - b_{22}}(1 + b_{12}||\hat{S}_1(\hat{A}-\hat{B})^{-1}\hat{S}_2||) . \end{aligned}$$

We now begin the proofs of the above results, neglecting Theorem 7.8.1 and Lemma 7.8.3 as they may be derived (with minimal modification) from results in [289].

Proof of Lemma 7.8.6: Since the operator norm is consistent (equation (7.47)), we have that

$$||\hat{A}\hat{X}|| \leq \alpha||\hat{X}||$$

$$||\hat{X}|| = ||\hat{X}\hat{B}B^{-1}|| \leq \frac{||\hat{X}\hat{B}||}{\alpha+\beta} \implies$$

$$||\hat{X}\hat{B}|| \geq (\alpha+\beta)||\hat{X}||$$

By the triangle inequality we conclude that

$$||\hat{A}\hat{X} - \hat{X}\hat{B}|| \geq ||\hat{X}\hat{B}|| - ||\hat{A}\hat{X}|| \geq \beta||\hat{X}||$$

□

Proof of Lemma 7.8.7:

First, we show that $(\hat{A} - \hat{B})$ is invertible. It suffices to show that $||\hat{B}\hat{A}^{-1}|| < 1$, as then $(1 - \hat{B}\hat{A}^{-1}) = \left((\hat{A} - \hat{B})\hat{A}^{-1}\right)$ is invertible. Let a normalized $|v_i\rangle \in \mathbf{S}_i$ be given. Then $\hat{A}^{-1}|v_i\rangle = c\,|v_i'\rangle$ for some (normalized) $|v_i'\rangle \in \mathbf{S}_i$ and $|c| < 1/G_i$. Using the above equation, one gets

$$\begin{aligned}
||\hat{B}\hat{A}^{-1}|v_i\rangle||^2 &= \langle v_i|\,\hat{A}^{-1}\hat{B}\hat{B}\hat{A}^{-1}\,|v_i\rangle \\
&< \frac{1}{G_i^2}\langle v_i'|\,\hat{B}\left(\hat{S}_1 + \hat{S}_2\right)\hat{B}\,|v_i'\rangle \\
&\leq \frac{b_{ii}^2 + b_{12}^2}{G_i^2} \\
&< 1/2\,.
\end{aligned}$$

For any normalized state $|v\rangle$, one may write $|v\rangle = a\,|v_1\rangle + b\,|v_2\rangle$, with $|v_i\rangle \in \mathbf{S}_i$ and $|a|^2 + |b|^2 = 1$, and by the triangle inequality

$$\begin{aligned} ||\hat{B}\hat{A}^{-1}\,|v\rangle\,|| &\leq |a| \cdot ||\hat{B}\hat{A}^{-1}\,|v_1\rangle\,|| + |b| \cdot ||\hat{B}\hat{A}^{-1}\,|v_2\rangle\,|| \\ &< \frac{1}{\sqrt{2}}(|a| + |b|) \leq 1\,, \end{aligned}$$

where the last inequality follows from writing $|a| = \sqrt{s}, |b| = \sqrt{1-s}$ for some $s \in [0,1]$. This shows that $||\hat{B}\hat{A}^{-1}|| < 1$, which implies that $(1 - \hat{B}\hat{A}^{-1})$ has only positive eigenvalues and is therefore invertible.

Since we have shown that $(\hat{A} - \hat{B})$ is invertible, one may easily check that

$$(\hat{A} - \hat{B})^{-1} = \hat{A}^{-1} + \hat{A}^{-1}\hat{B}(\hat{A} - \hat{B})^{-1} \tag{7.48}$$

Decomposing into $\mathbf{S}_1$ and $\mathbf{S}_2$ components, one gets

$$\begin{aligned} \hat{S}_1(\hat{A} - \hat{B})^{-1}\hat{S}_1 &= \hat{S}_1\hat{A}^{-1}\hat{S}_1 + \\ &\quad \hat{S}_1\hat{A}^{-1}\hat{S}_1 \Big(\hat{S}_1\hat{B}\hat{S}_1(\hat{A} - \hat{B})^{-1}\hat{S}_1 \\ &\quad + \hat{S}_1\hat{B}\hat{S}_2(\hat{A} - \hat{B})^{-1}\hat{S}_1\Big) \end{aligned}$$

By the triangle inequality and the consistency relation $||\hat{C}\hat{D}|| \leq ||\hat{C}|| \cdot ||\hat{D}||$, we have

$$\begin{aligned} ||\hat{S}_1(\hat{A} - \hat{B})^{-1}\hat{S}_1|| &< \frac{1}{G_1} + \frac{b_{11}}{G_1}||\hat{S}_1(\hat{A} - \hat{B})^{-1}\hat{S}_1|| \\ &\quad + \frac{b_{12}}{G_1}||\hat{S}_1(\hat{A} - \hat{B})^{-1}\hat{S}_2|| \implies \\ ||\hat{S}_1(\hat{A} - \hat{B})^{-1}\hat{S}_1|| &< \frac{1}{G_1 - b_{11}}\Big(1 + b_{12}||\hat{S}_1(\hat{A} - \hat{B})^{-1}\hat{S}_2||\Big)\,, \end{aligned} \tag{7.49}$$

where we also used the fact that we may interchange the projectors $\hat{S}_1, \hat{S}_2$ when taking the operator norm. Interchanging the numbers 1 and 2, we obtain an equivalent result for $||\hat{S}_2(\hat{A} - \hat{B})^{-1}\hat{S}_2||$. This proves the last two statements in Lemma 7.8.7.

Likewise using equation (7.48), one may show that

$$\begin{aligned}||\hat{S}_1(\hat{A}-\hat{B})^{-1}\hat{S}_2|| &= ||\hat{S}_1\hat{A}^{-1}\hat{S}_1\left(\hat{S}_1\hat{B}\hat{S}_1(\hat{A}-\hat{B})^{-1}\hat{S}_2\right.\\ &\qquad \left.+\hat{S}_1\hat{B}\hat{S}_2(\hat{A}-\hat{B})^{-1}\hat{S}_2\right)||\\ &\leq \frac{b_{11}}{G_1}||\hat{S}_1(\hat{A}-\hat{B})^{-1}\hat{S}_2|| + \frac{b_{12}}{G_1}||\hat{S}_2(\hat{A}-\hat{B})^{-1}\hat{S}_2||\,.\end{aligned}$$

Hence,

$$||\hat{S}_1(\hat{A}-\hat{B})^{-1}\hat{S}_2|| \leq \frac{b_{12}}{G_1-b_{11}}||\hat{S}_2(\hat{A}-\hat{B})^{-1}\hat{S}_2||\,. \tag{7.50}$$

Substituting the result of (7.49) (with 1 and 2 interchanged) into the right hand side produces the first statement of Lemma 7.8.7.

□

Proof of Corollary 7.8.2:

By assumption, we have that $\hat{H} = \hat{P}\hat{H}\hat{P} + \hat{Q}\hat{H}\hat{Q}$, where $\hat{P}$ projects into the subspace of $\hat{H}$ with eigenvalue in $(\lambda_- + \Delta/2, \lambda_+ - \Delta/2)$. This defines the energy gap between $\hat{H}|_P$ and $\hat{H}|_Q$. For $\tilde{H} = \hat{H} + \hat{V}$, we define $\tilde{\boldsymbol{P}}$ as the subspace of $\tilde{H}$ with eigenvalue in (λ_-, λ_+). $\mathbf{P'} \subset \mathbf{P}$ is an subspace of $\hat{H}_{eff}$ and $\tilde{\boldsymbol{P}}' \subset \tilde{\boldsymbol{P}}$ is the associated subspace of $\tilde{H}$, obtained from the eigenvalue correspondence discussed in Theorem 7.8.1.

Let $|\tilde{v}_i\rangle \in \tilde{\boldsymbol{P}}'$ be an eigenstate of $\tilde{H}$, with corresponding eigenvalue $\tilde{E}_i$. We may write

$$|\tilde{v}_i\rangle = N_i\,|u_i\rangle + \hat{Q}\,|\tilde{v}_i\rangle\ ,$$

where $\hat{P}\,|\tilde{v}_i\rangle = N_i\,|u_i\rangle$ and $\langle u_i|\,u_i\rangle = 1$. Since $|\tilde{v}_i\rangle \in \tilde{\boldsymbol{P}}$, we may use Theorem 7.8.4

to conclude that

$$N_i^2 = \langle \tilde{v}_i | \hat{P} | \tilde{v}_i \rangle \geq 1 - \left(\frac{2||\hat{V}||}{\Delta} \right)^2 .$$

Now decompose $|u_i\rangle$ into components parallel and orthogonal to $\mathbf{P}'$:

$$|u_i\rangle = \hat{P}' |u_i\rangle + (\hat{P} - \hat{P}') |u_i\rangle$$

We wish to bound $\langle u_i | \hat{P}' | u_i \rangle$ from below. To do this we first note that, as in the proofs of Lemmas 5 and 6 of [289], $\hat{\Sigma}(\tilde{E}_i) |u_i\rangle = \tilde{E}_i |u_i\rangle$. From this we conclude that

$$\begin{aligned} &(\hat{\Sigma}(\tilde{E}_i) - \hat{H}_{eff}) |u_i\rangle + (\hat{H}_{eff} - \tilde{E}_i \mathbf{1}) \hat{P}' |u_i\rangle \\ &\qquad = -(\hat{H}_{eff} - \tilde{E}_i \mathbf{1})(\hat{P} - \hat{P}') |u_i\rangle \end{aligned}$$

By assumption, $||(\hat{\Sigma}(\tilde{E}_i) - \hat{H}_{eff})|| < \gamma$. Since E_i is an eigenvalue corresponding to $\mathbf{P}'$, the eigenvalues of operator $(\hat{H}_{eff} - E_i \mathbf{1}) \hat{P}'$ have magnitude at most ν (its spectral diameter), and since $|E_i - \tilde{E}_i| < \gamma$, $||(\hat{H}_{eff} - \tilde{E}_i \mathbf{1}) \hat{P}'|| < \gamma + \nu$. By the triangle inequality, the norm of the left hand side is less than $2\gamma + \nu$. Likewise, the eigenvalues of $(\hat{H}_{eff} - E_i \mathbf{1})|_{P-P'}$ have magnitude at least equal than the spectral distance η, so the eigenvalues of $(\hat{H}_{eff} - \tilde{E}_i \mathbf{1})|_{P-P'}$ are greater than $\eta - \gamma > 0$. Thus the norm of the right hand side is greater than $(\eta - \gamma) ||(\hat{P} - \hat{P}') |u_i\rangle ||$. Therefore

$$||(\hat{P} - \hat{P}') |u_i\rangle || < \frac{2\gamma + \nu}{\eta - \gamma} \implies$$

$$\langle u_i | \hat{P}' | u_i \rangle = 1 - \langle u_i | (\hat{P} - \hat{P}') | u_i \rangle > 1 - \left(\frac{2\gamma + \nu}{\eta - \gamma} \right)^2$$

The result follows by noting that $\langle \tilde{v}_i | \hat{P}' | \tilde{v}_i \rangle = N_i^2 \langle u_i | \hat{P}' | u_i \rangle$.

□

Proof of Theorem 7.8.4:

Define the numbers

$$\bar{\lambda} = \frac{\lambda_+ + \lambda_-}{2}$$

$$\Lambda = \frac{\lambda_+ - \lambda_-}{2}$$

Note that $\Lambda \geq \Delta/2$ since we assumed $[\lambda_- + \Delta/2, \lambda_+ - \Delta/2]$ is non-empty. Since $\hat{H}$ is Hermitian, there exists a unitary operator $\hat{U} = (\hat{X}_P, \hat{X}_Q)$ that diagonalizes $\hat{H}$, where the columns of $\hat{X}_P$ and $\hat{X}_Q$ form an orthonormal basis for $\mathbf{P}$ and $\mathbf{Q}$, respectively. By our assumption about the spectra of $\hat{H}$ in $\mathbf{P}$ and $\mathbf{Q}$, we see that

$$\hat{H} - \bar{\lambda}\mathbf{1} = \hat{X}_P \hat{L}_P \hat{X}_P^\dagger + \hat{X}_Q \hat{L}_Q \hat{X}_Q^\dagger \,,$$

where $\hat{L}_p$ and $\hat{L}_Q$ are diagonal matrices, with eigenvalues in $[-(\Lambda - \Delta/2), \Lambda - \Delta/2]$ and $(-\infty, -\Lambda - \Delta/2] \cup [\Lambda + \Delta/2, \infty)$, respectively. Analogously, we may define the decomposition of $\tilde{H} - \bar{\lambda}$:

$$\tilde{H} - \bar{\lambda}\mathbf{1} = \tilde{X}_{\tilde{P}} \tilde{L}_{\tilde{P}} \tilde{X}_{\tilde{P}}^\dagger + \tilde{X}_{\tilde{Q}} \tilde{L}_{\tilde{Q}} \tilde{X}_{\tilde{Q}}^\dagger \,,$$

where the eigenvalues of $\tilde{L}_{\tilde{P}}$ and $\tilde{L}_{\tilde{Q}}$ are in $[-\Lambda, \Lambda]$ and $(-\infty, -\Lambda] \cup [\Lambda, \infty)$.

Consider the operator

$$\hat{V}_E = \tilde{X}_{\tilde{P}}^\dagger \left(\tilde{H} - \hat{H} \right) \hat{X}_Q$$

From the identities above it follows that

$$\begin{aligned} \hat{V}_E &= \tilde{X}_{\tilde{P}}^\dagger (\tilde{H} - \bar{\lambda}\mathbf{1}) \hat{X}_Q - \tilde{X}_{\tilde{P}}^\dagger (\hat{H} - \bar{\lambda}\mathbf{1}) \hat{X}_Q \\ &= \tilde{L}_{\tilde{P}} \tilde{X}_{\tilde{P}}^\dagger \hat{X}_Q - \tilde{X}_{\tilde{P}}^\dagger \hat{X}_Q L_Q \end{aligned}$$

Noting that $||\tilde{L}_{\tilde{P}}|| \leq \Lambda$ and $||\hat{L}_Q^{-1}|| \leq \frac{1}{\Lambda+\Delta/2}$, we may use Lemma 7.8.6 with $\hat{A} = \tilde{L}_{\tilde{P}}$, $\hat{B} = \hat{L}_Q$, $\alpha = \Lambda$, $\beta = \Delta/2$, and $\hat{X} = \tilde{X}_{\tilde{P}}^\dagger \hat{X}_Q$ to conclude

$$\begin{aligned} ||\tilde{X}_{\tilde{P}}^\dagger \hat{X}_Q|| = ||\hat{X}|| &\leq \frac{2||\hat{A}\hat{X} - \hat{X}\hat{B}||}{\Delta} \\ &= \frac{2||\hat{V}_E||}{\Delta} \\ &= \frac{2||\tilde{X}_{\tilde{P}}^\dagger \left(\tilde{H} - \hat{H}\right) \hat{X}_Q||}{\Delta} \\ &\leq \frac{2||\tilde{H} - \hat{H}||}{\Delta}. \end{aligned}$$

Here the second line follows from the second definition of $\hat{V}_E$ and the last line follows from $||\hat{A}\hat{B}|| \leq ||\hat{A}|| \cdot ||\hat{B}||$.

Let $|\tilde{v}\rangle \in \tilde{\boldsymbol{P}}$ be given with $\langle \tilde{v}|\, \tilde{v}\rangle = 1$. Since the columns of $\tilde{X}_{\tilde{P}}$ form an orthonormal basis for $\tilde{\boldsymbol{P}}$, there exists a vector $|x\rangle$ such that $|\tilde{v}\rangle = \tilde{X}_{\tilde{P}}\,|x\rangle$ and $\langle x|x\rangle = 1$. From the previous line we conclude that

$$\begin{aligned} \langle \tilde{v}|\, \hat{Q}\, |\tilde{v}\rangle &= \langle \tilde{v}|\, \hat{X}_Q \hat{X}_Q^\dagger\, |\tilde{v}\rangle \\ &= \langle x|\, \tilde{X}_{\tilde{P}}^\dagger \hat{X}_Q \hat{X}_Q^\dagger \tilde{X}_{\tilde{P}}\, |x\rangle \\ &\leq ||\hat{X}_Q^\dagger \tilde{X}_{\tilde{P}}||^2 \\ &= ||\tilde{X}_{\tilde{P}}^\dagger \hat{X}_Q||^2 \leq \left(\frac{2||\tilde{H} - \hat{H}||}{\Delta}\right)^2 \end{aligned}$$

where in the last line we used the fact that the operator norm is unchanged when taking the Hermitian adjoint. The first statement follows by noting that $\hat{Q} = \mathbf{1} - \hat{P}$. To prove the second statement, we can make an identical argument using $\tilde{V}_E = \hat{X}_P^\dagger(\tilde{H} - \hat{H})\tilde{X}_{\tilde{Q}}$.

□

Proof of Corollary 7.8.5:

We may assume without loss of generality that each domain $[\lambda_{k-} + \Delta/2, \lambda_{k+} - \Delta/2]$ is at least 2Δ away from its neighboring domains. If this were not the case for two domains, the gap Δ between the spectra of $\hat{H}|_P$ and $\hat{H}|_Q$ would imply that $\hat{H}|_Q$ had no eigenvalues between the two domains, and thus they may be merged.

Let a normalized vector $|v\rangle \in \mathbf{P}$ be given. We may decompose $|v\rangle$ into its components within each $\mathbf{P}_k$:

$$|v\rangle = \sum_k \left(\hat{P}_k |v\rangle\right) = \sum_k c_k |v_k\rangle \ ,$$

where $\sum_k |c_k|^2 = 1$. Define r_k as the amplitude of $|v_k\rangle$ outside of $\tilde{\boldsymbol{P}}$,

$$|v_k\rangle = \tilde{P} |v_k\rangle + r_k \left|v_k^\perp\right\rangle \ ,$$

where $\left|v_k^\perp\right\rangle \in \tilde{Q}$ has norm 1. Applying Theorem 7.8.4 to the single subspace $\mathbf{P}_k$, we get

$$1 - |r_k|^2 = \langle v_k| \tilde{P} |v_k\rangle \geq \langle v_k| \tilde{P}_k |v_k\rangle \geq 1 - \left(\frac{2||\tilde{H} - \hat{H}||}{\Delta}\right)^2 \ ,$$

therefore

$$|r_k| \leq \frac{2||\tilde{H} - \hat{H}||}{\Delta} \, .$$

Substituting into the definition of $|v\rangle$, we get

$$\begin{aligned} |v\rangle &= \sum_k c_k \left(\tilde{P} |v_k\rangle + r_k \left|v_k^\perp\right\rangle\right) \\ &= \tilde{P} \left(\sum_k c_k |v_k\rangle\right) + r_{eff} \left|v^\perp\right\rangle \ , \end{aligned}$$

where $r_{eff} \left|v^\perp\right\rangle = \sum_k c_k r_k \left|v_k^\perp\right\rangle$ is a vector in $\tilde{Q}$. By the triangle and Cauchy-

Schwartz inequalities we conclude that

$$\begin{aligned} |r_{eff}| &\leq \sum_k |c_k r_k| \\ &\leq \sum_k |c_k| \left(\frac{2||\tilde{H} - \hat{H}||}{\Delta} \right) \\ &\leq \sqrt{L} \left(\frac{2||\tilde{H} - \hat{H}||}{\Delta} \right) . \end{aligned}$$

The first statement of the corollary follows by noting that $\langle v| \tilde{P} |v\rangle = 1 - |r_{eff}|^2$. The second statement follows by making the same argument and, except with the initial assumption, adding or removing $\sim$ to each projector and vector.

□

7.9 Appendix B: Deterministic QSC Analysis

This section describes the deterministic Quantum Simulated Cooling scheme, and gives sufficient conditions for its success up to an infidelity $O(\epsilon)$.

Theorem 7.9.1 *Let $\hat{H}_S$ be a Hamiltonian acting on n qubits, with subspaces* $\mathbf{S}$ *and* $\mathbf{S}_\perp$. *Assume that*

$$(\hat{H}_S)|_{\mathbf{S}} = \sum_{j=0}^{L} \omega_j |j\rangle\langle j| ,$$

where $0 = \omega_0 < \omega_1 < \omega_2 ... < \omega_L$ *and*

$$\Delta = \min_{\omega_i, E} \{ |E - \omega_i| : E \in \mathrm{Span}(\hat{H}_S), E \neq \omega_i \} > 0 .$$

Finally, assume that there exists operators $\hat{T}_S$, $\hat{\delta}_j$, such that

$$(\hat{T}_S)|_{\mathbf{S}} = \Omega_0 |G\rangle\langle G| ,$$

with

$$|G\rangle = \sum_{j=0}^{L} x_j \, |j\rangle \ ,$$

$|x_j| > 0$*, and for all* j*,*

$$\begin{aligned} r \equiv \Omega_0/\Delta &< 1/8 \\ \frac{||\hat{S}\hat{\delta}_j\hat{S}||}{\Delta} &< r^2 \cdot |x_0 x_j| \\ \frac{||\hat{S}(\hat{T}_S + \hat{\delta}_j)\hat{S}_\perp||^2}{\Delta^2} &< r^2 \cdot |x_0 x_j| \\ \frac{||\hat{S}_\perp(\hat{T}_S + \hat{\delta}_j)\hat{S}_\perp||}{\Delta} &< 1/2 \, . \end{aligned} \tag{7.51}$$

Then for $\epsilon > 0$ *and* $r \propto \frac{\epsilon}{L^2\sqrt{L}}$*, there exists a TCP map* $\mathcal{E}$*, consisting of* L *single qubit measurements and unitaries* $\hat{U}_j$ *on* $n+1$ *qubits of the form*

$$\hat{U}_j = \exp\left(-i\tau^{(j)}(\hat{H}_S + \omega_B^{(j)}\mathbf{1}_S \otimes \hat{P}_\uparrow + \hat{T}_S \otimes \sigma_x + \hat{\delta}_j)\right) \ , \tag{7.52}$$

such that for any density matrix $\hat{\rho}_S$ *with support in* $\mathbf{S}$*,*

$$\mathrm{Tr}[(|0\rangle\langle 0| \otimes \mathbf{1}_B)\mathcal{E}(|F\rangle\langle F| \otimes |\downarrow\rangle\langle\downarrow|)] = 1 - O(\epsilon) \, ,$$

as $\epsilon \to 0^+$*, with total simulation time*

$$\tau_{tot} = O\left(\frac{L^2\sqrt{L}}{\epsilon\Delta|x_0|}\right)\sum_{j=1}^{L}\frac{1}{|x_j|} \, .$$

The proof is constructive and the QSC protocol is described in the main text. In summary, $\mathcal{E}$ can be described by a loop of L cooling steps, labeled by the index j (starting at $j = L$). At the beginning of each iteration, the bath is measured in the logical basis. If it is in state $|\uparrow\rangle$, then the transition to the ground state has already occurred, so we effectively terminate by decrementing $j \to j-1$ and continuing to the next iteration. Otherwise, we evolve under Hamiltonian $\tilde{H}_j = \hat{H}_j + \hat{V} + \hat{\delta}_j$,

where $\hat{H}_j = \hat{H}_S + \omega_B^{(j)} \mathbf{1}_S \otimes \hat{P}_\uparrow$, $\hat{V} = \hat{T}_S \otimes \sigma_x$, and $\hat{\delta}_j$ represents an error term in the simulation. The bath energy $\omega_B^{(j)}$ (defined explicitly below) is near ω_j. The time evolved under this Hamiltonian is $\tau^{(j)} = \frac{\pi}{2\Omega_0 |x_0 x_j|}(1 + O(r^2))$, and the associated unitary evolution is labeled $\hat{U}_j$ (equation (7.52)). We then decrement $j \to j-1$ and continue to the next iteration.

Written in pseudo-code, $\mathcal{E}$ may be summarized as

```
For j= L, L-1, ... 1
     Measure bath qubit
     If bath is down:
          Apply U_j
Measure bath
```

Step j is associated with the following trace-preserving, completely positive (TCP) map:

$$\begin{aligned} \mathcal{E}_j(\hat{\rho}) = \hat{U}_j(\mathbf{1}_S \otimes \hat{P}_\downarrow)\, \hat{\rho}\, (\mathbf{1}_S \otimes \hat{P}_\downarrow)\hat{U}_j^\dagger \\ + (\mathbf{1}_S \otimes \hat{P}_\uparrow)\hat{\rho}(\mathbf{1}_S \otimes \hat{P}_\uparrow)\,, \end{aligned} \tag{7.53}$$

as defined previously. We define $\mathcal{E} = E_1 \circ E_2 ... \circ E_L$. Given the above assumptions, the lemmas below prove that the algorithm works as expected. The proofs of the lemmas are included at the end of this section.

Lemma 7.9.2 (Fidelity of the cooling step) *Let $\hat{U}_j$ be the unitary evolution associated with cooling state $|j\rangle\,|\downarrow\rangle$, as defined in equation* (7.52)*. Assume that the*

bounds (7.51) *hold. Then there exists a time evolution* $\tau^{(j)} = \frac{\pi}{2\Omega_0|x_0x_j|}(1 + O(r^2))$ *and* $\omega_B^{(j)} \in (\omega_j - \Delta/4, \omega_j + \Delta/4)$ *defining* $\hat{U}_j$ *such that*

$$\hat{U}_j |j\rangle |\downarrow\rangle = |0\rangle |\uparrow\rangle + O(r)\,,$$

where the bound $O(r)$ *is uniform over all* j*.*

Lemma 7.9.3 (Preservation of the lower bands) *Define*

$$\mathbf{M}_{j-1}^{\downarrow} = \mathrm{Span}\{|k\rangle |\downarrow\rangle\}_{k=0}^{j-1}$$

Then under the assumptions of Lemma 7.9.2, for any state $|v\rangle \in \mathbf{M}_{j-1}^{\downarrow}$*,*

$$\hat{U}_j |v\rangle = \hat{M}_{j-1}^{\downarrow} \hat{U}_j |v\rangle + \sqrt{j} \cdot O(r)$$

Lemma 7.9.4 (Projective mapping of TCP map) *Define*

$$\mathbf{M}_j \;=\; \mathbf{M}_j^{\downarrow} \oplus \mathrm{Span}\left(\{|0\rangle |\uparrow\rangle\}\right)$$

Then for $\hat{M}_j \hat{\rho} \hat{M}_j = \hat{\rho}$*,*

$$\mathcal{E}_j(\hat{\rho}) = \lambda_j \hat{\rho}_{j-1} + \hat{R}_j$$

where $\hat{\rho}_{j-1}$ *is a density matrix satisfying* $\hat{M}_{j-1}\hat{\rho}_{j-1}\hat{M}_{j-1} = \hat{\rho}_{j-1}$*,* $\lambda_j = 1 - \mathrm{Tr}[\hat{R}_j]$*,* $\mathrm{Tr}[\hat{R}_j] = j^{3/2} \cdot O(r)$*, and* $||\hat{R}_j|| = \sqrt{j} \cdot O(r)$*.*

Lemma 7.9.5 (Success of Deterministic Algorithm) *Given the assumptions in the previous lemmas, let* $\hat{\rho} = \hat{\rho}_S \otimes |\downarrow\rangle\langle\downarrow|$ *for any* $\hat{\rho}_S$ *whose support is in* $\mathbf{S}$*. Assume that* $r = \Omega_0/\Delta \propto \epsilon L^{-5/2}$*. Then*

$$\mathrm{Tr}[\hat{M}_0 \mathcal{E}(\hat{\rho})] = 1 - O(\epsilon)$$

as $\epsilon \to 0^+$*.*

Proof of Theorem 7.9.1: Since $\hat{M}_0 = |0\rangle\langle 0| \otimes \mathbf{1}_B$, Lemma 7.9.5 proves the first claim in Theorem 7.9.1. As shown in the proof of Lemma 7.9.2, unitary $\hat{U}_j$ requires an evolution time $\tau^{(j)} = \frac{\pi}{2\Omega}$, where $\Omega = \Omega_0 |x_0 x_j| (1 + O(r))$. The simulated time required for the algorithm is therefore

$$\begin{aligned} \tau_{tot} &= \sum_{j=1}^{L} \tau^{(j)} \\ &= \frac{\pi}{2\Omega_0} \sum_{j=1}^{L} \frac{1}{|x_0 x_j|} (1 + O(r)) \\ &= O\left(\frac{L^2\sqrt{L}}{\epsilon\Delta}\right) \sum_{j=1}^{L} \frac{1}{|x_0 x_j|}, \end{aligned}$$

where we used the fact that $\Omega_0^{-1} = (r\Delta)^{-1} = \Delta^{-1} L^{5/2} \cdot O(\epsilon^{-1})$.

□

7.9.1 Reduced Algorithm:

It is possible that the decomposition $|G\rangle = \sum_j x_j |j\rangle$ contains values of x_j that are exponentially small in n, meaning that the simulation time $\tau^{(j)}$ scales exponentially in n. Under certain conditions it is valid to neglect the cooling of such states, leading to an improved run time. This discussion allows us to derive bounds on the allowed error in the preparation of the initial system state $\hat{\rho}_S$.

Suppose that we choose to skip the cooling of all states $|j\rangle$ such that $|x_j| \leq \eta$, for some parameter η. Defining $\mathbf{S}' = \mathrm{Span}\{|j\rangle : |x_j| > \eta\} \subseteq \mathbf{S}$, we may write any initial system state $|F\rangle$ as

$$|F\rangle = \hat{S}' |F\rangle + f_\perp |F_\perp\rangle$$

Writing the compound initial state as $\hat{\rho} = |F\rangle\langle F| \otimes |\downarrow\rangle\langle\downarrow|$, we may compute

$$\hat{\rho} = (1 - |f_\perp|^2)|F'\rangle\langle F'| \otimes |\downarrow\rangle\langle\downarrow| + \hat{R}_\perp \tag{7.54}$$

where $|F'\rangle \in \hat{S}'$, and $\hat{R}_\perp$ is an error term with rank 2 and norm $||\hat{R}_\perp|| \leq \frac{3}{\sqrt{2}}|f_\perp|$.

We can define the complement to $\mathbf{S}'$ as $\mathbf{S}'_\perp = \mathbf{S}_\perp \oplus (\mathbf{S} - \mathbf{S}')$. From (7.51) and the triangle inequality, we get new norm bounds for these spaces,

$$\begin{aligned} ||\hat{S}'(\hat{V} + \hat{\delta})\hat{S}'_\perp|| &= O(\Delta r) \\ ||\hat{S}'_\perp(\hat{\delta})\hat{S}'_\perp|| &= \Delta(1/2 + O(r)) \end{aligned} \tag{7.55}$$

As these are the only assumptions necessary to prove Lemma 7.9.3, for sufficiently small r it still holds for the reduced space $(\mathbf{M}^{\downarrow}_{j-1})' = \mathbf{M}^{\downarrow}_{j-1} \cap \mathbf{S}'$. Combining this with Lemma 7.9.2, we see (as in its proof) that Lemma 7.9.4 also holds with respect to the space $\mathbf{M}'_j = \mathbf{M}_j \cap \mathbf{S}'$. We may then apply Lemma 7.9.5 to the density matrix $\hat{\rho}' = |F' \downarrow\rangle\langle F' \downarrow|$ and get the same fidelity ϵ for the reduced algorithm $\mathcal{E}' = \mathcal{E}_{i_1} \circ ... \circ \mathcal{E}_{i_{L'}}$, where $i_1 \leq i_2 ... \leq i_{L'}$ enumerate the eigenstates in $\mathbf{S}'$.

Since $\mathcal{E}'$ is applied to $\hat{\rho}$ and not $\hat{\rho}'$, we see that the reduced algorithm fidelity is

$$\begin{aligned} \mathrm{Tr}[\hat{M}_0\mathcal{E}'(\hat{\rho})] &= (1 - |f_\perp|^2)\mathrm{Tr}[\hat{M}_0\mathcal{E}'(\hat{\rho}')] + \mathrm{Tr}[\hat{M}_0\mathcal{E}'(\hat{R}_\perp)] \\ &= (1 - |f_\perp|^2)(1 - O(\epsilon)) + \mathrm{Tr}[\hat{M}_0\mathcal{E}'(\hat{R}_\perp)]\,. \end{aligned} \tag{7.56}$$

Because $\mathcal{E}'$ is a composition of L' single qubit measurements and unitary evolutions, as seen in the proof of Lemma 7.9.5 we have that $||\mathcal{E}'(\hat{R}_\perp)|| \leq L' \cdot ||\hat{R}_\perp|| = L' \cdot O(|f_\perp|)$, where $L' = \dim(\mathbf{S}')/2 - 1 \leq L$. Furthermore, as $\hat{M}_0$ is a rank 2 projector, $\hat{M}_0\mathcal{E}'(\hat{R}_\perp)$

has rank at most 2, so we conclude that

$$\begin{aligned} |\mathrm{Tr}[\hat{M}_0\mathcal{E}'(\hat{R}_\perp)]| &\leq \mathrm{rank}(\hat{M}_0\mathcal{E}'(\hat{R}_\perp)) \cdot ||\hat{M}_0\mathcal{E}'(\hat{R}_\perp)|| \\ &= L' \cdot O(|f_\perp|)\,. \end{aligned}$$

Using this result in (7.56), as long as $|f_\perp| = O(\epsilon/L')$, we may still achieve fidelity $1 - O(\epsilon)$. Notice this allows us to treat any error in the preparation of $|F\rangle\,|\downarrow\rangle$ as contributing to $|f_\perp|$.

Since we are only cooling states such that $|x_j| > \eta$, the timing of the algorithm is then

$$\begin{aligned} \tau'_{tot} &= O\left(\frac{1}{\Omega_0|x_0|}\sum_{k=1}^{L'}\frac{1}{|x_{i_k}|}\right) \\ &\leq O\left(\frac{1}{\Omega_0|x_0|}\frac{L'}{\eta}\right) \\ &= O\left(\frac{(L')^3\sqrt{L'}}{\epsilon\eta\Delta|x_0|}\right)\,. \end{aligned}$$

In the case where $|F\rangle = |G\rangle$ we see that $|f_\perp|^2 = \sum_{|x_j|\leq\eta}|x_j|^2 \leq L\eta^2$, so $L\cdot|f_\perp| \leq L^{3/2}\eta$ and in order to maintain an infidelity $O(\epsilon)$ it is sufficient to set $\eta = \epsilon/L^{3/2}$. This gives

$$\tau'_{tot} = O\left(\frac{L^5}{\epsilon^2\Delta|x_0|}\right)\,.$$

7.9.2 Proofs of Lemmas 7.9.2-7.9.5

The proof of Lemma 7.9.2 is the most involved. First, we analyze the simulated Hamiltonian $\tilde{H}_j = \hat{H}_S + \omega_B^{(j)}\mathbf{1}_S \otimes \hat{P}_\uparrow + \hat{T}_S \otimes \sigma_x + \hat{\delta}_j$ in the subspace corresponding to $\mathbf{S}$, and show that it has eigenstates near $|j\rangle\,|\downarrow\rangle \pm |0\rangle\,|\uparrow\rangle$, with eigenvalues near

$\omega_B \pm \Omega_0 x_0 x_j$. In order to do this we compute the self-energy operator $\hat{\Sigma}(z)$ for the manifold of eigenvalues near ω_j, and show how the value of $\omega_B^{(j)}$ may be calculated to account for energy shifts associated with $\hat{V}$. We then account for the static error term $\hat{\delta}_j$, and the possibility that $\hat{V}$ may couple between $\mathbf{S}$ and $\mathbf{S}_\perp$.

Proof of Lemma 7.9.2:

We begin by analyzing the case where $\hat{\delta}_j = 0$ and $\hat{V} = \hat{S}\hat{V}\hat{S} = \Omega_0 |G\rangle\langle G| \otimes \sigma_x$. Note that the compound subspace $\mathbf{S} \otimes \mathcal{H}_B$ is then invariant under

$$\begin{aligned}\tilde{H}_j^{(0)} &= \hat{H}_j + \Omega_0 |G\rangle\langle G| \otimes \sigma_x \\ &= \left(\hat{H}_S + \omega_B^{(j)} \mathbf{1}_S \otimes \hat{P}_\uparrow\right) + \Omega_0 |G\rangle\langle G| \otimes \sigma_x \,,\end{aligned}$$

which will simplify our analysis. In order to understand the dynamics of $\tilde{H}_j^{(0)}$, we compute the self-energy operator (equation (7.46)) to find an effective Hamiltonian for the eigenstates of $\tilde{H}_j^{(0)}$ with eigenvalue near ω_j. Let $\mathbf{P}$ be the subspace spanned by eigenvalues between $\lambda_- = \omega_j - \Delta/2$ and $\lambda_+ = \omega_j + \Delta/2$. Given that the eigenstates of $\hat{H}_S$ in $\mathbf{S}_\perp$ are at least Δ away from those in $\mathbf{S}$, and $|\omega_B^{(j)} - \omega_j| < \Delta/4$, we have that $\mathbf{P} \subset \mathbf{S}$ and

$$\begin{aligned}\hat{P} &= |j\rangle\langle j| \otimes |\downarrow\rangle\langle\downarrow| + |0\rangle\langle 0| \otimes |\uparrow\rangle\langle\uparrow| \\ \hat{Q} &= \sum_{k\neq 0} |k\rangle\langle k| \otimes |\uparrow\rangle\langle\uparrow| + \sum_{k\neq j} |k\rangle\langle k| \otimes |\downarrow\rangle\langle\downarrow| + \hat{S}_\perp \hat{Q} \hat{S}_\perp \\ \hat{P}\hat{H}_j\hat{P} &= \omega_j |j\rangle\langle j| \otimes |\downarrow\rangle\langle\downarrow| + \omega_B^{(j)} |0\rangle\langle 0| \otimes |\uparrow\rangle\langle\uparrow| \\ \hat{V} &= \Omega_0 |G\rangle\langle G| \otimes \sigma_x\end{aligned}$$

Using (7.46), we may now compute

$$\begin{aligned}\hat{\Sigma}(z) &= \hat{P}\hat{H}_j\hat{P} + \hat{P}\hat{V}\hat{P} + \hat{P}\hat{V}\frac{\hat{Q}}{z-\hat{Q}(\hat{H}_j+\hat{V})\hat{Q}}\hat{V}\hat{P} \\ &= \hat{P}\hat{H}_j\hat{P} + \hat{P}\hat{V}\hat{P} \\ &+ \hat{P}\hat{V}\left(\hat{G}_Q(z) + \hat{G}_Q(z)\hat{V}\hat{G}_Q(z) + ...\right)\hat{V}\hat{P}\end{aligned} \tag{7.57}$$

where $\hat{G}_Q(z) = \frac{\hat{Q}}{z-\hat{Q}\hat{H}_j\hat{Q}}$. Since the projector into $\mathbf{S}$ commutes with $\hat{P}, \hat{Q}, \hat{H}_j$, and $\hat{V}$, we may replace all operators by their projections into $\mathbf{S}$ above. This simplifies $\hat{\Sigma}(z)$, giving

$$\begin{aligned}\hat{\Sigma}(z) &= \omega_j|j\rangle\langle j| \otimes |\downarrow\rangle\langle\downarrow| + \omega_B^{(j)}|0\rangle\langle 0| \otimes |\uparrow\rangle\langle\uparrow| \\ &+ \Omega_0\hat{P}\,|G\rangle\left(\sigma_x + \Omega_0\sigma_x\,\langle G|\,\hat{G}_Q(z)\,|G\rangle\,\sigma_x\right)\sigma_*(z)\,\langle G|\,\hat{P}\end{aligned} \tag{7.58}$$

where σ_* is the bath operator

$$\begin{aligned}\sigma_*(z) &= 1 + \left(\Omega_0\,\langle G|\,\hat{G}_Q(z)\,|G\rangle\,\sigma_x\right)^2 \\ &+ \left(\Omega_0\,\langle G|\,\hat{G}_Q(z)\,|G\rangle\,\sigma_x\right)^4 + ...\end{aligned}$$

To compute $\sigma_*(z)$ explicitly, we note that

$$\langle G|\,\hat{G}_Q(z)\,|G\rangle = g_j(z)|\downarrow\rangle\langle\downarrow| + g_0(z)|\uparrow\rangle\langle\uparrow|$$

$$g_j(z) = \langle G|\,\langle\downarrow|\,\hat{G}_Q(z)\,|G\rangle\,|\downarrow\rangle = \sum_{k\neq j}\frac{|x_k|^2}{z-\omega_k}$$

$$g_0(z) = \langle G|\,\langle\uparrow|\,G_Q(z)\,|G\rangle\,|\uparrow\rangle = \sum_{k\neq 0}\frac{|x_k|^2}{z-(\omega_k+\omega_B^{(j)})}$$

so

$$\left(\Omega_0\,\langle G|\,G_Q\,|G\rangle\,\sigma_x\right)^{2n} = \left(\Omega_0^2 g_j g_0\right)^n\left(|\downarrow\rangle\langle\downarrow| + |\uparrow\rangle\langle\uparrow|\right).$$

Therefore

$$\sigma_*(z) = \frac{1}{1-\Omega_0^2 g_j(z) g_0(z)}(|\downarrow\rangle\langle\downarrow| + |\uparrow\rangle\langle\uparrow|) \tag{7.59}$$

Since $\hat{P}\,|G\rangle\,|\downarrow\rangle = x_j\,|j\rangle\,|\downarrow\rangle$ and $\hat{P}\,|G\rangle\,|\uparrow\rangle = x_0\,|0\rangle\,|\uparrow\rangle$, we may use (7.58) and (7.59) to get

$$\begin{aligned}
\hat{\Sigma}(z) &= \omega_j |j\rangle\langle j| \otimes |\downarrow\rangle\langle\downarrow| + \omega_B^{(j)} |0\rangle\langle 0| \otimes |\uparrow\rangle\langle\uparrow| \\
&\quad + \frac{\Omega_0}{1-\Omega_0^2 g_j g_0} \hat{P}\Big(|G\rangle\langle G| \otimes \big(|\downarrow\rangle\langle\uparrow| + |\uparrow\rangle\langle\downarrow| \\
&\quad + \Omega_0 g_j |\uparrow\rangle\langle\uparrow| + \Omega_0 g_0 |\downarrow\rangle\langle\downarrow| \big) \Big) \hat{P} \\
&= \begin{pmatrix} \omega_j & 0 \\ 0 & \omega_B^{(j)} \end{pmatrix} \\
&\quad + \frac{\Omega_0}{1-\Omega_0^2 g_j(z) g_0(z)} \begin{pmatrix} |x_j|^2 \Omega_0 g_0(z) & x_0 x_j \\ x_0 x_j & |x_0|^2 \Omega_0 g_j(z) \end{pmatrix}
\end{aligned} \tag{7.60}$$

where the above matrices are written in the $\{|j\rangle\,|\downarrow\rangle\,, |0\rangle\,|\uparrow\rangle\}$ basis.

Using the above expression, we define the effective Hamiltonian $\hat{H}_{eff} = \hat{\Sigma}(\omega_B^{(j)})$. We identify the diagonal elements of the second matrix above as the level shift, and observe these are composed of even powers in Ω_0. If the diagonal terms in $\hat{H}_{eff}$ were equal, it would cause coherent oscillations $|j\rangle\,|\downarrow\rangle \leftrightarrow |0\rangle\,|\uparrow\rangle$ at a rate $2\Omega \approx 2\Omega_0 |x_0 x_j|$. We may find $\omega_B^{(j)}$ such that this is the case, by solving the degree $L+1$ polynomial equation

$$\big((1-\Omega_0^2 g_j(z) g_0(z))(z-\omega_j) + \Omega_0^2 (|x_0|^2 g_j(z) - |x_j|^2 g_0(z)) \big) \Big|_{z=\omega_B^{(j)}} = 0 \tag{7.61}$$

Effectively, we are adjusting the value of $\omega_B^{(j)}$ so that the even order energy shifts induced by $\hat{V}$ are canceled out. Note that we need a solution for $\omega_B^{(j)}$ that is contained

in $(\omega_j - \Delta/4, \omega_j + \Delta/4)$. Using the fact that $\Omega_0 < \Delta/4$, as well as $|g_j|, |g_0| \leq \frac{4}{3\Delta}$ for $z = \omega_B^{(j)} \in [\omega_j - \Delta/4, \omega_j + \Delta/4]$, it is not difficult to show that the left hand side is negative for $\omega_B^{(j)} = \omega_j - \Delta/4$ and positive for $\omega_B^{(j)} = \omega_j + \Delta/4$. Since the left hand side is smooth over this range, by the Intermediate Value Theorem a root exists within $(\omega_j - \Delta/4, \omega_j + \Delta/4)$. If our computed root is $\delta\omega_B^{(j)}$ off from the exact solution, from (7.60) we see the two states retain a splitting $O(\delta\omega_B^{(j)})$. The necessary accuracy $\delta\omega_B^{(j)}$ can thus be incorporated into the error term $\hat{S}\hat{\delta}_j\hat{S}$, as long as $\delta\omega_B^{(j)} = O(||\hat{S}\hat{\delta}_j\hat{S}||) = \Omega_0|x_0x_j| \cdot O(r)$.

We therefore assume that $\omega_B^{(j)}$ has been chosen so that the diagonal terms in (7.60) are equal at $z = \omega_B^{(j)}$, which means

$$\hat{H}_{eff} = \omega_B^* \mathbf{1} + \Omega \left(|j\rangle\langle 0| \otimes |\downarrow\rangle\langle\uparrow| + |0\rangle\langle j| \otimes |\uparrow\rangle\langle\downarrow| \right)$$

where

$$\Omega = \frac{\Omega_0 x_0 x_j}{1 - \Omega_0^2 g_j g_0} = \Omega_0 x_0 x_j \left(1 + O(r^2)\right)$$
$$\omega_B^* = \omega_B^{(j)} + \Omega_0 |x_0 x_j| \frac{|x_0/x_j| \Omega_0 g_j}{1 - \Omega_0^2 g_j g_0} = \omega_B^{(j)} + \Omega \cdot O(r)$$

and we assume that $|x_0/x_j| \leq O(1)$.

$\hat{H}_{eff}$ has eigenstates $|v_\pm\rangle = \frac{1}{\sqrt{2}} \left(|j\rangle |\downarrow\rangle \pm |0\rangle |\uparrow\rangle \right)$ with energy $\omega_B^* \pm \Omega$, so dynamics under $\hat{H}_{eff}$ for time $\tau_j = \frac{\pi}{2\Omega}$ would map state $|j\rangle |\downarrow\rangle \rightarrow |0\rangle |\uparrow\rangle$. To show that evolution under $\tilde{H}_j^{(0)}$ achieves the same mapping, we use Theorem 7.8.1 and Corollary 7.8.2 to show it has eigenstates and eigenvalues near those of $\hat{H}_{eff}$. To do this, we must determine an error bound for $||\hat{\Sigma}(z) - \hat{H}_{eff}||$.

As in (7.57) above, since $\hat{H}_{eff} = \hat{\Sigma}(\omega_B^{(j)})$ we have

$$\hat{\Sigma}(z) - \hat{H}_{eff} \;=\; \hat{P}\hat{V} \left(\tilde{G}_Q(z) - \tilde{G}_Q(\omega_B^{(j)}) \right) \hat{V}\hat{P} \tag{7.62}$$

where

$$\tilde{G}_Q(z) = \frac{\hat{Q}}{z - \hat{Q}(\hat{H}_j + \hat{V})\hat{Q}} = \sum_s (z - E_s)^{-1} |\phi_s\rangle\langle\phi_s|$$

for $|\phi_s\rangle \in Q$. Since $|\omega_B^{(j)} - \omega_j| < \Delta/4$, the eigenvalues of $\hat{Q}\hat{H}_j\hat{Q}$ are at least $3\Delta/4$ away from ω_j. As $||\hat{V}|| < \Delta/4$, by Lemma 7.8.3 we then conclude that $E_s \in (-\infty, \omega_j - \Delta/2] \cup [\omega_j + \Delta/2, \infty)$ for all s. $\tilde{G}_Q(z)$ is therefore analytic for $z \in [\omega_j - \Delta/4, \omega_j + \Delta/4]$, so we may compute its Taylor series expansion about $\omega_B^{(j)} \in (\omega_j - \Delta/4, \omega_j + \Delta/4)$:

$$\tilde{G}_Q(z) = \sum_s \left[(\omega_B^{(j)} - E_s)^{-1} - (z - \omega_B^{(j)})(z_s - E_s)^{-2} \right] |\phi_s\rangle\langle\phi_s|$$

For some $z_s \in [\omega_j - \Delta/4, \omega_j + \Delta/4]$, between $\omega_B^{(j)}$ and z. Since $|z_s - E_s| \geq \Delta/4$, we conclude that

$$\begin{gathered} ||\tilde{G}_Q(z) - \tilde{G}_Q(\omega_B^{(j)})|| \leq |z - \omega_B^{(j)}| \left(\frac{4}{\Delta}\right)^2 \\ \Longrightarrow \\ ||\hat{\Sigma}(z) - \hat{H}_{eff}|| \leq |z - \omega_B^{(j)}| \left(\frac{4||\hat{V}||}{\Delta}\right)^2 \\ = |z - \omega_B^{(j)}|(4r)^2 \end{gathered} \tag{7.63}$$

As above, the spectrum of $\hat{H}_{eff}$ is contained in $[c, d]$, where $c = \omega_B^{(j)} - \Omega\,(1 + O(r))$, $d = \omega_B^{(j)} + \Omega\,(1 + O(r))$. In Theorem 7.8.1, we consider only values of z in $[c - \gamma, d + \gamma]$ (γ is the error in the eigenvalues of $\hat{H}_{eff}$, compared to $\tilde{H}_j^{(0)}$). Thus we can determine γ self-consistently by solving

$$\gamma = |z - \omega_B^{(j)}|(4r)^2$$

for $z = d + \gamma$ and $z = c - \gamma$. To leading order in r, this gives

$$\gamma = \Omega \cdot O(r) \tag{7.64}$$

(in fact $\gamma = \Omega \cdot O(r^2)$, but the following result holds for (7.64) as well). Applying Theorem 7.8.1, we have that the two eigenvalues of $\hat{H}_{eff}$, $E_\pm = \omega_B^* \pm \Omega$, are γ close to the eigenvalues of $\tilde{H}_j^{(j)}$. The relative error in the energy difference $(E_+ - E_-)$ is therefore $O(\gamma/\Omega) = O(r)$.

Now Corollary 7.8.2 can be used to show that the eigenvectors of $\hat{H}_{eff}$ are close to the corresponding eigenvectors of $\tilde{H}_j^{(0)}$. In the notation of that corollary, we can define $\hat{P}' = |v_+\rangle\langle v_+|$, and see that $\nu = 0, \eta = 2\Omega$. Denoting the analogous eigenvectors and eigenvalues of $\tilde{H}_j^{(0)}$ by $|\tilde{v}_\pm\rangle$ and $\tilde{E}_\pm$, using (7.64) we see that

$$\begin{aligned} |\langle \tilde{v}_+ | v_+ \rangle|^2 &= \langle \tilde{v}_+ | \hat{P}' | \tilde{v}_+ \rangle \\ &> \left(1 - \left(\frac{2||\hat{V}||}{\Delta}\right)^2\right)\left(1 - \left(\frac{2\gamma + \nu}{\eta - \gamma}\right)^2\right) \\ &= 1 - O(r^2) \end{aligned}$$

and likewise for $\langle \tilde{v}_- | v_- \rangle$. From this and Theorem 1 we conclude that

$$\begin{aligned} |\tilde{v}_\pm\rangle = |v_\pm\rangle + O(r) = \frac{1}{\sqrt{2}}(|j\rangle|\downarrow\rangle \pm |0\rangle|\uparrow\rangle) + O(r) \\ \tilde{E}_+ - \tilde{E}_- = (E_+ - E_-)(1 + O(r)) = 2\Omega(1 + O(r)) \end{aligned} \tag{7.65}$$

For time evolution $\tau_j = \frac{\pi}{E_+ - E_-} = \frac{\pi}{2\Omega}$, (7.65) implies the statement of Lemma 7.9.2. To complete the proof, we account for the case when $\hat{V} \neq \hat{S}\hat{V}\hat{S}$ or $\hat{\delta} \neq 0$ by including the effect of these terms in $||\hat{\Sigma}(z) - \hat{H}_{eff}||$. As long as (7.64) still holds, we conclude that (7.65) is still valid. The full Hamiltonian is now $\tilde{H}_j = \hat{H}_j + \hat{S}\hat{V}\hat{S} + \hat{\delta}_{eff}$, where $\hat{\delta}_{eff}$ accounts for the terms we previously neglected. Specifically,

$$\hat{\delta}_{eff} = \hat{\delta} + (\hat{V} - \hat{S}\hat{V}\hat{S})$$

We wish to compute the bound $||\hat{\Sigma}(z) - \hat{H}_{eff}||$, where now $\hat{\Sigma}(z)$ is defined with respect to the perturbation $\hat{S}\hat{V}\hat{S} + \hat{\delta}_{eff}$ (see (7.66) below). As before, we have $\hat{H}_{eff} =$

$\hat{\Sigma}(\omega_B^{(j)})|_{\hat{\delta}_{eff}=0}$, with $\hat{\Sigma}(z)|_{\hat{\delta}_{eff}=0}$ defined as in (7.57). Suppose $||\hat{\Sigma}(z) - \hat{\Sigma}(z)|_{\hat{\delta}_{eff}=0}|| = \gamma'$. By the triangle inequality,

$$||\hat{\Sigma}(z) - \hat{H}_{eff}|| \leq \gamma' + ||\hat{\Sigma}(z)|_{\hat{\delta}_{eff}=0} - \hat{H}_{eff}||$$

We could then repeat the previous analysis to compute γ, and get $\gamma = \Omega \cdot O(r) + O(\gamma')$. The results of Theorem 7.8.1 and Corollary 7.8.2 could then still be applied to get (7.65), as long as γ' also satisfies (7.64). Below we show that this is the case, as long as (7.51) is true.

Including $\hat{\delta}_{eff}$ in (7.46), we see that

$$\begin{aligned}\hat{\Sigma}(z) = \hat{P}\hat{H}_j\hat{P} + \hat{P}\hat{V}\hat{P} + \hat{P}\hat{\delta}_{eff}\hat{P} \\ + \hat{P}(\hat{S}\hat{V}\hat{S} + \hat{\delta}_{eff})\cdot \\ \frac{\hat{Q}}{z - \hat{Q}(\hat{H}_j + \hat{S}\hat{V}\hat{S} + \hat{\delta}_{eff})\hat{Q}}(\hat{S}\hat{V}\hat{S} + \hat{\delta}_{eff})\hat{P}\end{aligned} \tag{7.66}$$

In order to bound all terms proportional to $\hat{\delta}_{eff}$, we use the relation $(\hat{A} - \hat{B})^{-1} = \hat{A}^{-1} + \hat{A}^{-1}\hat{B}(\hat{A} - \hat{B})^{-1}$ to get

$$\begin{aligned}\frac{\hat{Q}}{z - \hat{Q}(\hat{H}_j + \hat{S}\hat{V}\hat{S} + \hat{\delta}_{eff})\hat{Q}} = \tilde{G}_Q(z) \\ +\tilde{G}_Q(z)\hat{\delta}_{eff}\frac{\hat{Q}}{z - \hat{Q}(\hat{H}_j + \hat{S}\hat{V}\hat{S} + \hat{\delta}_{eff})\hat{Q}}\end{aligned}$$

where $\hat{G}_Q(z) = \frac{\hat{Q}}{z - \hat{Q}(\hat{H}_j + S\hat{V}S)\hat{Q}}$. This allows us to write:

$$\begin{aligned}
&\hat{\Sigma}(z) - \hat{\Sigma}(z)|_{\hat{\delta}_{eff}=0} = \hat{P}\hat{\delta}_{eff}\hat{P} \\
&+ \hat{P}\hat{\delta}_{eff}\frac{\hat{Q}}{z - \hat{Q}(\hat{H}_j + \hat{S}\hat{V}\hat{S} + \hat{\delta}_{eff})\hat{Q}}\hat{S}\hat{V}\hat{S}\hat{P} + \text{h.c.} \\
&+ \hat{P}\hat{\delta}_{eff}\frac{\hat{Q}}{z - \hat{Q}(\hat{H}_j + \hat{S}\hat{V}\hat{S} + \hat{\delta}_{eff})\hat{Q}}\hat{\delta}_{eff}\hat{P} \\
&+ \hat{P}\hat{S}\hat{V}\hat{S}\tilde{G}_Q\hat{S}\hat{\delta}_{eff}\cdot \\
&\quad\frac{\hat{Q}}{z - \hat{Q}(\hat{H}_j + \hat{S}\hat{V}\hat{S} + \hat{\delta}_{eff})\hat{Q}}\hat{S}\hat{V}\hat{S}\hat{P}
\end{aligned} \tag{7.67}$$

We now bound this difference. The operator $\hat{Q}(z - \hat{H}_j - \hat{S}\hat{V}\hat{S})\hat{Q}$ can be diagonalized in blocks of $\mathbf{S}$ and $\mathbf{S}_\perp$. As before, for $z \in [\omega_j - \Delta/4, \omega_j + \Delta/4]$, within both $\mathbf{S}$ and $\mathbf{S}_\perp$ this operator has eigenvalues with magnitude at least $\Delta/2$. In the notation of Lemma 7.8.7, we may define $\hat{A} = \hat{Q}(z - \hat{H}_j - \hat{S}\hat{V}\hat{S})\hat{Q}$, $\hat{B} = \hat{Q}\hat{\delta}_{eff}\hat{Q}$, $G_1 = \Delta/2, G_2 = \Delta/2$, so that $(\hat{A} - \hat{B})^{-1} = \frac{\hat{Q}}{z - \hat{Q}(\hat{H}_j + \hat{S}\hat{V}\hat{S} + \hat{\delta}_{eff})\hat{Q}}$. Defining $R_i = ||\hat{S}_i\hat{Q}\hat{\delta}_{eff}\hat{Q}\hat{S}_i||/\Delta \leq ||\hat{S}_i\hat{\delta}_{eff}\hat{S}_i||/\Delta$, $R_\times = ||\hat{S}\hat{Q}\hat{\delta}_{eff}\hat{Q}\hat{S}_\perp||/\Delta \leq ||\hat{S}\hat{\delta}_{eff}\hat{S}_\perp||/\Delta$, by Lemma 7.8.7 one may show that

$$\begin{aligned}
||\hat{S}\frac{\hat{Q}}{z - \hat{Q}(\hat{H}_j + \hat{S}\hat{V}\hat{S} + \hat{\delta}_{eff})\hat{Q}}\hat{S}_\perp|| &= O(R_\times) \\
||\hat{S}\frac{\hat{Q}}{z - \hat{Q}(\hat{H}_j + \hat{S}\hat{V}\hat{S} + \hat{\delta}_{eff})\hat{Q}}\hat{S}|| &= O(1) \\
||\hat{S}_\perp\frac{\hat{Q}}{z - \hat{Q}(\hat{H}_j + \hat{S}\hat{V}\hat{S} + \hat{\delta}_{eff})\hat{Q}}\hat{S}_\perp|| &= O(1)
\end{aligned}$$

Writing all terms of (7.67) in $\mathbf{S}$, $\mathbf{S}_\perp$ blocks, we have for $z \in [\omega_j - \Delta/4, \omega_j + \Delta/4]$

$$\begin{aligned}
\hat{P}\hat{\delta}_{eff} &= \Delta \cdot \begin{pmatrix} O(R_1) & O(R_\times) \end{pmatrix} \\
\frac{\hat{Q}}{z - \hat{Q}(\hat{H}_j + \hat{S}\hat{V}\hat{S} + \hat{\delta}_{eff})\hat{Q}} &= \Delta^{-1} \cdot \begin{pmatrix} O(1) & O(R_\times) \\ O(R_\times) & O(1) \end{pmatrix} \\
\hat{S}\hat{V}\hat{S}\hat{P} &= \Delta \cdot \begin{pmatrix} O(r) \\ 0 \end{pmatrix} \\
\hat{P}\hat{S}\hat{V}\hat{S}\tilde{G}_Q\hat{S}\hat{\delta}_{eff} &= \Delta \cdot \begin{pmatrix} O(rR_1) & O(rR_x) \end{pmatrix}
\end{aligned}$$

With these components, using (7.67) one may calculate $\gamma' = ||\hat{\Sigma}(z) - \hat{\Sigma}(z)|_{\hat{\delta}_{eff}=0}|| = O(\Delta(R_1 + R_\times^2))$. We need $||\hat{\Sigma}(z) - \hat{\Sigma}(z)|_{\hat{\delta}_{eff}=0}|| = \Omega \cdot O(r)$, so we require

$$\begin{aligned}
R_1 &= O(r \cdot \Omega/\Delta) \\
R_\times^2 &= O(r \cdot \Omega/\Delta) \\
R_2 &\leq 1/2
\end{aligned}$$

where the last inequality comes from the bound on $\hat{\delta}_{eff}$ necessary to use Lemma 7.8.7. One may check that these statements are satisfied by (7.51).

□

Proof of Lemma 7.9.3:

As before, we have $\hat{H}_j = \hat{H}_S + \hat{H}_B$, $\tilde{H}_j = \hat{H}_j + \hat{V} + \hat{\delta}_j$. Define $\hat{P}_0$ as the subspace spanned by the eigenspaces of $\hat{H}_j$ with eigenvalues $\omega_0, \omega_1, ...\omega_j$. This corresponds to the space $\mathbf{M}_{j-1}^{\downarrow} \subseteq \mathbf{S}$ mentioned in the lemma. In the language of Corollary 7.8.5, it corresponds to $\lambda_{-k} = \lambda_{k+} = \omega_k$ and Δ as defined for $\hat{H}_S$. The proof comes in two

steps. We define the intermediate Hamiltonian

$$\tilde{H}'_j = \hat{H}_j + \hat{S}\hat{V}\hat{S}\,,$$

with a subspace $\mathbf{P}_1$ corresponding to eigenvalues within $(\omega_0 - \Delta/8, \omega_0 + \Delta/8) \cup (\omega_1 - \Delta/8, \omega_1 + \Delta/$
Likewise, $\mathbf{P}_2$ is the subspace of $\tilde{H}_j$ of eigenvalues within $(\omega_0 - \Delta/4, \omega_0 + \Delta/4) \cup (\omega_1 - \Delta/4, \omega_1 + \Delta/$
The proof follows by showing that (up to an error $O(r^2)$), any state in $\mathbf{P}_0$ is in $\mathbf{P}_1$, and any state in $\mathbf{P}_1$ is in $\mathbf{P}_2$. This will imply that a state in $\mathbf{P}_0$ undergoing evolution $\hat{U}_j$ will remain in $\mathbf{P}_0$. For simplicity of notation, for all equations below let $|v_i\rangle$ represent a normalized state in $\mathbf{P}_i$.

Since $\tilde{H}'_j$ and $\hat{H}_j$ are block diagonal in $\mathbf{S}$ and $\mathbf{S}_\perp$, as long as, $\mathbf{P}_1 \subseteq \mathbf{S}$ it is sufficient to reduce our analysis to $\mathbf{S}$. This holds if $\hat{S}_\perp(\hat{V} + \hat{\delta})\hat{S}_\perp$ does not change the eigenvalue of $\mathbf{S}_\perp$ states by more than $\Delta/2$, as implied by Lemma 7.8.3 and (7.51). Considering only $\mathbf{S}$, (7.51) implies the bound $||\hat{S}\left(\tilde{H}'_j - \hat{H}\right)\hat{S}||/\Delta = O(r)$. By Corollary 7.8.5, we have that

$$\langle v_0|\,\hat{P}_1\,|v_0\rangle = 1 - j \cdot O(r^2)$$

Writing $|v_0\rangle = a\,|v_1\rangle + b\,|v_1^\perp\rangle$ where $\hat{P}_1\,|v_1^\perp\rangle = 0$, one can easily show that

$$\hat{P}_1\,|v_0\rangle = \sqrt{1 - j \cdot O(r^2)}\,|v_1\rangle$$

Equations (7.51) also imply that $\mathbf{P}_1$ is energetically separate from its complement $\mathbf{Q}_1$ by at least $\Delta' = \Delta/4$, so that $||\tilde{H}_j - \tilde{H}'_j||/\Delta' = O(r)$, and as above,

$$\hat{P}_2\,|v_1\rangle = \sqrt{1 - j \cdot O(r^2)}\,|v_2\rangle$$

We can combine these statements to get

$$\begin{aligned}\langle v_0|\,\hat{P}_2\,|v_0\rangle &\geq \langle v_0|\,\hat{P}_1\hat{P}_2\hat{P}_1\,|v_0\rangle \\ &= (1-j\cdot O(r^2))\,\langle v_1|\,\hat{P}_2\,|v_1\rangle \\ &= (1-j\cdot O(r^2))^2\end{aligned}$$

Finally, writing $|v_0\rangle = a\,|v_2\rangle + b\left|v_2^{\perp}\right\rangle$, the above statement implies

$$\hat{P}_2\,|v_0\rangle = (1-j\cdot O(r^2))\,|v_2\rangle$$

and by an identical analysis, for any $|v_2\rangle \in \mathbf{P}_2$, there exists $|v_0\rangle \in \mathbf{P}_0$ such that

$$\hat{P}_0\,|v_2\rangle = (1-j\cdot O(r^2))\,|v_0\rangle$$

Notice that the diagonals of $\hat{P}_0$ are at least as large as those of $\hat{P}_2\hat{P}_0\hat{P}_2$. Since $\mathbf{P}_2$ is an subspace of $\tilde{H}_j$, it is clear that $\hat{P}_2\hat{U}_j = \hat{U}_j\hat{P}_2$. Using these facts and the above equalities, we compute the bound:

$$\begin{aligned}\langle v_0|\,\hat{U}_j^{\dagger}\hat{P}_0\hat{U}_j\,|v_0\rangle &\geq \langle v_0|\,\hat{U}_j^{\dagger}\hat{P}_2\hat{P}_0\hat{P}_2\hat{U}_j\,|v_0\rangle \\ &= \langle v_0|\,\hat{P}_2\hat{U}_j^{\dagger}\hat{P}_0\hat{U}_j\hat{P}_2\,|v_0\rangle \\ &= (1-j\cdot O(r^2))^2\,\langle v_2|\,\hat{P}_0\,|v_2\rangle \\ &= (1-j\cdot O(r^2))^4 = 1-j\cdot O(r^2)-j^3\cdot O(r^6) \\ &= 1-j\cdot O(r^2)\end{aligned}$$

where in the last line we use the fact that $r \propto L^{-5/2}$. Since $\hat{Q}_0 = \mathbf{1}-\hat{P}_0$ we get

$$||\hat{Q}_0\hat{U}_j\,|v_0\rangle\,||^2 \leq j\cdot O(r^2)$$

Writing $\hat{U}_j\,|v_0\rangle = \hat{P}_0\hat{U}_j\,|v_0\rangle + \hat{Q}_0\hat{U}_j\,|v_0\rangle$, we conclude the proof noting that $\hat{P}_0 = \hat{M}_{j-1}^{\downarrow}$ and that the bound $O(r^2)$ is dependent only on the ratio $r = \Omega_0/\Delta$.

□

Proof of Lemma 7.9.4:

Since the operation $\mathcal{E}_j$ starts with a bath measurement and since the $\hat{M}_j$ projector commutes with the bath projectors $\mathbf{1}_S \otimes \hat{P}_\downarrow$ and $\mathbf{1}_S \otimes \hat{P}_\uparrow$, we may assume without loss of generality that

$$\hat{\rho} = \hat{M}_j^\downarrow \hat{\rho} \hat{M}_j^\downarrow + p_0 |0\rangle\langle 0| \otimes |\uparrow\rangle\langle\uparrow|$$

where $\mathbf{M}_j^\downarrow = \mathrm{Span}\{|k\rangle |\downarrow\rangle\}_{k=0}^j$. Furthermore, since

$$\mathcal{E}_j(|0\rangle\langle 0| \otimes |\uparrow\rangle\langle\uparrow|) = |0\rangle\langle 0| \otimes |\uparrow\rangle\langle\uparrow| = \hat{M}_{j-1}\mathcal{E}_j(|0\rangle\langle 0| \otimes |\uparrow\rangle\langle\uparrow|)\hat{M}_{j-1}$$

by the linearity of TCP maps it suffices to analyze the component of $\hat{\rho}$ within $\mathbf{M}_j^\downarrow$. We may therefore assume that $\hat{\rho} = \hat{M}_j^\downarrow \hat{\rho} \hat{M}_j^\downarrow$. Since $\hat{\rho}$ is a density matrix, we have that

$$\hat{\rho} = \sum_l p_l |v_l\rangle\langle v_l| \otimes |\downarrow\rangle\langle\downarrow|$$

where $|v_l\rangle |\downarrow\rangle \in \mathbf{M}_j^\downarrow$ and l is a sum over at most $j+1 = \dim(\mathbf{M}_j^\downarrow)$ terms. Each $|v_l\rangle |\downarrow\rangle$ may be decomposed into components parallel and orthogonal to $|j\rangle |\downarrow\rangle$:

$$|v_l\rangle |\downarrow\rangle = a_l |j\rangle |\downarrow\rangle + b_l \left|v_l^\perp\right\rangle$$

where $\left|v_l^\perp\right\rangle \in \mathbf{M}_{j-1}^\downarrow$. By Lemma 7.9.3, we have that

$$\hat{U}_j \left|v_l^\perp\right\rangle = \hat{M}_{j-1}^\downarrow \hat{U}_j \left|v_l^\perp\right\rangle + \sqrt{j} \cdot O(r)$$

Likewise by Lemma 7.9.2,

$$\begin{aligned} \hat{U}_j |j\rangle |\downarrow\rangle &= |0\rangle |\uparrow\rangle + O(r) \\ &= \hat{M}_{j-1}\hat{U}_j |j\rangle |\downarrow\rangle + O(r) \end{aligned}$$

Since $\mathbf{M}_{j-1}^{\downarrow} \subset \mathbf{M}_{j-1}$, we conclude that

$$\hat{U}_j |v_l\rangle |\downarrow\rangle = \hat{M}_{j-1}\hat{U}_j |v_l\rangle |\downarrow\rangle + \sqrt{j} \cdot O(r)$$

Finally, since $\mathcal{E}_j$ is a linear operator, we see that

$$\begin{aligned}
\mathcal{E}_j(\hat{\rho}) &= \sum_l p_l \mathcal{E}_j \left(|v_l\rangle\langle v_l| \otimes |\downarrow\rangle\langle\downarrow| \right) \\
&= \sum_l p_l \left(\hat{U}_j |v_l\rangle\langle v_l| \otimes |\downarrow\rangle\langle\downarrow| \hat{U}_j^\dagger \right) \\
&= \sum_l p_l \left(\hat{M}_{j-1}\hat{U}_j |v_l\rangle |\downarrow\rangle + \sqrt{j} \cdot O(r) \right) \\
&\quad \cdot \left(\langle v_l| \langle\downarrow| \hat{U}_j^\dagger \hat{M}_{j-1} + \sqrt{j} \cdot O(r) \right) \\
&= \hat{M}_{j-1}\mathcal{E}_j(\hat{\rho})\hat{M}_{j-1} + \hat{R}_j
\end{aligned}$$

where $\hat{R}_j$ is the sum of all terms proportional to $O(r)$. Using the triangle inequality and the fact that the p_l sum to 1, we see that $||\hat{R}_j|| = \sqrt{j} \cdot O(r)$. Since $\hat{R}_j$ is a sum of at most $(j+1)$ operators, each of rank 2, we see that $\text{rank}(\hat{R}_j) \leq 2(j+1)$. Therefore $|\text{Tr}[\hat{R}_j]| \leq \text{rank}(\hat{R}_j) \cdot ||\hat{R}_j|| = j^{3/2} \cdot O(r)$. Since a projection of a density matrix is proportional to a density matrix, we may write $\hat{M}_{j-1}\mathcal{E}_j(\hat{\rho})\hat{M}_{j-1} = \lambda_j \hat{\rho}_{j-1}$, with $\lambda_j = \text{Tr}[\hat{M}_{j-1}\mathcal{E}_j(\hat{\rho})\hat{M}_{j-1}] = \text{Tr}[\mathcal{E}_j(\hat{\rho}) - \hat{R}_j] = 1 - j^{3/2} \cdot O(r)$.

□

Proof of Lemma 7.9.5:

$\mathcal{E}$ is defined by the chain of TCP maps,

$$\mathcal{E} = \mathcal{E}_1 \circ \mathcal{E}_2 ... \circ \mathcal{E}_L$$

The initial state of the system and bath is described by the density matrix $\hat{\rho}_L =$

$|F\downarrow\rangle\langle F\downarrow|$, where $|F\rangle|\downarrow\rangle \in \mathbf{M}_L$. Repeated application of Lemma 7.9.4 gives

$$\begin{aligned}
\mathcal{E}(\hat{\rho}_L) &= \mathcal{E}_1 \circ \mathcal{E}_2 ... \circ \mathcal{E}_{L-1}\left(\lambda_L \hat{\rho}_{L-1} + \hat{R}_L\right) \\
&= \mathcal{E}_1 \circ \mathcal{E}_2 ... \circ \mathcal{E}_{L-2}\Big(\lambda_L \lambda_{L-1} \hat{\rho}_{L-2} \\
&\quad + \lambda_L \hat{R}_{L-1} + \mathcal{E}_{L-1}(\hat{R}_L)\Big) \\
&\vdots \\
&= \left(\prod_{k=1}^{L} \lambda_k\right) \hat{\rho}_0 + \hat{R}_{tot}
\end{aligned}$$

where $\hat{M}_0 \hat{\rho}_0 \hat{M}_0 = \hat{\rho}_0$, $\hat{R}_{tot}$ represents all other terms, and $\mathrm{Tr}[\hat{R}_{tot}] = 1 - \left(\prod_{k=1}^{L} \lambda_k\right)$ since $\mathcal{E}$ is trace-preserving.

We will bound the infidelity, $1 - \mathrm{Tr}[\hat{M}_0 \mathcal{E}(\hat{\rho}_L)] = 1 - \left(\prod_{k=1}^{L} \lambda_k\right) - \mathrm{Tr}[\hat{M}_0 \hat{R}_{tot}]$, by showing that $1 - \left(\prod_{k=1}^{L} \lambda_k\right)$ and $\mathrm{Tr}[\hat{M}_0 \hat{R}_{tot}]$ are small. First, consider the quantity $y = \log\left(\prod_{k=1}^{L} \lambda_k\right) = \sum_{k=1}^{L} \log(\lambda_k)$. By Lemma 7.9.4, we see that $\lambda_k = 1 - \mathrm{Tr}(\hat{R}_k)$. Given that $|\log(1-x)| \leq 2|x|$ for $|x| < 1/2$, we conclude that for $|\mathrm{Tr}(\hat{R}_k)| < 1/2$,

$$\begin{aligned}
|y| &\leq \sum_{k=1}^{L} \Big|\log(1 - \mathrm{Tr}[\hat{R}_k])\Big| \\
&\leq \sum_{k=1}^{L} 2|\mathrm{Tr}[\hat{R}_k]| \\
&= \sum_{k=1}^{L} k^{3/2} \cdot O(r) \\
&= L^{5/2} \cdot O(r)
\end{aligned}$$

Thus, to leading order in r,

$$1 - \left(\prod_{k=1}^{L} \lambda_k\right) = 1 - e^y = L^{5/2} \cdot O(r)$$

To show the second term is small, we must bound $\hat{R}_{tot}$, which is the sum of all error terms:

$$\hat{R}_{tot} = \sum_{k=1}^{L} \left(\prod_{j=k+1}^{L} \lambda_j \right) \mathcal{E}_1 \circ ... \circ \mathcal{E}_{k-1}(\hat{R}_k)$$

From the simple form of $\mathcal{E}_j$ (see (7.53)), we see that

$$\mathcal{E}_1 \circ ... \circ \mathcal{E}_{k-1}(\hat{R}_k) = \sum_{j=1}^{k} \hat{A}_j \hat{R}_k \hat{A}_j^\dagger$$

where

$$\hat{A}_j = |\uparrow\rangle\langle\uparrow| \left(\hat{U}_j |\downarrow\rangle\langle\downarrow| \right) \cdot \left(\hat{U}_{j+1} |\downarrow\rangle\langle\downarrow| \right) \cdot ... \cdot \left(\hat{U}_{k-1} |\downarrow\rangle\langle\downarrow| \right)$$

for $2 \leq j \leq k$, and

$$\begin{aligned} \hat{A}_1 &= \left(\hat{U}_1 |\downarrow\rangle\langle\downarrow| \right) \cdot \left(\hat{U}_2 |\downarrow\rangle\langle\downarrow| \right) \cdot ... \cdot \left(\hat{U}_{k-1} |\downarrow\rangle\langle\downarrow| \right) \\ \hat{A}_k &= |\uparrow\rangle\langle\uparrow| \end{aligned}$$

Since $\hat{A}_j$ is a product of projectors and unitaries, we must have that $||\hat{A}_j \hat{R}_k \hat{A}_j^\dagger|| \leq ||\hat{R}_k||$, so by the triangle inequality and Lemma 7.9.4 it follows that

$$||\mathcal{E}_1 \circ ... \circ \mathcal{E}_{k-1}(\hat{R}_k)|| \leq k||\hat{R}_k|| = k^{3/2} \cdot O(r) \implies$$

$$||\hat{R}_{tot}|| = \sum_{k=1}^{L} k^{3/2} \cdot O(r) = L^{5/2} \cdot O(r)$$

Finally, we note that since $\hat{M}_0$ is a projector of rank two, $\hat{M}_0 \hat{R}_{tot} \hat{M}_0$ also has rank at most 2. By the cyclic property of the trace, we conclude that

$$\begin{aligned} |\mathrm{Tr}[\hat{M}_0 \hat{R}_{tot}]| &= |\mathrm{Tr}[\hat{M}_0 \hat{R}_{tot} \hat{M}_0]| \\ &\leq \mathrm{rank}(\hat{M}_0 \hat{R}_{tot} \hat{M}_0) \cdot ||\hat{M}_0 \hat{R}_{tot} \hat{M}_0|| \\ &= L^{5/2} \cdot O(r) \end{aligned}$$

Combining the two results, we have that

$$1 - \mathrm{Tr}[\hat{M}_0 \mathcal{E}(\hat{\rho}_L)] = L^{5/2} \cdot O(r)$$

Thus, as long as $r = O(\epsilon / L^{5/2})$, the algorithm succeeds with infidelity $O(\epsilon)$.

□

7.10 Appendix C: Extension Analysis

We now discuss an augmentation of the previous cooling technique which does not require knowledge of the overlaps x_k describing the coupling $\hat{T}_S$ (as in equation (7.10)). It is described in detail in Section 7.6, though we summarize it here. We assume that the system Hamiltonian $\hat{H}_S$ has the form

$$\hat{H}_S = \hat{P}_1 \hat{H}_S \hat{P}_1 + \hat{P}_2 \hat{H}_S \hat{P}_2$$

where $\mathbf{P}_1$ is the subspace of $\hat{H}_S$ spanned by eigenvalues between $(\omega_1 - \delta\omega)$ and $(\omega_1 + \delta\omega)$, $|0\rangle$ is the non-degenerate ground states $\hat{H}_S$ with energy $\omega_0 = 0$, and $\hat{P}_2$ is a projector into the space orthogonal to $\mathrm{Span}\{|0\rangle\} \oplus \mathbf{P}_1$. To relate to notation in the previous section, we define the projectors $\hat{S} = (|0\rangle\langle 0| + \hat{P}_1)$, $\hat{S}_\perp = \hat{P}_2$. We define the spectral gap between $\mathrm{Span}\{|0\rangle\}, \mathbf{P}_1$ and $\mathbf{P}_2$:

$$\Delta = \min \left\{ \omega_1, E, |E - \omega_1| : E \in \mathrm{Spec}(\hat{H}_S|_{\mathbf{S}_\perp}) \right\} \tag{7.68}$$

In full, the unperturbed Hamiltonian is

$$\begin{aligned} \hat{H} = \hat{H}_S \otimes (|C\rangle\langle C| + |R\rangle\langle R| - |L\rangle\langle L|) \\ + \omega_1 \mathbf{1}_S \otimes (|R\rangle\langle R| + |L\rangle\langle L|) \end{aligned} \tag{7.69}$$

where $|C\rangle, |R\rangle$ and $|L\rangle$ are orthogonal basis vectors for the bath Hilbert space. We start by preparing the state,

$$|F\rangle |C\rangle = f_1 |1\rangle |C\rangle + f_\perp |F_\perp\rangle |C\rangle$$

where $|1\rangle \in \mathbf{P}_1$, $\langle 1| F_\perp\rangle = 0$, and we are given a lower bound for $|f_1|$. The algorithm proceeds by simulating the evolution of Hamiltonians $\hat{H} + \hat{X}$, where $\hat{X}$ satisfies

$$\begin{aligned} \hat{X} &= \hat{T}_S \otimes (|C\rangle\langle B| + |B\rangle\langle C|) \\ |B\rangle &= \frac{1}{\sqrt{2}}(|L\rangle + |R\rangle) \\ \Omega |1\rangle &= \hat{P}_1 \hat{T}_S |0\rangle \end{aligned} \tag{7.70}$$

where by phase convention Ω is real. Again, although $||\hat{T}_S|| = \Omega_0$ is a known quantity, we are only given a lower bound Ω^* for Ω.

The algorithm is probabilistic, and involves a single evolution step for time $\tau \sim \frac{1}{\Omega}$, followed by a measurement of the bath. If the bath is measured in state $|B\rangle$, then the desired transition $|1\rangle |C\rangle \to |0\rangle |B\rangle$ could have occurred. We verify this by applying the bath unitary $|B\rangle \leftrightarrow |L\rangle, |D\rangle \leftrightarrow |R\rangle$, then evolving under $\hat{H} + \hat{Y}$ for time $\tau = \frac{\pi}{2\Omega_0}$ where

$$\hat{Y} = \Omega_0 \mathbf{1}_S \otimes (|L\rangle\langle R| + |R\rangle\langle L|) \tag{7.71}$$

A measurement of a bath transition $|L\rangle \to |R\rangle$ would indicate that the system is in its ground state, while in all other cases a transition $|\psi L\rangle \to |\psi R\rangle$ is suppressed by energy conservation. If either the first or second bath measurements fail, we reinitialize the system and start again.

As before, we again show that given some bounds, the algorithm is robust against simulation errors and coupling between $\mathbf{S}$ and $\mathbf{S}_\perp$:

$$\begin{aligned} & r = \Omega_0/\Delta < 1/8 \\ & \\ & \delta\omega < r \cdot \Omega(\hat{V}) \\ & \frac{|\langle 0| \hat{T}_S |0\rangle|^2}{\omega_1} < r \cdot \Omega(\hat{V}) \\ & \frac{||\hat{S}\hat{\delta}\hat{S}||}{\Delta} < r \cdot \frac{\Omega(\hat{V})}{\Delta} \\ & \frac{||\hat{S}(\hat{V}+\hat{\delta})\hat{S}_\perp||^2}{\Delta^2} < r \cdot \frac{\Omega(\hat{V})}{\Delta} \\ & \frac{||\hat{S}_\perp(\hat{V}+\hat{\delta})\hat{S}_\perp||}{\Delta} < \Delta/2 \end{aligned} \tag{7.72}$$

where $\Omega(\hat{V}) = \Omega_0$ for $\hat{V} = \hat{Y}$, and $\Omega(\hat{V}) = \langle 1| \hat{T}_S |0\rangle = \Omega$ for $\hat{V} = \hat{X}$. As seen below, for the probabilistic scheme to succeed with fidelity $1 - O(\epsilon)$, we must scale r as $O(|f_1|\epsilon^{3/2})$.

Lemma 7.10.1 (Fidelity of the Unitary Evolutions) *Let* $\hat{U}(\tau) = e^{-i\tau(\hat{H}+\hat{X}+\hat{\delta})}$ *and assume* (7.72)*. Then*

$$\hat{U}(\tau) |1\rangle |C\rangle = \cos(\phi_t) |1\rangle |C\rangle - i \sin(\phi_t) |0\rangle |B\rangle + O(r) \tag{7.73}$$

where $\phi_t = \tau\Omega(1 + O(r))$*. The error term in* ϕ_t *and in* (7.73) *is uniform over* τ*. Likewise, let* $\hat{U}_v(\tau) = e^{-i\tau(\hat{H}+\hat{Y}+\hat{\delta})}$*. Then*

$$\hat{U}_v(\tau) |0\rangle |L\rangle = \cos(\phi_v) |0\rangle |L\rangle - i \sin(\phi_v) |0\rangle |R\rangle + O(r) \tag{7.74}$$

where $\phi_v = \tau\Omega_0$*.*

Lemma 7.10.2 (Verification Step)

$$\begin{aligned} \max_{|\psi\rangle} \langle\psi| \langle L| \hat{U}_v^\dagger (\mathbf{1}_S \otimes |R\rangle\langle R|) \hat{U}_v |\psi\rangle |L\rangle = & \quad O(r^2) \\ \max_{|\psi\rangle} \langle\psi| \langle R| \hat{U}_v^\dagger (\mathbf{1}_S \otimes |L\rangle\langle L|) \hat{U}_v |\psi\rangle |R\rangle = & \quad O(r^2) \end{aligned} \tag{7.75}$$

where the maximum is taken over all normalized system states $|\psi\rangle$ *such that* $\langle\psi|\,0\rangle = 0$.

Theorem 7.10.3 (Success of the Probabilistic Scheme) *Say that* $r = O(|f_1|\epsilon^{3/2})$ *as* $\epsilon \to 0^+$, *and that the* $\hat{U}_t$ *simulation time* τ *is sampled randomly within the range* $[\frac{\pi}{\Omega^*}, \frac{2\pi}{\Omega^*}]$, *where* $\Omega^* < \Omega$. *Then the verification step accepts with probability* $p_v = \frac{1}{|f_1|^2} \cdot O(1)$. *Given an acceptance, the probability of the system being in its ground state is* $p_{success} = 1 - O(\epsilon)$. *Since* $\Omega < r\Delta$, *the average simulation time* $\langle T\rangle$ *satisfies*

$$o\left(\frac{1}{|f_1|^3}\frac{1}{\epsilon^{3/2}\Delta}\right) = \langle T\rangle = O\left(\frac{1}{|f_1|^2}\frac{1}{\Omega^*}\right)$$

The proof of Lemma 7.10.1 is analogous to the proof of Lemma 7.9.2. We first analyze the success of the unitary evolutions under the assumption the most unwanted terms are zero, and show that it leads to the desired outcome. We then bound the effect of the unwanted terms on the unitary evolution.

Proof of Lemma 7.10.1:

We begin by proving the first statement of the lemma, for $\hat{V} = \hat{X} = \hat{T}_S \otimes (|B\rangle\langle C| + |C\rangle\langle B|)$. As in the proof of Lemma 7.9.2, instead of analyzing $\hat{H} + \hat{V} + \hat{\delta}$ we start by looking at the evolution of $\hat{H} + \hat{S}\hat{V}\hat{S}$, then obtain a bound on the errors caused by $\hat{\delta}_{eff} = \hat{V} - \hat{S}\hat{V}\hat{S} + \hat{\delta}$. Define $\mathbf{P}$ as the subspace spanned by the eigenvectors of $\hat{H}$ with energy in $[\omega_1 - \Delta/4, \omega_1 + \Delta/4]$. Notice that the projector $\hat{P}$ is

$$\hat{P} = \hat{P}_1 \otimes |C\rangle\langle C| + |0\rangle\langle 0| \otimes (|D\rangle\langle D| + |B\rangle\langle B|)\,,$$

where $|B\rangle = \frac{1}{\sqrt{2}}(|L\rangle + |R\rangle)$, $|D\rangle = \frac{1}{\sqrt{2}}(|L\rangle - |R\rangle)$, and that $\mathbf{P} \subset \mathbf{S}$. Before we

calculate the self-energy operator $\hat{\Sigma}(z)$ at $z = \omega_1$, we note the following relations:

$$\begin{aligned}
\hat{P} &= |0\rangle\langle 0| \otimes (|L\rangle\langle L| + |R\rangle\langle R|) + \hat{P}_1 \otimes |C\rangle\langle C| \\
&= |0\rangle\langle 0| \otimes (|D\rangle\langle D| + |B\rangle\langle B|) + \hat{P}_1 \otimes |C\rangle\langle C| \\
\hat{Q} &= \hat{P}_1 \otimes (|L\rangle\langle L| + |R\rangle\langle R|) + |0\rangle\langle 0| \otimes |C\rangle\langle C| + \hat{S}_\perp \\
\hat{P}\hat{H}\hat{P} &= \omega_1 |0\rangle\langle 0| \otimes (|D\rangle\langle D| + |B\rangle\langle B|) + \hat{P}_1 \hat{H}_S \hat{P}_1 \otimes |C\rangle\langle C| \\
\hat{Q}\hat{H}\hat{Q} &= (\hat{P}_1 \hat{H}_S \hat{P}_1 + \hat{S}_\perp \hat{H}_S \hat{S}_\perp) \otimes (-|L\rangle\langle L| + |R\rangle\langle R|) \\
&\quad + \omega_1 (\hat{P}_1 + \hat{S}_\perp) \otimes (|L\rangle\langle L| + |R\rangle\langle R|) \\
&\quad + \hat{S}_\perp \hat{H}_S \hat{S}_\perp \otimes |C\rangle\langle C| \\
\hat{P}\hat{V}\hat{P} &= \hat{P} \left(\hat{T}_S \otimes (|C\rangle\langle B| + |B\rangle\langle C|) \right) \hat{P} \\
&= \Omega \left(|1\, C\rangle\langle 0\, B| + |0\, B\rangle\langle 1\, C| \right)
\end{aligned}$$

The next term required in (7.46) is the unperturbed Green's function, $\hat{G}_Q(z) = \frac{\hat{Q}}{z\hat{Q} - \hat{Q}\hat{H}\hat{Q}}$. Since $\mathbf{P} \subset \mathbf{S}$ and $\hat{S}\hat{V}\hat{S}$, $\hat{H}$ are both block diagonal in $\mathbf{S}$ and $\mathbf{S}_\perp$, we may ignore the $\mathbf{S}_\perp$ component of $\hat{G}_Q(z)$:

$$\begin{aligned}
\hat{S}\hat{G}_Q(z)\hat{S} &= \frac{\hat{P}_1 \otimes (|L\rangle\langle L| + |R\rangle\langle R|)}{(z - \omega_1) - \hat{P}_1 \hat{H}_S \hat{P}_1 \otimes (|R\rangle\langle R| - |L\rangle\langle L|)} \\
&\quad + \frac{1}{z} |0\rangle\langle 0| \otimes |C\rangle\langle C|
\end{aligned}$$

so that

$$\begin{aligned}
\hat{S}\hat{G}_Q(\omega_1)\hat{S} &= \frac{\hat{P}_1}{\hat{P}_1 \hat{H}_S \hat{P}_1} \otimes (|L\rangle\langle L| - |R\rangle\langle R|) \\
&\quad + \frac{1}{\omega_1} |0\rangle\langle 0| \otimes |C\rangle\langle C|
\end{aligned}$$

Notice that $\langle B|\, \hat{S}\hat{G}_Q(\omega_1)\hat{S}\, |B\rangle = 0$. From the definition of $\hat{S}\hat{V}\hat{S} = \hat{S}\hat{T}_S\hat{S} \otimes$

$(|C\rangle\langle B| + |B\rangle\langle C|)$, we immediately observe that

$$\hat{S}\hat{V}\hat{S}\hat{G}_Q(\omega_1)\hat{S}\hat{V}\hat{S} = \frac{1}{\omega_1}\hat{S}\hat{T}_S|0\rangle\langle 0|\hat{T}_S\hat{S} \otimes |B\rangle\langle B|$$

Multiplication by $\hat{G}_Q(\omega_1)$ again produces a term proportional to $|D\rangle$. Since $\hat{V}|D\rangle = 0$, this implies that the series (7.46) with perturbation $\hat{S}\hat{V}\hat{S}$ truncates at second order in $\hat{V}$. Therefore $\hat{H}_{eff} \equiv \hat{\Sigma}(\omega_1)$ may be computed to all orders as

$$\begin{aligned}
\hat{H}_{eff} &= \hat{P}\hat{H}\hat{P} + \hat{P}\hat{V}P + \hat{P}\hat{V}\hat{S}\hat{G}_Q(\omega_1)\hat{S}\hat{V}\hat{P} \\
&= \omega_1|0\rangle\langle 0| \otimes (|D\rangle\langle D| + |B\rangle\langle B|) + \hat{P}_1\hat{H}_S\hat{P}_1 \otimes |C\rangle\langle C| \\
&\quad +\Omega\left(|1\rangle\langle 0| \otimes |C\rangle\langle B| + |0\rangle\langle 1| \otimes |B\rangle\langle C|\right) \\
&\quad +\frac{|\langle 0|\hat{T}_S|0\rangle|^2}{\omega_1}|0\rangle\langle 0| \otimes |B\rangle\langle B|
\end{aligned}$$

The system Hamiltonian is written $\hat{H}_S = \hat{P}_1\hat{H}_S\hat{P}_1 + \hat{S}_\perp\hat{H}_S\hat{S}_\perp$, where the spectrum of $\hat{H}_S|_{P_1}$ is contained in $(\omega_1 - \delta\omega, \omega_1 + \delta\omega)$. The state $|1\rangle \propto \hat{P}_1\hat{T}_S|0\rangle$ is not necessarily an eigenstate of $\hat{H}_S$, but $\omega_1^* = \langle 1|\hat{H}_S|1\rangle$ is contained in $(\omega_1 - \delta\omega, \omega_1 + \delta\omega)$. We write the projector into the remainder of $\mathbf{P}_1$ as $\hat{P}_1' = \hat{P}_1 - |1\rangle\langle 1|$. To see that $\hat{H}_{eff}$ produces the desired evolution, we rewrite it as

$$\begin{aligned}
\hat{H}_{eff} &= \omega_1\left(|0\rangle\langle 0| \otimes |B\rangle\langle B| + |1\rangle\langle 1| \otimes |C\rangle\langle C|\right) \\
&\quad + \left(\omega_1|0\rangle\langle 0| \otimes |D\rangle\langle D| + \hat{P}_1'\hat{H}_S\hat{P}_1' \otimes |C\rangle\langle C|\right) \\
&\quad + \Omega\left(|1\rangle\langle 0| \otimes |C\rangle\langle B| + |0\rangle\langle 1| \otimes |B\rangle\langle C|\right) \\
&\quad + \left((\omega_1^* - \omega_1)|1\rangle\langle 1| + \hat{P}_1'\hat{H}_S|1\rangle\langle 1| + \text{h.c.}\right) \otimes |C\rangle\langle C| \\
&\quad + \frac{|\langle 0|\hat{T}_S|0\rangle|^2}{\omega_1}|0\rangle\langle 0| \otimes |B\rangle\langle B|
\end{aligned} \tag{7.76}$$

Observe that if we neglect the terms on the third line of (7.76), $\hat{H}_{eff}$ has eigenvectors $|v_\pm\rangle = \frac{1}{\sqrt{2}}\left(|1\rangle|C\rangle \pm |0\rangle|B\rangle\right)$ with eigenvalues $\omega_1 \pm \Omega$, which exactly produce

the desired evolution (7.73). Since $||\hat{P}_1'(\hat{H}_S - \omega_1\hat{P}_1')\hat{P}_1'|| \leq ||\hat{P}_1(\hat{H}_S - \omega_1\hat{P}_1)\hat{P}_1|| \leq \delta\omega$, by Lemma 7.8.3 all other eigenvalues of the approximate $\hat{H}_{eff}$ are in $(\omega_1 - \delta\omega, \omega_1 + \delta\omega)$. The eigenvalues $\omega_1 \pm \Omega$ are therefore non-degenerate and energetically separated from the rest of the spectrum by a gap $\Omega - \delta\omega$. This fact will allow us to use Theorem 7.8.4 below to show that, up to an error of order $O(r)$, $|v_\pm\rangle$ correspond to eigenvectors of $\hat{H}_{eff}$.

The terms in the third line of (7.76) are bounded by $\Omega \cdot O(r)$. To see this, note that $\frac{|\langle 0|\hat{T}_S|0\rangle|^2}{\omega_1} \leq \Omega \cdot O(r)$ is already an explicit assumption. The bound for $\Big((\omega_1^* - \omega_1)|1\rangle\langle 1| + \hat{P}_1'\hat{H}_S|1\rangle\langle 1| + \text{h.c.}\Big) = \hat{P}_1(\hat{H}_s - \omega_1\hat{P}_1)\hat{P}_1 - \hat{P}_1'(\hat{H}_s - \omega_1\hat{P}_1')\hat{P}_1'$ comes from the fact that $||\hat{P}_1'(\hat{H}_S - \omega_1\hat{P}_1')\hat{P}_1'|| \leq ||\hat{P}_1(\hat{H}_S - \omega_1\hat{P}_1)\hat{P}_1|| \leq \delta\omega = \Omega \cdot O(r)$. By invoking Lemma 7.8.3 and Theorem 7.8.4 we conclude that $\hat{H}_{eff}$ has eigenvectors $\left|\tilde{\pm}\right\rangle$ with eigenvalues $\omega_1 \pm \Omega \cdot (1 + O(r))$ such that $|\left\langle \pm\right| \left.\tilde{\pm}\right\rangle|^2 \geq 1 - O(r^2)$, and that the rest of the spectrum of $\hat{H}_{eff}$ is $\Omega \cdot (1 + O(r))$ away from these eigenvalues.

The rest of the proof of (7.73) is now identical to the argument in Lemma 7.9.2. Using the bound for $\Omega_0 = ||\hat{T}_S||$, in the case when $\hat{\delta}_{eff} = 0$ we bound $||\hat{\Sigma}(z)|_{\hat{\delta}_{eff}} - \hat{H}_{eff}||$ for $z \in [\omega_1 - \Omega \cdot (1 + O(r)), \omega_1 + \Omega \cdot (1 + O(r))]$ using the Taylor's expansion of $\frac{\hat{Q}}{z\hat{Q} - \hat{Q}(\hat{H} + \hat{S}\hat{V}\hat{S})\hat{Q}}$. Then, using Lemma 7.8.7 we bound the error in $\hat{\Sigma}(z)$ obtained by neglecting $\hat{\delta}_{eff} = \hat{V} - \hat{S}\hat{V}\hat{S} + \hat{\delta}$, and show that it is equal to $\Omega \cdot O(r)$ under our assumed bounds (7.72). Since $||\hat{\Sigma}(z) - \hat{H}_{eff}||$ is still sufficiently small, we conclude by Theorem 7.8.1 and corollary 7.8.2 that $\hat{H} + \hat{V} + \hat{\delta}$ has eigenvalues $\omega_1 \pm \Omega \cdot (1 + O(r))$, and that these eigenvalues correspond to $\frac{1}{\sqrt{2}}\left(|1\rangle\,|C\rangle + |0\rangle\,|B\rangle\right) + O(r)$.

The proof of the second statement is nearly identical to the first. Noting that now $\hat{V} = \Omega_0 \mathbf{1}_S \otimes (|R\rangle\langle L| + |L\rangle\langle R|)$, we have $\hat{P}\hat{V}\hat{P} = \Omega_0|0\rangle\langle 0| \otimes |R\rangle\langle L| + \text{h.c.}$ and

$\hat{P}\hat{V}\hat{Q} = 0$. Assuming that $\hat{\delta} = 0$, the self-energy operator $\hat{\Sigma}(z)$ is now exactly equal to $\hat{P}\hat{H}\hat{P} + \hat{P}\hat{V}P$, so $\hat{H}_{eff} = \hat{\Sigma}(\omega_1)$ satisfies

$$\begin{aligned}\hat{H}_{eff} &= \omega_1 \left(|0\rangle\langle 0| \otimes |L\rangle\langle L| + |0\rangle\langle 0| \otimes |R\rangle\langle R|\right) + \hat{P}_1 \hat{H}_S \hat{P}_1 \otimes |C\rangle\langle C| \\ &+ \Omega_0 |0\rangle\langle 0| \otimes \left(|L\rangle\langle R| + |R\rangle\langle L|\right)\end{aligned}$$

which clearly has eigenvalues $\omega_1 \pm \Omega_0$ corresponding to $\frac{1}{\sqrt{2}}(|0\rangle |L\rangle \pm |0\rangle |R\rangle)$, with the rest of its spectrum in $(\omega_1 - \delta\omega, \omega_1 + \delta\omega)$. $\hat{H}_{eff}$ therefore produces the desired evolution. The rest of the proof, in which we bound $||\hat{\Sigma}(z) - \hat{H}_{eff}||$, again continues in the same way as in Lemma 7.9.2, with the substitution of Ω_0 in place of Ω.

□

Proof of Lemma 7.10.2:

The proof of this analogous to the proof of Lemma 7.9.3. As before, let $\mathbf{P}$ represent the subspace spanned by eigenvectors of $\hat{H}$ with eigenvalue contained in $(-\infty, \omega_1 - \Delta]$. Notice that $\mathbf{P}$ corresponds only to bath states in state $|C\rangle$ or $|L\rangle$. The complement, $\mathbf{Q}$, corresponds to eigenvalues within $[\omega_1, \infty)$. In the language of Theorem 7.8.4, we have $\lambda_- = -\infty, \lambda_+ = \omega_1 - \Delta/2$, and Δ defined as in (7.68).

Given (7.72), by the triangle inequality we conclude that $||\hat{Y} + \hat{\delta}||/\Delta = O(r)$. Define $\tilde{\boldsymbol{P}}$ as the direct sum of eigenspaces of $\tilde{H}_{=}\hat{H} + \hat{Y} + \hat{\delta}$ with eigenvalue in $(\lambda_-, \lambda_+) = (-\infty, \omega_1 - \Delta/2)$. By Theorem 7.8.4, for any state $|v\rangle \in \mathbf{P}$, we see that

$$\begin{aligned}\langle v| \tilde{P} |v\rangle &> 1 - \left(\frac{2||\tilde{H} - \hat{H}||}{\Delta}\right)^2 \\ &= 1 - O(r^2)\end{aligned}$$

This implies that $\tilde{P}\left|v\right\rangle = \sqrt{1-O(r^2)}\left|\tilde{v}\right\rangle$, where $\left|\tilde{v}\right\rangle$ represents an arbitrary normalized vector in $\tilde{\boldsymbol{P}}$. Likewise, for $\left|\tilde{v}\right\rangle \in \tilde{\boldsymbol{P}}$, $\left\langle\tilde{v}\right|\hat{P}\left|\tilde{v}\right\rangle = 1 - O(r^2)$. Since $\tilde{\boldsymbol{P}}$ is spanned by eigenvectors of $\tilde{H}$, for $\hat{U}_v = \exp(-i\tau\tilde{H})$, $\tilde{P}\hat{U}_v = \hat{U}_v\tilde{P}$. Noting that $\left\langle\psi\right|\tilde{P}\hat{P}\tilde{P}\left|\psi\right\rangle \leq \left\langle\psi\right|\hat{P}\left|\psi\right\rangle$ for all $\left|\psi\right\rangle$, we conclude that for any $\left|v\right\rangle \in \mathbf{P}$,

$$\begin{aligned}
\left\langle v\right|\hat{U}_v^\dagger\hat{P}\hat{U}_v\left|v\right\rangle &\geq \left\langle v\right|\hat{U}_v^\dagger\tilde{P}\hat{P}\tilde{P}\hat{U}_v\left|v\right\rangle \\
&= \left(\left\langle v\right|\tilde{P}\hat{U}_v^\dagger\right)\hat{P}\left(\hat{U}_v\tilde{P}\left|v\right\rangle\right) \\
&= (1-O(r^2))\left\langle\tilde{v}\right|\hat{P}\left|\tilde{v}\right\rangle \\
&= (1-O(r^2))^2 = 1-O(r^2)
\end{aligned}$$

Let $\left|\psi\right\rangle\left|L\right\rangle$ be given such that $\left\langle\psi|0\right\rangle = 0$. By examining the spectrum of $\hat{H}$, one sees that $\left|\psi\right\rangle\left|L\right\rangle \in \mathbf{P}$, and that the subspace $\mathcal{H}_S \otimes \mathrm{Span}\{\left|R\right\rangle\}$ is contained within $\mathbf{Q}$, so that the operator $\mathbf{1}_S \otimes \left|R\right\rangle\!\left\langle R\right| \leq \hat{Q} = (\mathbf{1} - \hat{P})$. From the above inequality we conclude that

$$\begin{aligned}
\left\langle\psi\right|\left\langle L\right|\hat{U}_v^\dagger\left(\mathbf{1}_S \otimes \left|R\right\rangle\!\left\langle R\right|\right)\hat{U}_v\left|\psi\right\rangle\left|L\right\rangle &\leq \left\langle\psi\right|\left\langle L\right|\hat{U}_v^\dagger\left(\mathbf{1}-\hat{P}\right)\hat{U}_v\left|\psi\right\rangle\left|L\right\rangle \\
&= 1 - \left\langle\psi\right|\left\langle L\right|\hat{U}_v^\dagger\hat{P}\hat{U}_v\left|\psi\right\rangle\left|L\right\rangle \\
&= O(r^2)
\end{aligned}$$

By an identical argument, we may prove the second statement of the claim as well.

□

Proof of Theorem 7.10.3:

Given initial state $\left|F\right\rangle\left|C\right\rangle$ and time evolution $\hat{U}_t(\tau)$ (as defined in Lemma 7.10.1), the probability of a verification event is given by

$$p_v = \left\langle F\right|\left\langle C\right|\hat{U}_t^\dagger\hat{X}^\dagger\hat{X}\hat{U}_t\left|F\right\rangle\left|C\right\rangle$$

where

$$\hat{X} = |R\rangle\langle R|\hat{U}_v|L\rangle\langle B|$$

and $\hat{U}_v$ is evaluated for time $\frac{\pi}{2\Omega_0}$. Likewise, the probability of the system being in the ground state after the verification has occurred is

$$p_{vs} = \langle F| \langle C| \hat{U}_t^\dagger \hat{X}^\dagger |0\rangle\langle 0|\hat{X}\hat{U}_t |F\rangle |C\rangle$$

where $|0\rangle$ is the ground state of $\hat{H}_S$. Along with finding p_v, we wish to calculate the success probability of the algorithm conditional on a verification event, $p_{s|v} = p_{vs}/p_v$. These three probabilities are functions of the parameter ϕ, where $\phi/\tau = \Omega(1+O(r))$ is half the energy splitting of the eigenstates $|\tilde{v}_\pm\rangle \approx \frac{1}{\sqrt{2}}(|1\rangle |C\rangle \pm |0\rangle |B\rangle)$ used in the evolution $\hat{U}_t(\tau)$.

By the first result of Lemma 7.10.1, for any time evolution $\hat{U}_t(\tau)$ we may write

$$\begin{aligned} \hat{U}_t(\tau) |F\rangle |C\rangle &= f_1 \left(\cos(\phi_t) |1\rangle |C\rangle - i \sin(\phi_t) |0\rangle |B\rangle + O(r)\right) \\ &\quad + f_\perp \hat{U}_t |f_\perp\rangle |C\rangle \end{aligned}$$

Since Lemma 7.10.1 implies coherent oscillations between $|1\rangle |C\rangle$ and $|0\rangle |B\rangle$, it must be that $\langle 0| \langle B| \hat{U}_t(\tau) |f_\perp\rangle |C\rangle = O(r)$, so that $\langle 0| \langle B| \hat{U}_t(\tau) |F\rangle |C\rangle = -i(f_1 \sin(\phi_t) + O(r))$. We mention that the bound $O(r)$ is independent of τ, i.e. as $r \to 0^+$ there is a constant $c > 0$ such that $|\langle 0| \langle B| \hat{U}_t(\tau) |F\rangle |C\rangle + i f_1 \sin(\phi_t)| < c \cdot r$ for all τ.

Likewise, the second result of Lemma 7.10.1 implies that

$$\hat{U}_v \left(\tau = \frac{\pi}{2\Omega_0}\right) |0\rangle |L\rangle = |0\rangle |R\rangle + O(r)$$

so

$$\hat{X} |0\rangle |B\rangle = |0\rangle |R\rangle + O(r)$$

For system states $|\psi\rangle$ such that $\langle\psi|\,0\rangle = 0$, by Lemma 7.10.2 we have that

$$\max_{\langle\psi|\psi\rangle=1} \langle\psi|\,\langle L|\,\hat{U}_v^\dagger|R\rangle\langle R|\hat{U}_v\,|\psi\rangle\,|L\rangle = O(r^2)$$

and since $\hat{U}_v^\dagger|R\rangle\langle R|\hat{U}_v$ is a projector, it must be that $\hat{U}_v^\dagger|R\rangle\langle R|\hat{U}_v\,|\psi\rangle\,|L\rangle = O(r)$, where the error bound is uniform over all $|\psi\rangle$. We conclude that for all composite states $|\psi_{SB}\rangle$ such that $\langle\psi_{SB}|\,0\rangle\,|B\rangle = 0$,

$$\hat{X}\,|\psi_{SB}\rangle = \hat{U}_v\left(\hat{U}_v^\dagger|R\rangle\langle R|\hat{U}_v\right)\cdot(|L\rangle\langle B|\psi_{SB}\rangle) = O(r)$$

and that this bound is the same over all such $|\psi_{SB}\rangle$. Since $\langle 0|\,\langle B|\,\hat{U}_t(\tau)\,|F\rangle\,|C\rangle = -i(f_1\sin(\phi_t) + O(r))$, we may write

$$\hat{U}_t(\tau)\,|F\rangle\,|C\rangle = -i(f_1\sin(\phi_t) + O(r))\,|0\rangle\,|B\rangle + c(\tau)\,|\psi_{SB}(\tau)\rangle$$

where $|c(\tau)| < 1$ and $\langle\psi_{SB}(\tau)|\,0\rangle\,|B\rangle = 0$ for all τ.

Applying $\hat{X}$ gives

$$\begin{aligned}
\hat{X}\hat{U}_t(\tau)\,|F\rangle\,|C\rangle &= -i(f_1\sin(\phi_t) + O(r))\,|0\rangle\,|R\rangle + O(r) \\
&= -i(f_1\sin(\phi_t) + A(\phi_t))\,|0\rangle\,|R\rangle \\
&\quad +B(\phi_t)\,|\psi_\perp(\tau)\rangle\,|R\rangle
\end{aligned}$$

where $\langle\psi_\perp(\tau)|\,0\rangle = 0$ for all τ. As the bounds derived from Lemmas 7.10.1 and 7.10.2 are independent of τ, we have that $A = \max|A(\phi_t)| = O(r)$ and $B = \max|B(\phi_t)| = O(r)$. We may now directly compute p_v and p_{vs}:

$$\begin{aligned}
p_v(\phi_t) &= |f_1\sin(\phi_t) + A(\phi_t)|^2 + |B(\phi_t)|^2 \\
p_{vs}(\phi_t) &= |f_1\sin(\phi_t) + A(\phi_t)|^2
\end{aligned}$$

so the success probability for a given ϕ_t is

$$p_{s|v}(\phi_t) = \frac{|f_1 \sin(\phi_t) + A(\phi_t)|^2}{|f_1 \sin(\phi_t) + A(\phi_t)|^2 + |B(\phi_t)|^2}$$

Suppose that when sampling over values of ϕ_t, with probability at least $1-\epsilon/2$ we have $p_{s|v}(\phi_t) > (1-\epsilon/2)$. Then $p_{success} > (1-\epsilon/2)^2 > 1-\epsilon$ for $0 < \epsilon < 1$, which is the desired result. In terms of the relation above, this condition equivalent to

$$|f_1 \sin(\phi_t) + A(\phi_t)| > |B(\phi_t)| \sqrt{\frac{2}{\epsilon} - 1}$$

As $|f_1 \sin(\phi_t) + A(\phi_t)| > |f_1 \sin(\phi_t)| - A$ and $|B(\phi_t)| < B$, this relation is satisfied if

$$|\sin(\phi_t)| \geq \frac{A + B\sqrt{\frac{2}{\epsilon}}}{|f_1|} = O\left(\frac{r}{\sqrt{\epsilon}|f_1|}\right) \tag{7.77}$$

Hence we obtain an infidelity at most ϵ as long (7.77) is violated with probability at most $\epsilon/2$. Note that if ϕ_t is sampled uniformly over a range larger than $\pi/2$ (as ensured by our sampling scheme for τ), the probability that $|\sin(\phi_t)| < c$ for some small number $c > 0$ is $p_{fail} = O(c)$ as $c \to 0$. We require $p_{fail} < \epsilon/2$ in (7.77), which is satisfied for $r = O(|f_1|\epsilon^{3/2})$. This gives success the bound $p_{success} > 1-\epsilon$ stated in the Lemma. Using the same argument, we see that to have $|f_1 \sin(\phi_t)| > 2A = O(r)$ with probability at least $1/2$, we only require $r = O(|f_1|)$, so under the more stringent scaling we may also conclude that the verification probability $p_v(\phi_t)$ is greater than $|f_1|^2/4$ with probability $O(1)$. This gives the desired scaling, $p_{accept} = O\left(\frac{1}{|f_1|^2}\right)$.

□

Bibliography

[1] A. Einstein, B. Podolsky, and N. Rosen. Can quantum-mechanical description of physical reality be considered complete? *Phys. Rev.*, 47:777–780, May 1935.

[2] E. Schrödinger. Discussion of probability relations between separated systems. *Mathematical Proceedings of the Cambridge Philosophical Society*, 31:555–563, 10 1935.

[3] Richard Jozsa and Noah Linden. On the role of entanglement in quantum-computational speed-up. *Proceedings of the Royal Society of London A: Mathematical, Physical and Engineering Sciences*, 459(2036):2011–2032, 2003.

[4] Marcos Curty, Maciej Lewenstein, and Norbert Lütkenhaus. Entanglement as a precondition for secure quantum key distribution. *Phys. Rev. Lett.*, 92:217903, May 2004.

[5] Géza Tóth and Iagoba Apellaniz. Quantum metrology from a quantum information science perspective. *Journal of Physics A: Mathematical and Theoretical*, 47(42):424006, 2014.

[6] W. S. Bakr, A. Peng, M. E. Tai, R. Ma, J. Simon, J. I. Gillen, S. Flling, L. Pollet, and M. Greiner. Probing the superflui to mott insulator transition at the single-atom level. *Science*, 329(5991):547–550, 2010.

[7] Immanuel Bloch, Jean Dalibard, and Sylvain Nascimbene. Quantum simulations with ultracold quantum gases. *Nat Phys*, 8(4):267–276, 04 2012.

[8] Maciej Lewenstein, Anna Sanpera, Veronica Ahufinger, Bogdan Damski, Aditi Sen(De), and Ujjwal Sen. Ultracold atomic gases in optical lattices: mimicking condensed matter physics and beyond. *Advances in Physics*, 56(2):243–379, 2007.

[9] A. Auerbach. *Interacting Electrons and Quantum Magnetism*. Springer New York, 1994.

[10] Patrick A. Lee, Naoto Nagaosa, and Xiao-Gang Wen. Doping a mott insulator: Physics of high-temperature superconductivity. *Rev. Mod. Phys.*, 78:17–85, Jan 2006.

[11] Michael H. Freedman, Alexei Kitaev, and Zhenghan Wang. Simulation of topological field theories by quantum computers. *Communications in Mathematical Physics*, 227(3):587–603, 2002.

[12] Christof Zalka. Simulating quantum systems on a quantum computer. *Proceedings of the Royal Society of London A: Mathematical, Physical and Engineering Sciences*, 454(1969):313–322, 1998.

[13] RichardP. Feynman. Simulating physics with computers. *International Journal of Theoretical Physics*, 21(6-7):467–488, 1982.

[14] Seth Lloyd. Universal quantum simulators. *Science*, 273(5278):1073–1078, August 1996.

[15] Barbara M. Terhal and David P. DiVincenzo. Problem of equilibration and the computation of correlation functions on a quantum computer. *Phys. Rev. A*, 61(2):022301, Jan 2000.

[16] Charles H Bennett and Gilles Brassard. Quantum cryptography: Public key distribution and coin tossing. *Theoretical Computer Science*, 560:7–11, 2014.

[17] Dominic Mayers. Unconditional security in quantum cryptography. *Journal of the ACM (JACM)*, 48(3):351–406, 2001.

[18] Artur K. Ekert. Quantum cryptography based on bell's theorem. *Phys. Rev. Lett.*, 67:661–663, Aug 1991.

[19] C.H. Bennett, G. Brassard, C. Crepeau, and U.M. Maurer. Generalized privacy amplification. *Information Theory, IEEE Transactions on*, 41(6):1915–1923, Nov 1995.

[20] Thomas Jennewein, Ulrich Achleitner, Gregor Weihs, Harald Weinfurter, and Anton Zeilinger. A fast and compact quantum random number generator. *Review of Scientific Instruments*, 71(4):1675–1680, 2000.

[21] André Stefanov, Nicolas Gisin, Olivier Guinnard, Laurent Guinnard, and Hugo Zbinden. Optical quantum random number generator. *Journal of Modern Optics*, 47(4):595–598, 2000.

[22] Nicolas Gisin, Grégoire Ribordy, Wolfgang Tittel, and Hugo Zbinden. Quantum cryptography. *Rev. Mod. Phys.*, 74:145–195, Mar 2002.

[23] L. Essen and J. V. L. Parry. An atomic standard of frequency and time interval: A caesium resonator. *Nature*, 176(4476):280–282, 08 1955.

[24] Andrei Derevianko and Hidetoshi Katori. *Colloquium* : Physics of optical lattice clocks. *Rev. Mod. Phys.*, 83:331–347, May 2011.

[25] A. D. Ludlow, T. Zelevinsky, G. K. Campbell, S. Blatt, M. M. Boyd, M. H. G. de Miranda, M. J. Martin, J. W. Thomsen, S. M. Foreman, Jun Ye, T. M. Fortier, J. E. Stalnaker, S. A. Diddams, Y. Le Coq, Z. W. Barber, N. Poli, N. D. Lemke, K. M. Beck, and C. W. Oates. Sr lattice clock at 1 10–16 fractional uncertainty by remote optical evaluation with a ca clock. *Science*, 319(5871):1805–1808, 2008.

[26] C. W. Chou, D. B. Hume, J. C. J. Koelemeij, D. J. Wineland, and T. Rosenband. Frequency comparison of two high-accuracy al^+ optical clocks. *Phys. Rev. Lett.*, 104:070802, Feb 2010.

[27] International Bureau of Weights & Measures, Barry N Taylor, and Ambler Thompson. The international system of units (si). 2001.

[28] Jean-Philippe Uzan. The fundamental constants and their variation: observational and theoretical status. *Rev. Mod. Phys.*, 75:403–455, Apr 2003.

[29] S. Blatt, A. D. Ludlow, G. K. Campbell, J. W. Thomsen, T. Zelevinsky, M. M. Boyd, J. Ye, X. Baillard, M. Fouché, R. Le Targat, A. Brusch, P. Lemonde, M. Takamoto, F.-L. Hong, H. Katori, and V. V. Flambaum. New limits on coupling of fundamental constants to gravity using ^{87}Sr optical lattice clocks. *Phys. Rev. Lett.*, 100:140801, Apr 2008.

[30] S S Y Chua, B J J Slagmolen, D A Shaddock, and D E McClelland. Quantum squeezed light in gravitational-wave detectors. *Classical and Quantum Gravity*, 31(18):183001, 2014.

[31] M. T. Jaekel and S. Reynaud. Quantum limits in interferometric measurements. *EPL (Europhysics Letters)*, 13(4):301, 1990.

[32] A. A. Clerk, M. H. Devoret, S. M. Girvin, F. Marquardt, and R. J. Schoelkopf. Introduction to quantum noise, measurement and amplification. 10 2008.

[33] Seth Lloyd. Almost any quantum logic gate is universal. *Phys. Rev. Lett.*, 75:346–349, Jul 1995.

[34] Igor Devetak. The private classical capacity and quantum capacity of a quantum channel. *IEEE Transactions on Information Theory*, 51(1):44–55, 2005.

[35] Joseph Emerson, Robert Alicki, and Karol Zyczkowski. Scalable noise estimation with random unitary operators. *Journal of Optics B: Quantum and Semiclassical Optics*, 7(10):S347, 2005.

[36] E. Knill, D. Leibfried, R. Reichle, J. Britton, R. B. Blakestad, J. D. Jost, C. Langer, R. Ozeri, S. Seidelin, and D. J. Wineland. Randomized benchmarking of quantum gates. *Phys. Rev. A*, 77:012307, Jan 2008.

[37] Marcus P. da Silva, Olivier Landon-Cardinal, and David Poulin. Practical characterization of quantum devices without tomography. *Phys. Rev. Lett.*, 107:210404, Nov 2011.

[38] Steven T. Flammia and Yi-Kai Liu. Direct fidelity estimation from few pauli measurements. *Phys. Rev. Lett.*, 106:230501, Jun 2011.

[39] Daniel Gottesman. Theory of fault-tolerant quantum computation. *Phys. Rev. A*, 57:127–137, Jan 1998.

[40] D. Aharonov and M. Ben-Or. Fault-tolerant quantum computation with constant error. In *Proceedings of the Twenty-ninth Annual ACM Symposium on Theory of Computing*, STOC '97, pages 176–188, New York, NY, USA, 1997. ACM.

[41] Seth Lloyd. Capacity of the noisy quantum channel. *Phys. Rev. A*, 55:1613–1622, Mar 1997.

[42] Scott Aaronson and Alex Arkhipov. The computational complexity of linear optics. In *Proceedings of the Forty-third Annual ACM Symposium on Theory of Computing*, STOC '11, pages 333–342, New York, NY, USA, 2011. ACM.

[43] H. J. Briegel, D. E. Browne, W. Dur, R. Raussendorf, and M. Van den Nest. Measurement-based quantum computation. *Nat Phys*, pages 19–26, 01 2009.

[44] Charles H. Bennett, Gilles Brassard, Sandu Popescu, Benjamin Schumacher, John A. Smolin, and William K. Wootters. Purification of noisy entanglement and faithful teleportation via noisy channels. *Phys. Rev. Lett.*, 76(5):722–725, January 1996.

[45] Michal Horodecki, Jonathan Oppenheim, and Andreas Winter. Quantum information can be negative. *NATURE*, 436:673, 2005.

[46] AndrewM. Childs, David Gosset, and Zak Webb. The bose-hubbard model is qma-complete. In Javier Esparza, Pierre Fraigniaud, Thore Husfeldt, and Elias Koutsoupias, editors, *Automata, Languages, and Programming*, volume 8572 of *Lecture Notes in Computer Science*, pages 308–319. Springer Berlin Heidelberg, 2014.

[47] E. Farhi, J. Goldstone, S. Gutmann, and M. Sipser. Quantum Computation by Adiabatic Evolution. *ArXiv Quantum Physics e-prints*, January 2000.

[48] D. Deutsch. Quantum computational networks. *Proceedings of the Royal Society of London. A. Mathematical and Physical Sciences*, 425(1868):73–90, 1989.

[49] C. Monroe and J. Kim. Scaling the ion trap quantum processor. *Science*, 339(6124):1164–1169, 2013.

[50] M. H. Devoret and R. J. Schoelkopf. Superconducting circuits for quantum information: An outlook. *Science*, 339(6124):1169–1174, March 2013.

[51] Gilles Brassard, Norbert Lütkenhaus, Tal Mor, and Barry C. Sanders. Limitations on practical quantum cryptography. *Phys. Rev. Lett.*, 85:1330–1333, Aug 2000.

[52] Valerio Scarani, Helle Bechmann-Pasquinucci, Nicolas J. Cerf, Miloslav Dušek, Norbert Lütkenhaus, and Momtchil Peev. The security of practical quantum key distribution. *Rev. Mod. Phys.*, 81:1301–1350, Sep 2009.

[53] D. Leibfried, M. D. Barrett, T. Schaetz, J. Britton, J. Chiaverini, W. M. Itano, J. D. Jost, C. Langer, and D. J. Wineland. Toward heisenberg-limited spectroscopy with multiparticle entangled states. *Science*, 304(5676):1476–1478, 2004.

[54] M. Kessler, E. P. Kómár, M. Bishof, L. Jiang, S. Sørensen, A. J. Ye, and D. Lukin, M.˙Heisenberg-limited atom clocks based on entangled qubits. *Phys. Rev. Lett.*, 112:190403, May 2014.

[55] D. J. Larson, J. C. Bergquist, J. J. Bollinger, Wayne M. Itano, and D. J. Wineland. Sympathetic cooling of trapped ions: A laser-cooled two-species nonneutral ion plasma. *Phys. Rev. Lett.*, 57:70–73, Jul 1986.

[56] C. J. Myatt, E. A. Burt, R. W. Ghrist, E. A. Cornell, and C. E. Wieman. Production of two overlapping bose-einstein condensates by sympathetic cooling. *Phys. Rev. Lett.*, 78:586–589, Jan 1997.

[57] John Weiner, Vanderlei S. Bagnato, Sergio Zilio, and Paul S. Julienne. Experiments and theory in cold and ultracold collisions. *Rev. Mod. Phys.*, 71:1–85, Jan 1999.

[58] K. Hammerer, K. Stannigel, C. Genes, P. Zoller, P. Treutlein, S. Camerer, D. Hunger, and T. W. Hänsch. Optical lattices with micromechanical mirrors. *Phys. Rev. A*, 82:021803, Aug 2010.

[59] James S Bennett, Lars S Madsen, Mark Baker, Halina Rubinsztein-Dunlop, and Warwick P Bowen. Coherent control and feedback cooling in a remotely coupled hybrid atom–optomechanical system. *New Journal of Physics*, 16(8):083036, 2014.

[60] Andreas Jöckel, Aline Faber, Tobias Kampschulte, Maria Korppi, Matthew T. Rakher, and Philipp Treutlein. Sympathetic cooling of a membrane oscillator in a hybrid mechanical–atomic system. *Nat Nano*, 10(1):55–59, 01 2015.

[61] Alexey V. Gorshkov, Rejish Nath, and Thomas Pohl. Dissipative many-body quantum optics in rydberg media. *Phys. Rev. Lett.*, 110:153601, Apr 2013.

[62] Eliot Kapit, Mohammad Hafezi, and Steven H. Simon. Induced self-stabilization in fractional quantum hall states of light. *Phys. Rev. X*, 4:031039, Sep 2014.

[63] S. Komiyama, O. Astafiev, V. Antonov, T. Kutsuwa, and H. Hirai. A single-photon detector in the far-infrared range. *Nature*, 403(6768):405–407, 01 2000.

[64] Kristine M. Rosfjord, Joel K. W. Yang, Eric A. Dauler, Andrew J. Kerman, Vikas Anant, Boris M. Voronov, Gregory N. Gol'tsman, and Karl K. Berggren. Nanowire single-photon detector with an integrated optical cavity and anti-reflection coating. *Opt. Express*, 14(2):527–534, Jan 2006.

[65] Haruka Tanji-Suzuki, Wenlan Chen, Renate Landig, Jonathan Simon, and Vladan Vuletić. Vacuum-induced transparency. *Science*, 333(6047):1266–1269, 2011.

[66] E. Knill, R. Laflamme, and G. J. Milburn. A scheme for efficient quantum computation with linear optics. *Nature*, 409(6816):46–52, January 2001.

[67] Michael A. Nielsen. Optical quantum computation using cluster states. *Phys. Rev. Lett.*, 93:040503, Jul 2004.

[68] Daniel E. Browne and Terry Rudolph. Resource-efficient linear optical quantum computation. *Phys. Rev. Lett.*, 95(1):010501, June 2005.

[69] D. Leibfried, R. Blatt, C. Monroe, and D. Wineland. Quantum dynamics of single trapped ions. *Rev. Mod. Phys.*, 75(1):281–324, March 2003.

[70] John Clarke and Frank K. Wilhelm. Superconducting quantum bits. *Nature*, 453(7198):1031–1042, June 2008.

[71] John S. Bell. On the Einstein-Podolsky-Rosen paradox. *Physics*, 1:195–200, 1964.

[72] John F. Clauser, Michael A. Horne, Abner Shimony, and Richard A. Holt. Proposed experiment to test local hidden-variable theories. *Phys. Rev. Lett.*, 23:880–884, Oct 1969.

[73] Graeme Smith. Quantum channel capacities. 07 2010.

[74] I. Devetak and P. W. Shor. The capacity of a quantum channel for simultaneous transmission of classical and quantum information. *Communications in Mathematical Physics*, 256(2):287–303, 2005.

[75] Benjamin Schumacher and Michael D. Westmoreland. Quantum privacy and quantum coherence. *Phys. Rev. Lett.*, 80:5695–5697, Jun 1998.

[76] D. Gross. Recovering low-rank matrices from few coefficients in any basis. *Information Theory, IEEE Transactions on*, 57(3):1548–1566, March 2011.

[77] John A. Smolin, Jay M. Gambetta, and Graeme Smith. Efficient method for computing the maximum-likelihood quantum state from measurements with additive gaussian noise. *Phys. Rev. Lett.*, 108:070502, Feb 2012.

[78] Joel J Wallman and Steven T Flammia. Randomized benchmarking with confidence. *New Journal of Physics*, 16(10):103032, 2014.

[79] Yun-Feng Huang, Bi-Heng Liu, Liang Peng, Yu-Hu Li, Li Li, Chuan-Feng Li, and Guang-Can Guo. Experimental generation of an eight-photon greenberger–horne–zeilinger state. *Nat Commun*, 2:546, 11 2011.

[80] Thomas M Cover and Joy A Thomas. *Elements of information theory*. John Wiley & Sons, 2012.

[81] Julia Kempe and Oded Regev. 3-local hamitonian is qma-complete. *Quantum Info. Comput.*, 3:258–264, May 2003.

[82] K. Temme, T. J. Osborne, K. G. Vollbrecht, D. Poulin, and F. Verstraete. Quantum metropolis sampling. November 2009.

[83] Man-Hong Yung and Alán Aspuru-Guzik. A quantum metropolis algorithm. *Proceedings of the National Academy of Sciences*, 109(3):754–759, 2012.

[84] Maris Ozols, Martin Roetteler, and Jérémie Roland. Quantum rejection sampling. In *Proceedings of the 3rd Innovations in Theoretical Computer Science Conference*, ITCS '12, pages 290–308, New York, NY, USA, 2012. ACM.

[85] Dorit Aharonov, Wim van Dam, Julia Kempe, Zeph Landau, Seth Lloyd, and Oded Regev. Adiabatic quantum computation is equivalent to standard quantum computation. *SIAM Journal of Computing*, 37(1):166–194, 2007.

[86] Andris Ambainis. Quantum query algorithms and lower bounds. In *Classical and New Paradigms of Computation and their Complexity Hierarchies*, pages 15–32. Springer, 2004.

[87] A. Ambainis, L. Magnin, M. Roetteler, and J. Roland. Symmetry-assisted adversaries for quantum state generation. In *Computational Complexity (CCC), 2011 IEEE 26th Annual Conference on*, pages 167–177, June 2011.

[88] Troy Lee, Rajat Mittal, Ben W Reichardt, Robert Spalek, and Mario Szegedy. Quantum query complexity of state conversion. In *Foundations of Computer Science (FOCS), 2011 IEEE 52nd Annual Symposium on*, pages 344–353. IEEE, 2011.

[89] L. DiCarlo, J. M. Chow, J. M. Gambetta, Lev S. Bishop, B. R. Johnson, D. I. Schuster, J. Majer, A. Blais, L. Frunzio, S. M. Girvin, and R. J. Schoelkopf. Demonstration of two-qubit algorithms with a superconducting quantum processor. *Nature*, 460(7252):240–244, July 2009.

[90] J Clarke and AI Braginsky. The squid handbook: Applications of squids and squid systems, volume ii, 2004.

[91] Alexandre Blais, Ren-Shou Huang, Andreas Wallraff, S. M. Girvin, and R. J. Schoelkopf. Cavity quantum electrodynamics for superconducting electrical circuits: An architecture for quantum computation. *Phys. Rev. A*, 69:062320, Jun 2004.

[92] Eva Zakka-Bajjani, Francois Nguyen, Minhyea Lee, Leila R. Vale, Raymond W. Simmonds, and Jose Aumentado. Quantum superposition of a single microwave photon in two different "colour" states. *Nat Phys*, 7(8):599–603, August 2011.

[93] JJ Bollinger, DJ Heizen, WM Itano, SL Gilbert, and DJ Wineland. A 303-mhz frequency standard based on trapped be/sup+/ions. *Instrumentation and Measurement, IEEE Transactions on*, 40(2):126–128, 1991.

[94] C. Roos, G. Lancaster, M. Riebe, H. Häffner, W. Hänsel, S. Gulde, C. Becher, J. Eschner, F. Schmidt-Kaler, and R. Blatt. Bell states of atoms with ultralong lifetimes and their tomographic state analysis. *Phys. Rev. Lett.*, 92:220402, Jun 2004.

[95] C. Langer, R. Ozeri, J. Jost, J. Chiaverini, B. DeMarco, A. Ben-Kish, R. Blakestad, J. Britton, D. Hume, W. Itano, D. Leibfried, R. Reichle, T. Rosenband, T. Schaetz, P. Schmidt, and D. Wineland. Long-lived qubit memory using atomic ions. *Phys. Rev. Lett.*, 95:060502, Aug 2005.

[96] T. P. Harty, D. T. C. Allcock, C. J. Ballance, L. Guidoni, H. A. Janacek, N. M. Linke, D. N. Stacey, and D. M. Lucas. High-fidelity preparation, gates, memory, and readout of a trapped-ion quantum bit. *Phys. Rev. Lett.*, 113:220501, Nov 2014.

[97] H. Dehmelt. Proposed 10^{14} $\Delta\nu < \nu$ Laser Fluorescence Spectroscopy on Tl^+ Mono-Ion Oscillator II (spontaneous quantum jumps). *Bull. Am. Phys. Soc.*, 20(60), 1975.

[98] J. I. Cirac and P. Zoller. Quantum computations with cold trapped ions. *Phys. Rev. Lett.*, 74(20):4091–4094, May 1995.

[99] Klaus Mølmer and Anders Sørensen. Multiparticle entanglement of hot trapped ions. *Phys. Rev. Lett.*, 82(9):1835–1838, Mar 1999.

[100] Rainer Blatt and David Wineland. Entangled states of trapped atomic ions. *Nature*, 453(7198):1008–1015, June 2008.

[101] T. Monz, K. Kim, W. Hänsel, M. Riebe, A. S. Villar, P. Schindler, M. Chwalla, M. Hennrich, and R. Blatt. Realization of the quantum Toffoli gate with trapped ions. *Phys. Rev. Lett.*, 102(4):040501, January 2009.

[102] D.J. Wineland, C. Monroe, W.M. Itano, D. Leibfried, B.E. King, and D.M. Meekhof. Experimental issues in coherent quantum-state manipulation of trapped atomic ions. *Journal of Research of the National Institute of Standards and Technology*, 103(259), 1998.

[103] Q. Turchette, Kielpinski, B. King, D. Leibfried, D. Meekhof, C. Myatt, M. Rowe, C. Sackett, C. Wood, W. Itano, C. Monroe, and D. Wineland. Heating of trapped ions from the quantum ground state. *Phys. Rev. A*, 61:063418, May 2000.

[104] L. Deslauriers, P. Haljan, P. Lee, K-A. Brickman, B. Blinov, M. Madsen, and C. Monroe. Zero-point cooling and low heating of trapped $^{111}Cd^{+}$ ions. *Phys. Rev. A*, 70:043408, Oct 2004.

[105] Anders S. Sørensen, Caspar H. van der Wal, Lilian I. Childress, and Mikhail D. Lukin. Capacitive coupling of atomic systems to mesoscopic conductors. *Phys. Rev. Lett.*, 92:063601, Feb 2004.

[106] L. Tian, P. Rabl, R. Blatt, and P. Zoller. Interfacing quantum-optical and solid-state qubits. *Phys. Rev. Lett.*, 92(24):247902, June 2004.

[107] P. Rabl, D. DeMille, J. M. Doyle, M. D. Lukin, R. J. Schoelkopf, and P. Zoller. Hybrid quantum processors: Molecular ensembles as quantum memory for solid state circuits. *Phys. Rev. Lett.*, 97(3):033003, July 2006.

[108] David Petrosyan, Guy Bensky, Gershon Kurizki, Igor Mazets, Johannes Majer, and Jörg Schmiedmayer. Reversible state transfer between superconducting qubits and atomic ensembles. *Phys. Rev. A*, 79(4):040304, April 2009.

[109] David C. Burnham and Donald L. Weinberg. Observation of simultaneity in parametric production of optical photon pairs. *Phys. Rev. Lett.*, 25(2):84–87, July 1970.

[110] L. Mandel and Emil Wolf. *Optical Coherence and Quantum Optics*. Cambridge University Press, September 29, 1995.

[111] N. Bergeal, R. Vijay, V. E. Manucharyan, I. Siddiqi, R. J. Schoelkopf, S. M. Girvin, and M. H. Devoret. Analog information processing at the quantum limit with a Josephson ring modulator. *Nat Phys*, 6(4):296–302, April 2010.

[112] M. A. Castellanos-Beltran, K. D. Irwin, G. C. Hilton, L. R. Vale, and K. W. Lehnert. Amplification and squeezing of quantum noise with a tunable josephson metamaterial. *Nat Phys*, 4(12):929–931, December 2008.

[113] R. Vijay, M.H. Devoret, and Siddiqi I. Invited review article: The Josephson bifurcation amplifiers. *Rev. Sci. Instrum.*, 80, 2009.

[114] R. Vijay, D. H. Slichter, and I. Siddiqi. Observation of quantum jumps in a superconducting artificial atom. *Phys. Rev. Lett.*, 106(11):110502, March 2011.

[115] Félix Beaudoin, Marcus P. da Silva, Zachary Dutton, and Alexandre Blais. First-order sidebands in circuit QED using qubit frequency modulation. *Phys. Rev. A*, 86(2):022305, August 2012.

[116] J. D. Strand, Matthew Ware, Félix Beaudoin, T. A. Ohki, B. R. Johnson, Alexandre Blais, and B. L. T. Plourde. First-order sideband transitions with flux-driven asymmetric transmon qubits. *Phys. Rev. B*, 87(22):220505, June 2013.

[117] M. Allman, S. D. Whittaker, J. M. Castellanos-Beltran, K. Cicak, F. da Silva, P. DeFeo, M. F. Lecocq, A. Sirois, D. Teufel, J. J. Aumentado, and W. Simmonds, R.˙ Tunable resonant and nonresonant interactions between a phase qubit and *lc* resonator. *Phys. Rev. Lett.*, 112:123601, Mar 2014.

[118] D. Kielpinski, D. Kafri, M. J. Woolley, G. J. Milburn, and J. M. Taylor. Quantum interface between an electrical circuit and a single atom. *Phys. Rev. Lett.*, 108(13):130504, March 2012.

[119] M. Devoret. Quantum fluctuations in electrical circuits. *Les Houches Session LXIII, Elsevier Science B. V.*, 1995.

[120] Konstantin K. Likharev. *Dynamics of Josephson Junctions and Circuits*. CRC Press, 1986.

[121] Lowell S. Brown. Quantum motion in a Paul trap. *Phys. Rev. Lett.*, 66(5):527–529, February 1991.

[122] W. Magnus and S. Winkler. *Hill's equation*. Dover books on advanced mathematics. Dover Publications, 1979.

[123] Walter G. Kelley. *The Theory of Differential Equations: Classical and Qualitative*. Springer, 2010.

[124] N. W. McLachlan. *Theory and Application of Mathieu Functions*. Oxford University Press, 1947.

[125] Wilhelm Magnus. On the exponential solution of differential equations for a linear operator. *Communications on Pure and Applied Mathematics*, 7(4):649–673, 1954.

[126] S. Blanes, F. Casas, J.A. Oteo, and J. Ros. The magnus expansion and some of its applications. *Physics Reports*, 470(5-6):151 – 238, 2009.

[127] V Kaplunenko and Gerd M Fischer. Josephson junction arrays as a variable inductor in rf circuits and tunable filters. *Superconductor Science and Technology*, 17(5):S145, 2004.

[128] C. Monroe. Quantum information processing with atoms and photons. *Nature*, 416:238, 2002.

[129] R. Blatt and D. Wineland. Entangled states of trapped atomic ions. *Nature*, 453:1008–1015, 2008.

[130] J. Clarke and F. K. Wilhelm. Superconducting quantum bits. *Nature*, 453:1031–1042, 2008.

[131] J. Verdú, H. Zoubi, Ch. Koller, J. Majer, H. Ritsch, and J. Schmiedmayer. Strong magnetic coupling of an ultracold gas to a superconducting waveguide cavity. *Phys. Rev. Lett.*, 103:043603, 2009.

[132] D. Leibfried, B. DeMarco, V. Meyer, D. Lucas, M. Barrett, J. Britton, W. M. Itano, B. Jelenković, C. Langer, T. Rosenband, and D. J. Wineland. Experimental demonstration of a robust, high-fidelity geometric two ion-qubit phase gate. *Nature*, 422:412, 2003.

[133] J. Benhelm, G. Kirchmair, C. F. Roos, and R. Blatt. Towards fault-tolerant quantum computing with trapped ions. *Nature Phys.*, 4:463–466, 2008.

[134] D. Leibfried, R. Blatt, C. Monroe, and D. Wineland. *Rev. Mod. Phys.*, 75:281, 2003.

[135] C. Ospelkaus, U. Warring, Y. Colombe, K. R. Brown, J. M. Amini, D. Leibfried, and D. J.Wineland. Microwave quantum logic gates for trapped ions. *Nature*, 476:181–185, 2011.

[136] N. Timoney, I. Baumgart, M. Johanning, A. F. Varón, M. B. Plenio, A. Retzker, and Ch. Wunderlich. Quantum gates and memory using microwave-dressed states. *Nature*, 476:185–189, 2011.

[137] J. Chiaverini, R. B. Blakestad, J. Britton, J. D. Jost, C. Langer, D. Leibfried, R. Ozeri, and D. J. Wineland. Surface-electrode architecture for ion-trap quantum information processing. *Quant. Info. Comp.*, 5:419, 2005.

[138] S. Seidelin, J. Chiaverini, R. Reichle, J. J. Bollinger, D. Leibfried, J. Britton, J. H. Wesenberg, R. B. Blakestad, R. J. Epstein, D. B. Hume, W. M. Itano, J. D. Jost, C. Langer, R. Ozeri, N. Shiga, and D. J. Wineland. Microfabricated surface-electrode ion trap for scalable quantum information processing. *Phys. Rev. Lett.*, 96(25):253003, Jun 2006.

[139] Z. Kim, C. P. Vlahacos, J. E. Hoffman, J. A. Grover, K. D. Voigt, B. K. Cooper, C. J. Ballard, B. S. Palmer, M. Hafezi, J. M. Taylor, J. R. Anderson, A. J. Dragt, C. J. Lobb, L. A. Orozco, S. L. Rolston, and F. C. Wellstood. Thin-film superconducting resonator tunable to the ground-state hyperfine splitting of 87rb. *AIP Adv.*, 1(4):042107, 2011.

[140] J. Labaziewicz, Y. Ge, P. Antohi, D. Leibrandt, K. R. Brown, and I. L. Chuang. Suppression of heating rates in cryogenic surface-electrode ion traps. *Phys. Rev. Lett.*, 100:013001, 2008.

[141] Q. A. Turchette et al. *Phys. Rev. A*, 61:063418, 2000.

[142] Matthias Keller, Birgit Lange, Kazuhiro Hayasaka, Wolfgang Lange, and Herbert Walther. Continuous generation of single photons with controlled waveform in an ion-trap cavity system. *Nature*, 431:1075–1078, 2004.

[143] S. Olmschenk, D. N. Matsukevich, P. Maunz, D. Hayes, L.-M. Duan, and C. Monroe. Quantum teleportation between distant matter qubits. *Science*, 323(5913):486–489, 2009.

[144] G. J. Milburn, S. Schneider, and D. F. V. James. Ion trap quantum computing with warm ions. *Fortschr. Phys.*, 48:801, 2000.

[145] Adriano Barenco, Charles H. Bennett, Richard Cleve, David P. DiVincenzo, Norman Margolus, Peter Shor, Tycho Sleator, John A. Smolin, and Harald Weinfurter. Elementary gates for quantum computation. *Phys. Rev. A*, 52:3457–3467, Nov 1995.

[146] W. J. Munro, K. Nemoto, G. J. Milburn, and S. L. Braunstein. Weak-force detection with superposed coherent states. *Phys. Rev. A*, 66(2):023819, Aug 2002.

[147] Klaus Mølmer and Anders Sørensen. Multiparticle entanglement of hot trapped ions. *Phys. Rev. Lett.*, 82(9):1835–1838, Mar 1999.

[148] Anders Sørensen and Klaus Mølmer. Entanglement and quantum computation with ions in thermal motion. *Phys. Rev. A*, 62(2):022311, Jul 2000.

[149] Asher Peres. Separability criterion for density matrices. *Phys. Rev. Lett.*, 77(8):1413–1415, Aug 1996.

[150] H. Häffner, C.F. Roos, and R. Blatt. Quantum computing with trapped ions. *Physics Reports*, 469(4):155 – 203, 2008.

[151] Robin Blume-Kohout, Jun O. S. Yin, and S. J. van Enk. Entanglement verification with finite data. *Phys. Rev. Lett.*, 105:170501, Oct 2010.

[152] Barbara M. Terhal. Bell inequalities and the separability criterion. *Physics Letters A*, 271(5–6):319 – 326, 2000.

[153] Fernando G. S. L. Brandão. Quantifying entanglement with witness operators. *Phys. Rev. A*, 72:022310, Aug 2005.

[154] Alain Aspect, Philippe Grangier, and Gérard Roger. Experimental tests of realistic local theories via bell's theorem. *Phys. Rev. Lett.*, 47:460–463, Aug 1981.

[155] D. Leibfried, E. Knill, S. Seidelin, J. Britton, R. B. Blakestad, J. Chiaverini, D. B. Hume, W. M. Itano, J. D. Jost, C. Langer, R. Ozeri, R. Reichle, and D. J. Wineland. Creation of a six-atom /'schrodinger cat/' state. *Nature*, 438(7068):639–642, 12 2005.

[156] Marcin Wieśniak, Vlatko Vedral, and Časlav Brukner. Magnetic susceptibility as a macroscopic entanglement witness. *New Journal of Physics*, 7(1):258, 2005.

[157] Leonid Gurvits. Classical deterministic complexity of edmonds' problem and quantum entanglement. In *Proceedings of the thirty-fifth annual ACM symposium on Theory of computing*, pages 10–19. ACM, 2003.

[158] Steven T Flammia, David Gross, Yi-Kai Liu, and Jens Eisert. Quantum tomography via compressed sensing: error bounds, sample complexity and efficient estimators. *New Journal of Physics*, 14(9):095022, 2012.

[159] F Caruso, J Eisert, V Giovannetti, and A S Holevo. Multi-mode bosonic gaussian channels. *New Journal of Physics*, 10(8):083030, 2008.

[160] A. S. Holevo and R. F. Werner. Evaluating capacities of bosonic gaussian channels. *Phys. Rev. A*, 63:032312, Feb 2001.

[161] P. Ehrenfest. Bemerkung ãber die angenãherte gãltigkeit der klassischen mechanik innerhalb der quantenmechanik. *Zeitschrift fÃr Physik*, 45(7-8):455–457, 1927.

[162] H.P. Breuer and F. Petruccione. *The Theory of Open Quantum Systems*. Clarendon Press, 2007.

[163] A S Holevo and V Giovannetti. Quantum channels and their entropic characteristics. *Reports on Progress in Physics*, 75(4):046001, 2012.

[164] Teiko Heinosaari, Alexander S. Holevo, and Michael M. Wolf. The semigroup structure of gaussian channels. *Quantum Info. Comput.*, 10(7):619–635, July 2010.

[165] R. Simon. Peres-horodecki separability criterion for continuous variable systems. *Phys. Rev. Lett.*, 84:2726–2729, Mar 2000.

[166] Geza Giedke, Lu-Ming Duan, J. Ignacio Cirac, and Peter Zoller. Distillability criterion for all bipartite gaussian states. *Quantum Info. Comput.*, 1(3):79–86, October 2001.

[167] E.H. Kennard. Zur quantenmechanik einfacher bewegungstypen. *Zeitschrift fÃr Physik*, 44(4-5):326–352, 1927.

[168] H. Weyl. *Gruppentheorie und Quantenmechanik. - Leipzig, Hirzel 1928. VIII, 288 S.* Leipzig, 1928.

[169] H. P. Robertson. The uncertainty principle. *Phys. Rev.*, 34:163–164, Jul 1929.

[170] Charles H. Bennett, Gilles Brassard, Claude Crépeau, Richard Jozsa, Asher Peres, and William K. Wootters. Teleporting an unknown quantum state via dual classical and einstein-podolsky-rosen channels. *Phys. Rev. Lett.*, 70(13):1895–1899, Mar 1993.

[171] Géza Giedke and J. Ignacio Cirac. Characterization of gaussian operations and distillation of gaussian states. *Phys. Rev. A*, 66:032316, Sep 2002.

[172] Earl T. Campbell, Marco G. Genoni, and Jens Eisert. Continuous-variable entanglement distillation and noncommutative central limit theorems. *Phys. Rev. A*, 87:042330, Apr 2013.

[173] G. Lindblad. On the generators of quantum dynamical semigroups. *Communications in Mathematical Physics*, 48:119–130, 1976.

[174] G.J. Milburn, S. Schneider, and D.F.V. James. Ion trap quantum computing with warm ions. *Fortschritte der Physik*, 48(9-11):801–810, 2000.

[175] J. J. García-Ripoll, P. Zoller, and J. I. Cirac. Coherent control of trapped ions using off-resonant lasers. *Phys. Rev. A*, 71(6):062309, Jun 2005.

[176] Michael A. Nielsen and Isaac. Chuang. *Quantum Computation and Quantum Information*. Cambridge University Press, 2000.

[177] Carlton M. Caves and G. J. Milburn. Quantum-mechanical model for continuous position measurements. *Phys. Rev. A*, 36:5543–5555, Dec 1987.

[178] H.M. Wiseman and L. Diósi. Complete parameterization, and invariance, of diffusive quantum trajectories for markovian open systems. *Chemical Physics*, 268(1–3):91 – 104, 2001.

[179] Kurt Jacobs and Daniel A. Steck. A straightforward introduction to continuous quantum measurement. *Contemporary Physics*, 47(5):279–303, 2006.

[180] Samuel L. Braunstein, Christopher A. Fuchs, and H. J. Kimble. Criteria for continuous-variable quantum teleportation. *Journal of Modern Optics*, 47(2-3):267–278, 2000.

[181] K. Hammerer, M. M. Wolf, E. S. Polzik, and J. I. Cirac. Quantum benchmark for storage and transmission of coherent states. *Phys. Rev. Lett.*, 94:150503, Apr 2005.

[182] M Owari, M B Plenio, E S Polzik, A Serafini, and M M Wolf. Squeezing the limit: quantum benchmarks for the teleportation and storage of squeezed states. *New Journal of Physics*, 10(11):113014, 2008.

[183] E. Arthurs and J. L. Kelly Jr. B.s.t.j. brief: On the simultaneous measurement of a pair of conjugate observables. *Bell System Technical Journal*, 44(04):725–729, April 1965.

[184] D.F. Walls and G.J. Milburn. *Quantum Optics*. SpringerLink: Springer e-Books. Springer, 2008.

[185] J. E. Gough, M. R. James, and H. I. Nurdin. Squeezing components in linear quantum feedback networks. *Phys. Rev. A*, 81:023804, Feb 2010.

[186] GÃran Lindblad. Cloning the quantum oscillator. *Journal of Physics A: Mathematical and General*, 33(28):5059, 2000.

[187] A. Holevo. *Probabilistic and Statistical Aspects of Quantum Theory*. Monographs quaderni. Scuola Normale Superiore, 2011.

[188] J. Eisert and M. B. Plenio. Introduction to the basics of entanglement theory in continuous-variable systems. *International Journal of Quantum Information*, 01(04):479–506, 2003.

[189] William Marshall, Christoph Simon, Roger Penrose, and Dik Bouwmeester. Towards quantum superpositions of a mirror. *Phys. Rev. Lett.*, 91:130401, Sep 2003.

[190] O. Romero-Isart, A. C. Pflanzer, F. Blaser, R. Kaltenbaek, N. Kiesel, M. Aspelmeyer, and J. I. Cirac. Large quantum superpositions and interference of massive nanometer-sized objects. *Phys. Rev. Lett.*, 107:020405, Jul 2011.

[191] Oriol Romero-Isart. Quantum superposition of massive objects and collapse models. *Phys. Rev. A*, 84:052121, Nov 2011.

[192] Igor Pikovski, Michael R. Vanner, Markus Aspelmeyer, M. S. Kim, and Caslav Brukner. Probing planck-scale physics with quantum optics. *Nat Phys*, 8(5):393–397, 05 2012.

[193] F. Karolyhazy. Gravitation and quantum mechanics of macroscopic objects. *Il Nuovo Cimento A*, 42(2):390–402, 1966.

[194] Roger Penrose. On gravity's role in quantum state reduction. *General Relativity and Gravitation*, 28(5):581–600, 1996.

[195] Lajos Diósi, Hans-Thomas Elze, Leone Fronzoni, Jonathan Halliwell, Enrico Prati, Giuseppe Vitiello, and James Yearsley. 5th international workshop dice2010: Space-time-matter – current issues in quantum mechanics and beyond. *Journal of Physics: Conference Series*, 306(1):011001, 2011.

[196] Gordon Baym and Tomoki Ozawa. Two-slit diffraction with highly charged particles: Niels bohr's consistency argument that the electromagnetic field must be quantized. *Proceedings of the National Academy of Sciences*, 106(9):3035–3040, 2009.

[197] Dvir Kafri and J.M. Taylor. A noise inequality for entanglement generation, 2013.

[198] L. Diósi. Relativistic theory for continuous measurement of quantum fields. *Phys. Rev. A*, 42:5086–5092, Nov 1990.

[199] O. Romero-Isart, L. Clemente, C. Navau, A. Sanchez, and J. I. Cirac. Quantum magnetomechanics with levitating superconducting microspheres. *Phys. Rev. Lett.*, 109:147205, Oct 2012.

[200] K. Audenaert, J. Eisert, M. B. Plenio, and R. F. Werner. Entanglement properties of the harmonic chain. *Phys. Rev. A*, 66:042327, Oct 2002.

[201] G.J. Milburn, S. Schneider, and D.F.V. James. Ion trap quantum computing with warm ions. *Fortschritte der Physik*, 48(9-11):801–810, 2000.

[202] D. Leibfried, B. DeMarco, V. Meyer, D. Lucas, M. Barrett, J. Britton, W. M. Itano, B. Jelenkovic, C. Langer, T. Rosenband, and D. J. Wineland. Experimental demonstration of a robust, high-fidelity geometric two ion-qubit phase gate. *Nature*, 422(6930):412–415, 03 2003.

[203] Howard M Wiseman and Gerard J Milburn. *Quantum measurement and control*. Cambridge University Press, 2009.

[204] J. J. Halliwell and E. Zafiris. Decoherent histories approach to the arrival time problem. *Phys. Rev. D*, 57:3351–3364, Mar 1998.

[205] Huan Yang, Haixing Miao, Da shin Lee, Bassam Helou, and Yanbei Chen. Macroscopic quantum mechanics in a classical spacetime. 10 2012.

[206] A. W. Overhauser and R. Colella. Experimental test of gravitationally induced quantum interference. *Phys. Rev. Lett.*, 33:1237–1239, Nov 1974.

[207] R. Colella, A. W. Overhauser, and S. A. Werner. Observation of gravitationally induced quantum interference. *Phys. Rev. Lett.*, 34:1472–1474, Jun 1975.

[208] S. A. Werner, J. L. Staudenmann, and R. Colella. Effect of earth's rotation on the quantum mechanical phase of the neutron. *Phys. Rev. Lett.*, 42:1103–1106, Apr 1979.

[209] Lajos Diósi. Notes on certain newton gravity mechanisms of wavefunction localization and decoherence. *Journal of Physics A: Mathematical and Theoretical*, 40(12):2989, 2007.

[210] Lajos Diósi. Hybrid quantum-classical master equations. 01 2014.

[211] Nikolai Kiesel, Florian Blaser, Uroš Delić, David Grass, Rainer Kaltenbaek, and Markus Aspelmeyer. Cavity cooling of an optically levitated submicron particle. *Proceedings of the National Academy of Sciences*, 110(35):14180–14185, 2013.

[212] Tongcang Li, Simon Kheifets, and Mark G. Raizen. Millikelvin cooling of an optically trapped microsphere in vacuum. *Nat Phys*, 7(7):527–530, 07 2011.

[213] Peter Asenbaum, Stefan Kuhn, Stefan Nimmrichter, Ugur Sezer, and Markus Arndt. Cavity cooling of free silicon nanoparticles in high vacuum. *Nat Commun*, 4, 11 2013.

[214] G. Guccione, M. Hosseini, S. Adlong, M. T. Johnsson, J. Hope, B. C. Buchler, and P. K. Lam. Scattering-free optical levitation of a cavity mirror. *Phys. Rev. Lett.*, 111:183001, Oct 2013.

[215] ZHANG-QI YIN, ANDREW A. GERACI, and TONGCANG LI. Optomechanics of levitated dielectric particles. *International Journal of Modern Physics B*, 27(26):1330018, 2013.

[216] M. Cirio, G. K. Brennen, and J. Twamley. Quantum magnetomechanics: Ultrahigh-q-levitated mechanical oscillators. *Phys. Rev. Lett.*, 109:147206, Oct 2012.

[217] Asher Peres and Daniel R. Terno. Hybrid classical-quantum dynamics. *Phys. Rev. A*, 63:022101, Jan 2001.

[218] William Hall. Multipartite reduction criteria for separability. *Phys. Rev. A*, 72:022311, Aug 2005.

[219] H. Haffner, C. Roos, C. Becher, W. Hansel, T. Korber, F. Schmidt-Kaler, M. Riebe, J. Benhelm, G. Lancaster, D. Chek-al Kar, and R. Blatt. Quantum computing with trapped ions. page 307, jun. 2005.

[220] Isaac L. Chuang and M. A. Nielsen. Prescription for experimental determination of the dynamics of a quantum black box. *Journal of Modern Optics*, 44(11-12):2455–2467, 1997.

[221] J. F. Poyatos, J. I. Cirac, and P. Zoller. Complete characterization of a quantum process: The two-bit quantum gate. *Phys. Rev. Lett.*, 78:390–393, Jan 1997.

[222] Seth T. Merkel, Jay M. Gambetta, John A. Smolin, Stefano Poletto, Antonio D. Córcoles, Blake R. Johnson, Colm A. Ryan, and Matthias Steffen. Self-consistent quantum process tomography. *Phys. Rev. A*, 87:062119, Jun 2013.

[223] David Gross, Yi-Kai Liu, Steven T. Flammia, Stephen Becker, and Jens Eisert. Quantum state tomography via compressed sensing. *Phys. Rev. Lett.*, 105:150401, Oct 2010.

[224] A. Shabani, R. L. Kosut, M. Mohseni, H. Rabitz, M. A. Broome, M. P. Almeida, A. Fedrizzi, and A. G. White. Efficient measurement of quantum dynamics via compressive sensing. *Phys. Rev. Lett.*, 106:100401, Mar 2011.

[225] Graeme Smith and John A. Smolin. Detecting incapacity of a quantum channel. *Phys. Rev. Lett.*, 108:230507, Jun 2012.

[226] Bo Qi, Zhibo Hou, Li Li, Daoyi Dong, Guoyong Xiang, and Guangcan Guo. Quantum state tomography via linear regression estimation. *Sci. Rep.*, 3, 12 2013.

[227] Max S. Kaznady and Daniel F. V. James. Numerical strategies for quantum tomography: Alternatives to full optimization. *Phys. Rev. A*, 79:022109, Feb 2009.

[228] Jeffrey M. Epstein, Andrew W. Cross, Easwar Magesan, and Jay M. Gambetta. Investigating the limits of randomized benchmarking protocols. *Phys. Rev. A*, 89:062321, Jun 2014.

[229] John Preskill. Reliable quantum computers. *Proceedings of the Royal Society of London A: Mathematical, Physical and Engineering Sciences*, 454(1969):385–410, 1998.

[230] Emanuel Knill, Raymond Laflamme, and Wojciech H. Zurek. Resilient quantum computation. *Science*, 279(5349):342–345, 1998.

[231] Scott Aaronson and Alex Arkhipov. Bosonsampling is far from uniform. 09 2013.

[232] Nicolo Spagnolo, Chiara Vitelli, Marco Bentivegna, Daniel J. Brod, Andrea Crespi, Fulvio Flamini, Sandro Giacomini, Giorgio Milani, Roberta Ramponi, Paolo Mataloni, Roberto Osellame, Ernesto F. Galvao, and Fabio Sciarrino. Experimental validation of photonic boson sampling. *Nat Photon*, 8(8):615–620, 08 2014.

[233] Jacques Carolan, MeineckeJasmin D. A., Peter J. Shadbolt, Nicholas J. Russell, Nur Ismail, Kerstin Wörhoff, Terry Rudolph, Mark G. Thompson, Jeremy L. O'Brien, MatthewsJonathan C. F., and Anthony Laing. On the experimental verification of quantum complexity in linear optics. *Nat Photon*, 8(8):621–626, 08 2014.

[234] Iulia Buluta and Franco Nori. Quantum simulators. *Science*, 326(5949):108–111, 2009.

[235] J. Ignacio Cirac and Peter Zoller. Goals and opportunities in quantum simulation. *Nat Phys*, 8(4):264–266, 04 2012.

[236] Pierre Pfeuty. The one-dimensional ising model with a transverse field. *ANNALS of Physics*, 57(1):79–90, 1970.

[237] Sergey Bravyi, David P. DiVincenzo, and Daniel Loss. Schrieffer–wolff transformation for quantum many-body systems. *Annals of Physics*, 326:2793–2826, 2011.

[238] Edward Farhi and Sam Gutmann. Quantum computation and decision trees. *Phys. Rev. A*, 58:915–928, Aug 1998.

[239] W. Forrest Stinespring. Positive functions on c*-algebras. *Proceedings of the American Mathematical Society*, 6(2):pp. 211–216, 1955.

[240] Michal Horodecki, Pawel Horodecki, and Ryszard Horodecki. Separability of mixed states: necessary and sufficient conditions. *Physics Letters A*, 223(1–2):1 – 8, 1996.

[241] Roger A. Horn and Charles R. Johnson. *Matrix Analysis*. Cambridge University Press, second edition, 2012. Cambridge Books Online.

[242] H. Haffner, W. Hansel, C. F. Roos, J. Benhelm, D. Chek-al kar, M. Chwalla, T. Korber, U. D. Rapol, M. Riebe, P. O. Schmidt, C. Becher, O. Guhne, W. Dur, and R. Blatt. Scalable multiparticle entanglement of trapped ions. *Nature*, 438(7068):643–646, 12 2005.

[243] G.-D. Lin, S.-L. Zhu, R. Islam, K. Kim, M.-S. Chang, S. Korenblit, C. Monroe, and L.-M. Duan. Large-scale quantum computation in an anharmonic linear ion trap. *EPL (Europhysics Letters)*, 86(6):60004, 2009.

[244] R. Blatt and C. F. Roos. Quantum simulations with trapped ions. *Nat Phys*, 8(4):277–284, 04 2012.

[245] D. T. C. Allcock, T. P. Harty, C. J. Ballance, B. C. Keitch, N. M. Linke, D. N. Stacey, and D. M. Lucas. A microfabricated ion trap with integrated microwave circuitry. *Applied Physics Letters*, 102(4):–, 2013.

[246] Philip Richerme, Zhe-Xuan Gong, Aaron Lee, Crystal Senko, Jacob Smith, Michael Foss-Feig, Spyridon Michalakis, Alexey V. Gorshkov, and Christopher Monroe. Non-local propagation of correlations in quantum systems with long-range interactions. *Nature*, 511(7508):198–201, 07 2014.

[247] H. C. Nägerl, D. Leibfried, H. Rohde, G. Thalhammer, J. Eschner, F. Schmidt-Kaler, and R. Blatt. Laser addressing of individual ions in a linear ion trap. *Phys. Rev. A*, 60:145–148, Jul 1999.

[248] M. Johanning, A. Braun, N. Timoney, V. Elman, W. Neuhauser, and Chr. Wunderlich. Individual addressing of trapped ions and coupling of motional and spin states using rf radiation. *Phys. Rev. Lett.*, 102:073004, Feb 2009.

[249] Shirin Enferad, Mahdi Amniat-Talab, and Maghsud Saadati-Niari. Creation of cluster state of four ions in ion-trap system by individual addressing. *Optik - International Journal for Light and Electron Optics*, 125(21):6395–6403, 11 2014.

[250] C. Piltz, T. Sriarunothai, A. F. Varón, and C. Wunderlich. A trapped-ion-based quantum byte with 105 next-neighbour cross-talk. *Nat Commun*, 5, 08 2014.

[251] C. Bruder, R. Fazio, and G. Schön. The bose-hubbard model: from josephson junction arrays to optical lattices. *Annalen der Physik*, 14(9-10):566–577, 2005.

[252] Waseem S. Bakr, Jonathon I. Gillen, Amy Peng, Simon Folling, and Markus Greiner. A quantum gas microscope for detecting single atoms in a hubbard-regime optical lattice. *Nature*, 462(7269):74–77, 11 2009.

[253] Daniel Greif, Thomas Uehlinger, Gregor Jotzu, Leticia Tarruell, and Tilman Esslinger. Short-range quantum magnetism of ultracold fermions in an optical lattice. *Science*, 340(6138):1307–1310, 2013.

[254] Jacob F. Sherson, Christof Weitenberg, Manuel Endres, Marc Cheneau, Immanuel Bloch, and Stefan Kuhr. Single-atom-resolved fluorescence imaging of an atomic mott insulator. *Nature*, 467(7311):68–72, 09 2010.

[255] ElliottH. Lieb and DerekW. Robinson. The finite group velocity of quantum spin systems. *Communications in Mathematical Physics*, 28(3):251–257, 1972.

[256] S. Bravyi, M. B. Hastings, and F. Verstraete. Lieb-robinson bounds and the generation of correlations and topological quantum order. *Phys. Rev. Lett.*, 97:050401, Jul 2006.

[257] Charles H. Bennett and Stephen J. Wiesner. Communication via one- and two-particle operators on einstein-podolsky-rosen states. *Phys. Rev. Lett.*, 69:2881–2884, Nov 1992.

[258] Lov K. Grover. A fast quantum mechanical algorithm for database search. In *Proceedings of the Twenty-eighth Annual ACM Symposium on Theory of Computing*, STOC '96, pages 212–219, New York, NY, USA, 1996. ACM.

[259] P.W. Shor. Polynomial-time algorithms for prime factorization and discrete logarithms on a quantum computer. *SIAM Review*, 41(2):303–332, 1999.

[260] Aija Berzina, Andrej Dubrovsky, Rusins Freivalds, Lelde Lace, and Oksana Scegulnaja. *Quantum Query Complexity for Some Graph Problems*, volume 2932 of *Lecture Notes in Computer Science*. Springer Berlin / Heidelberg, 2004.

[261] Aram W. Harrow, Avinatan Hassidim, and Seth Lloyd. Quantum algorithm for linear systems of equations. *Phys. Rev. Lett.*, 103:150502, Oct 2009.

[262] J. D. Biamonte, V. Bergholm, J. D. Whitfield, J. Fitzsimons, and A. Aspuru-Guzik. Adiabatic quantum simulators. *AIP Advances*, 1:022126, 2011.

[263] Hendrik Weimer, Markus Muller, Igor Lesanovsky, Peter Zoller, and Hans Peter Buchler. A rydberg quantum simulator. *Nat Phys*, 6(5):382–388, 05 2010.

[264] Ivan Kassal, Stephen P. Jordan, Peter J. Love, Masoud Mohseni, and Alán Aspuru-Guzik. Polynomial-time quantum algorithm for the simulation of chemical dynamics. *Proceedings of the National Academy of Sciences*, 105(48):18681–18686, 2008.

[265] Ivan Kassal, James D. Whitfield, Alejandro Perdomo-Ortiz, Man-Hong Yung, and Alán Aspuru-Guzik. Simulating chemistry using quantum computers. *Annual Review of Physical Chemistry*, 62:185–207, May 2011.

[266] FHL Essler, H Frahm, F Göhmann, A Klümper, and V Korepin. The one-dimensional hubbard model. 2003.

[267] Alan Aspuru-Guzik, Anthony D. Dutoi, Peter J. Love, and Martin Head-Gordon. Simulated quantum computation of molecular energies. *Science*, 309(5741):1704–1707, 2005.

[268] Herbert Spohn and Joel L Lebowitz. Irreversible thermodynamics for quantum systems weakly coupled to thermal reservoirs. *Advances in Chemical Physics: For Ilya Prigogine, Volume 38*, pages 109–142, 2007.

[269] Corinna Kollath, Andreas M. Läuchli, and Ehud Altman. Quench dynamics and nonequilibrium phase diagram of the bose-hubbard model. *Phys. Rev. Lett.*, 98:180601, Apr 2007.

[270] Marcos Rigol, Vanja Dunjko, and Maxim Olshanii. Thermalization and its mechanism for generic isolated quantum systems. *Nature*, 452(7189):854–858, 04 2008.

[271] Kristan Temme. Lower bounds to the spectral gap of davies generators. *Journal of Mathematical Physics*, 54(12):–, 2013.

[272] Edward Farhi and Sam Gutmann. Analog analogue of a digital quantum computation. *Phys. Rev. A*, 57(4):2403–2406, Apr 1998.

[273] Harry Buhrman and Ronald de Wolf. Complexity measures and decision tree complexity: a survey. *Theoretical Computer Science*, 288(1):21 – 43, 2002. Complexity and Logic.

[274] Lov K. Grover. Quantum mechanics helps in searching for a needle in a haystack. *Phys. Rev. Lett.*, 79(2):325–328, Jul 1997.

[275] Michel Boyer, Gilles Brassard, Peter Høyer, and Alain Tapp. Tight bounds on quantum searching. *Fortschritte der Physik*, 46(4-5):493–505, 1998.

[276] Daniel R Simon. On the power of quantum computation. *SIAM journal on computing*, 26(5):1474–1483, 1997.

[277] Scott Aaronson and Yaoyun Shi. Quantum lower bounds for the collision and the element distinctness problems. *J. ACM*, 51(4):595–605, July 2004.

[278] Richard Cleve, Daniel Gottesman, Michele Mosca, Rolando D. Somma, and David Yonge-Mallo. Efficient discrete-time simulations of continuous-time quantum query algorithms. In *Proceedings of the Forty-first Annual ACM Symposium on Theory of Computing*, STOC '09, pages 409–416, New York, NY, USA, 2009. ACM.

[279] Dominic Berry, Graeme Ahokas, Richard Cleve, and Barry Sanders. Efficient quantum algorithms for simulating sparse hamiltonians. *Communications in Mathematical Physics*, 270:359–371, 2007. 10.1007/s00220-006-0150-x.

[280] Dominic W Berry, Andrew M Childs, Richard Cleve, Robin Kothari, and Rolando D Somma. Exponential improvement in precision for simulating sparse hamiltonians. In *Proceedings of the 46th Annual ACM Symposium on Theory of Computing*, pages 283–292. ACM, 2014.

[281] Dominic W. Berry, Andrew M. Childs, Richard Cleve, Robin Kothari, and Rolando D. Somma. Simulating hamiltonian dynamics with a truncated taylor series. *Phys. Rev. Lett.*, 114:090502, Mar 2015.

[282] G. W. Stewart and Ji guan Sun. *Matrix Perturbation Theory*. Academic Press, Inc., 1990.

[283] Claude Cohen-Tannoudji, Jacques Dupont-Roc, and Gilbert Grynberg. *Atom-Photon Interactions: Basic Processes and Applications*. Wiley-Interscience, March 1992.

[284] Jérémie Roland and Nicolas J. Cerf. Quantum search by local adiabatic evolution. *Phys. Rev. A*, 65:042308, Mar 2002.

[285] Christoph Dankert, Richard Cleve, Joseph Emerson, and Etera Livine. Exact and approximate unitary 2-designs and their application to fidelity estimation. *Phys. Rev. A*, 80:012304, Jul 2009.

[286] Gilles Brassard, Peter Hoyer, Michele Mosca, and Alain Tapp. Quantum amplitude amplification and estimation. 2007.

[287] Scott Aaronson and Andris Ambainis. The need for structure in quantum speedups. *Theory OF Computing*, 10(6):133–166, 2014.

[288] A. Kitaev, Shen A. H. Yu, and M. N. Vyalyi. *Classical and Quantum Computation*. American Mathematical Society, 2002.

[289] Julia Kempe, Alexei Kitaev, and Oded Regev. The complexity of the local hamiltonian problem. *SIAM J. Comput.*, 35(5):1070–1097, May 2006.

[290] Walter Rudin. *Functional analysis*. International series in pure and applied mathematics. McGraw-Hill, Inc., New York, 1991.

[291] Man-Duen Choi. Completely positive linear maps on complex matrices. *Linear Algebra and its Applications*, 10(3):285 – 290, 1975.

[292] K Kraus. General state changes in quantum theory. *Annals of Physics*, 64(2):311 – 335, 1971.

[293] Ingemar Bengtsson, Karol Zyczkowski, and Gerard J. Milburn. Geometry of quantum states: an introduction to quantum entanglement by ingemar bengtsson and karol zyczkowski. *Quantum Information & Computation*, 8(8):860, 2008.

[294] Richard Feynman. Quantum mechanical computers. *Foundations of Physics*, 16:507–531, 1986. 10.1007/BF01886518.

[295] Wen-Chyuan Yueh. Eigenvalues of several tridiagonal matrices. *Appl Math ENotes*, 5:66–74, 2005.

[296] Stephen P. Jordan and Edward Farhi. Perturbative gadgets at arbitrary orders. *Phys. Rev. A*, 77(6):062329, June 2008.

[297] Sergey Bravyi, David P. DiVincenzo, Daniel Loss, and Barbara M. Terhal. Quantum simulation of many-body hamiltonians using perturbation theory with bounded-strength interactions. *Phys. Rev. Lett.*, 101:070503, Aug 2008.

[298] Hans J. Briegel and Robert Raussendorf. Persistent entanglement in arrays of interacting particles. *Phys. Rev. Lett.*, 86:910–913, Jan 2001.

[299] Ari Mizel, M. W. Mitchell, and Marvin L. Cohen. Energy barrier to decoherence. *Phys. Rev. A*, 63:040302, Mar 2001.

[300] Chetan Nayak, Steven H. Simon, Ady Stern, Michael Freedman, and Sankar Das Sarma. Non-abelian anyons and topological quantum computation. *Rev. Mod. Phys.*, 80(3):1083–1159, September 2008.

[301] Andrew M. Childs. Universal computation by quantum walk. *Phys. Rev. Lett.*, 102:180501, May 2009.

[302] Frank Verstraete, Michael M. Wolf, and J. Ignacio Cirac. Quantum computation and quantum-state engineering driven by dissipation. *Nat Phys*, 5(9):633–636, September 2009.

[303] Daniel Nagaj. Universal two-body-hamiltonian quantum computing. *Phys. Rev. A*, 85:032330, Mar 2012.

[304] E. B. Davies. Markovian master equations. *Communications in Mathematical Physics*, 39:91–110, 1974. 10.1007/BF01608389.